International Journal of Photoenergy

Selected Papers from the Second International Conference on Semiconductor Photochemistry

Guest Editors: Russell F. Howe, Peter K. J. Robertson, and Andrew Mills

Selected Papers from the Second International Conference on Semiconductor Photochemistry

International Journal of Photoenergy

Selected Papers from the Second International Conference on Semiconductor Photochemistry

Guest Editors: Russell F. Howe, Peter K. J. Robertson, and Andrew Mills

Contents

Hindawi Publishing Corporation
International Journal of Photoenergy
Volume 2008, Article ID 258561, 2 pages
doi:10.1155/2008/258561

Editorial

Preface to the Special Issue on Selected Papers from the Second International Conference on Semiconductor Photochemistry SP-2

Russell F. Howe,[1] Peter K. J. Robertson,[2] and Andrew Mills[3]

[1] *Department of Chemistry, The University of Aberdeen, Old Aberdeen AB24 3UE, UK*
[2] *Centre for Research in Energy and the Environment, The Robert Gordon University, Schoolhill, Aberdeen AB10 1FR, UK*
[3] *Department of Pure and Applied Chemistry, University of Strathclyde, Thomas Graham Building, 295 Cathedral Street, Glasgow G1 IXL, UK*

Correspondence should be addressed to Peter K. J. Robertson, peter.robertson@rgu.ac.uk

Received 24 December 2008; Accepted 24 December 2008

The Second International Conference on Semiconductor Photochemistry (SP-2) was set up following the highly successful SP-1 meeting held in Glasgow in July 2001. The conference was scheduled over three days from Monday 23rd July to Wednesday 25th of July 2007 (coincidentally the same days over which SP-1 was held in 2001) at The Robert Gordon University in Aberdeen in the north east of Scotland. As with SP-1, the primary objective of the organisers was to host an inclusive and affordable conference designed to reach as wide an audience as possible. As a result, the meeting again was organised on a nonprofit basis, with an intense programme and few additional "added extras." The delegate fee was established at an affordable rate of £150 for full delegates and £75 for students which covered attendance of the full conference programme, morning and afternoon tea, and lunch. The ability to allow the low registration fee was facilitated by the very generous support of the conference sponsors and we are extremely grateful to these sponsors who included: Degussa-Huels, Millennium Chemicals, Johnson Matthey, Pilkington Technology, Apache, Halliburton, the Robert Gordon University, the Society of Chemical Industry (SCI), and Hindawi Publishing Corporation for their support. This sponsorship was in various forms, including, money (Degussa-Huels, Millennium Chemicals, Johnson Matthey, Pilkington Technology, and the Society of Chemical Industry), the conference venue (The Robert Gordon University), conference bags (Halliburton and Apache), and support for the conference proceedings (Hindawi Publishing Corporation). The Aberdeen Ambassadors provided an accommodation booking service covering a range of hotel accommodation across the city, and alternative accommodation in the university halls of residence was also available.

The programme started each day at 8.30 am and finished at 18.00. In order to ensure that all participants were able to attend the whole programme, no parallel sessions were scheduled. On Monday and Tuesday evenings, a poster session was held with some liquid refreshment to "facilitate" the networking process. All those who wanted to lecture were given the opportunity to speak, usually for 25 minutes and only three specially invited lecturers were given extended lecture slots of 40 minutes. It was very heartening to find that all the big names in the field agreed unhesitatingly to be present at the conference, even when offered only a 25-minute slot so as to allow many others, possibly less well known, to speak. The conference proved to be exceptionally popular, attracting 200 participants from 34 nations; and the papers contained in this special edition provide just some measure of the diversity of subjects presented and discussed. The conference concluded with a civic reception at the historic Town House in Aberdeen City kindly provided by the Lord Provost and Aberdeen City Council. Plans for SP-3 are already well developed and it is planned to hold this in Glasgow in 12–16th April, 2010 (see http://sp3.ukspc.org.uk/ for further details).

Semiconductor photochemistry has been a topic of intense research interest over the past 25 years, especially with respect to studies utilising titanium dioxide. The research activity has significantly diversified from the early

work on photomineralisation of contaminants in water. This is demonstrated by the range of subjects covered in this special edition which include materials preparation, water and air purification, antibacterial effects, sensing properties of semiconductor films, and reactor engineering.

The properties of titania sol-gel catalysts depend strongly on the preparation conditions. The factors involved are discussed in the article by Marugan et al. Visible-light activation of titania photocatalysts is a widely sought objective; Irvine et al. describe a new approach to the preparation of such catalysts. Although titania has been the most widely studied photocatalyst, other transition metal oxides also warrant attention: Liang et al. report the photoelectrochemical characterisation of iron-oxide thin films. Yates et al. describe the visible and UV activity of thin silver films prepared by atmospheric pressure chemical vapour deposition (CVD). Mills and Crow have investigated the factors influencing the wettability of titania films, while Sheel et al. describe the photoactivity of thin silver films and of silver-titania composite films, particularly for biocidal activity. The thin-film theme is continued by Skubal et al., who reviewed their work on self detection and decontamination. The use of oxide semiconductors to detect oxygen through UV-activated luminescence is reported by Mills et al. Dye-sensitized solar cells were reviewed in a plenary presentation by Michael Grätzel; in this volume Holliman et al. describe studies of the uptake of dyes by titania. Mills et al. report a new rapid method for assessing the photocatalytic activity of thin titania films. Reaction pathways in the gas-phase degradation of decane and methanol have been investigated by Balcerski et al., using DRIFT spectroscopy, while Pucher et al. have combined adsorption and photocatalysis in a reactor for gas cleaning. Flores et al. have assessed the durability of silver-modified titania catalysts for degradation of dichloroacetic acid. Removal of hydrocarbons from water, with particular emphasis on reactor design, is covered by Adams et al., while photocatalytic degradation of pesticides is described by Boxall and Muneer. Finally, Mohamed et al. report on the partial oxidation of organic compounds via photocatalysis, a rather neglected subject in comparison with complete oxidation or degradation.

In conclusion, semiconductor photochemistry remains a very active field of research from which a range of practical applications with vast commercial potential is emerging. It will be interesting to see how the field has further developed at SP-3 in 2010. This conference will build on the aims of the previous meetings and feature an additional 1 day international *postgraduate* symposium so that the younger researchers in the field have an opportunity to present.

Russell F. Howe
Peter K. J. Robertson
Andrew Mills

Hindawi Publishing Corporation
International Journal of Photoenergy
Volume 2008, Article ID 759561, 7 pages
doi:10.1155/2008/759561

Research Article

Influence of the Synthesis pH on the Properties and Activity of Sol-Gel TiO_2 Photocatalysts

Javier Marugán,[1] Paul Christensen,[2] Terry Egerton,[2] and Herry Purnama[2]

[1] *Department of Chemical and Environmental Technology (ESCET), Universidad Rey Juan Carlos, C/ Tulipán s/n, Móstoles 28933, Madrid, Spain*
[2] *School of Chemical Engineering and Advanced Materials, University of Newcastle upon Tyne, Bedson Building, Newcastle upon Tyne NE1 7RU, UK*

Correspondence should be addressed to Javier Marugán, javier.marugan@urjc.es

Received 24 August 2007; Accepted 5 January 2008

Recommended by Russell Howe

The activity of titania photocatalysts is highly dependent on the synthesis procedure. This work reports a study of the correlation between the photocatalytic activity and the physicochemical and photoelectrochemical properties of sol-gel TiO_2 powders and electrodes synthesized using different pH values and temperatures. The activity of the materials has been evaluated using the decolorization of Reactive Orange 16 (RO16) as model reaction. In contrast with the large number of studies reporting the influence of the temperature, our results point out that preparation pH has even more influence on the crystalline phases and the photocatalytic activity of TiO_2 powders and photocurrents of the electrodes. However, the effects on the activity and the photocurrents recorded after immobilization on a conducting support do not vary accordingly. Consequently, our results indicate that the measurement of the photocurrent in an electrolyte media is not a good indicator of the photocatalytic activity of the unsupported system.

1. INTRODUCTION

The fundamentals of semiconductor photocatalysis and its application to the removal of chemical pollutants have been extensively reviewed [1–5]. However, commercialization of photocatalysis for water treatment has been hindered both by difficulties of postreaction catalyst recovery [6] and by low-quantum efficiencies [7], which means that large reactors are required for small-capacity plants. Consequently, although immobilized TiO_2 has been shown to be less active than slurry systems, much effort has been devoted to the development of highly active fixed catalysts. One approach is to immobilize the TiO_2 on a conducting support and apply a potential bias. This, simultaneously, addresses both problems [8].

The activity of titania powders and electrodes is highly dependent on the synthesis procedure [9, 10]. A common way of synthesizing TiO_2 electrodes is to coat conducting materials with titania sol-gel suspensions, as this procedure provides fine control of the physicochemical properties of the TiO_2 crystalline phase and hence of its photocatalytic activity [11]. The heat treatment temperature used to crystallize the titania has been shown to be critical in the activity of sol-gel coatings [12]. However, to the best of our knowledge, there are no reports about the influence of the synthesis pH or of the pH of coating suspensions on the activity and photoelectrochemical properties of the catalysts.

In this work we have studied the correlation between the photocatalytic activity and the physicochemical and photoelectrochemical properties of sol-gel TiO_2 synthesized using two different pH routes. The activity of the materials has been evaluated using the decolorization of Reactive Orange 16 as model reaction.

2. EXPERIMENTAL

2.1. Synthesis of the materials

Titanium dioxide sols were prepared by hydrolysis and condensation of titanium tetraisopropoxide (TTIP) (97%,

Sigma Aldrich, Gillingham, UK) at different pH values, following a procedure based on that described by O'Regan et al. [13]. Powder photocatalysts were obtained from the colloidal suspensions by increasing the pH to 7 with sodium hydroxide and vacuum filtering through a 2.7 μm paper filter (Whatman plc, Maidstone, UK). The filter cake was resuspended in deionized water three times to remove the ions from the solution until the filtrate conductivity fell below 200 $\mu S \cdot cm^{-1}$, and finally was rinsed twice with 2-propanol to minimize particle agglomeration. The solids were dried at room temperature and then calcined at the desired temperature for two hours.

To prepare the electrodes, the titania colloidal suspension was first concentrated to *ca.* 150 $g \cdot L^{-1}$, using a vacuum rotary evaporator, to increase the viscosity. Thin-film electrodes were fabricated by dropping suspension onto 1 cm × 1 cm titanium plates (99.6%, Goodfellow, Huntingdon, UK) and spinning at 2800 rpm prior to calcination for 10 minutes at the desired temperature. The dropping, spinning, and heating sequence were repeated five times. The white coating was more apparent on the neutral (pH 6.5) plates than on the acid (pH 1.5) electrodes.

2.2. Characterization techniques

X-ray diffractograms (XRD) were collected in the range $10 < 2\theta < 90^\circ$ in a Philips X'Pert diffractometer using nickel-filtered monochromatic Cu Kα radiation. In all cases, only anatase and rutile crystalline phases were detected. To investigate the morphology of the TiO_2 electrodes, scanning electron microscopy (SEM) micrographs were taken on a JEOL JSM5300LV working at an acceleration voltage of 25 kV under environmental conditions, without conductive coating on the sample.

Diffuse reflectance spectra (DRS) of the small plate electrodes were recorded from 200–500 nm relative to a polytetrafluoroethylene reference with a Varian Cary 500 Scan U-VIS-NIR spectrophotometer equipped with an integrating sphere diffuse reflectance accessory. Reflectances were reported as the Kubelka-Munk function, F(R), whose value, for constant scattering, is proportional to the absorption.

Electrochemical characterization of the small plate electrodes was carried out by cyclic voltammetry, with a sweep rate of 100 mV s^{-1}, using an Eco-Chemie μAutolab Type II potentiostat. Potentials were quoted with respect to an Ag/AgCl reference electrode and a 10 cm in diameter nickel gauze was employed as counter electrode. Photocurrents were recorded under illumination by two 36 W actinic UV lamps (Philips Lighting, Guildford, UK).

2.3. Photoreactions procedure

The photoreactor was a cylindrical concentric system with two axially located 8 W UV lamps (Sylvania: Light Bulbs Direct, Amersham, UK), two Pyrex glass walls containing the suspension of catalyst in the dye solution, and a sintered frit distributing the sparge oxygen. More details about the reactor can be found elsewhere [12]. The photocatalytic activity of the photocatalysts was evaluated using the decolorization

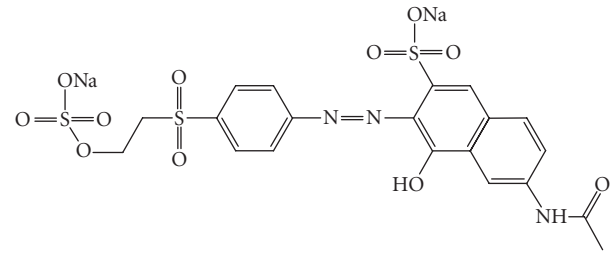

Scheme 1: Reactive Orange 16 (RO16).

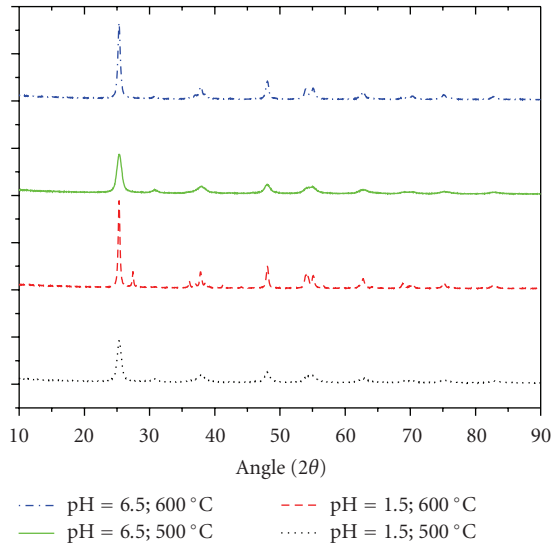

Figure 1: X-ray diffraction pattern of pure titania powder photocatalysts.

of the azo dye Reactive Orange 16 (RO16), represented in Scheme 1, as a model reaction. The initial concentration of dye was 0.05 mM. The pH obtained after dissolution of the dye in deionized water was used without further adjustment. The catalyst loading was 0.5 $g \cdot L^{-1}$ in all the experiments.

Prior to the start of the reaction, the dye solutions were equilibrated in the dark for 30 minutes in contact with the TiO_2 material and the oxygen bubbles. After switching on the lamps, the evolution of the reaction was followed by colorimetric measurements ($\varepsilon_{493\,nm}$ = 23.45 $L \cdot mmol^{-1} \cdot cm^{-1}$) using a Shimadzu UV/vis spectrophotometer.

3. RESULTS AND DISCUSSION

3.1. Characterization results

The initial synthesis of the pure titania powder photocatalysts followed the original acidic procedure of O'Regan et al. [13], described above. The influence of the calcination temperature was investigated first. As shown in Figure 1, the diffraction line breadth demonstrates that the TiO_2 existed as small crystallites of anatase after calcination at 500°C but that after calcination at 600°C, these crystals grew substantially and transformed to rutile.

Table 1: Synthesis conditions, crystallinity, and photocatalytic activity in terms of the first- order kinetic constant for RO16 decolorization of powder photocatalysts.

Name	pH	Temp. (°C)	XRD Data			k_{RO} (h^{-1})
			Anatase (%)	D_{anat} (nm)	S_g† (m^2g^{-1})	
P-TiO_2-1	1.5	500	100	14	110	0.22
P-TiO_2-2	1.5	600	89	42	37	0.32
P-TiO_2-3	6.5	500	100	12	128	0.38
P-TiO_2-4	6.5	600	100	24	64	1.09

†Estimated assuming nonporous spherical particles with a density corresponding to bulk anatase.

An equivalent set of materials was then prepared following a sol-gel route at pH 6.5. According to Wang and Ying [14], neutral aqueous media lead to anatase materials that undergo neither phase transition to rutile nor significant grain growth, whereas the use of nitric acid favours the formation of rutile. The XRD patterns (Figure 1) of these pH 6.5 materials show that at both 500°C or 600°C, pure anatase materials were obtained with only traces of rutile. Table 1 summarizes the composition calculated from the areas of the 101 anatase peak ($2\theta \sim 25.3°$) and the 110 rutile peak ($2\theta \sim 27.4°$) according to the procedure of Zhang and Banfield [15]:

$$\text{Anatase (wt\%)} = \frac{0.884 \times A_{\text{anatase}}}{0.884 \times A_{\text{anatase}} + A_{\text{rutile}}}. \quad (1)$$

The average crystallite sizes were estimated from the width of signals using the Scherrer equation (Table 1). The average anatase size increased with calcination temperature, especially for materials synthesized at acidic pH, which favours the thermal transformation to rutile.

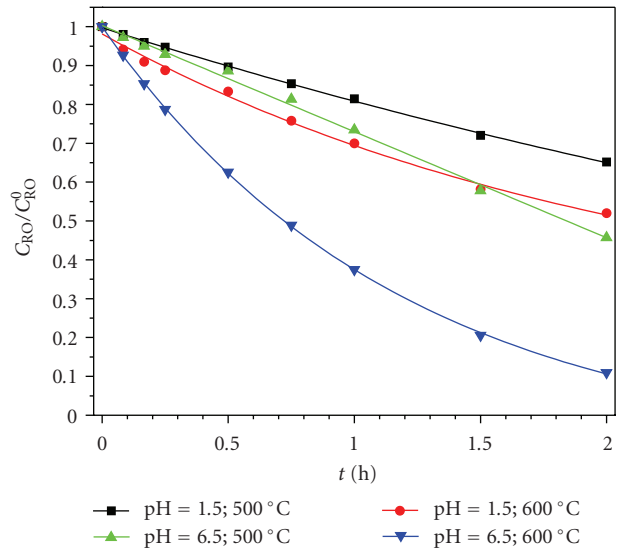

Figure 2: First-order kinetics fit of the RO16 photocatalytic decolorization.

3.2. Photocatalytic results

Figure 2 shows the photocatalytic activity of dispersions of these catalyst materials measured as the decrease with irradiation time of the absorption at 493 nm. In all cases, a pseudo-first-order kinetics model satisfactorily represents the results and the derived first-order rate constants are shown in Table 1. In both cases, an increase in the temperature of the heat treatment from 500°C to 600°C leads to a significant increase in the activity even though the surface area, estimated from the average anatase size, decreases. However, the clear and important conclusion is that titania materials synthesized via the neutral sol-gel route are more photoactive than samples prepared in acid media.

The lack of correlation between photocatalytic activity and the specific surface area suggests that the reaction rate may be more influenced by the generally assumed higher activity of anatase. Although this would be consistent with the increased activity of P-TiO_2-4 (100% anatase) relative to P-TiO_2-2 (11% rutile), it is inconsistent with the lower activity of P-TiO_2-2 relative to (100% anatase) P-TiO_2-1. We cannot exclude the possibility that since the P-TiO_2-1 was calcined at lower temperature, it may have significant amounts of amorphous TiO_2, which reduces the photocatalytic activity.

3.3. Photoelectrochemical results

The striking increase in photocatalytic activity associated with the particle preparation at pH 6.5 prompted a corresponding photoelectrochemical study on electrodes prepared by coating sol-gel TiO_2 coated onto 1 cm^2 titanium plates. Photocurrents were calculated as the difference between the current recorded in a cyclic voltammetry experiments in which the electrode was irradiated with UV light and the current recorded in the dark.

Figure 3(a) shows the influence of the pH on the photocurrent recorded in 0.1 M Na_2SO_4. As can be seen, the shape of the current voltage curve depended on the pH of the TiO_2 coating suspension and on the treatment temperature. The curve for the electrode coated with a neutral TiO_2 solution and heated at 500°C showed a progressive increase of the photocurrent with increase of the applied potential, in agreement with classical semiconductor theory. In contrast, for the electrode coated with an acidic TiO_2 sol the photocurrent seems to be independent on the voltage. This previously observed [9] behaviour is attributed to particles, which are smaller than the thickness of the depletion layer. Because of this, increasing the electric field does not increase charge separation [16]. At higher temperatures, this effect disappears,

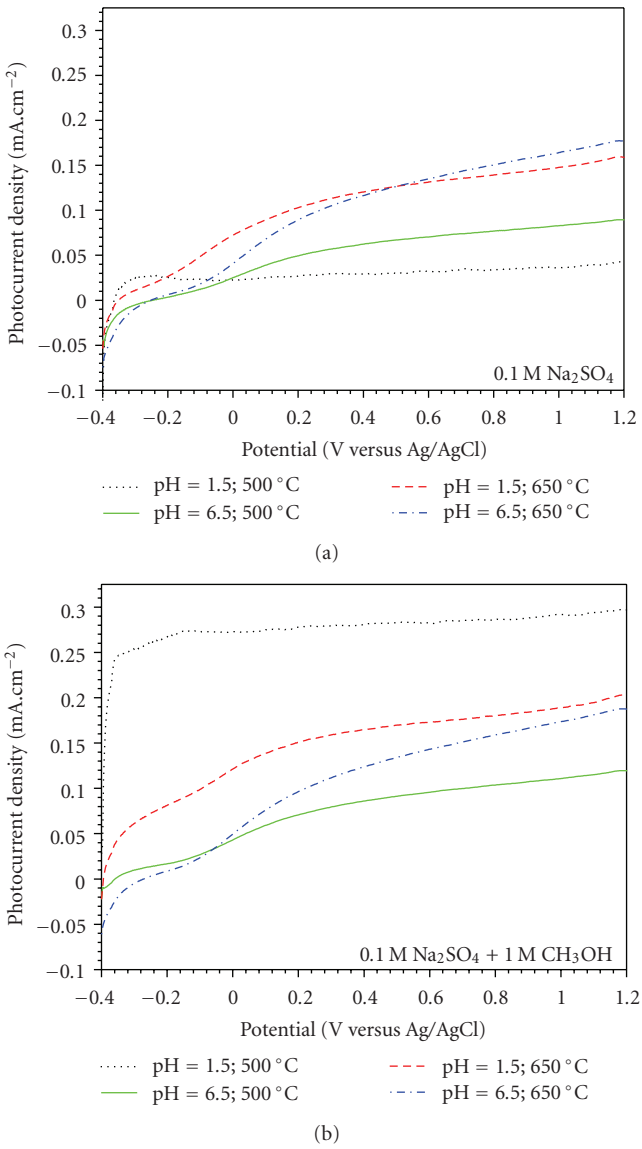

Figure 3: Influence of pH and temperature on the photocurrent density of TiO_2 electrodes in (a) 0.1 M Na_2SO_4 and (b) 0.1 M Na_2SO_4 + 1 M CH_3OH.

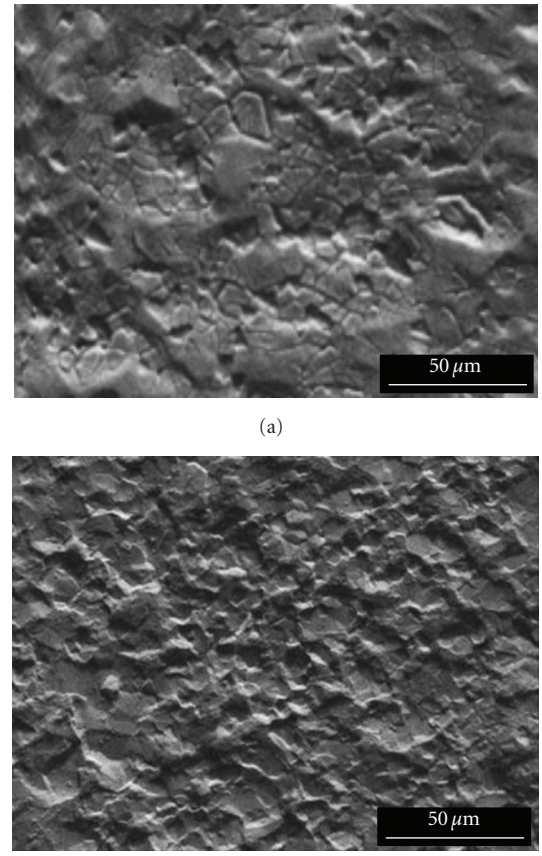

Figure 4: SEM micrographs spectra of TiO_2 electrodes calcined at 500°C: (a) pH = 1.5 and (b) pH = 6.5.

probably by growing of the titania particles, and the cyclic voltammetries of both kind of electrodes are quite similar. In all cases, the photocurrents of neutral TiO_2 electrodes at high potential values are higher than the photocurrent of acid TiO_2 electrodes at high potentials.

Figure 3(b) also displays the corresponding current voltage curves after addition of 1 M methanol to the electrolyte solution. Whereas the behaviour of the neutral TiO_2 electrodes is quite similar to that in the absence of methanol, the photocurrents recorded for the acid TiO_2 electrodes increase dramatically. This methanol enhancement has been previously reported by Christensen et al. [12] when comparing the photoelectrochemical properties of sol-gel electrodes (synthesized in acid media) with TiO_2 electrodes obtained thermally from titanium plates. Similarly, Mintsouli et al. [10] have reported a photocurrent enhancement in particulate electrodes (prepared from Degussa P25 suspensions) when adding oxalate to the electrolyte. In both cases, the organic compound is considered to scavenge photogenerated holes, decreasing charge recombination and hence increasing the photocurrent. This effect is reported to be especially marked in particulate electrodes of high roughness and titania surface area, but almost negligible for thermal electrodes [12]. The SEM micrographs, Figure 4, shows that the acid TiO_2 electrode presents a more fractured but less rough surface, whereas the neutral TiO_2 electrode calcined at 500°C consists of a continuous but rough film. At higher temperature, the two electrode types are more similar, although the neutral electrode seems to be more particulate.

Figures 5(a) and 5(b) show the influence of the heat treatment temperature on the photocurrent, measured at 1.0 V, with and without the addition of methanol for the pH 1.5 and pH 6.5 electrodes. In Na_2SO_4 (only) solution, both electrodes show a maximum photocurrent at 650°C comparable with the maximum at 600–650°C reported by Christensen et al. [17]. For the pH 6.5 electrodes, the methanol photocurrent enhancement, calculated as the difference of the two plots, is vanishingly small for all heat treatment temperatures. For the pH 1.5 electrodes, the methanol

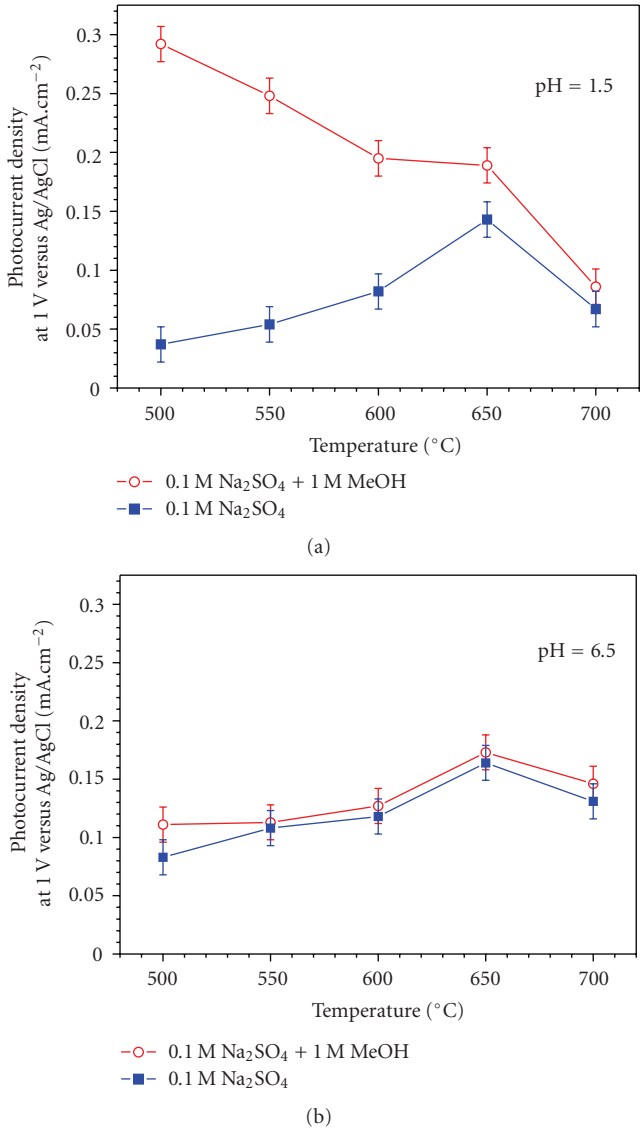

FIGURE 5: Influence of temperature on the photocurrent density of TiO_2 electrodes: (a) pH = 1.5 and (b) pH = 6.5. The error bars have been estimated from the spread of 2 independent measurements.

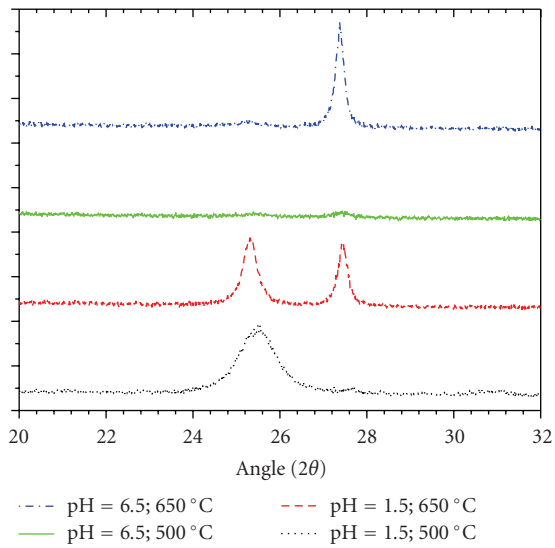

FIGURE 6: Influence of pH and temperature on the X-ray diffraction pattern of TiO_2 small electrodes.

photocurrent enhancement decreases to zero at ~700°C, which compares well with the 750°C reported in earlier work [17]. Consequently, the differences between electrodes synthesized in acid and neutral media disappear progressively when the calcination temperature is increased, probably due to the growth of the titania particles and the increase in the density of the titania film.

Figure 6 shows the X-ray diffraction patterns of the four electrodes. Acid sol-gel electrodes show the presence of anatase crystals at 500°C. Narrowing of the diffraction lines confirms the crystallite growth between 500°C and 650°C (The crystal sizes calculated for the acid pH electrodes are 10.2, 23.0, 30.9, and 68.3 nm for calcination temperatures of 500, 600, 650, and 700°C, resp.). Although the anatase peak height is little altered, the integrated intensity has reduced suggesting that anatase has transformed to rutile (A rutile phase is detected above 600°C). Remarkably, no anatase phase was detected in neutral pH TiO_2 electrodes below a treatment temperature of 700°C. However, rutile crystals were formed at lower temperatures, as was reported earlier for "thermal electrodes" prepared by heating titanium metal [17]. Therefore, these results suggest that either, unlike the pH 1.5 coating, the crystal growth of the pH 6.5 coating is controlled by the titanium substrate, or the rutile phase mainly grows directly from the oxidation of the titanium support.

Finally, the diffuse reflectance spectra of electrodes heated at 500°C are shown in Figure 7. It is immediately obvious that these spectra are unlike the "typical" spectra of TiO_2 and it is probable that they include a contribution from the underlying oxidized titanium metal. Separate studies [18] show that uncoated titanium metal is blue when heated to 500°C but grey or black when heated to 650°C. The influence of the colored substrate is likely to be increased when the particle size of the sol-gel-derived TiO_2 is small, and because it is not an efficient scatterer, it is not completely opaque. Despite these complications, the spectra show that for electrodes calcined at 500°C the peak absorption of the neutral pH electrode is ~20 nm below that of the acid electrode whose peak is near 350 nm. This blue shift could be explained by the extremely small crystallite size of the titanium dioxide particles (in agreement with the almost negligible intensity of the X-ray diffraction signals). Small particles can cause the apparent absorption maximum to shift to shorter wavelengths—as described by Mie theory [19]—and may also lead to an increased band gap in quantum-size semiconductor particles [20].

At 650°C, the increased absorption of the underlying oxidized titanium metal dominates the spectrum and its strong visible absorption means that the normally observed absorption edge is difficult to discern (therefore the 650°C spectra

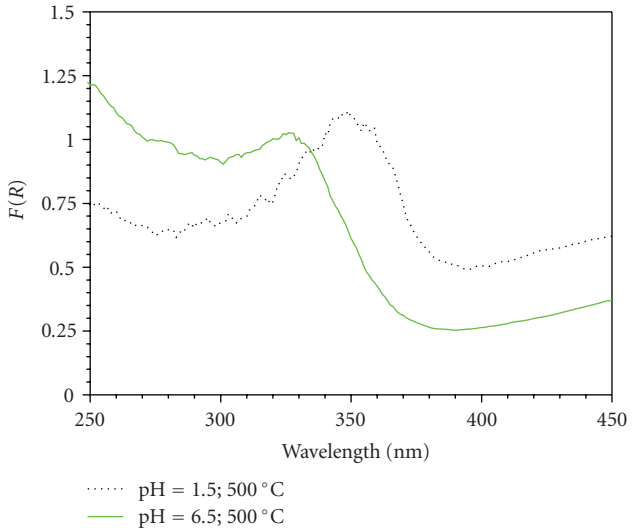

Figure 7: Influence of pH on the diffuse reflectance spectra of TiO_2 electrodes.

are not reported). However, the difference between the neutral and acid electrodes appeared to have disappeared.

Summarising, the physicochemical characterization of the materials seems to point out that the use of a neutral sol-gel route leads to titania catalysts constituted by extremely small anatase crystals of higher activity in comparison with those obtained at acidic pH values. However, despite the strong dependence of the photoelectrochemical properties of the materials on the synthesis pH, the photocurrents recorded under potentiostatic control do not correlate the activity exhibited by the materials for the decolorization of an azo dye solution.

4. CONCLUSIONS

The main conclusion of this work is the significance of the synthesis pH of sol-gel titania powders and electrodes for photocatalytic applications. In contrast with the large number of studies reporting the influence of the temperature on the physicochemical and photoelectrochemical properties of titania powders and coatings, our results indicate that pH is even more influential in controlling both the crystalline phases, and the photocatalytic activity of TiO_2 powders and photocurrents of the electrodes. However, the photocatalytic activities of the TiO_2 slurries are not proportional to the photocurrents recorded after immobilization on a conducting support. Consequently, these results indicate that the measurement of the photocurrent in an electrolyte media is not necessarily a good indicator of the photocatalytic activity of the unsupported system.

ACKNOWLEDGMENTS

Javier Marugán gratefully acknowledges the financial support of the Ministerio de Educación y Ciencia of Spain through the program Consolider-Ingenio 2010 (Project CSD2006-00044 TRAGUA) and Comunidad de Madrid through the program REMTAVARES S-0505/AMB/0395.

REFERENCES

[1] D. F. Ollis and H. Al-Ekabi, Eds., *Photocatalytic Purification and Treatment of Water and Air*, Elsevier, Amsterdam, The Netherlands, 1993.

[2] M. R. Hoffmann, S. T. Martin, W. Choi, and D. W. Bahnemann, "Environmental applications of semiconductor photocatalysis," *Chemical Reviews*, vol. 95, no. 1, pp. 69–96, 1995.

[3] A. Mills and S. Le Hunte, "An overview of semiconductor photocatalysis," *Journal of Photochemistry and Photobiology A*, vol. 108, no. 1, pp. 1–35, 1997.

[4] J.-M. Herrmann, "Heterogeneous photocatalysis: fundamentals and applications to the removal of various types of aqueous pollutants," *Catalysis Today*, vol. 53, no. 1, pp. 115–129, 1999.

[5] A. Mills and S. K. Lee, "Semiconductor photocatalysis," in *Advanced Oxidation Processes for Water and Wastewater Treatment*, S. Parsons, Ed., IWA Publishing, London, UK, 2004.

[6] J. Marugán, D. Hufschmidt, G. Sagawe, V. Selzer, and D. Bahnemann, "Optical density and photonic efficiency of silica-supported TiO_2 photocatalysts," *Water Research*, vol. 40, no. 4, pp. 833–839, 2006.

[7] L. Sun and J. R. Bolton, "Determination of the quantum yield for the photochemical generation of hydroxyl radicals in TiO_2 suspensions," *Journal of Physical Chemistry*, vol. 100, no. 10, pp. 4127–4134, 1996.

[8] T. Egerton and P. Christensen, "Photoelectrocatalysis processes," in *Advanced Oxidation Processes for Water and Wastewater Treatment*, S. Parsons, Ed., IWA Publishing, London, UK, 2004.

[9] J. C. Harper, P. Christensen, T. Egerton, T. P. Curtis, and J. Gunlazuardi, "Effect of catalyst type on the kinetics of the photoelectrochemical disinfection of water inoculated with *E. coli*," *Journal of Applied Electrochemistry*, vol. 31, no. 6, pp. 623–628, 2001.

[10] I. Mintsouli, N. Philippidis, I. Poulios, and S. Sotiropoulos, "Photoelectrochemical characterisation of thermal and particulate titanium dioxide electrodes," *Journal of Applied Electrochemistry*, vol. 36, no. 4, pp. 463–474, 2006.

[11] J. Aguado, R. van Grieken, M.-J. López-Muñoz, and J. Marugán, "A comprehensive study of the synthesis, characterization and activity of TiO_2 and mixed TiO_2/SiO_2 photocatalysts," *Applied Catalysis A*, vol. 312, no. 1-2, pp. 202–212, 2006.

[12] P. Christensen, T. P. Curtis, T. Egerton, S. A. M. Kosa, and J. R. Tinlin, "Photoelectrocatalytic and photocatalytic disinfection of *E. coli* suspensions by titanium dioxide," *Applied Catalysis B*, vol. 41, no. 4, pp. 371–386, 2003.

[13] B. O'Regan, J. Moser, M. Anderson, and M. Grätzel, "Vectorial electron injection into transparent semiconductor membranes and electric field effects on the dynamics of light-induced charge separation," *Journal of Physical Chemistry*, vol. 94, no. 24, pp. 8720–8726, 1990.

[14] C.-C. Wang and J. Y. Ying, "Sol-gel synthesis and hydrothermal processing of anatase and rutile titania nanocrystals," *Chemistry of Materials*, vol. 11, no. 11, pp. 3113–3120, 1999.

[15] H. Zhang and J. F. Banfield, "Understanding polymorphic phase transformation behaviour during growth of nanocrystalline aggregates: insights from TiO_2," *Journal of Physical Chemistry B*, vol. 104, no. 15, pp. 3481–3487, 2000.

[16] K. Vinodgopal, U. Stafford, K. A. Gray, and P. V. Kamat, "Electrochemically assisted photocatalysis. 2. The role of oxygen and reaction intermediates in the degradation of 4-chlorophenol on immobilized TiO_2 particulate films," *Journal of Physical Chemistry*, vol. 98, no. 27, pp. 6797–6803, 1994.

[17] P. Christensen, T. Egerton, S. A. M. Kosa, J. R. Tinlin, and K. Scott, "The photoelectrocatalytic oxidation of aqueous nitrophenol using a novel reactor," *Journal of Applied Electrochemistry*, vol. 35, no. 7-8, pp. 683–692, 2005.

[18] J. R. Tinlin, "Photoelectrocatalysis by TiO_2 electrodes," University of Newcastle upon Tyne, Newcastle upon Tyne, UK, 2002.

[19] C. F. Bohren and D. R. Huffman, *Absorption and Scattering of Light by Small Particles*, John Wiley & Sons, New York, NY, USA, 1983.

[20] Z. Zhang, C. C. Wang, R. Zakaria, and J. Y. Ying, "Role of particle size in nanocrystalline TiO_2-based photocatalysts," *Journal of Physical Chemistry B*, vol. 102, no. 52, pp. 10871–10878, 1998.

Hindawi Publishing Corporation
International Journal of Photoenergy
Volume 2008, Article ID 426872, 6 pages
doi:10.1155/2008/426872

Research Article

Synthesis of Visible-Light-Activated Yellow Amorphous TiO_2 Photocatalyst

Chamnan Randorn,[1] John T. S. Irvine,[1] and Peter Robertson[2]

[1] *School of Chemistry, University of St. Andrews, St. Andrews, Fife KY16 9ST, UK*
[2] *Centre for Research in Energy and the Environment, School of Engineering, The Robert Gordon University, Schoolhill, Aberdeen AB10 1FR, UK*

Correspondence should be addressed to John T. S. Irvine, jtsi@st-and.ac.uk

Received 10 March 2008; Accepted 22 April 2008

Recommended by Russell. Howe

Visible-light-activated yellow amorphous TiO_2 (yam-TiO_2) was synthesised by a simple and organic-free precipitation method. TiN, an alternative precursor for TiO_2 preparation, was dissolved in hydrogen peroxide under acidic condition (pH∼1) adjusted by nitric acid. The yellow precipitate was obtained after adjusting pH of the resultant red brown solution to 2 with NH_4OH. The BET surface area of this sample was 261 m^2/g. The visible light photoactivity was evaluated on the basis of the photobleaching of methylene blue (MB) in an aqueous solution by using a 250 W metal halide bulb equipped with UV cutoff filter ($\lambda > 420$ nm) under aerobic conditions. Yam-TiO_2 exhibits an interesting property of being both surface adsorbent and photoactive under visible light. It was assigned to the η^2-peroxide, an active intermediate form of the addition of H_2O_2 into crystallined TiO_2 photocatalyst. It can be concluded that an active intermediate form of titanium peroxo species in photocatalytic process can be synthesised and used as a visible-light-driven photocatalyst.

1. INTRODUCTION

Titaniumdioxide(TiO_2)has been the prevailing material in the fields of photocatalysis and solar energy conversion due to being chemically and biologically inert and environmentally friendly. Although TiO_2 is now used in various practical applications, only a small UV fraction of solar light can be utilised because of its large band gap of 3.2 eV. The development of a titania-related photocatalyst that shows a high level of activity under visible light would therefore be a major advance. Yellow TiO_2 prepared by nitrogen doping has been regarded as a visible-light-sensitive photocatalyst [1–4] as well as Cr or V doped TiO_2 [5, 6]. Additionally, metal ion doped $SrTiO_3$ [7–9], some metal sulfides such as $AgGaS_2$ and $AgInZn_7S_9$ [10], $(Ga_{1-y}Zn_y)(N_{1-x}O_x)$ [11], and $Sm_2Ti_2O_7$ [12] have been reported as visible-light-driven photocatalysts. There may be some disadvantages of doped materials, for instance, low surface area because of using high temperature, the requirement of the expensive chemicals and synthetic methods, and an increase in carrier recombination.

Amorphous TiO_2 is of interest for photocatalysis because of its high surface area and high adsorption. Moreover, simple synthesis with elimination of the calcination step would mean lower costs for chemicals and energy consumption. There have been only a few works that studied or mentioned amorphous TiO_2. Among them, it was found that commercial amorphous TiO_2 had negligible photoactivity because it contains high concentrations of defects which cause rapid e^--h^+ recombination [13]. However, synthetic amorphous TiO_2 has been recently shown to exhibit significantly photoactivity rates in aqueous methanol solutions under full solar spectrum (200 to >1000 nm) using a 400 W Xe arc lamp [14].

Hydrogen peroxide (H_2O_2) has been reported as an important factor in the photocatalytic process because it has occurred as an intermediate in the mechanism of the photocatalytic process using TiO_2 as photocatalysts, and it has been reported that the reactivity can be accelerated by the addition of H_2O_2 [15–17]. Moreover, titanium-peroxo species were found to be the active species in the titanium silicalite-1 (TS-1)/H_2O_2/H_2O system for partial hydrocarbon oxidation [18, 19]. In general, titanium-peroxo species or aqueous peroxotitanate are yellow or yellow-green depending on pH. There have been some works that used

titanium peroxo complex as a starting material for TiO_2 preparation [20–22].

As mentioned in the above discussion, H_2O_2 is important in photocatalysis at TiO_2, amorphous TiO_2 offers some enhancement of activity and noting the yellow colour of the catalytically active titanium-peroxo species in the TS-1/H_2O_2/H_2O system, it would be interesting to see if yellow amorphous titanium-peroxo species can act as a photocatalyst under visible light. In this work, therefore, we investigate the visible-light-driven photoactivity of yellow amorphous TiO_2 (hereinafter referred to as "yam-TiO_2") prepared by a peroxide-based route, using titanium nitride (TiN) as a precursor.

2. EXPERIMENTAL

2.1. Materials

Yam-TiO_2 wassynthesised by a peroxide-based route using TiN as precursor. 50 mL of 30% H_2O_2 (Fisher Scientific, Leicestershire, UK) was added to 1.0 g of TiN (Alfa Aesar, Lancashire, UK) under acidic condition (pH $\leq$ 1) adjusted by HNO_3 acid solution. After aging at room temperature-without any stirring for 24 hours, a clear red-brown solution was obtained. The obtained precursor solution was stable for several days under ambient atmosphere. Yellow precipitate is formed from this solution after adjusting the pH of the solution to 2 by slowly adding ammonia solution with the constant stirring. The precipitate was filtered and washed with distilled water several times. It was then dried at room temperature. The dried powder was also calcined at a constant heating rate of 5°C/min at various temperatures and held at these temperatures for 2 hours.

XRD data were collected with a Stoe Stadi-P Transmission X-ray diffractometer, using Cu $K_{\alpha 1}$ radiation in the range 2θ = 20–80°. The BET surface area measurement and pore analysis were carried out by nitrogen adsorption with use of Micromeritics ASAP 2020 V3.00 H surface area analyser. The measurement was carried out at liquid nitrogen temperature after degassing the powder sample at 120°C. TEM imaging was obtained using a JEOL-JEM 2011 electron microscope. Diffuse reflectance spectroscopy was carried out with a Perkin Elmer Lambda35 UV/Vis spectrometer using $BaSO_4$ as a reference.

2.2. Evaluation of photocatalytic activity

Visible light activity was evaluated on the basis of the decomposition of methylene blue (MB) in an aqueous solution. The sample powder was suspended in 200 mL of an 1×10^{-4} M MB solution by air bubbling. This mixture was first suspended in the dark for 2 hours to reach the adsorption equilibrium before irradiation with a high intensity discharge 250 W iron doped metal halide UV bulb (UV Light Technology Ltd., Bermingham, UK) equipped with UV cutoff filter, $\lambda \geq 420$ nm (Borosilicate Coated Glass HM07, UQG(optic)Ltd., Cambridge UK). The mixture temperature was controlled at about 25°C using a water bath for infrared radiation and lamp heating removal. After irradiation, 2 mL of the mixture was collected and centrifuged at the irradiation time intervals (hourly). The photoactivity was examinedby monitoring the reduction of the absorbance at 665 nm. The spectrophotometric measurements were carried out using Perkin Elmer Lambda35 UV/Vis spectrometer. A ten-fold dilution was used for the high absorbance solutions.

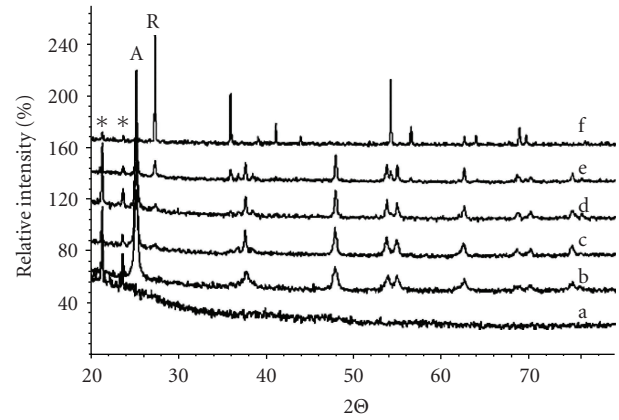

Figure 1: XRD patterns of as-prepared yam-TiO_2 (a) and after calcined at temperatures of (b) 400°C, (c) 800°C, (d) 850°C, (e) 900°C, (f) 1100°C (∗: Vaseline specific peaks, A: anatase, R: rutile).

3. RESULTS AND DISCUSSION

3.1. Characterisation

The XRD pattern of the as-prepared powder confirmed the amorphous structure of yam-TiO_2 as no diffraction peaks can be observed, Figure 1. Yam-TiO_2 was quite stable under air atmosphere (the sample used throughout this work was kept for several months in the aerobic vial). However, colour and phase transformation of yellow amorphous to white anatase/rutile occurred on heat treatment. Anatase was presented after calcination at 400°C and remained as a major phase until 900°C. This indicated that a high temperature stable anatase phase can be produced by this method. Phase transformation from anatase to rutile can be observed at about 800–850°C which was higher than TiO_2 prepared by conventional methods.

Furthermore, it was found that the particle sizes of TiO_2 after calcination at 600 and 900°C calculated by Scherrer equation were 31 and 51 nm, respectively. The obtained phase transformation temperature and particle size were consistent with the previous work that synthesised TiO_2 by peroxide-based route and using H_2TiO_3 as precursor [20]. However, the stability of anatase phase in this work was higher than TiO_2 synthesised by the peroxide-based route using $TiCl_3$ as precursor [21]. The peroxide-based route, therefore, is interesting for TiO_2 preparation because of the high temperature anatase-rutile phase transformation; however, it depends on precursor and synthesis condition. TiN is interesting to be used as an alternative precursor in a peroxide-based route because of its air and moisture stability, organic and chloride ion-free route, simplicity, and low cost.

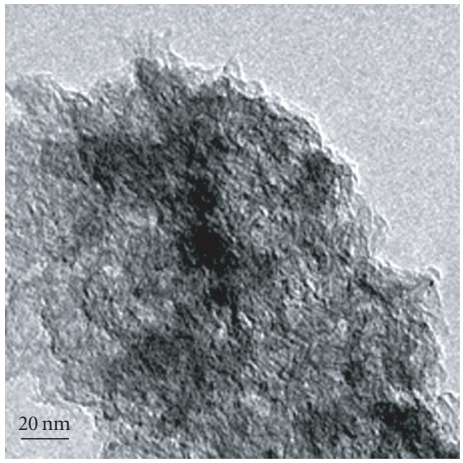

Figure 2: TEM image of as-prepared yam-TiO_2.

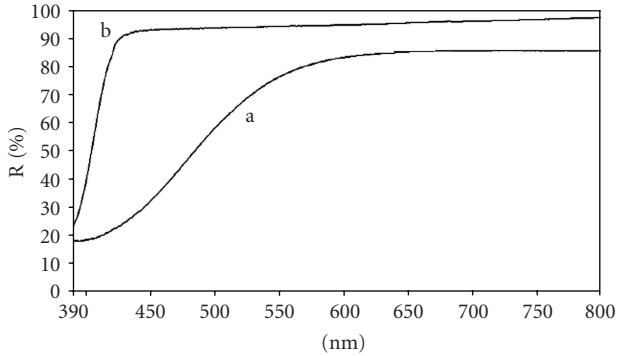

Figure 3: The UV-Vis diffuse reflectance of (a) yam-TiO_2, (b) commercial rutile TiO_2.

Accordingto our focus on evaluation of the visible light photoactivity of yellow amorphous TiO_2, TEM, BET and diffuse reflectance were only examined with the as-prepared powder. Figure 2 shows the TEM image of the as-prepared powder. The ultrafine particles with amorphous structure can be seen. As a result, a high BET surface area of 261 m^2/g was obtained. The diffuse reflectance spectrum shows the red shift of the absorption edge into the visible region (Figure 3(a)) compared with commercial rutile TiO_2 (TIOXIDE) (Figure 3(b)).

Yam-TiO_2 is attributed to the η^2-peroxide (η^2-TiOOH) because of the similar red shift and that yam-TiO_2 transformed to white powder on heating similar to the η^2-titanium peroxospecies in the TS-1/H_2O_2/H_2O system reported by Bonino et al. [18]. Lin and Frei [19] found that the η^2-peroxide species obtained upon loading H_2O_2 into TS-1 was photodissociated efficiently under irradiation with visible or near UV light. Moreover, η^2-peroxide was assigned to the adsorption structure formed by the addition of H_2O_2 on the surface of rutile TiO_2. This structure was preferable to produce hydroxyl radical that accelerates the photoactivity [17].

3.2. Visible light photocatalytic activity

The photobleaching of MB has been widely studied in heterogeneous photocatalysis. However, there are some concerns about the bleaching of MB due to the photoreduction to colourless form and photoabsorption of MB [23–25]. There are two main forms of MB, the blue colour of oxidised form (MB) and the colourless reduced form (leuco form, LMB). MB can be photoreduced to LMB by TiO_2 under UV light under anaerobic condition and in the presence of a sacrificial electron acceptor (SED). It was found that MB itself can act as an SED. However, this process is reversed on the addition of O_2 to the anaerobic system. Although LMB is readily oxidised back to MB by oxygen, this reaction depends on pH. The rate increases with pH, LMB is moderately stable under acidic condition but reacts rapidly with air under basic condition [23]:

$$\begin{aligned} \mathrm{MB} + \mathrm{SED} &\xrightarrow{\mathrm{TiO_2+UV}} \mathrm{LMB} + \mathrm{SED}^{2+}; \\ 2\mathrm{LMB} + \mathrm{O_2} &\longrightarrow 2\mathrm{MB} + 2\mathrm{H_2O}. \end{aligned} \tag{1}$$

As continuous air bubbling of a neutral solution was utilised in this work and no reducing agent was added to the system, it is likely that the dominant bleaching process is the photomineralisation of MB rather than the reductive formation of LMB. This system, MB/TiO_2/air-saturated water system, has widely been utilised for the demonstration of semiconductor photocatalysis, as reviewed by Mills and Wang [23]. It is possible or even probable that partial rather than complete mineralisation into CO_2, NH_4^+, NO_3^-, and SO_4^{2} is occurring as the main observable in bleaching MB.

The photoabsorption of MB can be an issue for visible-light-driven photocatalyst investigation because MB can absorb visible light, especially, in the range 600–700 nm. Yan et al. [25] concluded that MB was not an appropriate substrate for a visible-light photocatalytic activity test particularly in the range of 540–680 nm irradiation. However, the most important and intense emitting wavelength of the metal halide lamp used in this work is in the range of about 200–580 nm [26]. After equipping with a UV cutoff filter, the emitting wavelength is in the range of 420–580, which has little overlap with the absorption of MB as shown in Figure 4.

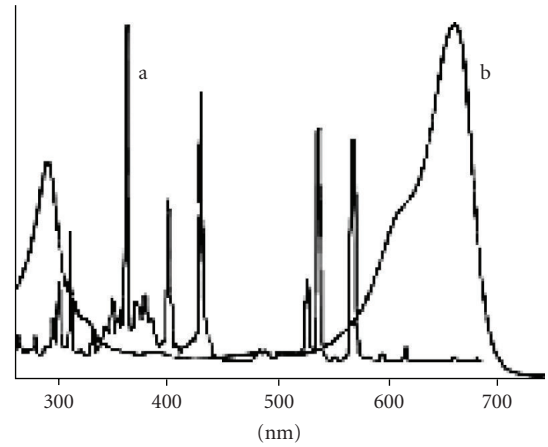

Figure 4: The emitting wavelength of metal halide lamp (a) and UV-Vis absorption spectrum of MB (b).

As a result, the photoabsorption of MB should not significantly effect the determination of visible light photocatalytic activity test in this work.

Figure 5 shows the photocatalytic degradation of MB comparing between amorphous TiO_2 prepared in acidic condition (yam-TiO_2) and in basic condition (labeled byam-TiO_2), including blanktest (2×10^{-5} M MB). It was found that 10% bleaching of MB was shown after visible light irradiation of only MB for 5 hours (Figure 5(a)), whereas slightly higher, 15% photobleaching of MB, was obtained by using 0.5 g/L byam-TiO_2 as photocatalyst (Figure 5(b)). However, the latter amount was obtained after 45% of 1×10^{-4} M MB was adsorbed, that indicated that the initial concentration of MB before photobleaching was about 5.5×10^{-5} M. Comparision with using 0.5 g/L yam-TiO_2, about 97% adsorption and 2% photocatalytic activity was measured (Figure 5(c)). It can be concluded that the adsorption capacity of yam-TiO_2 was significantly higher than byam-TiO_2; however, the extent of adsorption must hinder the hetereogeneous photoactivity. Therefore, a decreased amount of yam-TiO_2 to 0.2 g/L was performed for photoactivity comparison (Figure 5(d)). It can be seen that about 46% photobleaching of MB after adsorption was obtained, which was considerably higher than using byam-TiO_2 in spite of using less amount and higher concentration remained after adsorption. Moreover, only 9% photobleaching was observed for 0.5 g/L of Degussa P25 in 1×10^{-5} MB under visible light for 2 hours (compared to 93% under UV for 1 hour) showing that the yam-TiO_2 was much more effective, ~40% under visible light for 2 hours. An important point to note is that the adsorbed MB seemed much less intense in colour and indeed the colour had changed to pale purple/violet. This could indicate an oxidative adsorption process in the dark with the oxidised form, $MB^{\bullet+}$ being formed and adsorbed onto the yam-TiO_2; however, confirmation requires further study.

The irreversibility of the photobleaching process on continuous air bubbling for 24 hours in the dark after complete decolourisation of MB and the disappearance of the bands associated with MB (294 nm and 665 nm) with no appearance of band associated with LMB (256 nm) [24] as shown in Figure 6. were observed, further confirming that photoreduction of MB to LMB was not the dominant process.

These results show that yam-TiO_2 can act as a visible-light-driven photocatalyst better than byam-TiO_2, in parallel with a red shift of the absorption edge into the visible region as shown in Figure 7. However, an increase in visible absorption edge does not guarantee consistency in visible light photoactivity, the recombination and surface area are also important factors.

Recyclability and stability of photocatalyst are important factors for any practical applications. Therefore, we have attempted to investigate cyclability and stability. In general, the photoactivity of crystalline TiO_2 is observed by monitoring the degradation of MB in an aqueous solution, and adsorbed MB is not an issue probably due to small amount of MB that was adsorbed on crystallined TiO_2. The recyclability of crystallined TiO_2 normally performed by elimination of adsorbed MB on TiO_2 by oxidation

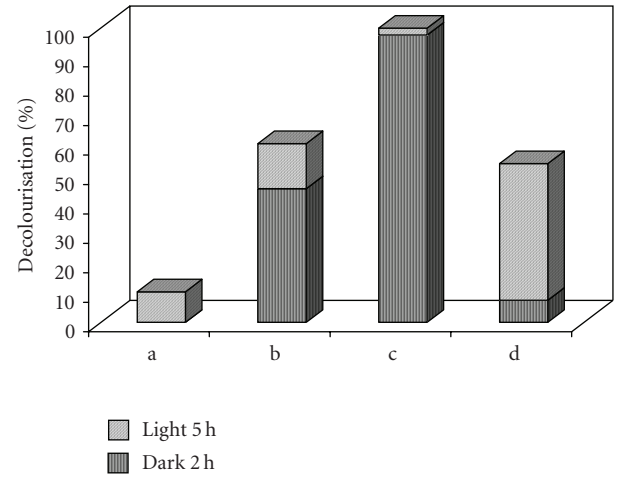

Figure 5: % decolourisation of MB under the condition of dark 2 hours and light 5 hours of (a) MB, (b) MB + 0.5 g/L byam-TiO_2, (c) MB + 0.5 g/L yam-TiO_2, (d) MB + 0.2 g/L yam-TiO_2.

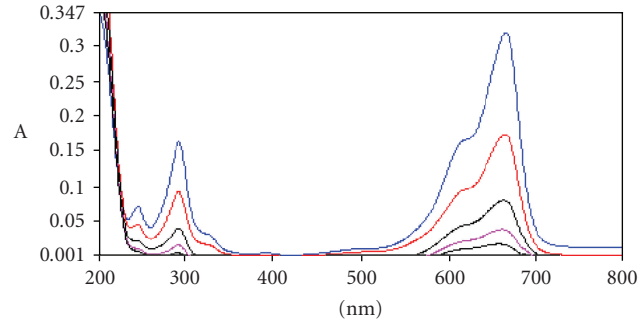

Figure 6: UV-Vis absorption spectra of MB.

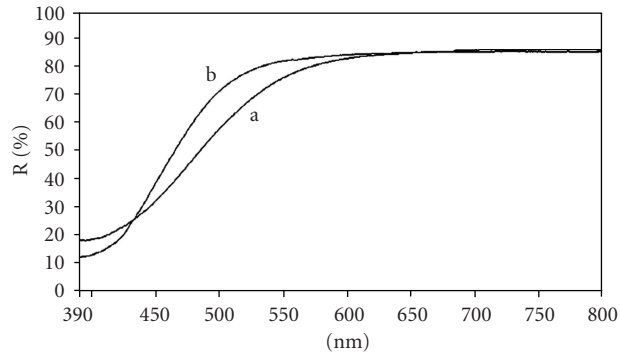

Figure 7: The UV-Vis diffuse reflectance of (a) yam-TiO_2, (b) byam-TiO_2.

at temperatures higher than about 200°C, which is the decomposition temperature of MB. However, removal of adsorbed MB by calcination cannot be used in the case of amorphous form because crystallisation will be induced.

As a result, the cyclability of yam-TiO_2 was measured by two different methods, with and without removal of

adsorbed MB. The first way, to completely remove adsorbed MB on the surface by using photoactivity itself until the original colour of yam-TiO_2 was recovered. Due to a large amount of MB being adsorbed on the surface, 48 hours UV irradiation was used for adsorbed MB removal, after colourless solution was obtained by visible light photoactivity test, in order to reduce the duration of adsorbed MB removal and to evaluate the stability of yam-TiO_2 under UV light simultaneously. Figure 8 shows the recyclability by using UV irradiation for adsorbed MB removal. The 0.5 g/L ratio of catalyst to volume of MB was chosen because of the incomplete MB adsorption, hence, the visible-light photoactivity can be monitored, and a quantity of catalyst will be sufficient for removal of the high amount of adsorbed MB in 48 hours. About 97% adsorption and 2% photoactivity in 5 hours were obtained in the preliminary photoactivity test (Figure 8(a)). After the mixture was irradiated with UV light for 48 hours, the violet powder of visible light irradiated/adsorbed MB was changed to yellow powder as the original colour with a small amount of violet specks. Some violet specks indicated incomplete removal of adsorbed MB. Thereafter, the colourless aqueous solution was removed from the mixture by rinsing and the remaining powder left to dry at room temperature.

The first reuse was performed by readding 200 mL of 1×10^{-4} M MB. A slight decrease of adsorption and photoactivity was obtained for the first and second recycles (Figure 8(b), (c)). A small decrease of adsorption capacity and photoactivity presumably caused by incomplete adsorbed MB removal and decrease of efficiency or stability of amorphous structure after prolonged UV irradiation, which the colour changing from yellow to pale yellow can be observed by the naked eye (XRD data showed that it remained amorphous structure). However, if considering only photoactivity by using MB concentration after adsorption, about 2×10^{-5} M estimated from the percentage of bleaching, as an initial concentration, about 80% bleaching of MB under visible light irradiation can be reached in 5 hours both in the first and second recycles (Figure 8(d), (e)).

The second way of recyclability testing was performed by readding 200 mL 1×10^{-4} M MB without removal of adsorbed MB. The results are shown in Figure 9. The adsorption capacity significantly decreased in the first and second reuses as expected, 75% and 22%, respectively (Figure 9(b), (c)), due to MB was adsorbed 97% of 1×10^{-4} M MB in the preliminary photoactivity test before recycling (Figure 9(a)). The photobleaching of MB in the first reuse, including adsorption and photoactivity, was 85% in 4 hours and 99% in 24 hours (Figure 9(b)), while 51% and 95%, respectively, in the second reuse (Figure 9(c)). However, considering only the photoactivity, the percentage of bleaching of MB under visible light irradiation can be about 40% in 5 hours and more than 90% in 24 hours both in the first and second recycles (Figure 9(d), (e)). These results show the reusability of yam-TiO_2.

As mentioned above about the gradual colour changing of yam-TiO_2 from yellow to pale yellow after irradiation, it was found that it remained pale yellow and can be a visible-light-driven photocatalyst even on prolonged irradiation, although the reaction rate decreased. The color change probably due to some η^2-peroxide being converted to a hydroxide form upon photo irradiation [17, 19]. The intense yellow can be recovered after further addition of H_2O_2 as well known for crystalline TiO_2. For this reason, yam-TiO_2 can be reused several times with addition of H_2O_2.

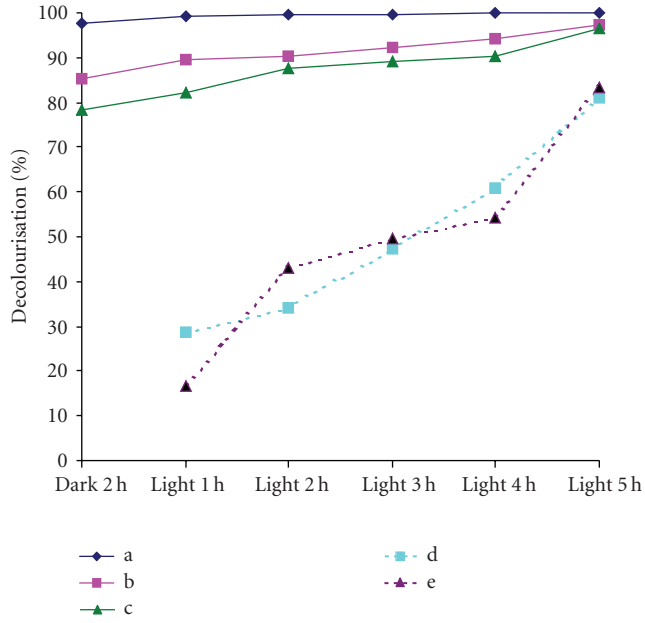

Figure 8: Recyclability with removal of adsorbed MB (a) MB + 0.5 g/L yam-TiO_2, (b) 1st reuse, (c) 2nd reuse, (d) only photoactivity of 1st reuse, (e) only photoactivity of 2nd reuse.

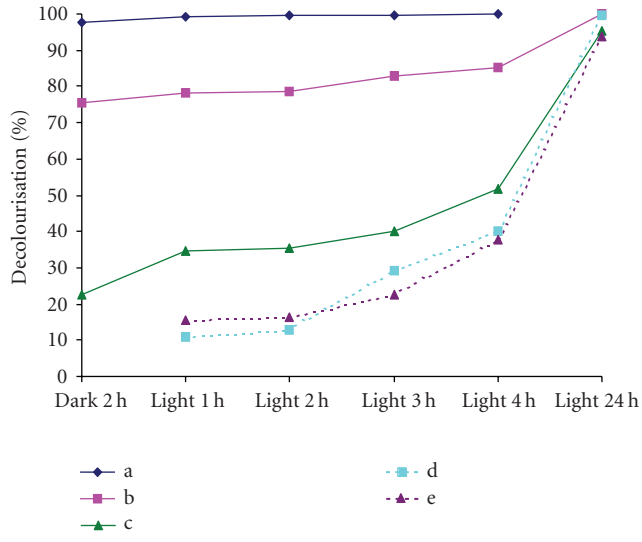

Figure 9: Recyclability without removal of adsorbed MB (a) MB + 0.5 g/L yam-TiO_2, (b) 1st reuse, (c) 2nd reuse, (d) only photoactivity of 1st reuse, (e) only photoactivity of 2nd reuse.

4. CONCLUSION

An active intermediate form of an addition of H_2O_2 into crystallined TiO_2 photocatalyst can be synthesised by peroxide-based route. It can be used as a visible-light-driven photocatalyst itself with the high surface area of amorphous form.

ACKNOWLEDGMENT

The authors would like to thank the Royal Thai Government for Chamnan Randorn's scholarship and EPSRC.

REFERENCES

[1] T. Sano, N. Negishi, K. Koike, K. Takeuchi, and S. Matsuzawa, "Preparation of a visible light-responsive photocatalyst from a complex of Ti^{4+} with a nitrogen-containing ligand," *Journal of Materials Chemistry*, vol. 14, no. 3, pp. 380–384, 2004.

[2] T. Ihara, M. Miyoshi, Y. Iriyama, O. Matsumoto, and S. Sugihara, "Visible-light-active titanium oxide photocatalyst realized by an oxygen-deficient structure and by nitrogen doping," *Applied Catalysis B*, vol. 42, no. 4, pp. 403–409, 2003.

[3] C. Shifu, L. Xuqiang, L. Yunzhang, and C. Gengyu, "The preparation of nitrogen-doped $TiO_{2-x}N_x$ photocatalyst coated on hollow glass microbeads," *Applied Surface Science*, vol. 253, no. 6, pp. 3077–3082, 2007.

[4] T. Matsumoto, N. Iyi, Y. Kaneko, et al., "High visible-light photocatalytic activity of nitrogen-doped titania prepared from layered titania/isostearate nanocomposite," *Catalysis Today*, vol. 120, no. 2, pp. 226–232, 2007.

[5] J. C.-S. Wu and C.-H. Chen, "A visible-light response vanadium-doped titania nanocatalyst by sol-gel method," *Journal of Photochemistry and Photobiology A*, vol. 163, no. 3, pp. 509–515, 2004.

[6] H. Kato and A. Kudo, "Visible-light-response and photocatalytic activities of TiO_2 and $SrTiO_3$ photocatalysts codoped with antimony and chromium," *Journal of Physical Chemistry B*, vol. 106, no. 19, pp. 5029–5034, 2002.

[7] R. Konta, T. Ishii, H. Kato, and A. Kudo, "Photocatalytic activities of noble metal ion doped $SrTiO_3$ under visible light irradiation," *Journal of Physical Chemistry B*, vol. 108, no. 26, pp. 8992–8995, 2004.

[8] S. Otsuka-Yao-Matsuo and M. Ueda, "Visible light-induced photobleaching of methylene blue aqueous solution using $(Sr_{1-x}La_x)TiO_{3+\delta}-TiO_2$ composite powder," *Journal of Photochemistry and Photobiology A*, vol. 168, no. 1-2, pp. 1–6, 2004.

[9] S. Otsuka-Yao-Matsuo, T. Omata, and M. Yoshimura, "Photocatalytic behavior of cerium titanates, $CeTiO_4$ and $CeTi_2O_6$ and their composite powders with $SrTiO_3$," *Journal of Alloys and Compounds*, vol. 376, no. 1-2, pp. 262–267, 2004.

[10] A. Kudo, "Development of photocatalyst materials for water splitting," *International Journal of Hydrogen Energy*, vol. 31, no. 2, pp. 197–202, 2006.

[11] M. Yashima, K. Maeda, K. Teramura, T. Takata, and K. Domen, "Crystal structure and optical properties of $(Ga_{1-x}Zn_x)(N_{1-x}O_x)$ oxynitride photocatalyst ($x = 0.13$)," *Chemical Physics Letters*, vol. 416, no. 4–6, pp. 225–228, 2005.

[12] M. Uno, A. Kosuga, M. Okui, K. Horisaka, and S. Yamanaka, "Photoelectrochemical study of lanthanide titanium oxides, $Ln_2Ti_2O_7$ (Ln = La, Sm, and Gd)," *Journal of Alloys and Compounds*, vol. 400, no. 1-2, pp. 270–275, 2005.

[13] B. Ohtani, Y. Ogawa, and S. Nishimoto, "Photocatalytic activity of amorphous-anatase mixture of titanium(IV) oxide particles suspended in aqueous solutions," *Journal of Physical Chemistry B*, vol. 101, no. 19, pp. 3746–3752, 1997.

[14] Z. Zhang and P. A. Maggard, "Investigation of photocatalytically-active hydrated forms of amorphous titania, $TiO_2 \cdot nH_2O$," *Journal of Photochemistry and Photobiology A*, vol. 186, no. 1, pp. 8–13, 2007.

[15] M. R. Hoffmann, S. T. Martin, W. Choi, and D. W. Bahnemann, "Environmental applications of semiconductor photocatalysis," *Chemical Reviews*, vol. 95, no. 1, pp. 69–96, 1995.

[16] A. Houas, H. Lachheb, M. Ksibi, E. Elaloui, C. Guillard, and J.-M. Herrmann, "Photocatalytic degradation pathway of methylene blue in water," *Applied Catalysis B*, vol. 31, no. 2, pp. 145–157, 2001.

[17] T. Hirakawa, K. Yawata, and Y. Nosaka, "Photocatalytic reactivity for $O_2^{\cdot-}$ and $OH^{\cdot}$ radical formation in anatase and rutile TiO_2 suspension as the effect of H_2O_2 addition," *Applied Catalysis A*, vol. 325, no. 1, pp. 105–111, 2007.

[18] F. Bonino, A. Damin, G. Ricchiardi, et al., "Ti-peroxo species in the TS-1/H_2O_2/H_2O system," *Journal of Physical Chemistry B*, vol. 108, no. 11, pp. 3573–3583, 2004.

[19] W. Lin and H. Frei, "Photochemical and FT-IR probing of the active site of hydrogen peroxide in Ti silicalite sieve," *Journal of the American Chemical Society*, vol. 124, no. 31, pp. 9292–9298, 2002.

[20] Y. Gao, Y. Masuda, W.-S. Seo, H. Ohta, and K. Koumoto, "TiO_2 nanoparticles prepared using an aqueous peroxotitanate solution," *Ceramics International*, vol. 30, no. 7, pp. 1365–1368, 2004.

[21] K. Melghit, S. S. Al-Rabaniah, and I. Al-Amri, "Low temperature preparation and characterization of nanospherical anatase TiO_2 and its photocatalytic activity on Congo red degradation under sunlight," *Ceramics International*, vol. 34, no. 3, pp. 479–483, 2008.

[22] E. Kanezaki, T. Sakamoto, A. Ookubo, and K. Ooi, "Solid-state chemistry of thermally induced yellow colouring in synthetic hydrous titanium oxide from $TiCl_3$," *Journal of the Chemical Society, Faraday Transactions*, vol. 88, no. 24, pp. 3583–3586, 1992.

[23] A. Mills and J. Wang, "Photobleaching of methylene blue sensitised by TiO_2: an ambiguous system?" *Journal of Photochemistry and Photobiology A*, vol. 127, no. 1–3, pp. 123–134, 1999.

[24] S.-K. Lee and A. Mills, "Novel photochemistry of *leuco*-Methylene blue," *Chemical Communications*, no. 18, pp. 2366–2367, 2003.

[25] X. Yan, T. Ohno, K. Nishijima, R. Abe, and B. Ohtani, "Is methylene blue an appropriate substrate for a photocatalytic activity test? A study with visible-light responsive titania," *Chemical Physics Letters*, vol. 429, no. 4–6, pp. 606–610, 2006.

[26] M. Cristea and B. Lafitte, "On the emitted spectrum changing in metal-halide lamps," *Journal of Optoelectronics and Advanced Materials*, vol. 6, no. 1, pp. 87–94, 2004.

Hindawi Publishing Corporation
International Journal of Photoenergy
Volume 2008, Article ID 739864, 7 pages
doi:10.1155/2008/739864

Research Article

Photoelectrochemical Characterization of Sprayed α-Fe_2O_3 Thin Films: Influence of Si Doping and SnO_2 Interfacial Layer

Yongqi Liang, Cristina S. Enache, and Roel van de Krol

Department DelftChemTech/Materials for Energy Conversion and Storage, Faculty of Applied Sciences, Delft University of Technology, P.O. Box 5045, 2600 GA Delft, The Netherlands

Correspondence should be addressed to Yongqi Liang, y.liang@tudelft.nl

Received 24 July 2007; Accepted 20 December 2007

Recommended by Russell Howe

α-Fe_2O_3 thin film photoanodes for solar water splitting were prepared by spray pyrolysis of $Fe(AcAc)_3$. The donor density in the Fe_2O_3 films could be tuned between 10^{17}–10^{20} cm^{-3} by doping with silicon. By depositing a 5 nm SnO_2 interfacial layer between the Fe_2O_3 films and the transparent conducting substrates, both the reproducibility and the photocurrent can be enhanced. The effects of Si doping and the presence of the SnO_2 interfacial layer were systematically studied. The highest photoresponse is obtained for Fe_2O_3 doped with 0.2% Si, resulting in a photocurrent of 0.37 mA/cm^2 at 1.23 V_{RHE} in a 1.0 M KOH solution under 80 mW/cm^2 AM1.5 illumination.

1. INTRODUCTION

Not long after the first report of stable photoelectrochemical O_2 evolution on single crystalline TiO_2 [1], significant research efforts were made to search for new oxide materials with smaller bandgaps to enhance visible light absorption [2]. Fe_2O_3 stands out with its nearly ideal bandgap of 2.2 eV [3] and its high-photochemical stability in aqueous solutions [4]. Though high-photoconversion efficiencies were already shown for polycrystalline Fe_2O_3 pellets [5] and single crystalline Fe_2O_3 samples [6], thin films are generally preferred in order to avoid the high resistivities encountered in, for example, single crystals, and to reduce the cost for fabrication. Very recently, an exceptionally high photocurrent of 2.7 mA/cm^2 at a bias of 1.23 V relative to the reversible hydrogen electrode (RHE) under simulated AM1.5 sunlight was reported for porous films synthesized using atmospheric pressure chemical vapor deposition (APCVD) [7]. While this breakthrough represents a major step forward, practical applications still require an additional ~4 times improvement in photocurrent. In order to achieve this, more detailed insights into the origin of the high photoresponse are required.

The key ingredients for the high performance of the APCVD films seem to be (i) Si doping, which is thought to induce a favorable morphology during film growth [8], (ii) the presence of a thin SiO_2 interfacial layer between the Fe_2O_3 and the transparent conducting substrate [7], and (iii) the addition of a cobalt catalyst [7]. The aim of the present study is to reveal the effects of Si doping and the addition of a thin interfacial layer (in this case SnO_2) between the transparent conducting substrate (TCO) and the Fe_2O_3. Toward this end, thin dense undoped and Si-doped Fe_2O_3 films are deposited onto conductive glass substrates by spray pyrolysis. Although spray pyrolysis will not generally yield the high degree of texturing that is required for optimal performance, the ease of doping and smooth film morphology greatly simplifies the photoelectrochemical characterization of the material. The photoresponse and the electrical characteristics of the deposited films are studied for various Si concentrations and the effect of a thin SnO_2 interfacial film is investigated.

2. EXPERIMENTAL

Thin films of α-Fe_2O_3 (hematite) were prepared by spray pyrolysis of a 0.04 M $Fe(AcAc)_3$ (Alfa Aesar, Karlsruhe, Germany) solution in a mixed solvent (2 : 1) of ethyl acetate and ethanol. To avoid large fluctuations of the temperature during spraying and to give the solvent enough

time to evaporate, the spray pyrolysis was carried out using 15 seconds on cycle, 45 seconds off cycle. Compressed air was used as the carrier gas.

Silicon doping was achieved by addition of different amounts of TEOS (99.9%, Alfa Aesar, Karlsruhe, Germany) to the precursor solution. All the Si concentrations mentioned hereafter refer to the atomic Si : Fe ratio in the spray solution, though the Si concentration that actually ends up in the deposited Fe_2O_3 films may be somewhat different. The SnO_2 interfacial layer was deposited by spray pyrolysis of a 0.1 M $SnCl_4$ (99%, Acros organics, NJ, USA) solution in ethyl acetate (99.5%, J. T. Baker, Deventer, Holland).

FTO glass (SnO_2:F, TEC-15, Libbey-Owens-Ford, Hartford, IN, USA, 2.5-mm thick) was used as a transparent conducting substrate for photoelectrochemical experiments. Fused silica (ESCO, S1-UV grade, thickness of 1 mm) was used as a substrate for the film thickness determination by UV-vis absorption measurements. All the substrates were cleaned by ultrasonic rinsing in pure ethanol, and subsequently dried under N_2 flow. During deposition, the substrate was heated using a temperature-controlled hotplate.

Structural characterization of the films was carried out using a Bruker D8 Advance X-ray diffractometer in the grazing incidence mode. A Renishaw 1000 spectrometer was used for microscopic Raman analysis.

To determine the film thickness, UV-vis absorption spectra of the SnO_2 and Fe_2O_3 films on fused silica were measured with a Lambda 900 UV-vis spectrophotometer (Perkin Elmer). For the Fe_2O_3 films, the thickness was further verified by inspection of the cross-section of the films using a JSM-6500F field emission scanning electron microscope (SEM).

A home-made three-electrode electrochemical cell, fitted with a fused silica window, was used for photoelectrochemical characterization. An aqueous solution of 1.0 M KOH (pH 14) was used as the electrolyte. The potential of the Fe_2O_3 working electrode (area: 0.283 cm^2) was controlled by a potentiostat (EG&G PAR 283), which was combined with a frequency response analyzer (Solartron 1255, Schlumberger, Hampshire, England) for impedance analysis. An Ag/AgCl electrode (REF321, Radiometer Analytical, Villeurbanne, France) was used as a reference and a coiled Pt wire was adopted as the counter electrode. All the potentials mentioned in this article are referred to Ag/AgCl (0.208 V versus NHE at 25°C), unless stated otherwise.

For spectral response measurements, light from a 200 W tungsten halogen lamp was coupled into a grating monochromator (Acton SpectraPro 150i) via a 50-mm diameter fused silica lens. Between the monochromator and the sample, an electronic shutter (Uniblitz LS6) was placed, and high-pass colored glass filters (Schott, 2×3 mm) were used to remove second-order diffracted light. The intensity of the monochromatic light was measured with a calibrated photodiode (Ophir, Jerusalem, Israel, PD300-UV). For white-light measurements, a solar simulator (EPS 1200S, KH Steuernagel Lichttechnik GmbH, Mörfelden-Walldorf, Germany) was used to provide simulated AM1.5 sunlight. The light from the solar simulator was directed to the sample by mirror (UV-enhanced aluminum, Melles Griot, Cambridge, England) placed under a 45° angle. This resulted in an illumination intensity of 80 mW/cm^2 (i.e., 80% of AM1.5 light) at the position of the sample, as measured with a calibrated Si photodiode. An AM1.5 standard spectrum reported by NREL [9] was used for integrating the monochromatic photocurrent and comparing it to the white light response.

3. RESULTS AND DISCUSSION

Figure 1(a) shows X-ray diffraction results for the 0.1% Si-doped Fe_2O_3 films. At 350°C, the peak intensity distribution corresponds to that of regular polycrystalline hematite. As the temperature is increased, the intensity of the (110) diffraction peak becomes stronger, while the (104) diffraction becomes less pronounced. For the samples without Si dopant, the same trend is observed. Hence, (110) is preferred growth direction for sprayed Fe_2O_3 films at deposition temperatures of 400°C and higher.

The preferred (110) orientation implies that the c-axes of the crystal domains in the Fe_2O_3 film are parallel to the substrate surface. Since electron transport along the c-axis is known to be about four orders of magnitude slower than in the other directions [10, 11], the (110) orientation observed here is much more favorable for electron transport than the (001) oriented hematite films deposited with, for example, ion-beam assisted CVD [12]. Moreover, the conductivity along the c-axis has been suggested to be p-type in character [13, 14]. This implies that a (110) preferred orientation would also be favorable for photoanodes made of vertically aligned hematite nanowires, where efficient hole transport in the direction parallel to the substrate is desired.

In addition to the hematite peaks, two other phases seem to be present in minor amounts as indicated by small peaks at 29.8° and 32.1°. The small peak at 29.8°, which is attributed to the presence of Fe_3O_4 [15], appears only in the samples deposited at low temperatures (≤450°C). The origin of the peak at 32.1° is not yet clear and can not be attributed to any of the known iron oxides. The closest candidate would be β-Fe_2O_3 with a peak at 32.9°, but this seems to be too far from the observed peak position. Moreover, β-Fe_2O_3 has been reported to disappear after annealing at high temperatures (550°C) [16], whereas Figure 1(a) shows the peak at 32.9° to actually increase with temperature.

Figure 1(b) shows the Raman spectra of Fe_2O_3 doped with 0.2% Si. Compared to the α-Fe_2O_3 peaks, the intensity of the Fe_3O_4 peak at 656 cm^{-1} [17] decreases with increasing deposition temperature. This is consistent with the XRD results in Figure 1(a), and supports our conclusion that Fe_3O_4 is only formed at temperatures ≤450°C under the currently used conditions for spray pyrolysis.

As can be observed in Figures 1(c) and 1(d), spray pyrolysis of the $Fe(AcAc)_3$ solution yields compact films of uniform thickness. A thickness of 200 nm was reached after 40 spray cycles (each cycle consists of 15 seconds spray on +45 seconds spray off), resulting in an average deposition rate of 20 nm/min for spraying at 450°C. No significant differences

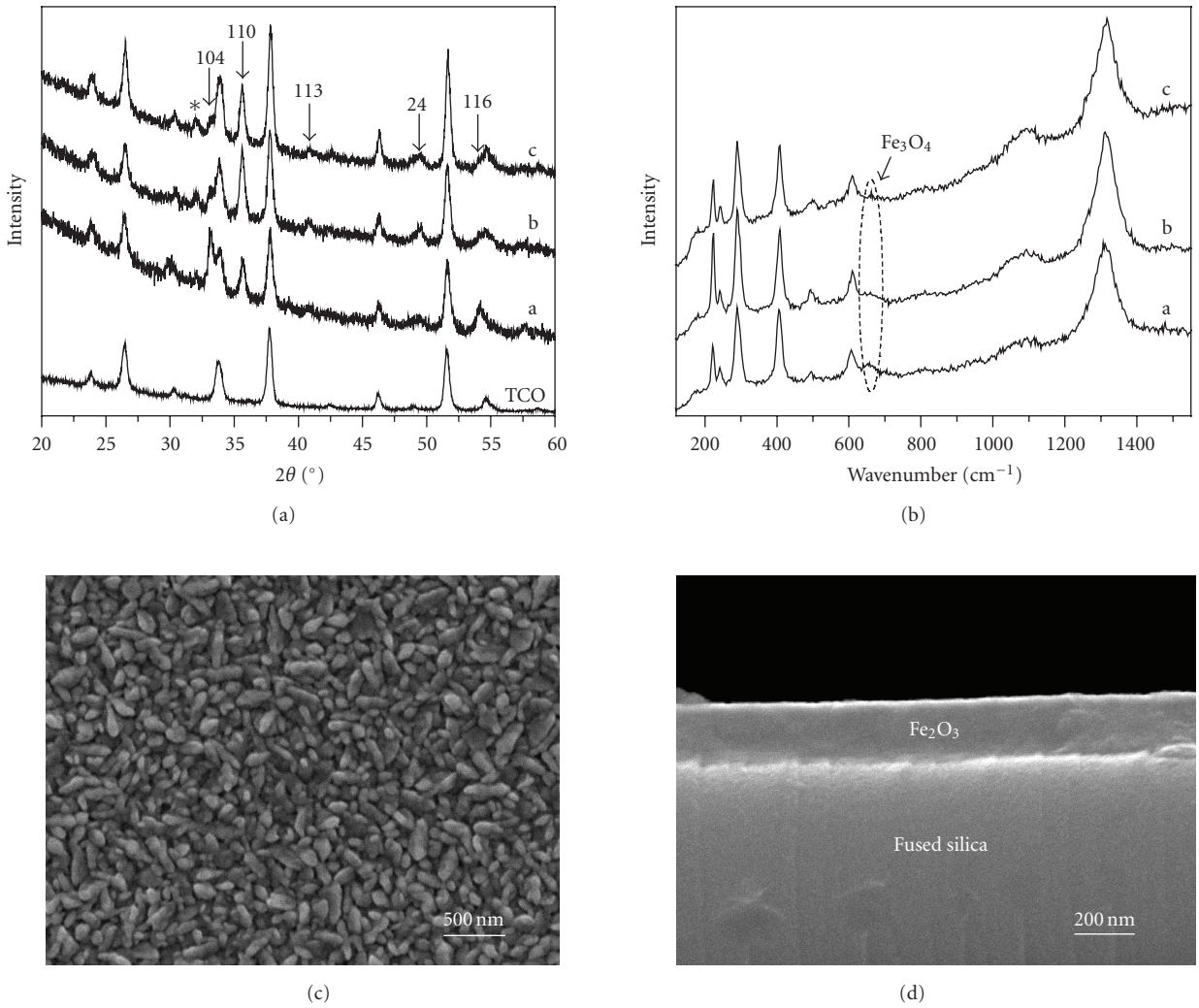

FIGURE 1: (a) XRD of Fe_2O_3 films doped with 0.1% Si deposited at (a) 350°C, (b) 400°C, (c) 450°C. The diffraction pattern of the TCO substrate fired at 400°C in the air is also shown for comparison. Undefined peaks are marked with *. (b) Raman spectra of Fe_2O_3 samples doped with 0.2% Si deposited at (a) 350°C, (b) 450°C, (c) 500°C. (c) SEM micrographs showing the typical morphology of the Fe_2O_3 films on TCO. (d) Cross-section of a 200 nm Fe_2O_3 film on a fused silica substrate.

in film morphology are observed between undoped and Si-doped films.

Figure 2(a) shows the measured photocurrent versus potential curves for Fe_2O_3 films doped with 0.2% Si. Comparison between curves a and b shows a significant improvement of the photocurrent response, when a 5 nm SnO_2 interfacial layer is present between the TCO substrate and the Fe_2O_3 film. This improvement is especially pronounced at lower potentials. Specifically, at a potential of 0.23 V versus Ag/AgCl, which corresponds to a reversible hydrogen potential of 1.23 V_{RHE}, the photocurrent increases from 0.04 mA/cm^2 to 0.33 mA/cm^2. In fact, Figure 2(a) shows that the interfacial layer shifts the photocurrent onset potential by ~0.2 V in the cathodic direction. Another effect of the interfacial layer is a significant improvement of the reproducibility of the photoresponse, especially for undoped samples. Without the interfacial layer, photocurrent variations of up to a factor of five or more are observed between samples made under the same conditions. With the interfacial layer, these variations are within a factor of 2.

For the Si-doped samples, front-side (electrolyte-side) illumination (curve a in Figure 2(a)) always gives a higher photocurrent than back-side (substrate-side) illumination (curve a' in Figure 2(a)). This shows that the rate-limiting step in the Si-doped samples is hole transport. In contrast, electron transport is found to be rate limiting in undoped Fe_2O_3 samples. The introduction of the SnO_2 interfacial layer does not change the ratio between the front-side photocurrent and the back-side photocurrent (curves b and b'). Since front-side illumination shows higher photocurrents, all the data discussed from this point forward are measured using front-side illumination.

The thickness of the SnO_2 films was determined by UV-vis absorption measurements, corrected for reflection, assuming an absorption coefficient of 1.3×10^5 cm^{-1} at 300 nm [18]. For these measurements, the SnO_2 films were

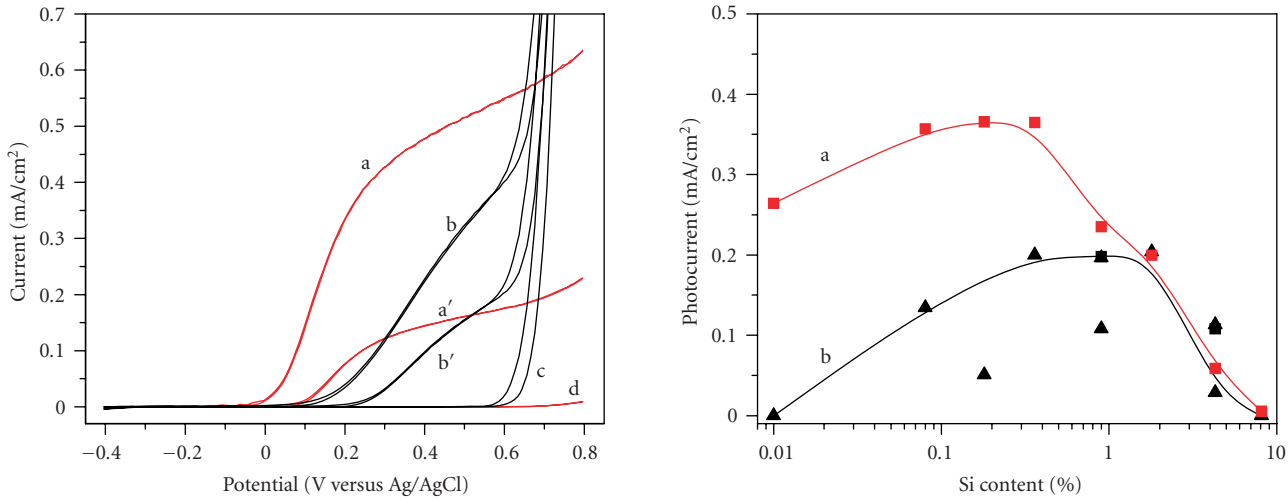

FIGURE 2: (a) Current-potential measurements under simulated 80 mW/cm^2 AM1.5 sunlight for Fe_2O_3 doped with 0.2% Si with (a: front-side illumination; a': back-side illumination; d: dark) and without (b: front-side illumination; b': back-side illumination; c: dark) 5 nm SnO_2 interfacial layer. The scan rate is 20 mV/s. (b) Dependence of the photocurrent (front-side illumination) at 0.23 V versus Ag/AgCl on the Si dopant concentration; a: with SnO_2 interfacial layer; b: without SnO_2 interfacial layer.

deposited on fused silica substrates, and the growth rate was assumed to be similar to that on the TCO substrates. Because of the small thickness (~5 nm) and the large bandgap (>3.6 eV) of SnO_2, it can be safely assumed that the contribution of the interfacial layer to the photocurrent is negligible. Furthermore, X-ray diffraction revealed that the SnO_2 interfacial layer does not affect the preferred orientation of the Fe_2O_3 films.

Figure 2(b) shows the photocurrent at 0.23 V versus Ag/AgCl for Fe_2O_3 films with various amounts of Si doping. For the films without SnO_2 interfacial layer, the optimum Si concentration is ~1%, whereas an optimum concentration range between 0.2 and –0.4% is found for films with an interfacial SnO_2 layer. It should be noted that these concentrations are much lower than in previously reported studies on Si-doped Fe_2O_3 [19, 20], where a significant fraction of Si content was presumably present as a second phase. As can be seen in Figure 2(b), the presence of an SnO_2 interfacial layer is especially beneficial at low-Si concentrations.

Previous reports have shown that unintentional incorporation of donor-type species may also be responsible for improved photoefficiencies. Examples of impurities that are sometimes difficult to avoid are Si [8, 19], carbon in the case of organic Fe-precursors such as $Fe(AcAc)_3$, and chlorine when $FeCl_3$ or $FeCl_2$ are used as precursors [7]. The electrical conductivity can also be affected by the presence of other iron oxide phases, such as FeO, Fe_3O_4, or Fe_2O_3, which may be formed depending on the deposition conditions and the presence of trace impurities [2, 16, 17].

To rule out that the beneficial effect of the SnO_2 layer is caused by the diffusion of Sn into the Fe_2O_3 film (i.e., unintentional doping), a Mott-Schottky analysis was carried out. Figure 3(a) shows a Mott-Schottky plot of an undoped Fe_2O_3 film recorded in the dark. The presence of a 5 nm SnO_2 interfacial layer has no significant effect on the curve, which already indicates that no significant Sn diffusion into the Fe_2O_3 layer occurs. According to the depletion layer model, the capacitance of the semiconductor space charge layer C_{sc} changes with the applied potential V_A according to the Mott-Schottky equation,

$$\frac{1}{C_{sc}^2} = \frac{2}{e\varepsilon_r\varepsilon_0 N_d A^2}\left(V_A - V_{fb} - \frac{kT}{e}\right), \quad (1)$$

where ε_r is the semiconductor dielectric constant, A is the surface area of the electrode, N_d is the donor density, and V_{fb} is the flatband potential. At potentials positive of −0.6 V, the Fe_2O_3 is fully depleted and the slope of the curve reflects the donor density in the conducting FTO substrate. From the intercept of the dashed lines in Figure 3(a) and the dielectric constant of 80 for Fe_2O_3 [22], the film thickness is calculated according to $C = \varepsilon_0\varepsilon_r A/d$, yielding a thickness value of 135 nm. The discrepancy between the calculated value and the value determined from the SEM cross-section (200 nm, Figure 1(d)) is presumably caused by the surface roughness and/or the frequency dispersion in the Mott-Schottky plots, which will be discussed in more detail below. A donor density of 1.2×10^{17} cm^{-3} in the Fe_2O_3 is calculated from the slope of the Mott-Schottky plot between −0.8 V and −0.6 V. This value is quite small for a semiconducting metal oxide indicating that (i) the sprayed Fe_2O_3 films are of high quality with relatively few electronic defects and (ii) little, if any, Sn diffuses from either the interfacial layer or the F:SnO_2 conducting substrate into the Fe_2O_3 film. The beneficial effect of the SnO_2 interfacial layer is tentatively attributed either to the passivation of surface states or to an improvement of the band alignment between the Fe_2O_3 and the underlying TCO.

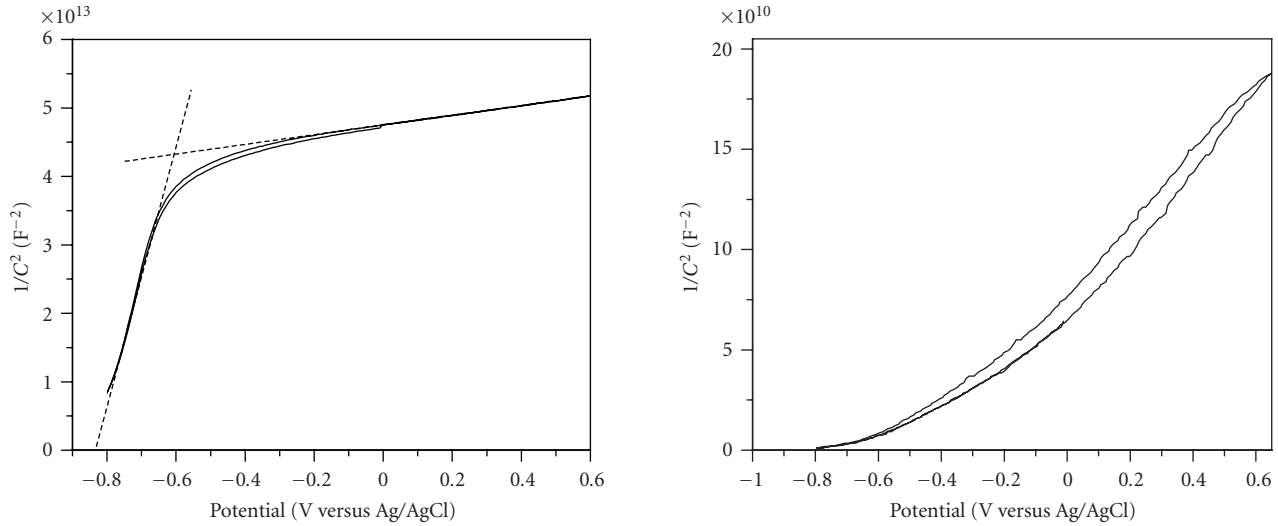

FIGURE 3: Mott-Schottky measurement of Fe_2O_3 films (a) undoped, measured at 30 kHz and (b) doped with 0.9% Si, measured at 1 kHz. The frequency was selected based on the impedance spectra (not shown), in the range where the slope of $\log|-Z''|$ versus $\log(\omega)$ is close to -1, and the real part of impedance is more or less constant [21].

After introducing 0.9% Si dopant in the precursor solution, dramatic changes in the Mott-Schottky plot are observed (Figure 3(b)). From these data, a donor density of $1 \times 10^{20}\,\text{cm}^{-3}$ is calculated. However, considering the roughness of the surface on a microscopic scale and the fact that the depletion layer extends only a few nanometers into the Fe_2O_3 film, the effective surface area will be larger than the geometrical area. As a result, the true donor density will be somewhat smaller than the calculated value. The fact that the curve concaves upwards in Figure 3(b) supports the interpretation in terms of surface roughness effects [23]. If all Si atoms present in the precursor solution are incorporated into the film and act as ionized donors, a maximum donor density of $4 \times 10^{20}\,\text{cm}^{-3}$ is expected. This is within the same order of magnitude as the measured donor density, indicating that a significant fraction of the Si atoms, is incorporated into the film where they indeed act as ionized donors. This is a somewhat unexpected result, since the pyrolysis of TEOS usually requires temperatures much higher than 450°C [7].

Another important parameter of the semiconductor that can be derived from Mott-Schottky measurements is the flat band potential. Although the flat band potential depends on the exposed crystal plane and on the donor density inside the Fe_2O_3, most reports agree that the flat band potential of Fe_2O_3 with a donor density of $\sim 10^{17}\,\text{cm}^{-3}$ is -0.7 V in a 1.0 M KOH solution [6, 24]. A somewhat more negative potential of -0.84 V versus Ag/AgCl is found for our spray-deposited undoped Fe_2O_3 films (Figure 3(a)). However, it should be mentioned that an accurate determination of the flat band potential is complicated by some degree of frequency dispersion observed in the Mott-Schottky plots [25, 26]. Specifically, in the frequency range between 1 kHz and 30 kHz, the flat band potential varies between -0.67 V and -0.96 V. The donor density shows much less variation; values between $1.3 \times 10^{17}\,\text{cm}^{-3}$ and $0.8 \times 10^{17}\,\text{cm}^{-3}$ are observed between 1 and 30 kHz. A more detailed analysis of the impedance spectra to elucidate the origin of the frequency dispersion is still ongoing, but is complicated by the fact that the equivalent circuits that are normally used to model semiconducting photoanodes are not able to describe the measured data in a satisfactory manner.

To objectively compare the photoelectrochemical performance of our films with the literature, the incidented photon-to-current conversion efficiency (IPCE) has been measured as a function of wavelength. The IPCE of the Fe_2O_3 films doped with 0.1% Si and deposited on top of a 5 nm SnO_2 interfacial layer is shown in Figure 4(a). A bias of 0.4 V versus Ag/AgCl was used, since no accurate steady-state photocurrent values could be obtained at more negative potentials due to a transient response when the light is switched on and off. A maximum IPCE of 20% is found at 370 nm, which is comparable to the best spray-deposited Fe_2O_3 samples reported so far [16], though still a factor of about 2.5 below the samples made by APCVD [7]. At wavelengths shorter than 370 nm, however, the IPCE shows a steeper decrease than that reported in the literature for Fe_2O_3 [7, 16]. While the origin of this difference is not clear, it does explain the relatively modest response of our samples to white-light illumination.

To compare the IPCE spectra with the photoresponse under simulated AM1.5 sunlight, the IPCE data are integrated over the standard AM1.5 solar spectrum and corrected for an actual intensity of $80\,\text{mW/cm}^2$ (Figure 4(b)). The photocurrent is assumed to depend linearly on the light intensity, which is reasonable for the low-light intensities used in this study (10–20 $\mu\text{W/cm}^2$). The integrated photocurrent of $0.53\,\text{mA/cm}^2$ is higher

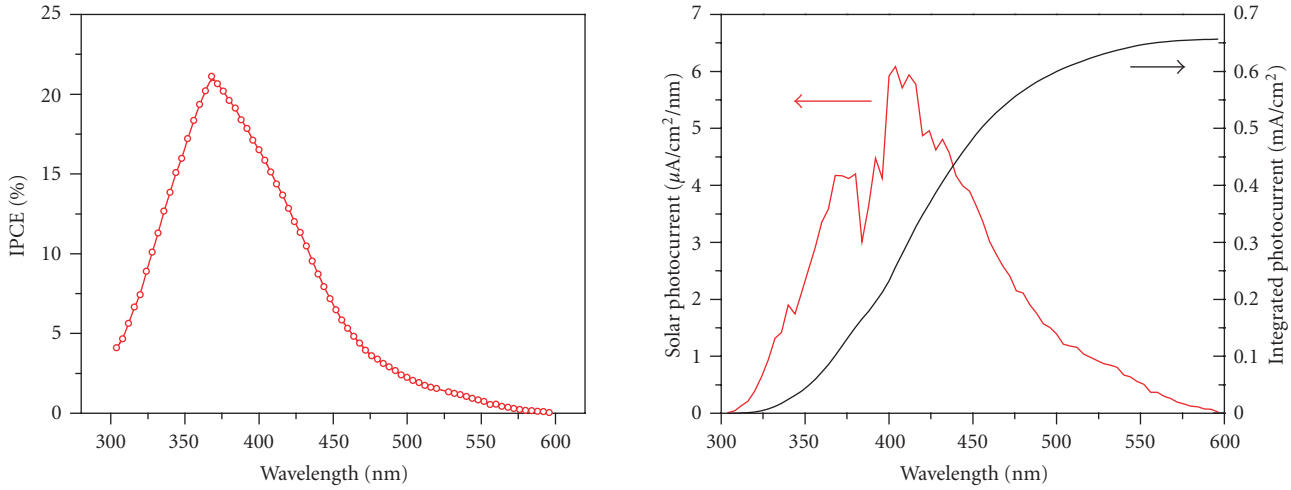

FIGURE 4: (a) IPCE curve for 0.1% Si-doped Fe_2O_3 measured at 0.4 V versus Ag/AgCl. (b) Momentary and integrated solar photocurrent of the sample obtained by multiplying IPCE with the photon flux spectrum of AM1.5 sunlight. When correcting for the actual experimental intensity of 80 mW/cm^2, an integrated photocurrent of $0.8 \times 0.66 = 0.53$ mA/cm^2 is obtained.

than the measured AM1.5 photocurrent of 0.44 mA/cm^2 (Figure 2(a)). Although the reason for this discrepancy is not yet clear, this perhaps rather conservative value for the photoresponse under simulated AM1.5 light is much better suited for comparison with results from other labs than the often reported photocurrents measured with xenon light sources. As pointed out recently by Murphy et al., the high-UV content of xenon lamps often leads to severe overestimation of the photoconversion efficiencies [3].

4. CONCLUSIONS

Thin-film hematite Fe_2O_3 photoanodes were deposited on transparent conducting glass substrates by spray pyrolysis. A thin, 5 nm SnO_2 interfacial layer between the Fe_2O_3 and TCO glass was found to be beneficial for both the reproducibility and the photocurrent efficiency of the Fe_2O_3 films. While the beneficial effect of an interfacial layer on the photoresponse of Fe_2O_3 has been previously reported for ultrathin (~1 nm) SiO_2 films, in this study we show that the beneficial effect of such an interfacial layer is not limited to the material SiO_2, and that electrons do not need to be able to tunnel through the interfacial layer. Silicon concentrations between 0.2 and 0.4% are found to give the highest photocurrents for spray-deposited Fe_2O_3 films. The highest photoresponse measured during this study was 0.37 mA/cm^2 at 0.23 V versus Ag/AgCl (1.23 V versus RHE) under 80 mW/cm^2 AM1.5 illumination for films doped with 0.2% Si and deposited on a 5 nm SnO_2 interfacial layer. Since hole transport is the rate limiting factor for these films, further improvements of the efficiency requires nanostructured electrodes with high aspect ratios in order to minimize the distance that the photogenerated holes have to travel before reaching the semiconductor/electrolyte interface. Development of suitable low-cost deposition techniques for such electrodes, that can be readily scaled-up and that allow accurate control over dopant concentrations, is one of the major challenges in the field of photocatalysis and solar water splitting.

ACKNOWLEDGMENTS

This work is financially supported under the sustainable hydrogen program (Project no. 053.61.009) by NWO-ACTS. The authors also want to express their thanks to Ilkay Cesar from EPFL for stimulating discussions on Fe_2O_3. Roel van de Krol gratefully acknowledges support from the Netherlands Organization for Scientific Research (NWO) in the form of a VENI Grant.

REFERENCES

[1] A. Fujishima and K. Honda, "Electrochemical photolysis of water at a semiconductor electrode," *Nature*, vol. 238, pp. 37–38, 1972.

[2] K. L. Hardee and A. J. Bard, "Semiconductor electrodes. X. Photoelectrochemical behavior of several polycrystalline metal oxide electrodes in aqueous solutions," *Journal of the Electrochemical Society*, vol. 124, no. 2, pp. 215–224, 1977.

[3] A. B. Murphy, P. R. F. Barnes, L. K. Randeniya, et al., "Efficiency of solar water splitting using semiconductor electrodes," *International Journal of Hydrogen Energy*, vol. 31, no. 4, pp. 1999–2017, 2006.

[4] J. H. Kennedy and M. Anderman, "Photoelectrolysis of water at α-Fe_2O_3 electrodes in acidic solution," *Journal of the Electrochemical Society*, vol. 130, no. 4, pp. 848–852, 1983.

[5] R. Shinar and J. H. Kennedy, "Photoactivity of doped α-Fe_2O_3 electrodes," *Solar Energy Materials*, vol. 6, no. 3, pp. 323–335, 1982.

[6] C. Sanchez, K. D. Sieber, and G. A. Somorjai, "The photoelectrochemistry of niobium doped α-Fe_2O_3," *Journal of Electroanalytical Chemistry*, vol. 252, no. 2, pp. 269–290, 1988.

[7] A. Kay, I. Cesar, and M. Grätzel, "New benchmark for water photooxidation by nanostructured α-Fe_2O_3 films," *Journal of*

the American Chemical Society, vol. 128, no. 49, pp. 15714–15721, 2006.

[8] I. Cesar, A. Kay, J. A. Gonzalez Martinez, and M. Grätzel, "Translucent thin film Fe_2O_3 photoanodes for efficient water splitting by sunlight: nanostructure-directing effect of Si-doping," *Journal of the American Chemical Society*, vol. 128, no. 14, pp. 4582–4583, 2006.

[9] http://rredc.nrel.gov/solar/spectra/am1.5/.

[10] T. Nakau, "Electrical conductivity of α-Fe_2O_3," *Journal of the Physical Society of Japan*, vol. 15, no. 4, p. 727, 1960.

[11] K. M. Rosso, D. M. A. Smith, and M. Dupuis, "An *ab initio* model of electron transport in hematite (α-Fe_2O_3) basal planes," *Journal of Chemical Physics*, vol. 118, no. 14, pp. 6455–6466, 2003.

[12] F. Yubero, M. Ocaña, A. Justo, L. Contreras, and A. R. González-Elipe, "Iron oxide thin films prepared by ion beam induced chemical vapor deposition: structural characterization by infrared spectroscopy," *Journal of Vacuum Science and Technology A*, vol. 18, no. 5, pp. 2244–2248, 2000.

[13] J. B. Goodenough, "Metallic oxides," *Progress in Solid State Chemistry*, vol. 5, pp. 145–398, 1971.

[14] N. Iordanova, M. Dupuis, and K. M. Rosso, "Charge transport in metal oxides: a theoretical study of hematite α-Fe_2O_3," *Journal of Chemical Physics*, vol. 122, no. 14, pp. 144305–144310, 2005.

[15] JCPDS reference card #19-0629, International Center for Diffraction Data, New York, NY, USA.

[16] C. J. Sartoretti, B. D. Alexander, R. Solarska, I. A. Rutkowska, and J. Augustynski, "Photoelectrochemical oxidation of water at transparent ferric oxide film electrodes," *Journal of Physical Chemistry B*, vol. 109, no. 28, pp. 13685–13692, 2005.

[17] A. Duret and M. Grätzel, "Visible light-induced water oxidation on mesoscopic α-Fe_2O_3 films made by ultrasonic spray pyrolysis," *Journal of Physical Chemistry B*, vol. 109, no. 36, pp. 17184–17191, 2005.

[18] K. B. Sundaram and G. K. Bhagavat, "Optical absorption studies on tin oxide films," *Journal of Physics D*, vol. 14, pp. 921–925, 1981.

[19] J. H. Kennedy, R. Shinar, and J. P. Ziegler, "α-Fe_2O_3 photoanodes doped with silicon," *Journal of the Electrochemical Society*, vol. 127, no. 10, pp. 2307–2309, 1980.

[20] C. Leygraf, M. Hendewerk, and G. A. Somorjai, "Mg- and Si-doped iron oxides for the photocatalyzed production of hydrogen from water by visible light ($2.2\,\text{eV} \leq h\nu \leq 2.7\,\text{eV}$)," *Journal of Catalysis*, vol. 78, no. 2, pp. 341–351, 1982.

[21] R. van de Krol, A. Goossens, and J. Schoonman, "Mott-Schottky analysis of nanometer-scale thin-film anatase TiO_2," *Journal of the Electrochemical Society*, vol. 144, no. 5, pp. 1723–1727, 1997.

[22] S. M. Wilhelm, K. S. Yun, L. W. Ballenger, and N. Hackerman, "Semiconductor properties of iron oxide electrodes," *Journal of the Electrochemical Society*, vol. 126, no. 3, pp. 419–424, 1979.

[23] J. Schoonman, K. Vos, and G. Blasse, "Donor densites in TiO_2 photoelectrodes," *Journal of the Electrochemical Society*, vol. 128, no. 5, pp. 1154–1157, 1981.

[24] J. H. Kennedy and K. W. Frese Jr., "Flatband potentials and donor densities of polycrystalline α-Fe_2O_3 determined from Mott-Schottky plots," *Journal of the Electrochemical Society*, vol. 125, no. 5, pp. 723–726, 1978.

[25] H. O. Finklea, "The preparation of TiO_2 electrodes with minimum Mott-Schottky frequency dispersion," *Journal of the Electrochemical Society*, vol. 129, no. 9, pp. 2003–2008, 1982.

[26] G. Oskam, D. Vanmaekelbergh, and J. J. Kelly, "A reappraisal of the frequency dependence of the impedance of semiconductor electrodes," *Journal of Electroanalytical Chemistry*, vol. 315, no. 1-2, pp. 65–85, 1991.

Hindawi Publishing Corporation
International Journal of Photoenergy
Volume 2008, Article ID 870392, 8 pages
doi:10.1155/2008/870392

Research Article

Photoactive Thin Silver Films by Atmospheric Pressure CVD

Heather M. Yates, Lucy A. Brook, and David W. Sheel

Institute for Materials Research, Salford University, Manchester M5 4WT, UK

Correspondence should be addressed to Heather M. Yates, h.m.yates@salford.ac.uk

Received 24 July 2007; Revised 22 November 2007; Accepted 26 March 2008

Recommended by Russell Howe

We report the visible and UV activity of thin silver films. The films are grown using a CVD process employing aqueous-based silver precursors, flame-assisted chemical vapour deposition. This approach overcomes many of the previously encountered limitations to silver deposition by employing an atmospheric pressure process, low-cost and low-toxicity precursors. The resultant films are assessed for activity using stearic acid destruction as a model compound. We also report on the addition of titania to these silver films to increase the potential functionality. This activity is also demonstrated, where the films appear largely transparent to the eye, further widening the potential application of this work. It is speculated that the nanoparticulate nature, of the CVD silver, is crucial in determining photoactivity.

1. INTRODUCTION

In recent years, photoactive films have attracted increasing attention, particularly based on titania. Significant efforts have been directed at developing the photoactivity of titania into the visible. Methods have included use of other photoactive materials in conjunction with TiO_2 including WO_3 [1] and PdO [2], or by doping with anionic [3, 4], or cationic [5] species. To date, the results have been mixed. In many cases, the doping itself leads to a reduction in photoactivity, often attributed to disruption of the crystal structure [6] and/or the introduction of compensation centres [7]. Some papers do claim visible activity [8], although the form and mechanism of how the photoactivity works is often in dispute [9].

The combination of Ag and TiO_2 produced mainly by sol-gel techniques has been shown to improve TiO_2 UV photoactivity, under the correct conditions. In some cases, this has been shown to relate to the modification of the sample morphology by the Ag with, for example, a change in crystallite size [10] or rutile/anatase [11]. The addition of Ag is considered to promote charge separation of the electron-hole pairs from TiO_2 after photon absorption by acting as an electron sink.

Research literature of the behaviour of just Ag under illuminated light relates mainly to its own transition rather than its effect on other chemical compounds. The reduction of Ag^+ ions to Ag metal is well documented, and use of UV to form the metal from ions is common practice. Commercial uses of the reduction of Ag^+ ions include photography [12] and photochromic glass [13]. Films of AgCl were found to be photocatalytic for the oxidation of water, but only in the presence of excess Ag^+. This activity expanding from the UV to visible due to self-sensitisation [14].

Other research relating to use of Ag in catalysis is usually in conjunction with zeolites, where the presence of Ag^+ clusters increases the photodecomposition rate of specific organics by acting as active sites, or electron trapping sites [15], or decomposition of inorganics such as NO and H_2O [16]. In these cases, the zeolite is needed to isolate and stabilize the Ag^+ ions (and their clusters). The zeolite itself is playing a role in the photoactivity of the catalyst, for example, the increased efficiency of the N_2O decomposition reaction with ZSM-5 opposed to zeolite Y [17]. There is only very limited literature available on the photoactivity of thin Ag films with organic materials. Research by Guo et al. [18] states that there is a possible photocatalyic reaction under laser excitation.

A wide range of techniques have been used to deposit thin film silver including electroless deposition [19], electrostatic deposition [20], and PVD processes (e.g., evaporation and sputtering) [21]. Previous studies on silver thin film structure have shown that continuous sheets of silver can be produced easily by PVD [22], and a granular structure can

be produced by MOCVD [23, 24]. Although these processes are effective at producing thin films, the degree of silver nanostructure control is typically limited.

In this paper, we report the use of flame-assisted chemical vapour deposition (FACVD) to produce silver nanostructured layers and coatings. The process can use aqueous precursors, which are in many cases very soluble, and of relatively low toxicity. Growth rates are also rapid in comparison to previous APCVD reports, and a high degree of nanostructure control can be achieved with this approach. Indeed, the nanostructured silver deposition control arising from our described approach appears to give an enhancement to photoactivity and also to the bioactivity of the various film structures, as previously shown [25]. We will report on the photoactivity of Ag films in both the visible and the UV, along with examples of Ag/TiO_2 films. The added attraction of the TiO_2/Ag combination is the increased durability of the samples, over that of Ag which is relatively soft and the additional high photoactivity expected of the TiO_2 under UV.

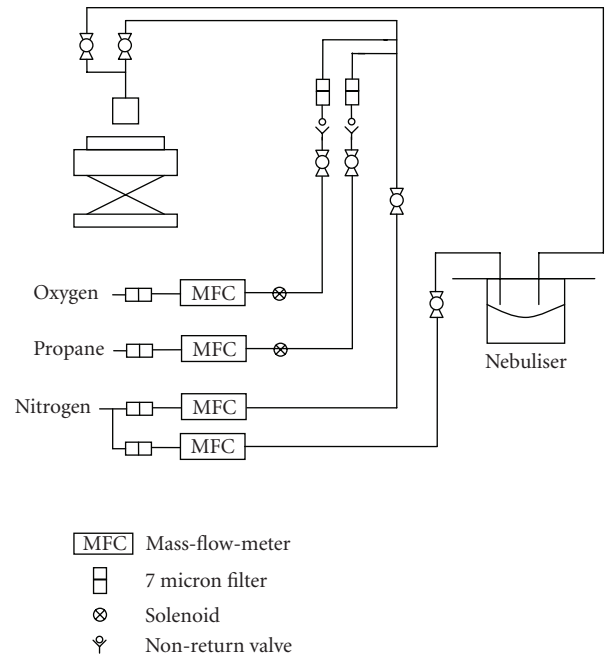

Figure 1: Schematic of the FACVD system.

2. EXPERIMENTAL

2.1. Growth

All films were grown on commercially supplied silica-coated barrier glass substrates. The barrier is a thin (60 nm), amorphous film of SiO_2 to prevent diffusion of impurity ions within the float glass. These would all cause a reduction in the quality and photoactivity of the films.

All silver films were produced by flame-assisted chemical vapour deposition (FACVD). The FACVD reactor used is of in-house construction. Basically, it consists of a burner head which allows gas mixing, a translational substrate stage and a precursor delivery system (electronic mass-flow controllers and a nebuliser). A schematic of the system is shown in Figure 1. The substrate stage is made up of a carbon block which can be translated beneath the flame at a rate of 3.6 cm/s. The number of passes under the burner head is related to the sample thickness. The carbon block was held at 300°C for optimum growth. The nebuliser is a commercially available ultrasonic system (ultra-neb2000 Devilbiss 200HS-042), with water used as the transmission medium. The precursor solution sits within a cup that in turn is in contact with the water in the nebuliser, such that ultrasonic waves are passed through to the precursor solution, hence producing droplets of precursor solution. Nitrogen carrier gas then passes through the nebuliser, collecting solution droplets, which are then transported to the flame. Fuelling the burner is a mixture of propane and oxygen gases, flowing at 0.99 L min^{-1} and 3.65 L min^{-1}, respectively, generating a flame output power of 1.50 kW. The precursor is carried in 1.70 L min^{-1} of nitrogen. These gases are also mixed with 13.90 L min^{-1} of make-up nitrogen for flame control. The precursor reagent used was silver nitrate supplied by Aldrich, with a purity of 99.99% dissolved in deionised water to the required concentration.

Electroplated silver was also deposited as a comparison to the FACVD films. These films were deposited using 0.15 M silver nitrate in deionised water (solution A), 0.8 M potassium hydroxide in deionised water (solution B), and a 0.49 M glucose solution (solution C). The glucose solution was made up of 88% deionised water, 11% ethanol, and 1% concentrated nitric acid. The solutions were mixed in the ratio 16 : 8 : 1 of A : B : C, respectively, and deionised water was added to control the speed of the reaction. Concentrated ammonia was used to react with any oxide precipitation.

Titania films were grown using an atmospheric pressure CVD coater. The precursors used were titanium tetrachloride (4.9×10^{-4} mol min^{-1}) and ethyl acetate (3.65×10^{-3} mol min^{-1}) (Aldrich), which were transported through the reactor by a carrier gas of nitrogen. The substrate temperature was 650°C. Silver was deposited both under and over these films by FACVD.

2.2. Characterisation

X-ray diffraction (Siemens D5000) was used to confirm the sample crystallinity. The morphology assessed by SEM (Philips XL30). Film thickness (for titania) was estimated by relating the reflected colour to a calibrated chart for thickness versus refractive index. Film thickness for the Ag was determined by cross-sectional SEM and the use of a surface profiler (Dektak 3ST) on an etched edge. X-ray photoelectron spectroscopy, XPS, (Kratos AXIS Ultra) with an Al (monochromated) K_α radiation source was used to check the surface composition and stoichiometry of the films.

To test the photocatalytic behaviour under UV (365 nm), the degradation of stearic acid was followed by FTIR (Bruker, Vector 22). The software allows integration of the area under the peaks over a range of 2800–3000 cm^{-1}. A typical stearic acid layer would have an integrated absorbance over this range of 1.0 cm^{-1} corresponding to ca. 3.13×10^{15}

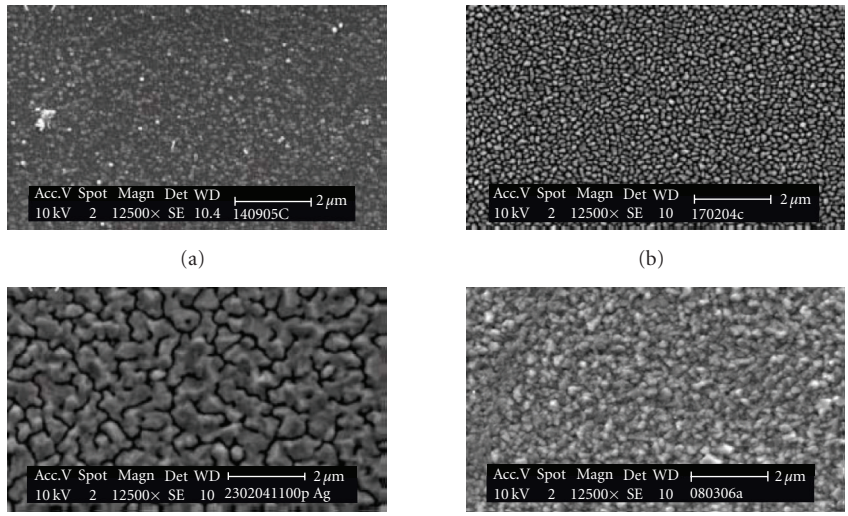

Figure 2: SEM images of (a) Ag 2 passes, (b) Ag 30 passes, (c) Ag 100 passes, (d) electroplate Ag.

molecules cm^{-2} [26]. The stearic acid (100 μl of 10 mmoL in methanol) was spun coated onto the sample. After drying in an oven, the sample was exposed to UV light with an intensity of 3 mW/cm^2. For visible light measurements, a high-intensity tungsten/halogen lamp (300 W) with a 400 nm cut-off filter was used.

3. RESULTS AND DISCUSSION

In order to understand the influence of the various layer structures, both silver (by FACVD) and titania (by thermal CVD) were grown. The silver films were analysed, and both the silver and titania films were tested for photoactivity in the visible and the UV regions.

3.1. Visual

The Ag films were produced with a range of thickness (60–250 nm), by increasing the number of passes of the moving substrate under the flame. The comparison TiO_2 films were all transparent (80 nm) with a brown tinge due to interference colouration. Visually, all the Ag films were highly reflective, with a pale pink tinge which darkens to purple for thicker coatings. The films could withstand gentle rubbing or sonification. Those with an upper layer of TiO_2 were slightly more robust.

3.2. X-ray diffraction

All Ag films (FACVD and electroplated) were crystalline showing metallic cubic Ag only (JCPDS 04-0783). That of the titania was anatase (JCPDS 21-1272) when grown directly on a glass substrate (or under Ag film), while it contained some rutile (calculated at 33 wt%) when grown on top of the Ag film. Use of Scherrers formula [27] allows calculation of crystallite size (Table 1). The calculation is ideally for a powder not a thin film, so will contain line width broadening from strain as well as crystallite size. Despite these reservations, the values obtained will give an idea of the changes occurring.

Table 1: Number of passes, thickness, and crystallite size.

Deposition time (number of passes)	Thickness, nm	Crystallite size, nm
2	60	11
4	61	12
30	93	20
100	250	38
Electroplate	104	33

3.3. Chemical composition

Confirmation that the Ag films consisted of metallic Ag, not oxides (or sulphides) came from the XPS. The high-resolution scan only showed the 3d signals at $3d_{5/2}$ = 368.7 eV and $3d_{3/2}$ = 374.7 eV with a splitting of 6 eV which are characteristic of metallic Ag. From the wide scan, a small amount of Si was detected, which almost certainly comes from the glass substrate. The O 1s signal consisted only of a single peak at 532.7 eV relating to absorbed water on the surface. No O 1s or Ag 3d signal was present for an oxide.

Both TiO_2 deposited over Ag and the inverse (Ag over TiO_2) established that there was both TiO_2 and Ag on the surface. Obviously, in the case of Ag over TiO_2 the intensity of the Ag signal was greater. The high-resolution scan showed Ti 2p signals at $2p_{1/2}$ = 464.7 eV and $2p_{3/2}$ = 459.0 eV, with a splitting of 5.7 eV, characteristic of TiO_2. This was confirmed by the O 1s signal at 530.2 eV.

3.4. Morphology

From the SEM can be seen (Figure 2) that in the early stages of thin film growth the Ag deposits as particles rather than

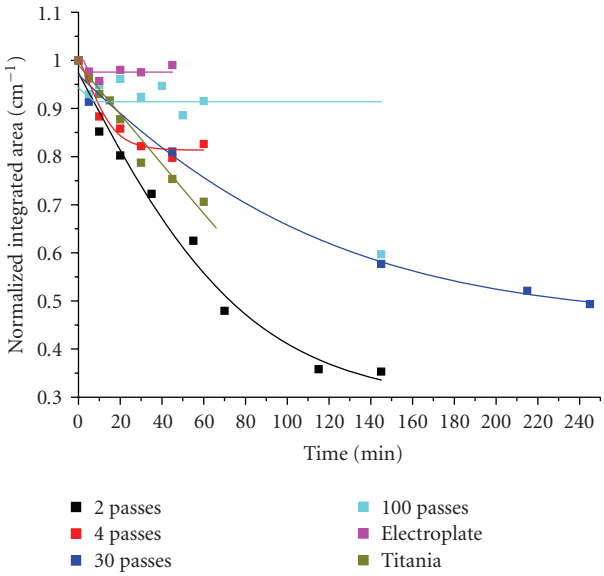

FIGURE 3: UV photoactivity for Ag films of differing thickness (2, 4, 30, and 100 passes). Also included are the results for the electroplate silver (■) and an 80 nm thick film of titania (■).

a continuous film. The exact size and spacing depend on the growth conditions [28]. It is also important to note that the sample thickness is more correctly the height of the individual islands. As the number of passes is increased the particles gradually coalesce and form a continuous sheet. As can be seen in Figure 2(d), the electroplate Ag forms a continuous film with a granular surface.

3.5. Photoactivity

The photoactivity was assessed by use of stearic acid as a model system, as stearic acid simulates a typical type of solid organic film that deposits on glass and ceramic surfaces. However, it is important to note that if a material is highly photoactive with one model compound, it does not necessarily mean that it is as active with another, or even that the same relative rates of activity can be determined. This has been previously clearly shown with titania [29, 30].

3.5.1. Photoactivity under UV radiation

The rate at which the stearic acid was decomposed is shown by the integrated area under the IR signals from the stearic acid (2957.5, 2922.8, and 2853.4 cm^{-1}), which are directly proportional to the concentration. For a period of up to 70 minutes, the FACVD Ag films showed signs of photoactivity, which then levelled out, as seen below in Figure 3. This is particularly obvious for the thinnest sample of 2 passes (60 nm). This behaviour does not occur for the thickest FACVD film of 100 passes (250 nm) or the electroplate film (104 nm).

There is an increased scatter in some of the measurements (enhanced by the normalisation). This is particularly obvious for the thickest film (100 passes) due to increased roughness and haziness. The hazy appearance of the thick samples is due to increased crystalline disorder and increased crystallite size (i.e., above a critical particles size a film is perceived as hazy as more light is scattered).

That these decay curves for silver are real and not an artefact of the experimental set up (or instrument fault), a film of TiO_2 was run over the same experimental period, showing the expected zero-order curve as the stearic acid decomposes, (as seen in Figure 3). This is of a similar order to the initial rate of reaction (0–70 minutes) of the thinnest Ag layer (60 nm). A linear fit giving $0.0026 \pm 0.0002\,\text{cm}^{-1}\,\text{min}^{-1}$ (8.13×10^{12} molecules $\text{cm}^{-2}\,\text{min}^{-1}$) for the TiO_2 film and $0.0025 \pm 0.0002\,\text{cm}^{-1}\,\text{min}^{-1}$ (7.81×10^{12} molecules $\text{cm}^{-2}\,\text{min}^{-1}$) for the initial rate of the Ag layer (2 passes). Most of the curves shown are obviously not linear, so have been fitted by a sigmoidal fit.

The lack of activity for the thick films may relate to differences in the morphology (continuous rather than island formation) and the crystallite size. As previously noted the thinner films have much smaller crystallite sizes (11–20 nm) than that for the thicker films (33–38 nm). This change in crystallite size relates to the extent of deposition. Also, the smaller the nanoparticles, the greater the surface area and hence increased rate of photoactivity.

From Figure 3, in particularly those for 4 and 2 passes, it can be seen that a point is reached at which no more stearic acid is decomposed. These coatings are noncontinuous, but previous research has shown that a pollutant can be removed from incomplete coatings of TiO_2 due to the mobile electron/hole during the photoactive process [31]. This is not occurring here, suggesting that the mechanism for TiO_2 photoactivity is different to that of the Ag.

3.5.2. Photoactivity under visible radiation

Before running the experiments, the emission of the "visible" lamp with and without the 400 nm cut-off filter was checked. This confirmed that no obvious emission below 398 nm was detected with the filter in place.

Considering the UV experiments, a sharp reduction of the stearic acid is followed by a point of no change for the thinner samples (Figure 4), while the thicker samples do not show this behaviour, and confirming lack of photoactivity. For reference, a film of TiO_2 (which is not expected to show any visible activity) has been added. This can be seen to show a slight reduction in values with time ($10^{-4}\,\text{cm}^{-1}\,\text{min}^{-1}$, 3.12×10^{12} molecules $\text{cm}^{-2}\,\text{min}^{-1}$), relating to stearic acid changes due to temperature fluctuations and possibly UV undetected by the emission spectra. This trend is in line with that seen for the thicker samples (100 pass FACVD and electroless plate). The thinner samples show a much more pronounced change.

As before, it is proposed that the initial activity seen relates to the formation of nanoparticles in the FACVD which do not occur in the electroplate silver, along with the difference in the morphology. As noted earlier, the thinner FACVD films exist as islands of Ag, rather than continuous film (100 pass and electroplate). Calzaferri et al. [14] suggest that Ag clusters on the surface sensitise the photocatalytic process. These clusters lead to the formation of empty Ag

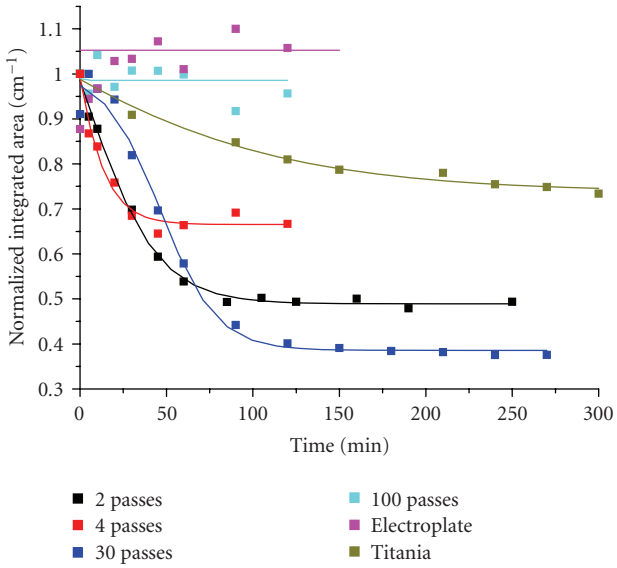

Figure 4: Visible photoactivity for Ag films of differing thickness (2, 4, 30, and 100 passes). Also included are the results for the electroplate silver (■) and an 80 nm thick film of titania (■).

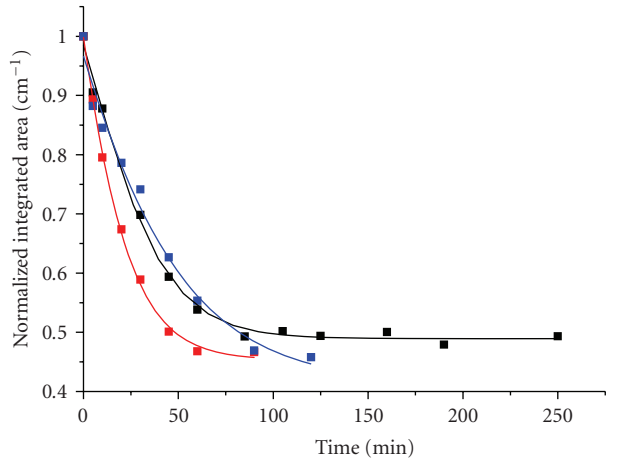

Figure 5: Repeated addition of stearic acid on a single Ag sample (2 passes). First stearic acid run ■, additional stearic acid added, and the experiment repeated once ■, twice ■.

energy levels lower than those in the bulk metal, and so enable a new transition, extending the process from the UV into the visible.

Interestingly, it was possible to repeat this behaviour on addition of more stearic acid, as shown in Figure 5 using the thinnest Ag layer (2 passes). After the standard stearic acid test had been carried out, more stearic acid was spun coated onto the sample and the test repeated. As can be seen the same trend occurs. The initial rate of the reaction (gradient) showed no significant change at $0.0033 \pm 0.0004\,\text{cm}^{-1}\,\text{min}^{-1}$ (1.25×10^{13} molecules $\text{cm}^{-2}\,\text{min}^{-1}$). In fact, this value is compatible to the UV activity of a TiO_2 film (80 nm).

A possible explanation for this behaviour is that the stearic acid would react with the Ag at the islands, but no

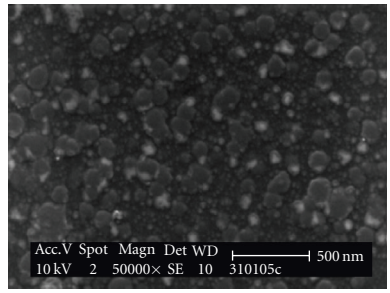

Figure 6: SEM image of an Ag sample (2 pass) after stearic acid decomposition has stopped.

reaction would occur between them (being on glass not Ag). When all the stearic acid on the island was used up, no more reaction would occur. On addition of more stearic acid, the process would begin again. This would seem to be in agreement with the SEM (Figure 6) taken after the reaction had finished, showing a patchy coating of stearic acid rather than a film.

As in the case of UV photoactivity, the presence of smaller nanoparticles will increase the surface area available and so increase any reaction between the stearic acid and the film.

As standard practice, the samples were exposed to UV light for 4 hours before the visible experiment as previous work had shown that this gave improved visible photoactivity of sol-gel produced, Ag-doped TiO_2 samples [32, 33]. This is considered due to the UV partially reducing the TiO_2 and favouring the electron transfer to Ag [34]. However, the above experiment with repeated layers of stearic acid showed that this was not necessary for just Ag films (opposed to TiO_2-Ag). Exposing the sample to UV light should reduce any Ag^+ ions to Ag metal, as is common practice for the formation of Ag/TiO_2 from $TiO_2/AgNO_3$ for sol-gel films [35].

It has previously been mentioned that under UV light any Ag^+ would be reduced to Ag metal. However, under visible light in the presence of O_2 this process can be reversed with O_2 acting as an electron acceptor for the photoexcited Ag. This was shown to be a reversible sequence (between UV/visible) by Ohko et al. [36]. Films of AgCl were found to be photocatalytic for the oxidation of water, but only in the presence of excess Ag^+. This photoactivity expanding from the UV to visible due to self-sensitisation [14]. The presence of the excess Ag^+ was considered to be responsible for the self-sensitisation with the band gap of AgCl being decreased due to these Ag ion 5s states. For our experiments, there is no initial high concentration of Ag^+ ions, as no other chemical species than Ag metal were detectable by the limits of XRD or XPS.

Similar experiments were done using multilayers of TiO_2 and Ag. As previously mentioned, if TiO_2 was deposited on top of Ag, anatase with a small amount of rutile was produced. Also, the layer was not continuous, so both Ag and TiO_2 were present on the top surface.

This again (Figure 7) shows the trend seen with the Ag films, along with the ability to repeat the experiment on adding more stearic acid on completion of the first

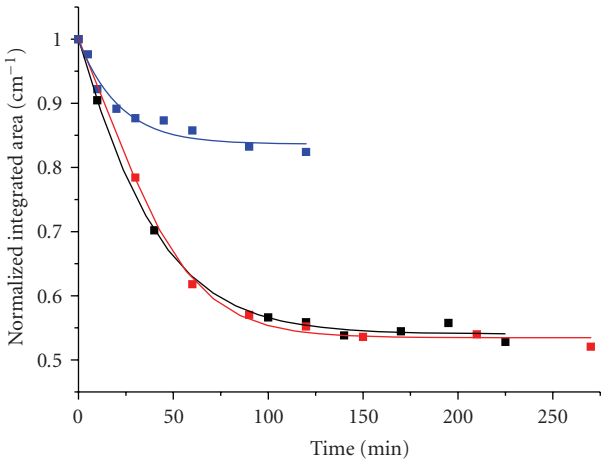

Figure 7: Visible stearic acid tests for TiO_2 over Ag (2 passes). First stearic acid run ■, additional stearic acid and experiment repeated ■, titania film ■.

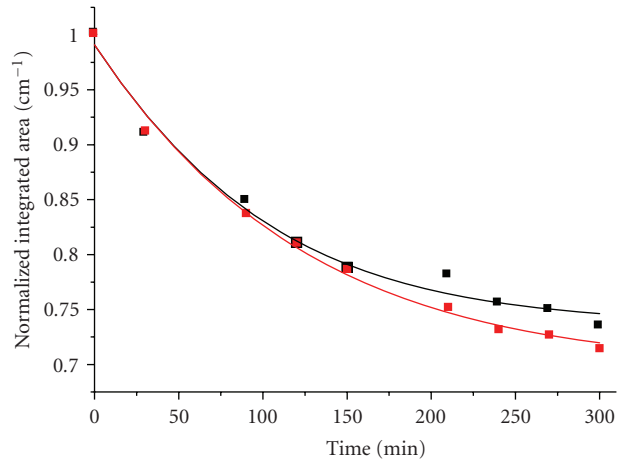

Figure 8: Visible activity of Ag on TiO_2 ■ compared to that of TiO_2 ■.

experiment. The TiO_2 film is also plotted, so the contrast between no activity (TiO_2) and activity (TiO_2 on Ag) can be more clearly seen.

Growth Ag (2 passes) on top of TiO_2 again led to a surface containing Ag and TiO_2 (anatase only). In this case, no sign of activity was seen (Figure 8), with the multilayer giving the same lack of activity as seen in the comparison TiO_2 sample. Both samples gave rates of $10^{-4}\,cm^{-1}\,min^{-1}$ (3.12×10^{12} molecules $cm^{-2}\,min^{-1}$), which are similar to that obtained by uncoated float glass. The complete lack of any activity due to the Ag is surprising given the previous results. Possibly there is an advantage having a mixture of rutile and anatase rather than just anatase as rutile absorbs a higher wavelength of light than anatase, which may in some way help the decomposition of stearic acid which occurs. Also, the presence of rutile may favour the TiO_2 over Ag sample, as it was previously shown by Sclafani et al. [34] that rutile, but not anatase improved the UV photoactivity of sol-gel mixed TiO_2/Ag samples. However, this cannot be the full explanation, as the films of just Ag show photoactivity. Alternatively, deposition of Ag on top of TiO_2, rather than directly on the barrier glass may alter either the amounts or dispersion of Ag being deposited and hence may reduce its effect on the stearic acid. If as earlier postulated the structure of the Ag is of importance and then by growth on a different effective substrate, this structure is changed, hence curtailing the photoactivity. However, the Ag crystallite size itself has not been altered whether grown on either material, so indicating the FACVD deposition process was controlling this property.

The mechanism by which Ag (under certain conditions) removes stearic acid is not clear at this stage. We can speculate on this, as to whether this is a photocatalytic process or a photoactive reduction/oxidation reaction. In this regard, some key points (noted in the above section) are as follows:

(i) under both UV and visible light, stearic acid can be decomposed;

(ii) such degradation only occurs for the thin films of Ag and TiO_2 over Ag (which actually consists of TiO_2 interspersed with Ag clusters);

(iii) the reaction tails off before completion;

(iv) the behaviour can be repeated on the same sample;

(v) the (active) thin films consist of noncontinuous island growth of small Ag clusters. Significantly, the two films where no reaction occurred were for the thick, continuous films of 100 passes FACVD, and the electroplate film. Both also have the largest crystallite sizes.

The decomposition of the stearic acid might initially suggest a photocatalytic process particularly as the behaviour seems to be repeatable on the same sample. However, the reaction tails off implying that the active species may be being depleted which would suggest a photoactive oxidation/reduction process. It is possible that under more extended testing, full depletion may be observable. However, such a simple silver depletion driven reaction is hard to rationalise with the observation that reaction does not occur (or is substantially slower) in two types of silver films. We could speculate that, in this instance, presence of the nanoparticulate films consisting of isolated clusters, and below a critical crystallite size, is of paramount importance for these UV and visible activated decompositions of stearic acid. Additional studies are planned to try to further elucidate the mechanism involved.

4. SUMMARY

By use of FACVD, with aqueous precursors, it has been shown possible to controllably deposit polycrystalline cubic Ag films. The thickness of the film and morphology can be controlled by the number of passes of the burner head over the substrate. The comparison TiO_2 is stoichiometric anatase. The silver films deposited in an island formation which gradually closed up becoming a continuous film by

a thickness of 250 nm. This nanostructure could be varied by controlling the growth conditions. These films were compared with a continuous film of Ag produced by the electroplate method. All the silver films which consisted of the noncontinuous nanostructure demonstrated an initial visible activity to stearic acid, which was shown to be repeatable on the same sample, although they did not go to completion. No activity was shown by the continuous films of 100 passes or the electroplate samples for UV or visible, suggesting that the nanostructure is a significant factor in the photoactivity seen with stearic acid in the thinner films.

By use of multilayers of thin coatings of Ag under TiO_2, it is possible to combine the visible photoactivity of the Ag and complement its UV activity with the excellent photoactivity of TiO_2. This has potential use in the commercial sector due to the shown repeatable measurement, along with the improved durability of the product over that of just Ag.

ACKNOWLEDGMENTS

This work is partially financed by the EC through GRD1-2001-40791, PHOTOCOAT project. LB thanks Corus Plc for financial support.

REFERENCES

[1] X. Z. Li, F. B. Li, C. L. Yang, and W. K. Ge, "Photocatalytic activity of WO_x-TiO_2 under visible light irradiation," *Journal of Photochemistry and Photobiology A*, vol. 141, no. 2-3, pp. 209–217, 2001.

[2] Q. Li, W. Liang, and J. K. Shang, "Enhanced visible-light absorption from PdO nanoparticles in nitrogen-doped titanium oxide thin films," *Applied Physics Letters*, vol. 90, no. 6, Article ID 063109, 3 pages, 2007.

[3] S. Sakthivel and H. Kisch, "Daylight photocatalysis by carbon-modified titanium dioxide," *Angewandte Chemie International Edition*, vol. 42, no. 40, pp. 4908–4911, 2003.

[4] R. Asahi, T. Morikawa, T. Ohwaki, K. Aoki, and Y. Taga, "Visible-light photocatalysis in nitrogen-doped titanium oxides," *Science*, vol. 293, no. 5528, pp. 269–271, 2001.

[5] H. Yamashita, M. Harada, J. Misaka, et al., "Application of ion beam techniques for preparation of metal ion-implanted TiO_2 thin film photocatalyst available under visible light irradiation: metal ion-implantation and ionized cluster beam method," *Journal of Synchrotron Radiation*, vol. 8, part 2, pp. 569–571, 2001.

[6] H. M. Yates, M. G. Nolan, D. W. Sheel, and M. E. Pemble, "The role of nitrogen doping on the development of visible light-induced photocatalytic activity in thin TiO_2 films grown on glass by chemical vapour deposition," *Journal of Photochemistry and Photobiology A*, vol. 179, no. 1-2, pp. 213–223, 2006.

[7] W. Choi, A. Termin, and M. R. Hoffmann, "The role of metal ion dopants in quantum-sized TiO_2: correlation between photoreactivity and charge carrier recombination dynamics," *Journal of Physical Chemistry*, vol. 98, no. 51, pp. 13669–13679, 1994.

[8] J. Wang, S. Yin, M. Komatsu, Q. Zhang, F. Saito, and T. Sato, "Photo-oxidation properties of nitrogen doped $SrTiO_3$ made by mechanical activation," *Applied Catalysis B*, vol. 52, no. 1, pp. 11–21, 2004.

[9] Y. Y. Mi, S. J. Wang, J. W. Chai, et al., "Effect of nitrogen doping on optical properties and electronic structures of $SrTiO_3$ films," *Applied Physics Letters*, vol. 89, no. 23, Article ID 231922, 3 pages, 2006.

[10] A. Dobosz and A. Sobczyński, "The influence of silver additives on titania photoactivity in the photooxidation of phenol," *Water Research*, vol. 37, no. 7, pp. 1489–1496, 2003.

[11] J.-W. Yoon, T. Sasaki, and N. Koshizaki, "Dispersion of nano-sized noble metals in TiO_2 matrix and their photoelectrode properties," *Thin Solid Films*, vol. 483, no. 1-2, pp. 276–282, 2005.

[12] T. H. James, *The Theory of the Photographic Process*, MacMillan, New York, NY, USA, 4th edition, 1977.

[13] W. H. Armistead and S. D. Stookey, "Photochromic silicate glasses sensitized by silver halides," *Science*, vol. 144, no. 3615, pp. 150–154, 1964.

[14] G. Calzaferri, D. Brühwiler, S. Glaus, D. Schürch, A. Currao, and C. Leiggener, "Quantum-sized silver, silver chloride and silver sulfide clusters," *Journal of Imaging Science and Technology*, vol. 45, no. 4, pp. 331–339, 2001.

[15] M. C. Kanan, S. M. Kanan, and H. H. Patterson, "Luminescence properties of silver(I)-exchanged zeolite Y and its use as a catalyst to photodecompose carbaryl in the presence of natural organic matter," *Research on Chemical Intermediates*, vol. 29, no. 7-9, pp. 691–704, 2003.

[16] M. Matsuoka, K. Iino, H. Chen, and M. Anpo, "Local structures of Ag (I) clusters prepared within zeolites by ion-exchange method and their photochemical properties," *Research on Chemical Intermediates*, vol. 31, no. 1–3, pp. 153–165, 2005.

[17] M. Matsuoka, W.-S. Ju, H. Yamashita, and M. Anpo, "In situ characterization of the Ag^+ ion-exchanged zeolites and their photocatalytic activity for the decomposition of N_2O into N_2 and O_2 at 298 K," *Journal of Photochemistry and Photobiology A*, vol. 160, no. 1-2, pp. 43–46, 2003.

[18] L. J. Guo, Q. Xing, X. L. Liu, Y. B. Huang, and Y. J. Mo, "The structure and properties of self-assembly complex LB films of silver nanoparticles," *Spectroscopy and Spectral Analysis*, vol. 25, no. 5, pp. 726–729, 2005.

[19] S. Chandra, J. N. Sharma, V. K. Mohabey, and R. C. Agrawal, "Superionic solid film. III. Preparation and electrical conductivity of cation substituted silver iodide based superionic solid $NH_4Ag_4I_5$," *Journal of Physics D*, vol. 13, no. 3, pp. 495–502, 1980.

[20] Z. Liu, X. Wang, H. Wu, and C. Li, "Silver nanocomposite layer-by-layer films based on assembled polyelectrolyte/dendrimer," *Journal of Colloid and Interface Science*, vol. 287, no. 2, pp. 604–611, 2005.

[21] Y. S. Jung, "Study on texture evolution and properties of silver thin films prepared by sputtering deposition," *Applied Surface Science*, vol. 221, no. 1–4, pp. 281–287, 2004.

[22] T. L. Alford, L. Chen, and K. S. Gadre, "Stability of silver films on underlying layers at elevated temperatures," *Thin Solid Films*, vol. 429, no. 1-2, pp. 248–254, 2003.

[23] M. Abourida, H. Guillon, C. Jimenez, et al., "Silver thin films deposited by injection MOCVD," in *Proceedings of the 203rd Meeting of the Electrochemical Society*, pp. 938–945, Paris, France, August 2003.

[24] L. Gao, P. Härter, C. Linsmeiner, A. Wiltner, R. Emling, and D. S. Landsied, "Silver MOCVD for advanced silver metallization," *Microelectronic Engineering*, vol. 82, no. 3-4, pp. 296–300, 2005.

[25] L. A. Brook, P. Evans, H. A. Foster, et al., "Highly bioactive silver and silver/titania composite films grown by chemical vapour deposition," *Journal of Photochemistry and Photobiology A*, vol. 187, no. 1, pp. 53–63, 2007.

[26] Y. Paz, Z. Luo, L. Rabenberg, and A. Heller, "Photo-oxidative self-cleaning transparent titanium dioxide films on glass," *Journal of Materials Research*, vol. 10, no. 11, pp. 2842–2848, 1995.

[27] B. D. Cullity, *Elements of XRD*, Addison-Wesley, Reading, Mass, USA, 1978.

[28] D. W. Sheel, L. A. Brook, and H. M. Yates, "Controlled nanostructured silver coated surfaces by atmospheric pressure chemical vapour deposition," *Chemical Vapour Deposition*, vol. 14, no. 1-2, pp. 14–24, 2008.

[29] W. Choi and J. Ryu, "Multi-aspects of photocatalytic activities of TiO_2: substrate specificity and implication for the activity test standardization," in *Proceedings of the 2nd International Conference on Semiconductor Photochemistry*, Aberdeen, UK, July 2007.

[30] A. Mills and S. Le Hunte, "An overview of semiconductor photocatalysis," *Journal of Photochemistry and Photobiology A*, vol. 108, no. 1, pp. 1–35, 1997.

[31] S.-K. Lee, S. McIntyre, and A. Mills, "Visible illustration of the *direct*, *lateral* and *remote* photocatalytic destruction of soot by titania," *Journal of Photochemistry and Photobiology A*, vol. 162, no. 1, pp. 203–206, 2004.

[32] E. Stathatos, T. Petrova, and P. Lianos, "Study of the efficiency of visible-light photocatalytic degradation of basic blue adsorbed on pure and doped mesoporous titania films," *Langmuir*, vol. 17, no. 16, pp. 5025–5030, 2001.

[33] J.-M. Herrmann, H. Tahiri, Y. Ait-Ichou, G. Lassaletta, A. R. Gonzalez-Elipe, and A. Fernandez, "Characterisation and photocatalytic activity in aq. medium of TiO_2 and Ag-TiO_2 coatings on quartz," *Applied Catalysis B*, vol. 13, no. 3-4, pp. 219–228, 1997.

[34] A. Sclafani and J.-M. Herrmann, "Influence of metallic silver and of platinum-silver bimetallic deposits on the photocatalytic activity of titania (anatase and rutile) in organic and aqueous media," *Journal of Photochemistry and Photobiology A*, vol. 113, no. 2, pp. 181–188, 1998.

[35] A. Sclafani, M.-N. Mozzanega, and J.-M. Herrmann, "Influence of silver deposits on the photocatalytic activity of titania," *Journal of Catalysis*, vol. 168, no. 1, pp. 117–120, 1997.

[36] Y. Ohko, T. Tatsuma, T. Fujii, et al., "Multicolour photochromism of TiO_2 films loaded with silver nanoparticles," *Nature Materials*, vol. 2, no. 1, pp. 29–31, 2003.

Hindawi Publishing Corporation
International Journal of Photoenergy
Volume 2008, Article ID 470670, 6 pages
doi:10.1155/2008/470670

Research Article

A Study of Factors that Change the Wettability of Titania Films

Andrew Mills and Matthew Crow

Department of Pure and Applied Chemistry, University of Strathclyde, 295 Cathedral Street, Glasgow, G1 1XL, UK

Correspondence should be addressed to Andrew Mills, a.mills@strath.ac.uk

Received 25 July 2007; Accepted 3 January 2008

Recommended by Russell Howe

The effect of several pretreatment methods on the wettability of polycrystalline titania-coated glass (Pilkington Activ) and plain glass are investigated. UV/ozone, immersion in aqua regia, and heating ($T > 500^\circ C$) render both substrates superhydrophilic (i.e., water contact angle (CA) $< 5^\circ$). The dark recovery of the contact angles of these superhydrophilic substrates, monitored after treatment in either an evacuated or an ambient atmosphere, led to marked increases in CA. Ultrasound treatment of superhydrophilic Activ and glass samples produced only small increases in CA for both substrates, but rubbing the samples with a cloth produced much larger increases. The results of this study are discussed in the context of the current debate over the mechanism of the photo-induced superhydrophilic effect.

1. INTRODUCTION

Titanium dioxide films have been widely observed to become superhydrophilic, that is, water droplet contact angle $< 5^\circ$, when exposed to ultraviolet (UV) light, a phenomenon termed photoinduced superhydrophilicity (PSH) [1–7]. Its effects have been pivotal in the development of self-cleaning surfaces for glazing and other applications, but the precise mechanism by which this change is effected remains the subject of some debate, although it is clear that PSH is initiated by the photogeneration of electron/hole pairs and their migration to the surface. An essential feature of the overall PSH phenomenon is not only the initial, photo-induced hydrophobic to hydrophilic change, but also the reverse, dark process, whereby a superhydrophilic titania film recovers its original hydrophobic form. Any mechanism of PSH must embrace both the light-induced superhydrophilic process and the dark hydrophobic recovery step.

In 1985 Kume and Nozu of Nihon Itagarasu, Japan reported that sheet glass coated with TiO_2 had the ability to stay clean by "…rapidly and automatically decomposing and removing organic stains adhered to the glass surface…" [8]. Most importantly, part of their patent application involved the observation that the contact angle made by a water droplet on the glass, that is, CA, was reduced as a function of UV irradiation time. This appears to be the first clear claim of a PSH effect relating to titania films on glass and explanation for the effect, namely, it is due to the removal of hydrophobic organic stains on the surface, via the following, well-established, photocatalytic oxidative (PCO) process:

$$\text{organic} + O_2 \xrightarrow[h\nu \geq 3.2\,\text{eV}]{TiO_2} \text{minerals} \quad (\text{e.g., } CO_2 \text{ and } H_2O). \quad (1)$$

In contrast, in 1997, Wang et al. [6], reporting on the UV-induced PSH of TiO_2/SiO_2 films, proposed that the effect was not due to PCO but rather the dissociative adsorption of water at surface defects created by UV light [9]. The defects, it was suggested, were formed by the trapping of holes at bridging oxygen lattice points close to the surface, the Ti^{4+} sites being reduced to Ti^{3+} by the electrons and oxygen atoms being ejected to form vacancies [10]. The oxygen vacancies were thought to cause an increase in the adsorbed hydroxyl group density and lead to the formation of hydrophilic regions. It was proposed that storage in the dark, in the presence of oxygen, removed the defects replacing the chemisorbed hydroxyl groups with oxygen and so returning the surface to its original hydrophobic state. A very simple summary of this surface reorganisation

mechanism for PSH is as follows:

$$\equiv \mathrm{Ti} - \mathrm{O} - \mathrm{Ti} \equiv + \mathrm{H_2O} \underset{\text{dark}}{\overset{\mathrm{O_2}, h\nu \geq E_{BG}}{\longleftrightarrow}} \equiv \mathrm{Ti} - \mathrm{OH}\ \mathrm{HO} - \mathrm{Ti} \equiv . \quad (2)$$

It has been suggested that the above mechanism is specific to only a few materials of which titania is most notable, for example, it is not exhibited by silica substrates, that is, glass. This photo-induced surface reorganisation (PISR) model of PSH has received support from a number of different studies including examination of the creation of Ti^{3+} defects on single-crystal rutile TiO_2 using XPS [11]; FTIR measurements that reveal anatase TiO_2 is able to adsorb water reversibly upon UV irradiation [10]; and AFM studies which show apparent "roughening" of the surface as a result of UV exposure (attributed to defect formation) [12]. The importance of bridging oxygen, an integral part of the PISR model, has also been illustrated using rutile single crystals, with the (001) face—which does not feature bridging oxygens—showing the least propensity to photo-induced hydrophilic change [10, 13].

Recently, support for the more simplistic PCO model of PSH, based on reaction (1), namely, the photocatalytic removal of hydrophobic organic surface contaminants, has increased with a number of different groups reporting evidence for this model using test hydrophobic surface contaminants such as trimethyl acetate [14] and hexane [15], and the detection of previously unobserved layers of hydrocarbons on titania surfaces [16]. These results have presented a significant challenge to the PISR model of PSH.

Key to any model of PSH is an explanation of the dark recovery step, and significant support for this aspect of the PISR model of PSH effectively a dark, dehydration step (see reaction (2)) has been provided by studies [10, 17, 18] which show that titania films regain their original hydrophobicity at an increased rate when stored at increased temperatures [18, 19] or under an evacuated (H_2O free) atmosphere [17]. The PISR model rationale behind this is that heat and vacuum cause the metastable water/hydroxyl groups, responsible for the superhydrophilic surface of titania, to dissociate more quickly. It has also been demonstrated that hydrophilic TiO_2-glass films exhibit a measurable increase in contact angle when subjected to ultrasound [20]. The use of ultrasound to render a superhydrophilic film slightly more hydrophobic was interpreted initially by advocates of the PISR model as being due to the reoxidation of the surface by sonically produced OH radicals [20], but more recently as simply the breaking down of the photo-induced hydrophilic metastable state by an external stimulus [18]. A similar interpretation has been used to explain the effect of wet rubbing [21], which reconverts superhydrophilic titania to its original hydrophobic state via a mechanochemical effect.

In this paper, the effects of UV/O_3, heating, and strong acid pretreatment on initially hydrophobic samples of Activ and plain glass were studied. In addition, the effects of vacuum, ultrasound, and rubbing on the wettability of clean, superhydrophilic samples of titania-coated, self-cleaning glass (Activ), and plain glass were examined and the results discussed in terms of the two different mechanisms of the PSH effect.

2. EXPERIMENTAL

All reagents, unless otherwise stated, were supplied by Aldrich and used as received. The titania-coated substrates used in this work were 2 cm × 2 cm Activ samples, supplied by Pilkington Glass, comprising 4 mm thick float glass coated with an approximately 15 nm layer of TiO_2, deposited by an inline CVD process [22]. The reverse side of Activ provided the samples of uncoated float-glass used in all "plain glass" blank experiments. Additional experiments revealed no difference in behaviour between that of the reverse side of Activ and uncoated float glass samples. Typically, all glass samples, that is, Activ or plain, were cleaned with chloroform and left in a sealed box in the dark for in excess of one month before use. Unless otherwise stated, both types of glass were rendered superhydrophilic by pretreating with UVC/ozone, effected by irradiation with 2 × 6 W UVC (254 nm) bulbs (Vilber-Lourmat, Torcy, France), irradiance ~1 mW cm^{-2}, in a water saturated, that is, 100% relative humidity (RH), oxygen atmosphere containing ~1700 ppm ozone, produced by a corona-discharge ozone generator (OZ500, Dryden Aqua, Edinburgh, UK).

Other pretreatment methods used included a heat-treatment process, using a muffle furnace, in which the samples were kept at the desired temperature for 1 hour before removing to cool to room temperature in a covered Petri dish. Aqua regia was also used as a pretreatment method and involved immersing the samples for 1 hour in the aqua regia before being removed, rinsed with doubly-distilled, deionised water and dried in a stream of cylinder air.

Water droplet contact angles, CAs, were measured using an FTA100 system comprising a CCTV camera interfaced with a computer, which provided a continuous stream of images of any water droplet after its initial deposition onto the surface of the substrate under test. Droplets were deposited using a 500 μL Gastight (Hamilton) syringe, via a 30-gauge stainless steel needle with 0° bevel (Kahnetics), which deposited reproducible 5 μL water droplets. The software package associated with the instrument allowed calculation of the contact angle made by the water droplet deposited on the substrate by curve fitting the droplet image outline. Three droplets were deposited per sample and the average of the contact angles determined with a typical variance of <5%.

The study of the kinetics of contact angle recovery of samples held under vacuum was carried out using a vacuum desiccator connected to a vacuum line. Noncovered samples were simply left on the benchtop in a light-free laboratory. For the investigation of ultrasonic (US) recovery, samples of superhydrophilic Activ or glass were immersed in doubly-distilled, deionised water and placed in a US bath (VWR model: USC100T). All glassware for this section was thoroughly cleaned with chloroform and rinsed with water before use. Sample handling was carried out using plastic

Table 1: Table of water contact angles for Activ and glass samples before and after pretreatment.

Pretreatment method	Activ		Glass	
	initial CA/°	final CA/°	initial CA/°	final CA/°
UVC/O_3[(a)]	71	<5	35	<5
Δ 500°C[(b)]	70	<5	37	<5
Aqua regia[(c)]	70	<5	38	<5

[(a)] Samples irradiated by 2 × 6 W UVC bulbs in ~1700 ppm O_3 for 1 hour.
[(b)] Samples heated to 500°C and held at temp for 1 hour before cooling under Petri dish.
[(c)] Immersion in 25 mL aqua regia for 1 hour before rinsing and drying.

forceps and the samples were dried with compressed air from a cylinder.

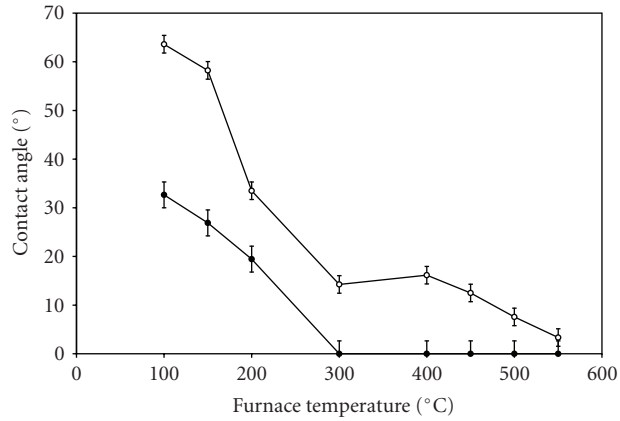

Figure 1: Plot of contact angle versus pretreatment temperature for Activ (∘) and for glass (•).

3. RESULTS AND DISCUSSION

3.1. Pretreatment cleaning methods

The combination of short wavelength ultraviolet light and ozone to create electronically excited ozone, O_3^*, a very effective oxidising agent, is well documented in its use for destroying organic materials and scouring the latter from surfaces such as semiconductor wafers [23, 24]. Recent work by this group has found that the combination of UVC and ozone as a pretreatment produces a superhydrophilic surface on Activand plain glass. These findings imply that the intrinsic state of a titania film or pristine glass is superhydrophilic, as indicated by other work on both plain glass [25] and titania [26]—such as found on Activ—and that this state requires simply the removal of all surface contaminants, particularly hydrophobic organics for its production.

The finding that UV/O_3 pretreatment renders Activ superhydrophilic fits in with both the PSIR and PCO models of PSH. However, the observation that plain glass is also rendered superhydrophilic indicates that the initial hydrophobic nature of the plain glass, and most probably Activ, is due to contamination of the surface by hydrophobic organics, at a level too low to be detected by simple FTIR. Thus, there appears no need to invoke a surface reorganisation mechanism, that is, PISR to explain PSH in titania, since the above results imply any oxidative process that removes hydrophobic surface organics, such as UVC/O_3, will render the surface of titania and glass superhydrophilic. The typical water droplet contact angles of plain and Activ glass samples before and after UV/O_3 treatment are given in Table 1.

A series of experiments were carried out to investigate a variety of other oxidising pretreatment methods, including heating and strong acid immersion, to ascertain if all were able to render Activ and plain glass superhydrophilic (i.e., CA < 5°). Thus, heating Activ and plain glass at different temperatures and testing their hydrophilic natures, via CA measurements, produced the results illustrated in Figure 1. These results show that for both substrates, the CA decreases with increasing temperature, with glass falling from an initial contact angle, CA_i, ~35° to <5° by 300°, and Activ from CA_i~70° to <5° by 550°.

That the titania substrates become hydrophilic with heat treatment appears at odds with the PSIR model of PSH, that is, reaction (2), which suggests that the dark dehydration process should be promoted by high temperatures [27], leading to either no change, or an increase in its hydrophobic nature and *not*, as observed in Figure 1, a decrease. Instead, the results in Figure 1 indicate that the initial hydrophobic character of Activ and plain glass is due to organic surface contaminants that are readily oxidised by high-heat treatment to reveal the intrinsic superhydrophilic nature of glass and titania films. From the data in Figure 1, it appears that the plain glass samples become hydrophilic at lower temperatures than Activ, probably due to a lower level of contamination on glass, which is much smoother than the titania films, rendering the latter more susceptible to organic adsorption.

In a final set of experiments, Activ and plain glass samples that were initially hydrophobic were pretreated with the very oxidising reagent, aqua regia, and all found to be rendered superhydrophilic (see Table 1).

From the above results, it appears that all three methods of pretreatment, that is, UVC/O_3, heat (>550°C), and aqua regia are able to effect the conversion of both Activ and plain glass samples from an initial hydrophobic state to a superhydrophilic state. All three methods use very strong oxidising agents/conditions to render plain and Activ glass samples superhydrophilic, most probably due to the oxidation of any surface hydrophobic organic species. These results provide significant support for the PCO model of PSH and reveal that the pristine, that is, organic-free, surfaces of these materials are superhydrophilic.

3.2. Studies of the "dark" hydrophilic to hydrophobic process

The "dark" recovery of contact angle, that is, the regeneration of hydrophobicity, exhibited by superhydrophilic titania films has been widely reported [10, 17, 22, 28], and opinion

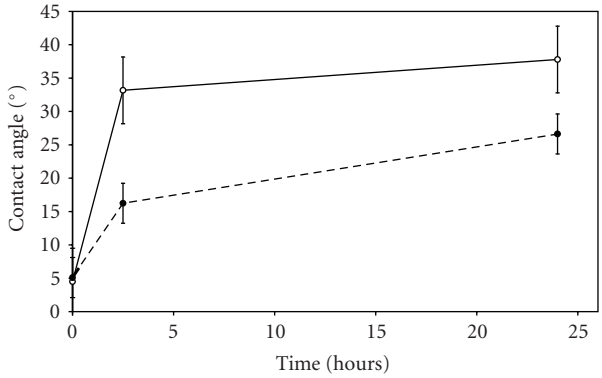

Figure 2: Water droplet contact (CA) angle versus exposure time in an evacuated atmosphere for Activ (∘) and glass (•); CA measurements recorded under ambient conditions.

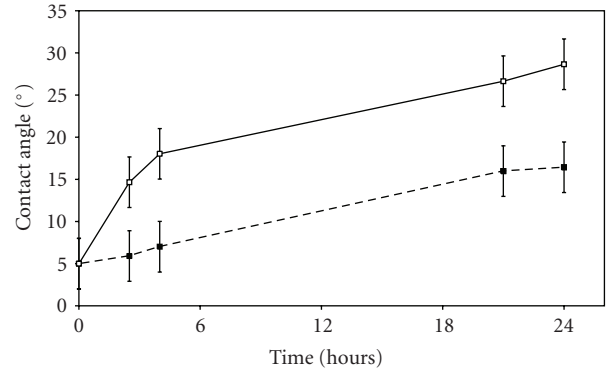

Figure 3: Variation in CA versus time for initially pristine superhydrophilic sample of Activ (□) and glass (■) under ambient laboratory conditions.

over its cause is polarised between a recontamination of the surface by airborne organics (the PCO model of PSH) and the reverse of reaction (2), that is, a dehydroxylation/dehydration process on the surface of the titania (the PISR model of PSH). Work carried out by others [17] shows that superhydrophilic samples of titania become more hydrophobic when stored in an evacuated atmosphere. These results are interpreted as providing strong evidence of the PISR model, in which vacuum storage accelerates water desorption and therefore CA recovery in superhydrophilic samples of titania. In replicating this work, we also found that the CA of Activ increases markedly when the samples are stored under vacuum, but also, and more revealing, that plain glass exhibits the same feature, although to a lesser extent. These results, illustrated in Figure 2, indicate that the phenomenon of the CA increasing for superhydrophilic titania films held under vacuum—used to support the "surface reorganisation" model, that is, reaction (2)—is not specific to titania films but is also exhibited by plain glass and so not likely to be associated with a PISR mechanism, which is attributed to titania but not to glass. Instead, the more likely explanation is that it is due to organic contamination of a clean surface, that is, glass or titania in this work, produced by exposing the sample to air when making the CA measurement after storage in a vacuum.

The effect of airborne contamination of a pristine, superhydrophilic glass, and Activ surface was demonstrated by leaving two freshly prepared samples out on the bench and monitoring the change in CA as a function of time. The results of this work are illustrated in Figure 3, from which it is clear that, on the open bench, a pristine, superhydrophilic sample of glass, or Activ can be rendered noticeably hydrophobic within few hours of exposure. Note that, as expected from its lower surface roughness, over the same time plain glass is rendered less hydrophobic than Activ due to this surface contamination. Simple IR analysis of these glass samples revealed no indication of contamination of their surfaces by hydrophobic organics, implying that the level is very low and below that detectable by conventional FTIR spectroscopy.

Table 2: Table of water contact angle for Activ and glass samples before and after either sonication or immersion for 10 minutes in deionised (DI) water.

Treatment	Activ		Glass	
	initial CA/°	final CA/°	initial CA/°	final CA/°
Sonication for 10 minutes in DI water	<5	8.9	3.8	8.2
DI water immersion for 10 minutes	<5	6.4	4.3	5.3

Previous work carried out by others [20] has shown that a superhydrophilic titania film is rendered more hydrophobic upon exposure to ultrasound (10 minutes). In another set of experiments, both glass and titania films, rendered superhydrophilic by treatment with UVC/O_3, were placed in high-purity water in clean beakers and treated with ultrasound. The measured CAs of these samples before and after exposure to ultrasound are given in Table 2 and show that for both samples upon sonication the CA rises slightly, by 3–5°, whereas without sonication the CA remains largely unchanged. These results imply that the effect of ultrasound on superhydrophilic films, be they glass or titania, is very small and most probably due to a roughening of the substrate, and/or some organic contamination. This effect is, once again, not specific to titania and would have been expected if the PISR model was appropriate.

Other work shows that any wiping or rubbing of a pristine superhydrophilic glass or titania film using a tissue or cloth renders the film hydrophobic, and this is attributed, once again, to organic contamination of the surfaces of these substrates. It appears unlikely that rubbing is able to effect the reverse of reaction (2) via a mechanochemical effect as claimed by others [21] since plain glass is affected in the same way as titania.

4. CONCLUSIONS

UV light is well known to render titania samples superhydrophilic, but this can also be effected for glass and titania

films by the combination of UVC and ozone or pretreatment with a highly oxidising solution (e.g., aqua regia) or by heating at $T > 500^{\circ}$C, suggesting that a common process is responsible for the cleaning of both substrates, namely, the removal of adventitious hydrophobic organic surface species via oxidation. These findings indicate that the pristine surfaces of plain glass and titania are intrinsically superhydrophilic and imply that the photocatalytic oxidation of organics on titania (PCO) is the most likely cause of the PSH effect.

Investigations of the recovery of the initial hydrophobicity exhibited by untreated titania or plain glass showed that, once rendered superhydrophilic, the dark hydrophilic to hydrophobic process is exhibited by both titania and plain glass films and is most likely due to contamination by airborne, hydrophobic organics. Thus, storage of titania or plain glass under vacuum, or on the open bench, leads to a noticeable increase in CA. The effect of ultrasonic treatment on contact angle recovery is very small for both plain and titania-coated glass, and probably due to surface roughening. Rubbing or wiping the hydrophilic plain glass or titania films produces a marked rise in hydrophobicity and is attributed to contamination of the surfaces by hydrophobic organics.

The work presented here provides further support for the proposal that the PSH effect is due to the UV-driven removal of hydrophobic surface organics by PCO, and the dark, slow readsorption of airborne organics.

REFERENCES

[1] M. Langlet, S. Permpoon, D. Riassetto, G. Berthomé, E. Pernot, and J. C. Joud, "Photocatalytic activity and photo-induced superhydrophilicity of sol-gel derived TiO_2 films," *Journal of Photochemistry and Photobiology A*, vol. 181, no. 2-3, pp. 203–214, 2006.

[2] A. Mills, G. Hill, S. Bhopal, I. P. Parkin, and S. A. O'Neill, "Thick titanium dioxide films for semiconductor photocatalysis," *Journal of Photochemistry and Photobiology A*, vol. 160, no. 3, pp. 185–194, 2003.

[3] M. Miyauchi, A. Nakajima, T. Watanabe, and K. Hashimoto, "Photocatalysis and photoinduced hydrophilicity of various metal oxide thin films," *Chemistry of Materials*, vol. 14, no. 6, pp. 2812–2816, 2002.

[4] I. P. Parkin and R. G. Palgrave, "Self-cleaning coatings," *Journal of Materials Chemistry*, vol. 15, no. 17, pp. 1689–1695, 2005.

[5] R.-D. Sun, A. Nakajima, A. Fujishima, T. Watanabe, and K. Hashimoto, "Photoinduced surface wettability conversion of ZnO and TiO_2 thin films," *Journal of Physical Chemistry B*, vol. 105, no. 10, pp. 1984–1990, 2001.

[6] R. Wang, K. Hashimoto, A. Fujishima, et al., "Light-induced amphiphilic surfaces," *Nature*, vol. 388, no. 6641, pp. 431–432, 1997.

[7] N. Stevens, C. I. Priest, R. Sedev, and J. Ralston, "Wettability of photoresponsive titanium dioxide surfaces," *Langmuir*, vol. 19, no. 8, pp. 3272–3275, 2003.

[8] S. Kume and T. Nozu, J. P. Patent Office, "Difficult stainable glass product," application no.: Sho 63-100042, 1988.

[9] A. Fujishima, K. Hashimoto, and T. Watanabe, *TiO_2 Photocatalysis: Fundamentals and Applications*, BKC, Tokyo, Japan, 1999.

[10] A. Fujishima, T. N. Rao, and D. A. Tryk, "Titanium dioxide photocatalysis," *Journal of Photochemistry and Photobiology C*, vol. 1, no. 1, pp. 1–21, 2000.

[11] A. N. Shultz, W. Jang, W. M. Hetherington III, D. R. Baer, L.-Q. Wang, and M. H. Engelhard, "Comparative second harmonic generation and X-ray photoelectron spectroscopy studies of the UV creation and O_2 healing of Ti^{3+} defects on (110) rutile TiO_2 surfaces," *Surface Science*, vol. 339, no. 1-2, pp. 114–124, 1995.

[12] K.-I. Katsumata, A. Nakajima, T. Shiota, et al., "Photoinduced surface roughness variation in polycrystalline TiO_2 thin films," *Journal of Photochemistry and Photobiology A*, vol. 180, no. 1-2, pp. 75–79, 2006.

[13] R. Wang, N. Sakai, A. Fujishima, T. Watanabe, and K. Hashimoto, "Studies of surface wettability conversion on TiO_2 single-crystal surfaces," *Journal of Physical Chemistry B*, vol. 103, no. 12, pp. 2188–2194, 1999.

[14] J. M. White, J. Szanyi, and M. A. Henderson, "The photon-driven hydrophilicity of titania: a model study using $TiO_2(110)$ and adsorbed trimethyl acetate," *Journal of Physical Chemistry B*, vol. 107, no. 34, pp. 9029–9033, 2003.

[15] T. Zubkoy, D. Stahl, T. L. Thompson, D. Panayotov, O. Diwald, and J. T. Yates Jr., "Ultraviolet light-induced hydrophilicity effect on $TiO_2(110)$ (1×1). Dominant role of the photooxidation of adsorbed hydrocarbons causing wetting by water droplets," *Journal of Physical Chemistry B*, vol. 109, no. 32, pp. 15454–15462, 2005.

[16] C.-Y. Wang, H. Groenzin, and M. J. Shultz, "Molecular species on nanoparticulate anatase TiO_2 film detected by sum frequency generation: trace hydrocarbons and hydroxyl groups," *Langmuir*, vol. 19, no. 18, pp. 7330–7334, 2003.

[17] H. Irie and K. Hashimoto, "Photocatalytic active surfaces and photo-induced high hydrophilicity/high hydrophobicity," in *Environmental Photochemistry Part II*, P. Boule, P. K. J. Robertson, and D. W. Bahnemann, Eds., Springer, Berlin, Germany, 2005.

[18] K. Hashimoto, H. Irie, and A. Fujishima, "TiO_2 photocatalysis: a historical overview and future prospects," *Japanese Journal of Applied Physics*, vol. 44, no. 12, pp. 8269–8285, 2005.

[19] M. Miyauchi, N. Kieda, S. Hishita, et al., "Reversible wettability control of TiO_2 surface by light irradiation," *Surface Science*, vol. 511, no. 1–3, pp. 401–407, 2002.

[20] N. Sakai, R. Wang, A. Fujishima, T. Watanabe, and K. Hashimoto, "Effect of ultrasonic treatment on highly hydrophilic TiO_2 surfaces," *Langmuir*, vol. 14, no. 20, pp. 5918–5920, 1998.

[21] M. Kamei and T. Mitsuhashi, "Hydrophobic drawings on hydrophilic surfaces of single crystalline titanium dioxide: surface wettability control by mechanochemical treatment," *Surface Science*, vol. 463, no. 1, pp. L609–L612, 2000.

[22] A. Mills, A. Lepre, N. Elliott, S. Bhopal, I. P. Parkin, and S. A. O'Neill, "Characterisation of the photocatalyst Pilkington Activ™: a reference film photocatalyst?" *Journal of Photochemistry and Photobiology A*, vol. 160, no. 3, pp. 213–224, 2003.

[23] J. R. Vig, "UV/ozone cleaning of surfaces," *Journal of Vacuum Science and Technology A*, vol. 3, no. 3, pp. 1027–1034, 1985.

[24] R. R. Sowell, R. E. Cuthrell, D. M. Mattox, and R. D. Bland, "Surface cleaning by ultraviolet radiation," *Journal of Vacuum Science and Technology*, vol. 11, no. 1, pp. 474–475, 1974.

[25] S. Takeda, M. Fukawa, Y. Hayashi, and K. Matsumoto, "Surface OH group governing adsorption properties of metal oxide films," *Thin Solid Films*, vol. 339, no. 1-2, pp. 220–224, 1999.

[26] M. Takeuchi, K. Sakamoto, G. Martra, S. Coluccia, and M. Anpo, "Mechanism of photoinduced superhydrophilicity on the TiO_2 photocatalyst surface," *Journal of Physical Chemistry B*, vol. 109, no. 32, pp. 15422–15428, 2005.

[27] A. Kanta, R. Sedev, and J. Ralston, "Thermally- and photoinduced changes in the water wettability of low-surface-area silica and titania," *Langmuir*, vol. 21, no. 6, pp. 2400–2407, 2005.

[28] N. Sakai, A. Fujishima, T. Watanabe, and K. Hashimoto, "Quantitative evaluation of the photoinduced hydrophilic conversion properties of TiO_2 thin film surfaces by the reciprocal of contact angle," *Journal of Physical Chemistry B*, vol. 107, no. 4, pp. 1028–1035, 2003.

Hindawi Publishing Corporation
International Journal of Photoenergy
Volume 2008, Article ID 168185, 11 pages
doi:10.1155/2008/168185

Review Article

Biocidal Silver and Silver/Titania Composite Films Grown by Chemical Vapour Deposition

D. W. Sheel, L. A. Brook, I. B. Ditta, P. Evans, H. A. Foster, A. Steele, and H. M. Yates

Institute for Materials Research, Salford University, Manchester, M5 4WT, UK

Correspondence should be addressed to D. W. Sheel, d.w.sheel@salford.ac.uk

Received 27 March 2008; Revised 27 March 2008; Accepted 19 May 2008

Recommended by Russell Howe

This paper describes the growth and testing of highly active biocidal films based on photocatalytically active films of TiO_2, grown by thermal CVD, functionally and structurally modified by deposition of nanostructured silver via a novel flame assisted combination CVD process. The resulting composite films are shown to be highly durable, highly photocatalytically active and are also shown to possess strong antibacterial behaviour. The deposition control, arising from the described approach, offers the potential to control the film nanostructure, which is proposed to be crucial in determining the photo and bioactivity of the combined film structure, and the transparency of the composite films. Furthermore, we show that the resultant films are active to a range of organisms, including Gram-negative and Gram-positive bacteria, and viruses. The very high-biocidal activity is above that expected from the concentrations of silver present, and this is discussed in terms of nanostructure of the titania/silver surface. These properties are especially significant when combined with the well-known durability of CVD deposited thin films, offering new opportunities for enhanced application in areas where biocidal surface functionality is sought.

1. INTRODUCTION

In recent years, TiO_2 has been widely investigated for its interesting photoexcited properties, for example, using photocatalysis can lead to the decomposition of organics into harmless products under UV light irradiation [1]. The extent of the photoactivity depends on a wide range of properties including morphology, crystallinity, and surface area.

The use of TiO_2 as a biocide was first demonstrated by Matsunaga et al. (1985) [2]. Subsequently, there have been a number of reports of disinfection of bacteria, viruses, and other micro-organisms. Most of this early work [3] used suspensions of TiO_2 and planktonic organisms. More recently, research has examined the interaction of organisms with biocidal thin films of TiO_2 anchored to solid surfaces [4–7]. Maness et al. have suggested that the mechanism by which titania is able to kill bacteria involves the disruption of the cell membrane following peroxidation of the membrane lipids by active oxygen species [3]. This is supported by the work of Sunada et al. [8] who studied killing of *Escherichia coli* on thin Cu/TiO_2 films and showed that firstly, the outer membrane was damaged followed by the cytoplamic membrane and that these processes then allowed the complete degradation of the cells. Amézaga-Madrid et al. [9] studied the inactivation of *Pseudomonas aeruginosa* and showed cell damage consistent with membrane and cell-wall damage.

Bulk Ag has been long used for coating many items including mirrors (for reflectance properties) and electrical contacts, as it is the most conductive of all metals. There is particular interest in nanoparticulate Ag due to its ability to act as both an electron sink and as redox catalyst. The antimicrobial properties of silver were well known to the ancient Egyptians and Greeks, for example, Hippocrates mentions silver as a treatment for ulcers [10]. Since then silver has been widely used as an antimicrobial agent in applications such as wound dressings and as surface coatings, for example, catheters [11, 12]. Silver has also been incorporated into bioglass [13]. Silver ions (Ag^+) interact strongly with electron donors, and the antimicrobial activity of Ag primarily involves interactions with sulphydryl groups in proteins [14–17]. Silver also reacts with other cellular components such as nucleic acids [18]. Silver has been shown to inhibit energy production by inhibition of the respiratory

chain of *Escherichia coli* [19]. Indirect toxicity may also arise from salt formation with silver ions that results in a chloride or anion limitation within the cell. Nanocrystalline silver [20] also releases Ag^0 and has been shown to rapidly kill bacteria and fungi [21]. Although Ag^+ is rapidly inactivated by interaction with organic matter, Ag^0 is much more stable [22].

The combination of Ag and TiO_2 for catalysis has been much studied for mainly sol-gel produced materials [23–25] with some colloid production of mixed [26] and core-shell composite clusters [27]. Most of these papers conclude that Ag is capable, under the correct conditions, of improving TiO_2 photoactivity. The addition of Ag promotes the charge separation of the electron-hole pairs from TiO_2 after photon absorption by acting as an electron sink. Also the plasmon resonance in metallic Ag nanoparticles is considered to locally enhance the electric field facilitating electron-hole production [28]. While most relate this improvement to electronic effects, it has been pointed out that the addition of Ag can modify the grain sizes of the TiO_2, so increasing the surface area and hence also the photoactivity [24].

FACVD is a low-cost relatively simple atmospheric pressure CVD technique that is compatible with small volume, batch, and high volume continuous coating processes. A flame is used to provide the energy required to crack the precursor species into fragments and subsequently forms the film upon the substrate. Use of this method with low hazard aqueous solutions of simple metal salts can yield thin films, which represents a major advantage in terms of precursor cost and environmental impact compared to alternative CVD methods. In a previous paper [29], we also reported the use of aerosol delivery of aqueous solutions of silver salts I combination with FACVD, overcoming the previous limitations that atmospheric pressure CVD growth requires precursors with moderately high-vapour pressures. In this publication, we reported the first use of FACVD for silver deposition in combination with titania. We showed that this composite had biocidal activity toward (gram negative) *Escherichia coli*.

In this paper, we have now extended the work to explore a wider range of films structures, demonstrate significantly enhanced activity levels, and widen the exploration of biocidal activity to include gram positive bacteria (*Staphylococcus epidermidis*), and a virus (bacteriophage).

2. EXPERIMENTAL

2.1. Growth

All films were grown on precoated (CVD) silica coated barrier glass substrates. The barrier was a (60 nm) amorphous film of SiO_2 designed to prevent diffusion of impurity ions within the float glass. These would all cause a reduction in the quality and photoactivity of the films. All TiO_2 films used for biocidal testing were grown using an atmospheric pressure CVD coater described previously [30]. The precursor used was titanium tetra-isopropoxide (7.79×10^{-4} mol min^{-1}) (TTIP from Sigma-Aldrich, Mo, USA), which was transported through the reactor by a carrier gas of nitrogen. The substrate temperature was 500°C for TTIP.

Additionally, some films were grown using $TiCl_4$ and ethyl acetate at a substrate temperature of 650°C, for comparison purposes. The Ag films were grown using an atmospheric pressure flame assisted CVD coater with a propane/oxygen flame, described in detail previously [31]. The substrate temperature was set at 300°C. An aqueous solution of 0.5 M $AgNO_3$ was nebulised, into a carrier of N_2, through the flame and onto the substrate.

2.2. Characterisation

Standard techniques of X-ray diffraction (Siemens D5000, Surrey, UK), micro-Raman 514.5 nm Ar line (Renishaw 1000, Gloucestershire, UK), UV/visible spectroscopy (Hewlett Packard HP895A, Bracknell, UK), and SEM (Philips XL30, Surrey, UK, equipped with a Rontec Quantax silicon drift diode detector 3rd generation (SDD3) energy dispersive X-ray spectrometer (EDAX)) were used to characterise the samples. Film thickness was estimated by relating the reflected colour to a calibrated chart for thickness versus refractive index. X-ray photoelectron spectroscopy, XPS, (Kratos AXIS Ultra, Calif, USA) with an Al (monochromated) K_α radiation source was used to check the surface characteristics of the films. It was necessary to use a charge neutraliser as all the samples were insulating, due mainly to the deposition on glass. This tends to shift the peak positions up to 2 eV so the measurements are referenced to the residual C 1s signal at 285 eV. Curve fitting used CASA XP software using a mixture of Gaussian-Lorentzian functions to deconvolute spectra.

To test the functional behaviour of the samples, both photoactivity and bioactivity were tested.

2.2.1. Photocatalytic behaviour

This was measured under UV (365 nm) at 20°C under open laboratory conditions. The emission spectrum of the UV tubes (Sylvania F15W/BLB-T8, Mass, USA) is shown in Figure 1. The degradation of stearic acid was followed by FTIR (Bruker, Coventry, UK, Vector 22). A typical stearic acid layer would have an integrated absorbance over this range of 1.0 cm^{-1} corresponding to ca. 3.13×10^{15} molecules cm^{-2} [32]. Stearic acid (100 μL of 10 mmol in methanol) was spun coated onto the sample. After drying in an oven at 55°C, the sample was exposed to UV light with an intensity of 3 mW/cm^2. The activity of the film was defined in cm^{-1} min^{-1}, which indicated the rate of reduction in selected stearic acid peaks in the IR region. The technique used was developed from work described previously [30, 32, 33].

2.2.2. Biocidal activity testing

The test used was a modification of the standard test described by BS EN 13697 : 2001. Samples were cleaned by shaking gently for 40 minutes in 40 mL of 100% methanol. Samples were removed aseptically, placed in a UVA transparent plastic Petri dish, coated side uppermost, and

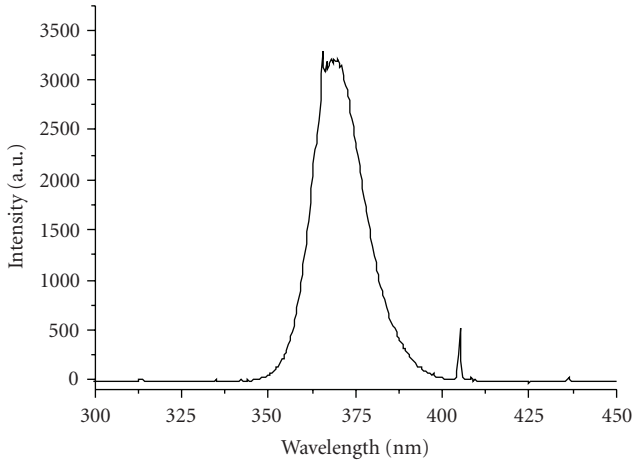

Figure 1: Emission spectrum of UV lamps.

preirradiated under 15 W UVA lamps (Sylvania F15W/BLB-T8) with a 2.24 mW cm^2 output for 24 hours.

Escherichia coli B NCIMB 9482, *E. coli* ATCC 10536, and bacteriophage T4 were obtained from the National Collection of Industrial and Marine Bacteria, Aberdeen UK, and *Staphylococcus epidermidis* NCTC11047 from the National Type Culture Collection, Colindale, UK. Bacteria were subcultured into Nutrient Broth (Oxoid, Basingstoke, UK), inoculated onto Cryobank beads (Mast Diagnostics, Liverpool, UK) and stored at –70°C. Beads were subcultured onto Nutrient Agar (Oxoid), incubated at 37°C for 24 hours and stored at 5°C. A 50 μL loopful (a plastic loop calibrated to give a defined volume) was inoculated in to 20 mL Nutrient broth (Oxoid) and incubated for 24 hours at 37°C. Cultures of *E. coli* ATCC 10536 and *S. epidermidis* were centrifuged at 5000 x g for 10 minutes in a bench centrifuge, and the cells washed in deionised water x 3 by centrifugation and resuspension. Controls show that this process does not affect cell viability over the test timescales. Cultures were resuspended in water and adjusted to OD 0.5 at 600 nm (Camspec, M330, Cambridge, UK) to give approximately 2×10^8 colony forming units (CFUs) mL^{-1}.

Stock bacteriophage suspension was produced by addition of bacteriophage T4 to a 24-hour culture of *E. coli B* and incubation at 37°C for a further 24 hour. Remaining cells and cell debris were removed by centrifugation at 5000 x g for 10 minutes. Bacteriophage were centrifuged by centrifugation at 20 000 x g in a Sorvall RC6 centrifuge. The pellet was washed 3 x by centrifugation and resuspension, plaque count determined and diluted appropriately and stored at −20°C.

Phage was assayed by the double agar layer method [34]. Phage suspension (0.1 mL) was mixed with 0.2 mL 24 hours *E. coli* B culture in nutrient broth (approx 2×10^8 CFU mL^{-1}) and 5 mL molten soft agar (Nutrient Broth +6 g l^{-1} agar; Oxoid, UK) and poured on to surface of a nutrient agar plate. When set, the plates were incubated at 37°C for 24 hours and plaques counted.

A suspension of 50 μL of bacterial or phage was inoculated on to each test sample and spread out using the edge of a flame sterilized microscope cover slip.

The samples were UV activated by exposure to three 15 W UVA lamps (the surface incident irradiation was 2.25 mW cm^{-2} on each occasion). A sample was removed immediately and the remaining samples removed at regular intervals. Samples exposed to UVA but covered with a poly laminar UVA protection film (Anglia Window Films UK) to block UVA but not infra-red, acted as controls.

The samples were immersed in 20 mL of sterile deionised water and vortexed for 60 seconds to resuspend the organisms. A viability count was performed by serial dilution and plating onto nutrient agar in triplicate or by plaque count and incubation at 37°C for 48 hours. Each experiment was performed in triplicate.

3. RESULTS AND DISCUSSION

In order to understand the influence of the various layer structures, four types of film were produced and characterised. That of just Ag, TiO_2/Ag deposited sequentially to form layers of Ag both over and under TiO_2 and TiO_2 for reference. The two multilayered structures were deposited, so that the effect of Ag either above or below the TiO_2 layer could be assessed. The Ag films were produced with a range of thickness (60–90 nm), by increasing the number of passes of the moving substrate under the flame (see [35] for a full description of the FACVD system). The number of passes is approximately linearly related to the thickness.

3.1. Optical properties

The TiO_2 films (single and combined) were all transparent, showing interference fringes of varying colour depending on their thickness (40–120 nm). All of these films were very strongly adhered to the substrate (measured by tape pull test). Visually all the Ag films were reflective, with a pale pink tinge, which darkened to purple for thicker coatings, and eventually developed a silver appearance. The multilayered films were again reflective, those with TiO_2 grown over the Ag exhibiting accentuation of the reflected colour relating to the TiO_2 thickness. There was an increased hardness of TiO_2/Ag over Ag, which was relatively soft. (Tested by scratch resistance with a variable load traversing needle.)

3.2. Crystallinity

3.2.1. XRD

All Ag films were crystalline showing metallic cubic Ag only (JCPDS 04-0783).

Those films of Ag/TiO_2 showed no mixed species only those of Ag and TiO_2. $TiO_2$was grown directly onto the glass substrate, as expected anatase only, as discussed in a previous publication [36].

Use of Scherrer's formula [37] allows the calculation of crystallite size. The calculation is ideally for a powder not for a thin film, so will contain line width broadening from strain as well as crystallite size. Despite these reservations, the values obtained will give an idea of the changes occurring.

Considering one of the thicker Ag samples, there was an apparent increase in Ag crystallite size from 21 nm to 59 nm on addition of the TiO_2 layer. Calculations, on Ag layers covered by over-layers of TiO_2, suggest crystallite size values of 33 nm and 51 nm for anatase. The anatase value was similar to that calculated from other TiO_2 films (of similar thickness) grown under identical conditions (average 30 nm). There was no obvious change in crystallite size in TiO_2 when it is the lower layer, as expected since relatively low temperatures (300°C) were used to deposit the Ag. In previous work [35], we have shown that at higher substrate temperatures, the Ag crystallite size increases when TiO_2 overgrowth is undertaken. In this case, this most likely arises due to the high TiO_2 growth temperature (650°C), leading to annealing and growth of the Ag crystallites. As an independent check, an Ag sample was heated (650°C, 10^0 min^{-1}) without the addition of more Ag. Although some vaporisation of the silver film appeared to have occurred, it was possible to calculate that the crystallite size still increased significantly (21 nm to 37 nm) on heating under these conditions.

Similarly, the crystallite size for Ag growth either on TiO_2 or directly on the barrier glass appeared to be equivalent in all cases, indicating that the FACVD deposition process was controlling this property.

Growth of TiO_2 layer, over the thin layer of Ag produced no changes in the Ag crystallite size. This is attributed to the relatively low-growth temperature (500°C) used for TTIP, which was probably not high enough to alter the Ag crystallite size. The anatase crystallite size was 30 nm.

3.2.2. Raman

Titania and titania underlayer samples confirmed the presence of anatase (398, 515, 636 cm^{-1}) (see Figure 2). There was an additional signal at 972 cm^{-1} which was the only signal seen for the reference thick Ag sample. This is tentatively assigned to a plasmon resonance, which is generally defined as a coupled oscillation of conductance electrons when interacting with an external electromagnetic wave of specific wavelength. The position of the plasmon relates to the size (shape or distribution) of the Ag particles [38, 39].

3.3. Chemical composition

XPS of all the samples containing Ag confirmed this to be metallic Ag with the $3d_{5/2}$ peak appearing at 368.7 eV and only an O 1s signal at 533 eV relating to absorbed water and no signal for an oxide (528.2–531 eV) [40] (see Figure 2). XPS of all the samples (Ag, TiO_2, TiO_2/Ag, Ag/TiO_2) showed no major impurities in the wide scan, save the expected presence of C (standard calibration reference) and small amounts of Cl in the case of TiO_2 grown from $TiCl_4$ and ethyl acetate. Of major importance was the fact that both multilayer samples show signals from both TiO_2 and Ag. As XPS only samples about 5 nm of the surface, this established that the surface consists of both Ag and TiO_2.

A high resolution scan of the Ag 3d region (see Figure 3(a)) for the reference Ag film (30 passes) showed a

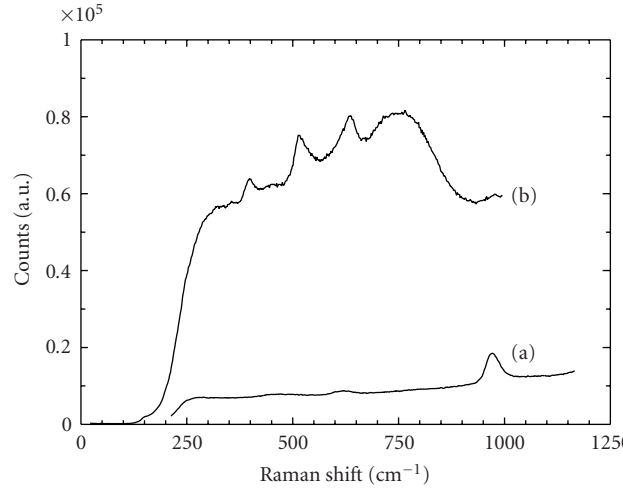

Figure 2: (a) Raman spectra for silver and (b) TiO_2 over silver film.

$3d_{5/2}$ peak at 368.7 eV and a $3d_{3/2}$ peak at 374.7 eV, which were both shifted to lower binding energies when TiO_2 was grown on the same Ag film ($3d_{5/2}$ = 367.9 eV and $3d_{3/2}$ = 373.9 eV).

The titania over Ag samples showed a slightly lower intensity of Ag (when spectra were overlaid). This is as expected, as it is partially masked by the TiO_2 layer, and in order to be located at the exposed surface of the sample the Ag atoms would have had to diffuse through the TiO_2 layer.

High resolution Ti 2p spectra (see Figure 3(b)) showing the $2p_{1/2}$ and $2p_{3/2}$ signals (464.7 eV, 459.0 eV) displayed no differences in position and width from that of a standard CVD deposited TiO_2 sample.

The O 1s (see Figure 3(c)) showed signals assigned to O bound to Ti^{4+} (530.2 eV) and O bound to H (532.8 eV) from absorbed water, on the lower trace. The upper trace for a thick layer of Ag (30 passes) showed only the O 1s signal for absorbed water.

From this, it can be confirmed that only Ag and TiO_2 were present. There was no shift in the positions of the Ti 2p and O 1s peaks when Ag was present, establishing that there was no significant chemical interaction of the Ag with the Ti and O. Quantitative calculation of the elements gave 1:1:2.2 ratio for Ag:Ti:O, that is, consistent with the presence of Ag metal and an oxide with the stoichiometry, $TiO_{2.2}$.

XPS results for Ag over TiO_2 gave very similar results to those above, confirming the presence of TiO_2 and Ag. As expected, the Ag signals were stronger as more Ag was expected to be present at the surface layer.

For Ag on top, it can be seen that the top surface contains both TiO_2 and Ag, despite the fact that they were grown as independent layers. The XPS characteristics for the multilayer of Ag on TiO_2 are readily explained on the basis that the Ag grows as nanocrystallites rather than as a continuous film. There are two possible explanations for the presence of Ag on the surface when it was originally formed as the lower layer. Either there was preferential growth of the TiO_2 on the barrier glass rather than the Ag (inhibited on Ag or faster growth on glass) or the Ag may diffuse to

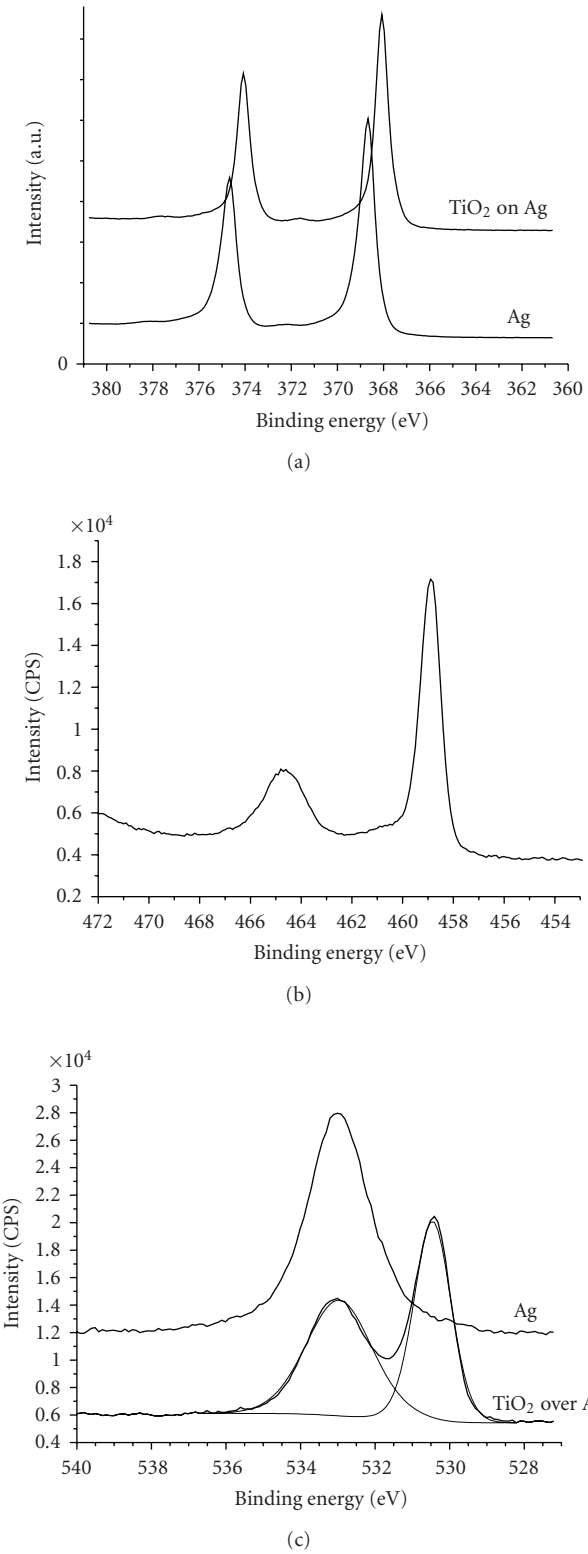

Figure 3: XPS high-resolution scan of (a) Ag 3d TiO_2 over Ag(30) (including sample Ag(30), (b) Ti 2p, (c) XPS high-resolution scan for O 1s.

the surface due to the growth temperature required for TiO_2 growth.

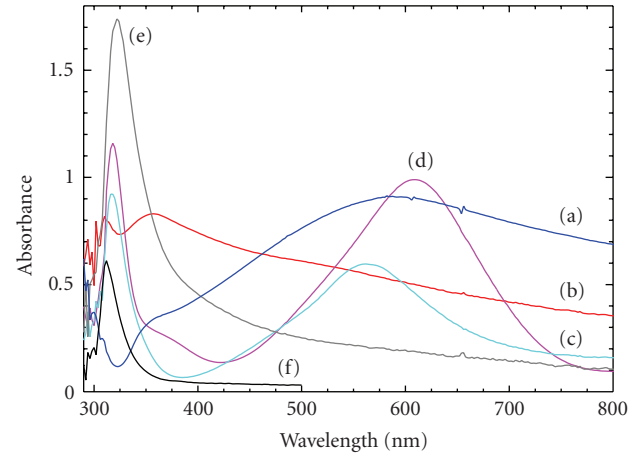

Figure 4: UV/Vis spectra of (a) thick layer of Ag (30 passes), (b) TiO_2 on Ag (30), (c) TiO_2 (TTIP) over Ag (4 passes), (d) Annealed TiO_2 (TTIP) over Ag (4 passes), (e) thin layer of Ag (2 passes) over TiO_2, (f) commercial TiO_2 on glass.

3.4. UV/Visible spectroscopic characteristics

Deposition of TiO_2 on top of silver (see Figure 4(b)) showed a UV/vis absorption signal at 310 nm which relates to the TiO_2 (see trace of commercial TiO_2 on glass, Figure 4(f)). There is also a signal at 357 nm, which may be of the same origin as the shoulder seen on the Ag film with a long broad tail (see Figure 4(a)). The spectra from a sample prepared by growing a thin over-layer of Ag (2 passes) (since the silver films are not continuous, the number of passes-giving relative amount of silver deposited—is considered more valuable than a nominal approximated thickness) on TiO_2showed only a signal relating to the TiO_2 and no sign of any Ag plasmon (see Figure 4(e)). Due to the small crystallite size (11 nm) and the lower Ag concentration, this is possibly hidden by the broad strong TiO_2 absorption band.

Spectra, for a sample prepared using TTIP as a reactant in order to deposit only anatase over Ag (4 passes), again gave absorption bands relating to both TiO_2 and an Ag plasmon (see Figure 4(c)). Interestingly on annealing this sample at 650°C, the surface plasmon shifted from 564 nm to 602 nm (see Figure 4(d)). This is in line with the expected change of wavelength as the particle size increases.

3.5. Surface structure

The FACVD process used leads to the growth of a nanostructured surface rather than a continuous Ag film. The density, size, and spacing of the nanostructured surface will depend critically on the growth conditions chosen. The image in Figure 5(a) shows growth of Ag (seen as bright particles) on top of TiO_2. Separated Ag particles between TiO_2 crystallites are readily observed.

The form of the TiO_2 round and under the Ag is similar to that expected for TiO_2 grown directly on a glass substrate. The example shown in Figure 5(b) for comparison (as this is the most commonly used alternative process for CVD of

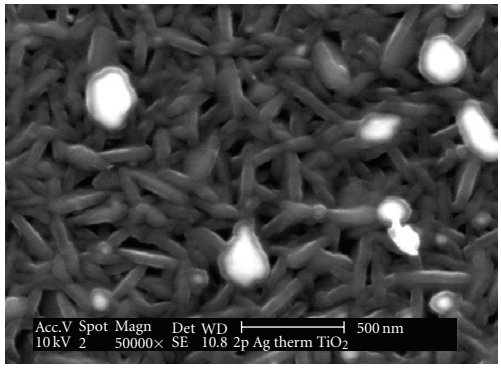

(a)

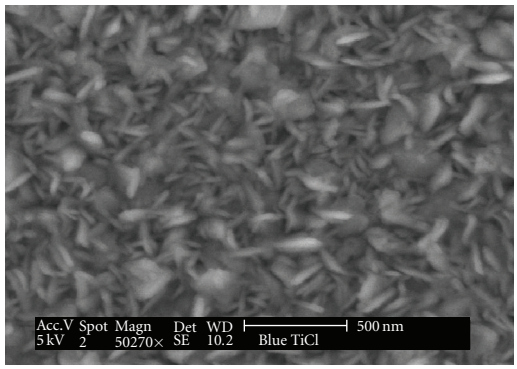

(b)

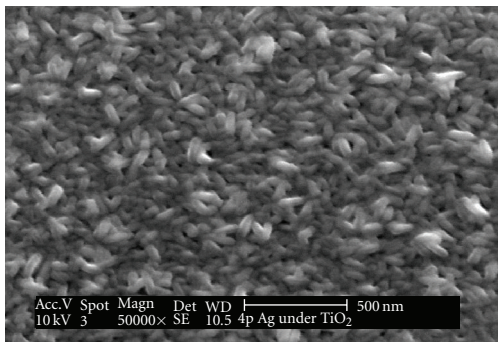

(c)

Figure 5: SEM images of (a) Ag(2) on top of TiO_2, (b) TiO_2 on barrier glass, (c) TiO_2 (TTIP) over Ag (4 passes).

titania) is for a TiO_2 layer grown using $TiCl_4$ and ethyl acetate with a thickness of ca. 120 nm.

The sample (see Figure 5(c)) with an over-layer of TiO_2 on Ag shows similar images, of the TiO_2 to that of TiO_2 grown direct on barrier glass. This is to be expected as both are only of anatase. In this instance, the SEM images look very similar, although with slightly smaller features resulting from growth on the Ag underlayer.

SEM images for TiO_2 over-layers on Ag do not show any obvious signs of Ag nanoparticles on the surface. However, use of EDAX at a series of reducing accelerating voltages (i.e., sampling closer to the surface) clearly showed that the Ag signal became stronger nearer the surface, supporting our

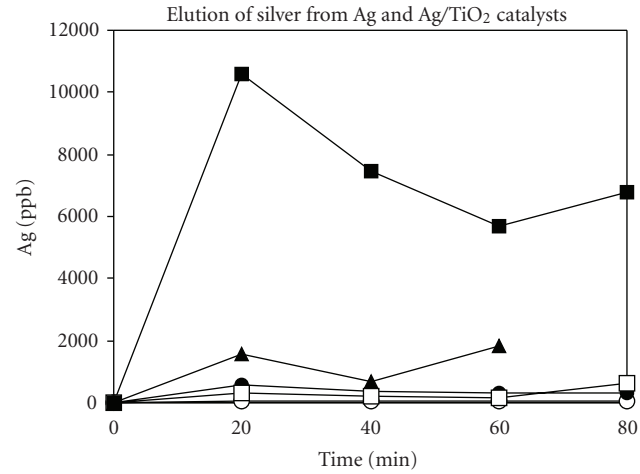

Figure 6: ▲ titania under, □ titania over, ■ silver only, ◦ titania over with UV.

contention that at least some Ag is likely to be either exposed or very close to the surface of the sample. Unfortunately, it is not possible to accurately determine the penetration depth as this will depend on many variables including the accelerating voltage, sample matrix, and chemical identity (extent of absorption). The depth will generally vary from a few hundreds of nm to a couple of μm.

3.6. Surface Ag elution

The rate of elution of silver was tested by aqueous solution extraction-simulating the biocidal testing procedure. The sample was treated as if undergoing a bacterial test, but water and no bacteria added. After set times additional water was added, and then withdrawn, to nitric acid and the Ag content checked by ICPMS. The intention was to explore if the levels of silver eluted were sufficient to explain the biocidal activity (see Figure 6). A further objective was to assess the longevity of the bacteriocidal activity (by repeated extraction cycles). The Ag elution results are in the order silver > titania > titania under silver > titania over silver > titania only.

The concentrations of silver in the bacteria sampling solutions, for titania/silver combinations, are ∼100 to 1000 ppb. For silver alone, this rises to ∼10 000 ppb. It is interesting to note that silver under titania gives higher elution rates. This is compatible with the biocidal activity results.

3.7. Functional properties

3.7.1. Photoactivity

Photocatalytic activity assessment was undertaken via degradation of stearic acid under UV light (365 nm). The rate at which the stearic acid was decomposed is shown by the integrated area under the IR signals from the stearic acid (2957.5, 2922.8, and 2853.4 cm^{-1}), which are directly proportional to the concentration. The rates were obtained from the gradient of a linear (first order) fit to the raw data. As an indication of the fit error, the variance has also been given.

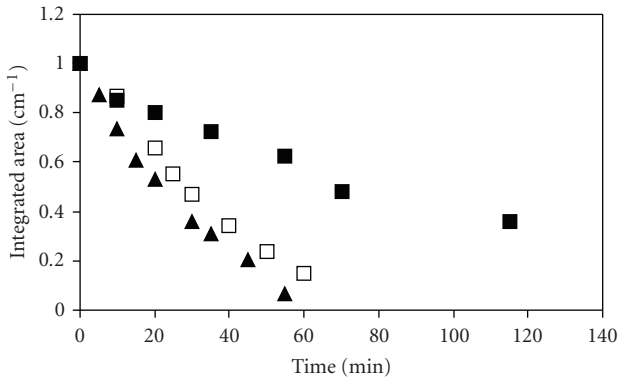

FIGURE 7: Photoactivity for the degradation of stearic acid (normalised) for ■ Ag(2), □ TiO_2 on Ag(2), ▲ TiO_2 on Ag repeat.

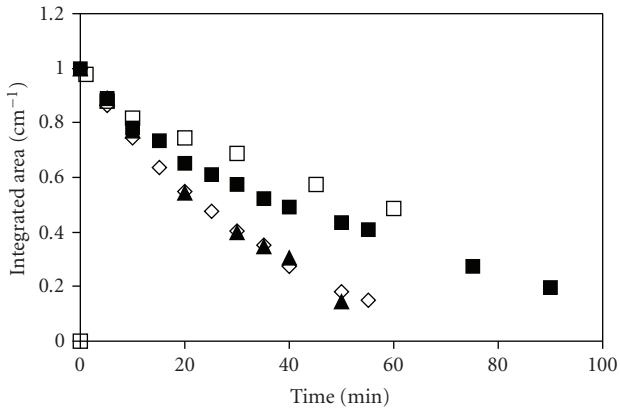

FIGURE 8: Photoactivity for the degradation of stearic acid (normalised) for Ag over TiO_2 (sample A ▲, sample B ■), reference TiO_2 ◇ and Ag on a commercial TiO_2 coating □.

This would give a value of 1 for a perfect fit. All Ag samples gave broadly similar results irrespective of the Ag deposition thickness. For example, a thick layer gave a stearic acid decomposition rate of 0.0017 cm^{-1} min^{-1} (variance 0.946) while that for a thin layer was 0.0020 cm^{-1} min^{-1}(variance 0.961). The multilayered films were UV active, although to varying degrees, depending on a range of factors.

(1) Titania over silver

TiO_2 over a thin layer of Ag (2 passes) (0.015, 0.010 cm^{-1} min^{-1}, variance 0.968) was more active than Ag and generally higher than TiO_2 alone (see Figure 7).

The comparison values for TiO_2 on barrier glass are for pure anatase. Growth of TiO_2 over Ag (4 passes) gave an activity of 0.0024 cm^{-1} min^{-1}(variance 0.974) for the combined layer, which is similar to that of just the Ag, but less than that for a single layer of TiO_2 (0.006 cm^{-1} min^{-1}, variance 0.963) of similar thickness.

The conditions of growth of TiO_2 have been shown to alter some of the physical properties of the underlying Ag (e.g., crystallite size) and so this in turn may effect the activity of the multilayer, along with the rutile/anatase ratio.

(2) Silver over titania

A thin layer of Ag (2 passes) was deposited on laboratory thermally grown TiO_2. Ag(2) on TiO_2 activity (0.0082 cm^{-1} min^{-1}, variance 0.981) (sample A in Figure 8) is referenced against TiO_2 chosen from the thickest area of the substrate before the Ag was grown. This reference should indicate the maximum activity available from anywhere on the CVD coated plate, (average 0.007 cm^{-1} min^{-1}). To illustrate the effect of thickness, a second point chosen from a thinner area gives a lower activity of 0.006 cm^{-1} min^{-1} and variance of 0.940 (see Figure 8, sample B).

For comparison with commercially grown CVD titania, Ag(2) was deposited on a (uniform) commercially available (Saint-Gobain Bioclean) CVD TiO_2 coated glass giving photoactivity of 0.0054 cm^{-1} min^{-1} and variance of 0.958 (over 60 minutes) against the commercial TiO_2 coating of average 0.003 cm^{-1} min^{-1} (variance 0.976) (see Figure 8).

3.7.2. Biocidal activity

The combined thermal and FACVD grown multilayer films were investigated for biocidal activity using the bacteria *Escherichia coli* (Gram-negative), *Staphylococcus epidermidis* (Gram-positive), and bacteriophage T4.

The extension of the biocidal work to Gram-positive bacteria is important because the different cell wall structure from the Gram-negative *E. coli* has been shown to decrease susceptibility to photocatalytic disinfection. The ability to disinfect viruses is also important, and bacteriophage is used as models for inactivation of mammalian viruses. There is also a large size difference between bacteria and viruses, and surface morphology may play a significant role. Plain glass was used as a control. The error bars represent the standard deviation from three separate biocidal tests. In some cases, the SD is very low and error bars are smaller than the data points. Comparisons were made between FACVD Ag layers alone, photoactive TiO_2 films, and FACVD Ag over-coated with TiO_2. All the Ag films used were about 60 nm thick (4 passes), while the comparison TiO_2 reference samples were approximately 80 nm thick.

The biocidal activity was measured by the technique outlined in Section 2. Example results (*E. coli*) are shown in Figure 9(a) for a TiO_2 layer only; see Figure 9(b) for Ag on glass and TiO_2 over Ag (see Figure 9(c)).

It can be seen that the thermally grown TiO_2 film was biocidally active for the Gram-negative *E. coli*, with a >5 log reduction in 180–240 minutes. All the Ag films tested were highly bacteriocidal, and most gave effectively 100% kill in under the minimum test time of 20 minutes. Although the rate of killing was slower on TiO_2 over Ag, the rate was much higher than on plain TiO_2 and these films also showed a significant enhancement of durability.

Gram-positive bacterium *Staphylococcus epidermidis* on Ag over TiO_2 was also completely killed (see Figure 10) but at a slower rate taking approx 60 minutes.

It took 80 minutes to achieve equivalent deactivation of Bacteriophage T4 (see Figure 11) on Ag over TiO_2.

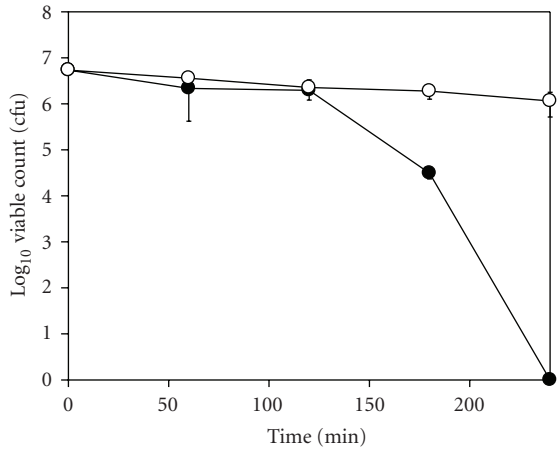

(a)

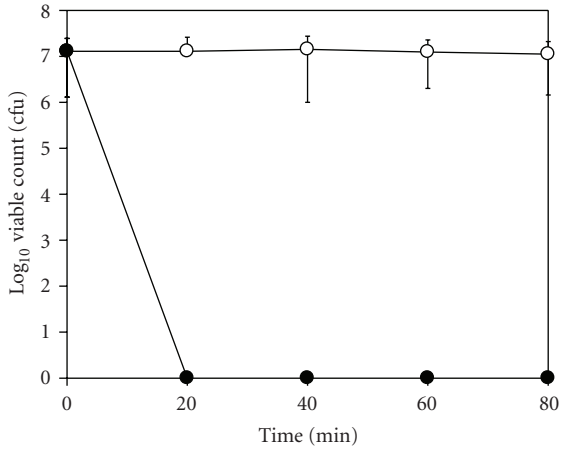

(b)

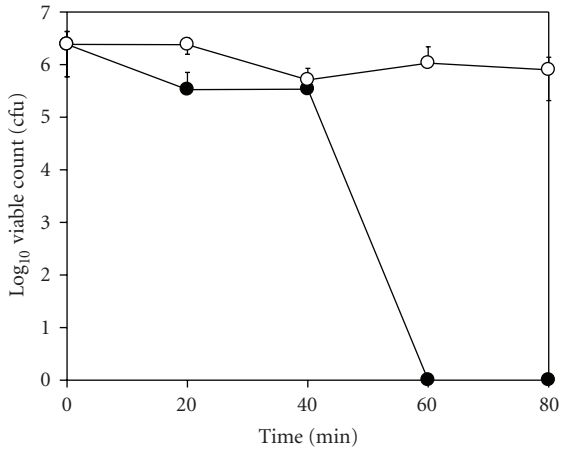

(c)

Figure 9: (a) Killing of *E. coli* on a TiO_2 film on glass • with control sample ◦. (b) Killing of *E. coli* on Ag layer on glass (note: minimum test time 20 minutes) • with control sample ◦. (c) Killing of *E. coli* on TiO_2 layer over Ag on glass • with control sample ◦.

4. DISCUSSION

All grown films were polycrystalline, consisting of cubic Ag and TiO_2. The TiO_2 is stoichiometric anatase when the bottom layer, and a mixture of anatase and rutile when over silver. XPS confirms that there is no chemical interaction between the Ag and the TiO_2. One of the interesting features of this work is that although the Ag and TiO_2 layers were grown sequentially the overall result shows that the surface consists of both Ag and TiO_2, for TiO_2 samples if the substrate temperature during growth (or after annealing post growth) is sufficiently high (> ~600C).

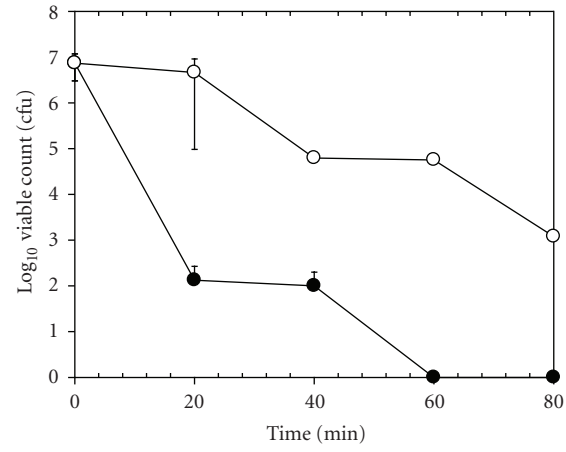

Figure 10: Killing of *S. epidermidis* on Ag over TiO_2.

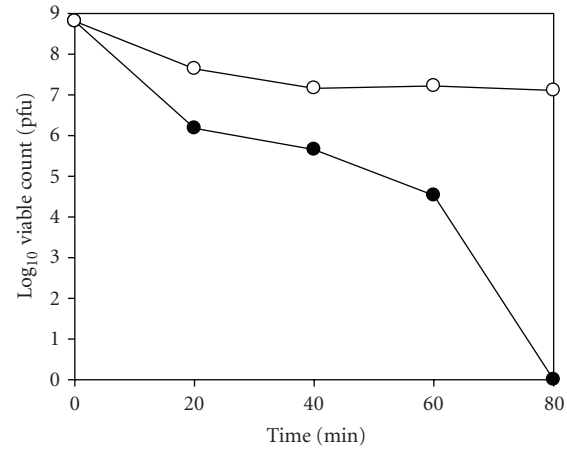

Figure 11: Killing of Bacteriophage T4 on Ag over TiO_2 • with control sample ◦.

All the samples had some UV photoactivity, which is of differing values depending on the exact arrangement of the layers. The addition of Ag layers gives comparable or improved photoactivity of the multilayers, particularly in the case of Ag on TiO_2, over that of single layer of Ag or TiO_2 of comparable thickness.

The biocidal results show a high degree of activity for both Ag and Ag/TiO_2 films and interestingly some of the most active results are from Ag under TiO_2.

Sökmen et al. [41] used TiO_2 loaded with 1% Ag but *in suspension* and got 100% kill in 15 minutes probably due to the presence of silver ions. On TiO_2 alone, Amézaga-Madrid [9] only got a 70% reduction after 40 minutes

whereas Sunada et al. [42] saw a 6 log kill after 90 minutes with similar bacteria loadings to our own, but kill time was longer with larger doses. Kikuchi et al. [43] reported a 4-log reduction in 1 hour. Kühn et al. [44] reported a 6-log reduction of *E. coli* on P25 coated plexiglass in 1 hour. Direct comparison of biocidal activity to other data available in the literature is complicated by the different test methods used. However, it appears clear that, for thin films-based biocidal activity, the films grown in this work are highly active.

The demonstration of high activity across organisms is particularly encouraging, as Gram-positive bacteria have been shown to be more resistant [45] to photocatalytic disinfection than Gram-negative bacteria, both in suspension and on air filters [46, 47] probably due to their different cell wall structure.

Similarly, the observed high activity against bacteriophage shows that nonenveloped DNA viruses can also be inactivated and suggests that the films can be active across a wide range of organism dimensions.

The proposed mechanism for this activity is one that is strongly influenced by the thickness of the TiO_2 (80 nm). Our data suggest that this should be sufficiently thick so as to develop critical level crystallinity, but thin enough to allow silver to diffuse through (and into) the TiO_2 film as it grows. This is supported by the reported XPS results.

It should be noted that the UV levels employed in this work are of similar intensity to that found in full sunlight.

The silver elution results show that for titania/silver combinations, the level of silver in the bacteria sampling solutions was ~100 to 1000 ppb. A silver level of around 1 ppm is normally considered the minimum for significant biocidal activity. The very high levels of bactericidal activity seen with the films grown by the combination CVD process seem unlikely to be due to silver alone. Furthermore, it was observed that no killing occurred in the dark, at times up to 80 minutes, demonstrating that photocatalytic activity was crucial for high-level biocidal activity.

We can speculate that the nanostructure of Ag deposited by FACVD may be crucial in determining biocidal activity. Ag grown on glass or Ag over-coated with TiO_2, both benefit from the high-structure control capability of the FACVD approach. When deposited onto TiO_2, the structure flexibility will be, at least, partially predefined by this underlayer. Silver molecules can be oxidised at the silver/titania interface, and thus we have designed the multilayer system to incorporate a diffusion-based replenishment capability, giving the potential for extended activity. It is interesting to note that atomic absorption measurements of the bacteria solutions above the films showed concentrations below 1 ppm (Atomic Abs. detection limit).

CVD films of titania are highly durable. Indeed photocatalytic titania films made by CVD are used in commercial window "easy clean" coatings which are used on external surfaces. We have, additionally, tested our films on simulated (humidity, temperature, and exposure) and compared them to commercial samples, demonstrating close to similar performance. The titania films thus (as well as being active) also act as a host for silver.

The combination of Ag by FACVD and TiO_2, by CVD, offers unique advantages in that the CVD TiO_2 coating imparts a major enhancement to durability and as we previously have shown [29] the activity was retained along with chemical and abrasion resistance compatible with potential application of the technology. In addition, it is noteworthy that the combined Ag/TiO_2 films are thin and as such impart only moderate changes to visual appearance.

This combined flexible process along with the associated transparency and durability offers opportunity for application in the increasing number of areas where bio-active surface functionality is sought. The demonstrated capability of the films to show highly efficient biocidal activity against a range of organisms reinforces this potential.

ACKNOWLEDGMENTS

This work was partially financed by the EC through GRD1-2001-40791, PHOTOCOAT project, and partly by EPSRC. The authors acknowledge the valuable assistance of Chris Liptrot and Amran Mohammed in biocidal testing.

REFERENCES

[1] A. Mills and S. Le Hunte, "An overview of semiconductor photocatalysis," *Journal of Photochemistry and Photobiology A*, vol. 108, no. 1, pp. 1–35, 1997.

[2] T. Matsunaga, R. Tomoda, T. Nakajima, and H. Wake, "Photoelectrochemical sterilization of microbial cells by semiconductor powders," *FEMS Microbiology Letters*, vol. 29, no. 1-2, pp. 211–214, 1985.

[3] P.-C. Maness, S. Smolinski, D. M. Blake, Z. Huang, E. J. Wolfrum, and W. A. Jacoby, "Bactericidal activity of photocatalytic TiO_2 reaction: toward an understanding of its killing mechanism," *Applied and Environmental Microbiology*, vol. 65, no. 9, pp. 4094–4098, 1999.

[4] Y. Kikuchi, K. Sunada, T. Iyoda, K. Hashimoto, and A. Fujishima, "Photocatalytic bactericidal effect of TiO_2 thin films: dynamic view of the active oxygen species responsible for the effect," *Journal of Photochemistry and Photobiology A*, vol. 106, no. 1–3, pp. 51–56, 1997.

[5] K. P. Kühn, I. F. Chaberny, K. Massholder, et al., "Disinfection of surfaces by photocatalytic oxidation with titanium dioxide and UVA light," *Chemosphere*, vol. 53, no. 1, pp. 71–77, 2003.

[6] J. C. Yu, W. Ho, J. Lin, H. Yip, and P. K. Wong, "Photocatalytic activity, antibacterial effect, and photoinduced hydrophilicity of TiO_2 films coated on a stainless steel substrate," *Environmental Science & Technology*, vol. 37, no. 10, pp. 2296–2301, 2003.

[7] K. Sunada, Y. Kikuchi, K. Hashimoto, and A. Fujishima, "Bactericidal and detoxification effects of TiO_2 thin film photocatalysts," *Environmental Science & Technology*, vol. 32, no. 5, pp. 726–728, 1998.

[8] K. Sunada, T. Watanabe, and K. Hashimoto, "Bactericidal activity of copper-deposited TiO_2 thin film under weak UV light illumination," *Environmental Science & Technology*, vol. 37, no. 20, pp. 4785–4789, 2003.

[9] P. Amézaga-Madrid, G. V. Nevárez-Moorillón, E. Orrantia-Borunda, and M. Miki-Yoshida, "Photoinduced bactericidal activity against *Pseudomonas aeruginosa* by TiO_2 based thin films," *FEMS Microbiology Letters*, vol. 211, no. 2, pp. 183–188, 2002.

[10] Hippocrates, "On Ulcers," 400 B.C.E.; translated by Francis Adams, http://classics.mit.edu/Browse/browse-Hippocrates.html.

[11] A. D. Russell and W. B. Hugo, "Antimicrobial activity and action of silver," in *Progress in Medicinal Chemistry*, G. P. Ellis and D. K. Luscombe, Eds., vol. 31, pp. 351–370, Elsevier Science, St. Louis, Mo, USA, 1994.

[12] S. Silver, "Bacterial silver resistance: molecular biology and uses and misuses of silver compounds," *FEMS Microbiology Reviews*, vol. 27, no. 2-3, pp. 341–353, 2003.

[13] E. Vernè, S. Di Nunzio, M. Bosetti, et al., "Surface characterization of silver-doped bioactive glass," *Biomaterials*, vol. 26, no. 25, pp. 5111–5119, 2005.

[14] R. O. Fernández and R. A. Pizarro, "Lethal effect induced in *Pseudomonas aeruginosa* exposed to ultraviolet-a radiation," *Photochemistry and Photobiology*, vol. 64, no. 2, pp. 334–339, 1996.

[15] K. S. Rogers, "Variable sulfhydryl activity toward silver nitrate by reduced glutathione and alcohol, glutamate and lactate dehydrogenases," *Biochimica et Biophysica Acta* , vol. 263, no. 2, pp. 309–314, 1972.

[16] S. Y. Liau, D. C. Read, W. J. Pugh, J. R. Furr, and A. D. Russell, "Interaction of silver nitrate with readily identifiable groups: relationship to the antibacterial action of silver ions," *Letters in Applied Microbiology*, vol. 25, no. 4, pp. 279–283, 1997.

[17] J. L. Clement and P. S. Jarrett, "Antibacterial silver," *Metal-Based Drugs*, vol. 1, no. 5-6, pp. 467–482, 1994.

[18] R. H. Jensen and N. Davidson, "Spectrophotometric, potentiometric, and density gradient ultracentrifugation studies of the binding of silver ion by DNA," *Biopolymers*, vol. 4, no. 1, pp. 17–32, 1966.

[19] P. D. Bragg and D. J. Rainnie, "The effect of silver ions on the respiratory chain of *Escherichia coli*," *Canadian Journal of Microbiology*, vol. 20, no. 6, pp. 883–889, 1974.

[20] F.-R. F. Fan and A. J. Bard, "Chemical, electrochemical, gravimetric, and microscopic studies on antimicrobial silver films," *Journal of Physical Chemistry B*, vol. 106, no. 2, pp. 279–287, 2002.

[21] S. Thomas and P. McCubbin, "A comparison of the antimicrobial effects of four silver-containing dressings on three organisms," *Journal of Wound Care*, vol. 12, no. 3, pp. 101–107, 2003.

[22] K. Dunn and V. Edwards-Jones, "The role of Acticoat^{TM} with nanocrystalline silver in the management of burns," *Burns*, vol. 30, supplement 1, pp. S1–S9, 2004.

[23] C. He, Y. Yu, X. Hu, and A. Larbot, "Influence of silver doping on the photocatalytic activity of titania films," *Applied Surface Science*, vol. 200, no. 1–4, pp. 239–247, 2002.

[24] A. Dobosz and A. Sobczyński, "The influence of silver additives on titania photoactivity in the photooxidation of phenol," *Water Research*, vol. 37, no. 7, pp. 1489–1496, 2003.

[25] E. Stathatos, T. Petrova, and P. Lianos, "Study of the efficiency of visible-light photocatalytic degradation of basic blue adsorbed on pure and doped mesoporous titania films," *Langmuir*, vol. 17, no. 16, pp. 5025–5030, 2001.

[26] P. D. Cozzoli, E. Fanizza, R. Comparelli, M. L. Curri, A. Agostiano, and D. Laub, "Role of metal nanoparticles in TiO_2Ag nanocomposite-based microheterogeneous photocatalysis," *Journal of Physical Chemistry B*, vol. 108, no. 28, pp. 9623–9630, 2004.

[27] T. Hirakawa and P. V. Kamat, "Charge separation and catalytic activity of Ag-TiO_2 core-shell composite clusters under UV-irradiation," *Journal of the American Chemical Society*, vol. 127, no. 11, pp. 3928–3934, 2005.

[28] J.-M. Herrmann, H. Tahiri, Y. Ait-Ichou, G. Lassaletta, A. R. González-Elipe, and A. Fernández, "Characterization and photocatalytic activity in aqueous medium of TiO_2 and Ag-TiO_2 coatings on quartz," *Applied Catalysis B*, vol. 13, no. 3-4, pp. 219–228, 1997.

[29] L. A. Brook, P. Evans, H. A. Foster, et al., "Highly bioactive silver and silver/titania composite films grown by chemical vapour deposition," *Journal of Photochemistry and Photobiology A*, vol. 187, no. 1, pp. 53–63, 2007.

[30] H. M. Yates, M. G. Nolan, D. W. Sheel, and M. E. Pemble, "Atmospheric pressure CVD growth of photocatalytic titanium dioxide thin films on tin oxide," in *Proceedings of the 15th European Conference on Chemical Vapor Deposition (EUROCVD '05)*, pp. 783–790, Electrochemical Society Proceedings, Bochum, Germany, September 2005.

[31] M. J. Davis, G. Benito, D. W. Sheel, and M. E. Pemble, "Growth of thin films of molybdenum and tungsten oxides by combustion CVD using aqueous precursor solutions," *Chemical Vapor Deposition*, vol. 10, no. 1, pp. 29–34, 2004.

[32] Y. Paz, Z. Luo, L. Rabenberg, and A. Heller, "Photo-oxidative self-cleaning transparent titanium dioxide films on glass," *Journal of Materials Research*, vol. 10, no. 11, pp. 2842–2848, 1995.

[33] A. Mills, G. Hill, S. Bhopal, I. P. Parkin, and S. A. O'Neill, "Thick titanium dioxide films for semiconductor photocatalysis," *Journal of Photochemistry and Photobiology A*, vol. 160, no. 3, pp. 185–194, 2003.

[34] A. Gratia, "Des relations numeriques entre bactéries lysogenes et particules de bactériophage," *Annales del'Institut Pasteur*, vol. 57, pp. 652–676, 1936.

[35] D. W. Sheel, L. A. Brook, and H. M. Yates, "Controlled nanostructured silver coated surfaces by atmospheric pressure chemical vapour deposition," *Chemical Vapor Deposition*, vol. 14, no. 1-2, pp. 14–24, 2008.

[36] P. Evans, T. English, D. Hammond, M. E. Pemble, and D. W. Sheel, "The role of SiO_2 barrier layers in determining the structure and photocatalytic activity of TiO_2 films deposited on stainless steel," *Applied Catalysis A*, vol. 321, no. 2, pp. 140–146, 2007.

[37] B. D. Cullity, *Elements of X-Ray Diffraction*, Addison-Wesley, Reading, Mass, USA, 1978.

[38] T. Ung, L. M. Liz-Marzán, and P. Mulvaney, "Gold nanoparticle thin films," *Colloids and Surfaces A*, vol. 202, no. 2-3, pp. 119–126, 2002.

[39] S. Link and M. A. El-Sayed, "Spectral properties and relaxation dynamics of surface plasmon electronic oscillations in gold and silver nanodots and nanorods," *Journal of Physical Chemistry B*, vol. 103, no. 40, pp. 8410–8426, 1999.

[40] J. Chastain and R. C. King Jr., Eds., "Handbook of X-Ray Photoelectron Spectroscopy," Physical Electronic, Eden Prairie, Minn, USA, 1995.

[41] M. Sökmen, F. Candan, and Z. Sümer, "Disinfection of *E. coli* by the Ag-TiO_2/UV system: lipidperoxidation," *Journal of Photochemistry and Photobiology A*, vol. 143, no. 2-3, pp. 241–244, 2001.

[42] K. Sunada, Y. Kikuchi, K. Hashimoto, and A. Fujishima, "Bactericidal and detoxification effects of TiO_2 thin film photocatalysts," *Environmental Science & Technology*, vol. 32, no. 5, pp. 726–728, 1998.

[43] Y. Kikuchi, K. Sunada, T. Iyoda, K. Hashimoto, and A. Fujishima, "Photocatalytic bactericidal effect of TiO_2 thin films: dynamic view of the active oxygen species responsible for the effect," *Journal of Photochemistry and Photobiology A*, vol. 106, no. 1–3, pp. 51–56, 1997.

[44] K. P. Kühn, I. F. Chaberny, K. Massholder, et al., "Disinfection of surfaces by photocatalytic oxidation with titanium dioxide and UVA light," *Chemosphere*, vol. 53, no. 1, pp. 71–77, 2003.

[45] A. Erkan, U. Bakir, and G. Karakas, "Photocatalytic microbial inactivation over Pd doped SnO_2 and TiO_2 thin films," *Journal of Photochemistry and Photobiology A*, vol. 184, no. 3, pp. 313–321, 2006.

[46] A.-G. Rincón and C. Pulgarin, "Use of coaxial photocatalytic reactor (CAPHORE) in the TiO_2 photo-assisted treatment of mixed *E. coli* and *Bacillus* sp. and bacterial community present in wastewater," *Catalysis Today*, vol. 101, no. 3-4, pp. 331–344, 2005.

[47] A. Pal, S. O. Pehkonen, L. E. Yu, and M. B. Ray, "Photocatalytic inactivation of Gram-positive and Gram-negative bacteria using fluorescent light," *Journal of Photochemistry and Photobiology A*, vol. 186, no. 2-3, pp. 335–341, 2007.

Hindawi Publishing Corporation
International Journal of Photoenergy
Volume 2008, Article ID 343714, 6 pages
doi:10.1155/2008/343714

Research Article

TiO_2 Films for Self-Detection and Decontamination

Laura R. Skubal,[1] Alan L. McArthur,[1] and Matthew Newville[2]

[1] *Chemical Sciences Division, Argonne National Laboratory, 9700 South Cass Avenue, Argonne, IL 60439, USA*
[2] *Consortium for Advanced Radiation Science, The University of Chicago, 9700 South Cass Avenue, Argonne, IL 60439, USA*

Correspondence should be addressed to Laura R. Skubal, l@anl.gov

Received 25 July 2007; Accepted 05 March 2008

Recommended by Russell Howe

Methods that rapidly detect, characterize, quantify, and decontaminate surfaces are essential following chemical or biological incidents. Our work focused on developing a "smart" surface, one that monitors itself and the overlying atmosphere and triggers a decontamination step when surface contamination is detected. Titanium dioxide was used to coat a ceramic surface containing skeletal impregnated platinum electrodes. The electrical resistance of the surface became altered by the introduction of a contaminant into the overlying atmosphere and its chemisorption to the surface. This change in resistance in turn initiated illumination by an external ultraviolet lamp to induce photocatalytic oxidation of the sorbed contaminant. Film resistance was concentration-dependent, allowing self-decontamination to be triggered at set pollutant levels. Preliminary results suggest that advanced surfaces and films can be developed to identify contaminant type and concentration and to initiate photocatalytic decontamination to meet regulatory or safety standards.

1. INTRODUCTION

Recent advancements in materials have prompted researchers to investigate new ways of combating chemical and biological incidents and contamination. The development and use of self-cleaning materials are prevalent. Numerous studies have been performed that detail the creation, effectiveness, and benefit of self-cleaning films and materials. These studies are especially prevalent for fabrics, glass, and building materials. These studies, however, are only precursors to "smart" materials of the future; materials that incorporate multifunctional particles that will have the ability to detect toxics on their surfaces, identify the toxic, decontaminate themselves, and know when to stop self-decontamination processes. The research presented in this study is a rudimentary approach to creating a material that fulfills these criteria.

In the 1990s, the number of articles describing the benefits of semiconductor photocatalysis for mineralizing organics and reducing metals increased exponentially as compared to the number of articles published before this era. Studies demonstrated that semiconductor photocatalysis was able to effectively decompose a huge variety of organic compounds on particle surfaces, despite the fact that these organics had structures and functional groups that were vastly different from each other. Alkanes, ketones, alcohols, phenols, aromatic compounds, and so forth all can be mineralized by photocatalysis with titanium dioxide [1–4]. The vast number of decomposition reactions attainable with TiO_2 has led to the incorporation of these particles in materials designed for practical applications.

One of the fastest growing areas of TiO_2 application is the incorporation of reactive particles in surface materials. As Mills and Wang eloquently note the reaction

$$\text{organic} + O_2 \xrightarrow[h\nu \geq E_{bg}]{TiO_2} CO_2 + H_2O + \text{Mineral acids}, \qquad (1)$$

where E_{bg}, the TiO_2 semiconductor bandgap (3.0 to 3.2 eV), has been used extensively to create self-cleaning surfaces, including glasses, tiles, and fabrics, and has led to the commercialization of these products and a booming industry for them [5]. Their own work reported on the effectiveness of using self-cleaning films composed of Degussa P25 TiO_2-coated quartz discs for the destruction of stearic acid [5]. Other researchers have studied a variety of coatings for decontamination purposes as well. Allen et al. reported on the longevity and effectiveness of anatase and rutile TiO_2 in

paints for self-cleansing and microbial destruction [6], and Abdullah et al. reported on the advantages and disadvantages of coating methods (dip coating, splatter coating, static brush coating, etc.) for various TiO_2 for self-cleaning applications [7]. Other popular applications include the incorporation of photocatalytic semiconductor particles in textiles. Bozzi et al. tried to increase the ability to bond TiO_2 to wool-polyamide and polyester fabrics to improve stain mineralization with some success [8]. Similarly, Qi et al. coated cotton textiles with TiO_2 to create a fabric to reduce bacterial activity and get rid of stains [9]. Research focusing on self-cleaning entities is in its infancy; as the characteristics of nanoparticles are better understood, advancements will be made in these applications.

One aspect of self-cleaning films that has not been well explored includes films that report when they are contaminated, identify the contaminant and concentration of the contaminant, initiate a mechanism to "self-clean," assess themselves as to when the film surface is restored, and stop the self-cleaning process. This group's previous work demonstrated that TiO_2 films could be used to detect and distinguish various compounds [10, 11]. The work presented in this paper describes the creation of a film that self-senses contaminants sorbed to it, identifies the concentration of the contaminant, and triggers a mechanism to clean itself.

2. EXPERIMENTAL

2.1. Film preparation

The support substrate for the films was created by depositing fine platinum electrodes on thin aluminum oxide substrates. The aluminum oxide substrates (Coors Corporation, Colo, USA) were screened with platinum electrodes using a conductor paste (Heraeus, Hanau, Germany conductor paste product LP11-4493) silk-screened using a Presco Model 873 screen printer outfitted with Ikegami optics. The electrodes were air-dried, then sintered in a Lindberg type 51524 furnace. The temperature was initially ramped to 350°C over two hours to remove the organic vehicle (Heraeus vehicle RV-025), in which the platinum particles were suspended. The temperature was then increased to 1300°C to sinter the platinum particles. Substrates containing the impregnated platinum electrodes were cooled to ambient temperatures. Degussa P25 TiO_2 was mixed with the organic vehicle in a ratio of 1.0 g TiO_2 to 6.5 g organic vehicle. The TiO_2 paste was screen printed on top of the platinum electrodes. Substrates housing the electrodes and TiO_2 were fired at 350°C to remove the organic vehicle. Studies in the literature show that a change in Degussa P25 TiO_2 photoreactivity does not accompany firing at this temperature [12].

2.2. Feedback system

The electrodes on finished coated substrates were connected to a system that included an ultraviolet (UV) light emitting diode (LED) (Part BP200CUV1K-250) (Ledtronics, Inc., Calif, USA,) powered by a BK Precision DC Power Supply 1635A. Electrode leads initially were connected to a Wavetek DM23XT multimeter to get baseline resistance readings that determined cutoff resistance points. Afterwards, the electrodes of the sensor were connected to the input of an electronic switching circuit that activated the UV LED. The coated substrates and UV diode were contained inside of a sealed quartz chamber. The system configuration is shown in Figure 1.

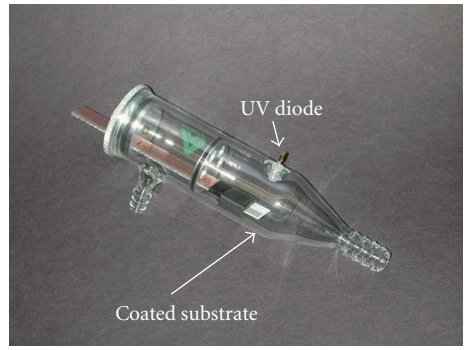

Figure 1: 100 mL reactor with two access ports, UV diode, and electrode-connected substrate holder.

2.3. Ethanol preparation

Reactor access ports, containing septa, were used to inject various concentrations of ethanol (Aaper Alcohol & Chemical Company, Ky, USA, absolute, 200 proof) into the reactor. Stock gaseous ethanol was prepared by injecting 5 mL of ethanol into a sealed glass bottle with a septum. The ethanol was allowed to equilibrate so that the headspace was saturated (approximately 59000 ppmv). Specific aliquots of ethanol vapor in the headspace were withdrawn via a gas-tight syringe and injected into the reactor to produce specific concentrations of ethanol in the reactor. Dry zero chromatographic air (AGA) periodically was injected into the reactor to replace the air removed. Saturated concentrations of ethanol in the reactor were created by injecting 0.2 mL of neat ethanol into the bottom of the reactor and allowing it to equilibrate. Reactor septa were removed for flushing the reactor with air between sample runs.

2.4. Sorption reactions/concentration recognition reactions

Initial work focused on self-recognition of surface contamination and contaminant concentration determinations. Two types of experiments were performed: those in dry zero chromatographic air (herein referred to as dry air) and those performed in humid air (40% relative humidity). In both types of reactions, the glass reactor housing all components was purged with air then was injected with the appropriate concentration of ethanol. The chemicals equilibrated for 20 minutes and the electrical resistances were recorded. The reactor was flushed with air until the sensor surface exhibited a resistance of greater than 2000 megaohms, and the next experiment commenced. The experiments were repeated using four sensors and results were averaged.

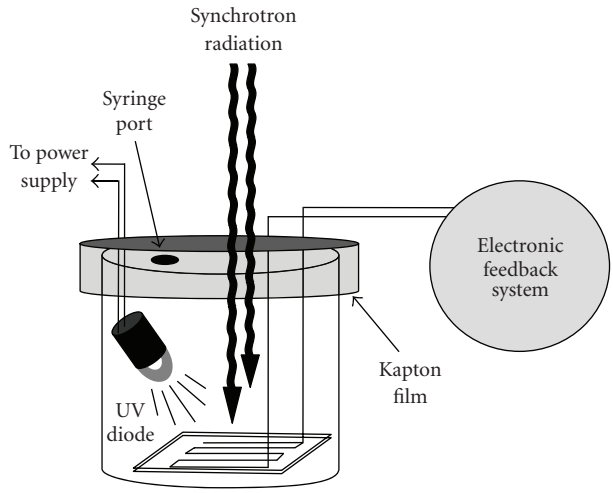

Figure 2: Test setup in XRF cups.

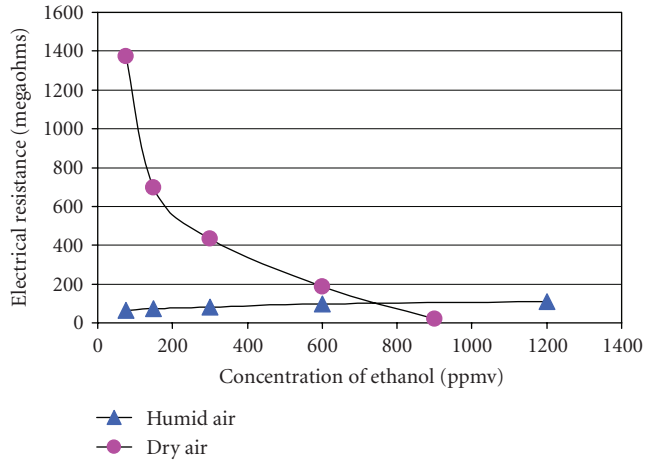

Figure 3: The electrical resistance of the coated substrates in dry air and in humid air in darkness as the ethanol concentration in the atmosphere above the substrates progressively increases.

2.5. Automated detection/automated decontamination reactions

The next group of experiments focused on contaminant detection, initiation of a decontamination process, and self-monitoring of the progress of the decontamination effort. Ethanol at various concentrations was injected into the reactor in darkness, while the system continuously self-monitored film resistance. The system was programmed to switch on the UV diode should the resistance of the surface decrease by more than 10 megaohms (from a maximum detection limit of 2000 megaohms). Triggering of the UV diode also signaled the system to record the surface resistance for the next 30 minutes during illumination.

2.6. Titanium nearest neighbor/valence state monitoring

Reactions were performed in X-ray fluorescence (XRF) cups so that the bulk state of titanium could be monitored for both valence state changes and the nearest neighbor changes with X-ray absorption fine spectroscopy (XAFS). XAFS experiments were conducted at Argonne National Laboratory's Advanced Photon Source. The experiments examined the state of Ti on the prepared films in lightness and darkness in air atmospheres, in nitrogen atmospheres, and in air atmospheres saturated with ethanol.

The test configuration was essentially the same as the one used in Figure 1, only the coated substrates were contained in XRF cups sealed with Kapton film. The experimental setup is shown in Figure 2.

XAFS work was performed at Argonne National Laboratory's Advanced Photon Source, at GSECARS beamline 13BM. Samples were positioned 45° to the beam. The extended X-ray absorption fine spectroscopy (EXAFS) spectra were recorded in fluorescence mode as a function of incident X-ray energy from a water-cooled Si(111) monochromator by measuring the integrated Ti K fluorescence intensity using a 16-element Ge detector placed in the horizontal plane along the polarization vector of the synchrotron radiation. Contaminants were injected into the XRF cup reactor and enclosed films were monitored for state changes after these injections.

3. RESULTS AND DISCUSSION

The electrical resistance of the TiO_2 surfaces changed as various concentrations of ethanol were introduced into the reactor. Figure 3 shows how the resistance of the TiO_2 film decreases as ethanol concentrations are increased in dry air and how the electrical resistance of the film slightly increases in humid air in the dark.

In dry air and in humid air, the film resistance was greater than 2000 megaohms in the absence of ethanol. In dry air in the dark, the electrical resistance rapidly decreases from 1374 megaohms at 75 ppmv ethanol to 22 megaohms at 900 ppmv ethanol. In humid air in darkness, the electrical resistance of the sensing surface slowly increases over time from 66 megaohms at 75 ppmv ethanol to 110 megaohms at 1200 ppmv ethanol. Figure 3 shows that water clearly competes for sorption sites on the TiO_2 sensing surface in darkness.

The known resistances gathered in Figure 3 were used to construct a feedback loop, whereby the sensing surface could trigger a UV LED positioned above it. Figure 4 shows how the resistance of the films in humid air (70% relative humidity) evolves as illumination proceeds.

As illumination proceeds, the resistance of the TiO_2 films decreases slightly indicating that activity is occurring on the sensing surface. Since the concentrations of injected ethanol were high and the film surface was small (1 cm by 1 cm), the oxidation of all ethanol in the reactor was not complete due to time and material constraints. However, the oxidation of gas-phase ethanol is a well-documented reaction and in the literature [13–18]. Briefly, part of the ethanol reacts on the Degussa P25 TiO_2 surface through the decomposition pathway of ethanol → acetaldehyde → acetic acid → carbon

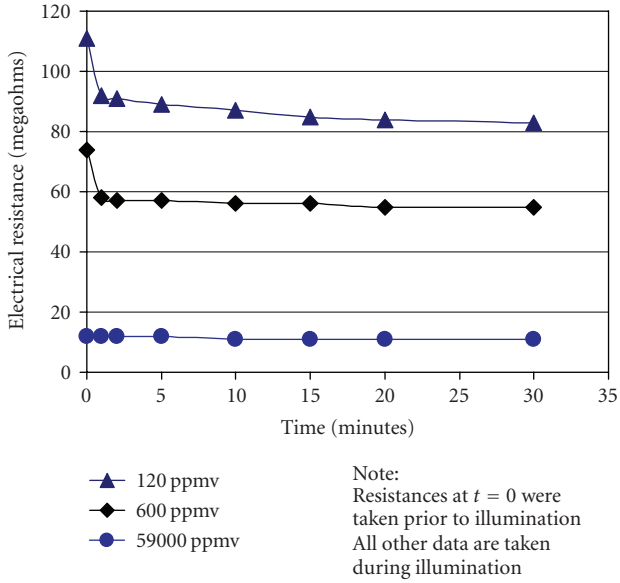

Figure 4: Substrate response after humid air was spiked ethanol and illuminated. Resistances at $t = 0$ reflect the surface's electrical resistance in the dark prior to the lights being turned on.

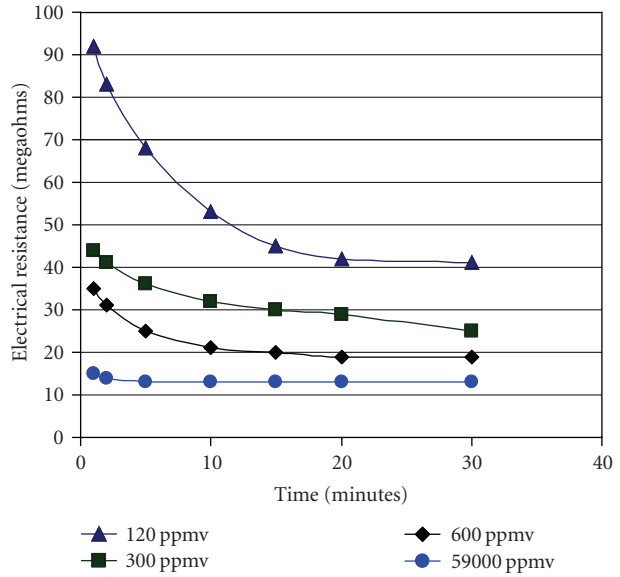

Figure 5: Response of substrates after dry air was spiked with ethanol and illuminated.

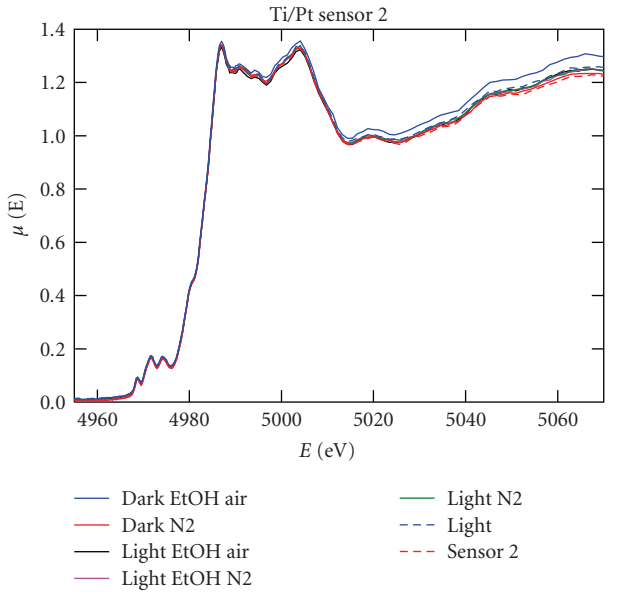

(a)

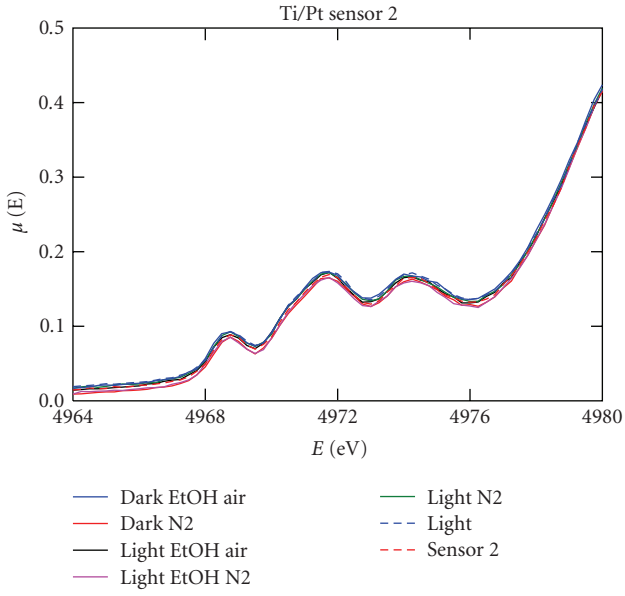

(b)

Figure 6: The XAFS spectra for the sensor. The labels designate the following atmospheric conditions during X-ray interrogation. "Dark EtOH air" indicates a saturated ethanol atmosphere in darkness; "dark N2" indicates a nitrogen atmosphere in darkness; "light EtOH air" indicates a saturated ethanol atmosphere while the sensing surface is illuminated; "light EtOH N2" indicates a nitrogen atmosphere saturated with ethanol while the sensing surface is illuminated; "light N2" indicates a nitrogen atmosphere while the sensing surface is illuminated; "light" indicates a dry air atmosphere while the sensor is illuminated; and "sensor 2" indicates a dry air atmosphere while the sensor is kept in darkness. Figure 6(b) is the magnified X-ray absorption near edge spectroscopy (XANES) portion of the spectra and describes the valence state of Ti.

dioxide + formaldehyde → formic acid → carbon dioxide. The other portion reacts via the decomposition pathway of ethanol → acetaldehyde → formic acid + formaldehyde → formic acid → carbon dioxide [18]. Ethanol and water do compete for reaction sites on the TiO_2 surface [17], and the rate of ethanol decomposition on the TiO_2 surface is partially limited by the adsorption of intermediates on the TiO_2 [14].

Analogous to the reactions described in Figure 4, various amounts of ethanol were injected into dry air in the reactor. Figure 5 shows the resistance of the films over time in humid air (70% relative humidity) as illumination proceeds.

From $t = 0$ minutes to $t = 30$ minutes, the resistance of the TiO_2 films drops slightly indicating that reactions are proceeding on the sensing surface. The results in both Figures 4 and 5 show that during illumination, humidity does not appear to affect the activity of surfaces exposed to *saturated* concentrations of ethanol; little change occurs in the resistance of the sensor over time. However, the presence of humidity does affect both the sorption of ethanol to the sensor surface (as shown in Figure 3) and the activity on the sensor surface at lower concentrations of ethanol. For example, exposure of the sensing surface to 600 ppmv of ethanol in the dark in humid air produces a resistance of 96 megaohms versus 185 megaohms in dry air. After the sensing surface is illuminated for 30 minutes, the resistance of the sensing surface in humid air decreases to 55 megaohms, while the resistance of sensing surface in dry air decreases to 19 megaohms. Humidity does play an important role in contaminant sorption to and photoactivity of Degussa P25. Muggli et al. note that water competes for sites when lights are off but at high concentrations of ethanol (100 ppm) water does not compete as effectively as ethanol [17]. Others also have noted in their oxidative work with gaseous toluene and acetone [19, 20].

Results from the XAFS studies of the bulk TiO_2 in the sensing surface are shown in Figures 6(a) and 6(b).

Figure 6 shows that in all cases, bulk Ti in the TiO_2 film remains in a Ti^{4+} state which is expected. Grazing incidence XAFS was not performed but may show variation in the state of surface Ti atoms. Films composed of smaller TiO_2 particles (i.e., nanoparticles less than 2 $\AA$ in diameter) might show variations in the state of Ti in the XANES spectra, but it is expected that the reactions with ethanol also would be different if nanoparticles were used. The spectra in Figure 6 aligns with the anatase form of TiO_2, which is the primary form of the Degussa P25 TiO_2 used to create films.

4. CONCLUSION

This study demonstrates that films combined with an appropriate feedback system can be used to detect contaminants on their surfaces, recognize the concentration of the contaminant, and trigger a decontamination step. Humidity did affect concentration measurements of ethanol and needed to be monitored in conjunction with the resistances to produce correct concentration information in the feedback loop. XANES measurements showed that the bulk TiO_2 composing the films was in the form of anatase and the Ti remained in a 4+ valence state throughout the experiments. We expect that with advancements in nanomaterials and nanocircuits, films and materials that are self-sense and self-decontaminate will be staples of future first responders and warfighters.

ACKNOWLEDGMENTS

The authors would like to thank Dr. Andrew Mills of the University of Strathclyde for supplying the Degussa P25 TiO_2, Mr. Joeseph Gregar of Argonne National Laboratory for fabricating the quartz reactor, and Mr. Rich Voogd of Argonne National Laboratory for fabricating the device in the reactor that connected the electronics to the sensor.

REFERENCES

[1] T. V. Malleswara Rao and G. Deo, "Ethane and propane oxidation over supported V_2O_5/TiO_2 catalysts: analysis of kinetic parameters," *Industrial and Engineering Chemistry Research*, vol. 46, no. 1, pp. 70–79, 2007.

[2] A. V. Vorontsov, D. V. Kozlov, P. G. Smirniotis, and V. N. Parmon, "TiO_2 photoctalytic oxidation: II. Gas-phase processes," *Kinetics and Catalysis*, vol. 46, no. 3, pp. 422–436, 2005.

[3] O. d'Hennezel, P. Pichat, and D. F. Ollis, "Benzene and toluene gas-phase photocatalytic degradation over H_2O and HCL pretreated TiO_2: by-products and mechanisms," *Journal of Photochemistry and Photobiology A*, vol. 118, no. 3, pp. 197–204, 1998.

[4] V. Brezová, A. Blažková, L. Karpinský, et al., "Phenol decomposition using M^{n+}/TiO_2 photocatalysts supported by the sol-gel technique on glass fibres," *Journal of Photochemistry and Photobiology A*, vol. 109, no. 2, pp. 177–183, 1997.

[5] A. Mills and J. Wang, "Simultaneous monitoring of the destruction of stearic acid and generation of carbon dioxide by self-cleaning semiconductor photocatalytic films," *Journal of Photochemistry and Photobiology A*, vol. 182, no. 2, pp. 181–186, 2006.

[6] N. S. Allen, M. Edge, G. Sandoval, J. Verran, J. Stratton, and J. Maltby, "Photocatalytic coatings for environmental applications," *Photochemistry and Photobiology*, vol. 81, no. 2, pp. 279–290, 2005.

[7] H. Z. Abdullah, H. Taib, and C. C. Sorrell, "Coating methods for self-cleaning thick films of titania," *Advances in Applied Ceramics*, vol. 106, no. 1-2, pp. 105–112, 2007.

[8] A. Bozzi, T. Yuranova, and J. Kiwi, "Self-cleaning of wool-polyamide and polyester textiles by TiO_2-rutile modification under daylight irradiation at ambient temperature," *Journal of Photochemistry and Photobiology A*, vol. 172, no. 1, pp. 27–34, 2005.

[9] K. Qi, W. A. Daoud, J. H. Xin, C. L. Mak, W. Tang, and W. P. Cheung, "Self-cleaning cotton," *Journal of Materials Chemistry*, vol. 16, no. 47, pp. 4567–4574, 2006.

[10] L. R. Skubal, N. K. Meshkov, and M. C. Vogt, "Detection and identification of gaseous organics using a TiO_2 sensor," *Journal of Photochemistry and Photobiology A*, vol. 148, no. 1–3, pp. 103–108, 2002.

[11] L. R. Skubal, M. C. Vogt, and N. K. Meshkov, "Monitoring the electrical response of photoinduced organic oxidation on TiO_2 surfaces," in *Water, Ground, and Air Pollution Monitoring Remediation*, T. Vo-Dinh and R. L. Spellicy, Eds., vol. 4199 of *Proceedings of SPIE*, pp. 157–164, Boston, Mass, USA, November 2000.

[12] J. F. Porter, Y.-G. Li, and C. K. Chan, "The effect of calcination on the microstructural characteristics and photoreactivity of Degussa P-25 TiO_2," *Journal of Materials Science*, vol. 34, no. 7, pp. 1523–1531, 1999.

[13] N. R. Blake and G. L. Griffin, "Selectivity control during the photoassisted oxidation of 1-butanol on titanium dioxide," *Journal of Physical Chemistry*, vol. 92, no. 20, pp. 5697–5701, 1988.

[14] M. R. Nimlos, E. J. Wolfrum, M. L. Brewer, J. A. Fennell, and G. Bintner, "Gas-phase heterogeneous photocatalytic oxidation

of ethanol: pathways and kinetic modeling," *Environmental Science and Technology*, vol. 30, no. 10, pp. 3102–3110, 1996.

[15] J. M. Coronado, S. Kataoka, I. Tejedor-Tejedor, and M. A. Anderson, "Dynamic phenomena during the photocatalytic oxidation of ethanol and acetone over nanocrystalline TiO_2: simultaneous FTIR analysis of gas and surface species," *Journal of Catalysis*, vol. 219, no. 1, pp. 219–230, 2003.

[16] A. V. Vorontsov and V. P. Dubovitskaya, "Selectivity of photocatalytic oxidation of gaseous ethanol over pure and modified TiO_2," *Journal of Catalysis*, vol. 221, no. 1, pp. 102–109, 2004.

[17] D. S. Muggli, K. H. Lowery, and J. L. Falconer, "Identification of adsorbed species during steady-state photocatalytic oxidation of ethanol on TiO_2," *Journal of Catalysis*, vol. 180, no. 2, pp. 111–122, 1998.

[18] D. S. Muggli, J. T. McCue, and J. L. Falconer, "Mechanism of the photocatalytic oxidation of ethanol on TiO_2," *Journal of Catalysis*, vol. 173, no. 2, pp. 470–483, 1998.

[19] Y. Ku, K.-Y. Tseng, and W.-Y. Wang, "Decomposition of gaseous acetone in an annular photoreactor coated with TiO_2 thin film," *Water, Air, & Soil Pollution*, vol. 168, no. 1–4, pp. 313–323, 2005.

[20] T. N. Obee, "Photooxidation of sub-parts-per-million toluene and formaldehyde levels on titania using a glass-plate reactor," *Environmental Science & Technology*, vol. 30, no. 12, pp. 3578–3584, 1996.

Hindawi Publishing Corporation
International Journal of Photoenergy
Volume 2008, Article ID 547301, 6 pages
doi:10.1155/2008/547301

Research Article

UV-Activated Luminescence/Colourimetric O_2 Indicator

Andrew Mills,[1] Cheryl Tommons,[1] Raymond T. Bailey,[1] M. Catriona Tedford,[2] and Peter J. Crilly[2]

[1] *Department of Pure and Applied Chemistry, Westchem Graduate School of Chemistry, University of Strathclyde, 295 Cathedral Street, Glasgow G1 1XL, Scotland*
[2] *Chemical and Biological Sciences, Bell College of Technology, University of the West of Scotland, Hamilton ML3 0JB, Scotland*

Correspondence should be addressed to Andrew Mills, a.mills@strath.ac.uk

Received 26 July 2007; Accepted 6 November 2007

Recommended by Russell Howe

An oxygen indicator is described, comprising nanoparticles of titania dispersed in hydroxyethyl cellulose (HEC) polymer film containing a sacrificial electron donor, glycerol, and the redox indicator, indigo-tetrasulfonate (ITS). The indicator is blue-coloured in the absence of UV light, however upon exposure to UV light it not only loses its colour but also luminesces, unless and until it is exposed to oxygen, whereupon its original colour is restored. The initial photobleaching spectral (absorbance and luminescence) response characteristics in air and in vacuum are described and discussed in terms of a simple reaction scheme involving UV activation of the titania photocatalyst particles, which are used to reduce the redox dye, ITS, to its *leuco* form, whilst simultaneously oxidising the glycerol to glyceraldehye. The response characteristics of the activated, that is, UV photobleached, form of the indicator to oxygen are also reported and the possible uses of such an indicator to measure ambient O_2 levels are discussed.

1. INTRODUCTION

The presence of oxygen in food packaging usually has a detrimental effect on the food products contained therein. Oxygen does not only react chemically with food to cause oxidative rancidity, but moulds, growths, and aerobic microorganisms—which discolour and decompose food and make it offensive to smell and dangerous to eat—thrive in the presence of oxygen [1]. Therefore, it is no surprise that the removal of oxygen in the food packaging industry is of immense importance. This is usually achieved via modified atmosphere packaging (MAP), a process in which the atmosphere within the food package is flushed and replaced with an inert gas, such as nitrogen or carbon dioxide, often combined with an efficient oxygen scavenger, resulting in an oxygen level of 0.1% or less within the food package [1, 2]. MAP increases the shelf life of many food products by a factor of 3-4 compared to that in air, making it a popular method of packaging food in the wholesale and retail food packaging industry.

There are many established methods for the detection of oxygen, which include the Clark electrode [3] and gas chromatography [4], however, such methods are too expensive and time consuming to allow 100% quality assurance. Consequently, there is an increasing interest in the development of cheap, easy-to-use oxygen indicators [5]. This area of research has been dominated by the quenching of a polymer-encapsulated lumophore, such as ruthenium(II)-tris(4,7-diphenyl-1,10-phenanthroline), $Ru(dpp)_3^{2+}$, by oxygen. One of the few commercially-available products based on this approach is the OxySense system [6], whereby, $Ru(dpp)_3^{2+}$ is encapsulated in silicone rubber dots, called O_2xyDots^{TM}, which can be attached to the inside of a package or bottle. The O_2xyDot is illuminated and the readily measured luminescence lifetime of the lumophore is equated to the oxygen level within the package. Unfortunately, the detection of oxygen using the OxySense system, or any optical sensor based on luminescence, requires the use of relatively expensive instrumentation for making the required lifetime or intensity measurements.

Unlike changes in luminescence intensity or lifetime, a sensor that changes colour in the presence of oxygen would be most desirable for MAP, given that the human eye can then act as the detector. Such indicators can take several forms, such as a tablet [7, 8] or a printed layer [9, 10]. This technology is typified by the Ageless Eye oxygen indicator, manufactured by the Mitsubishi Gas Company in Japan [7, 8, 11], that comprises a redox-indicator, usually methylene

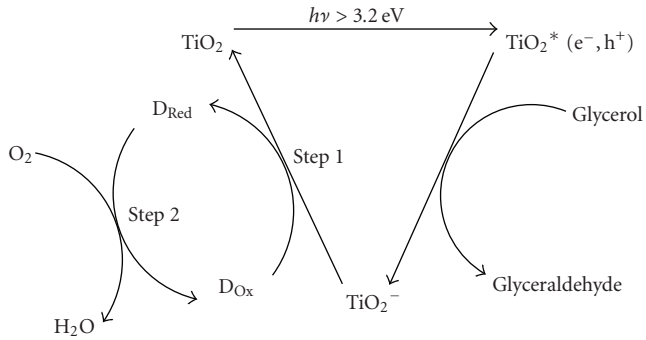

Figure 1: Schematic illustration of the key processes involved in the UV activation and subsequent response towards oxygen of a TO_2/redox dye, D_{OX}/glycerol/HEC oxygen indicator, such as that used in this work, where D_{OX} = ITS.

blue, which, in the absence of oxygen, is maintained in its colourless, chemically reduced, *leuco* form, by a reducing agent, such as glucose in an alkali medium. In the presence of oxygen *leuco,* methylene blue is oxidised to a highly coloured form. All components are mixed together, along with a nonredox dye, such as Acid Red 52, which provides a pink background colour, and pressed together to form a pellet, which is subsequently encapsulated in an oxygen-permeable, ion-impermeable plastic sachet to avoid any contact with the food. In the presence of oxygen, the Ageless Eye indicator changes from pink to purple in 2-3 hours, in a quasireversible process. However, this indicator needs to be stored and handled under anaerobic conditions. Such oxygen indicators are used in the food packaging industry, but mostly used as a research tool or fault diagnostic, since they have limited use elsewhere, because of cost and storage issues.

Lee et al. [12, 13] recently developed a new range of colourimetric oxygen indicators that are irreversible, reusable, and UV-light activated. Such "intelligent ink" oxygen sensors comprise a UV-absorbing semiconductor, such as TiO_2, a redox-indicator, such as methylene blue, a sacrificial electron donor, such as triethanolamine, and an encapsulating polymer such as hydroxyethyl cellulose; the ingredients are mixed together, with water as the solvent, to form an ink. The ink can be coated or printed subsequently onto a variety of substrates to produce a blue oxygen indicator film, which, when activated by UV light, becomes colourless. The activated, that is, UV-photobleached, film remains colourless unless, or until, exposed to oxygen, at which point the reduced methylene blue is reoxidised back to its original blue form.

The basic working principles, by which such an irreversible oxygen indicator works, are illustrated in Figure 1. Thus, upon UVA irradiation, ultraband gap illumination ($h\nu$) of the TiO_2 semiconductor particles create electron-hole pairs, $TiO_2{}^*(e^-,h^+)$. The photogenerated holes, h^+, oxidise the mild sacrificial electron donor (SED) present, glycerol in this case, in the ink film and the remaining photogenerated electrons, that is, e^- or $TiO_2{}^-$, as in Figure 1, reduce the redox-sensitive dye, D_{OX} to a reduced form, D_{Red}, which has a different colour to D_{OX}. In an ink film, the above key components are encapsulated in a polymer, such as hydroxyethyl cellulose (HEC) that is soluble in a common solvent (usually water). Thus, UV irradiation causes an O_2-sensitive ink film to change colour (step 1, Figure 1). In the absence of oxygen, the photobleached dye will stay in this reduced—usually colourless—state indefinitely. However, upon exposure to oxygen, it is reoxidised to its original, highly coloured form (step 2, Figure 1).

In this paper, we describe a very oxygen sensitive version of this type of UV-activated indicator, in which the sacrificial electron donor is glycerol and the redox dye is indigo-tetrasulfonate (ITS). The latter is highly coloured and nonluminescent in its oxidised state but virtually colourless, highly luminescent, and very oxygen-sensitive in its reduced state, *leuco* indigo-tetrasulfonate (*leuco*-ITS).

2. EXPERIMENTAL

2.1. Materials

Unless stated otherwise, all chemicals were purchased from Aldrich Chemical Company (Gillingham, Dorset, UK). The semiconductor, titanium dioxide (TiO_2), was P25 provided by Degussa (Frankfurt, Germany) and comprised particles *ca*. 30 nm in diameter, with an 80 : 20 anatase : rutile crystal phase composition.

2.2. Preparation of indigo-tetrasulfonate (ITS) based films

A typical example of an UV-activated luminescence/colourimetric oxygen-sensitive, ITS-based indicator ink, used to make the indicator films reported in this work, was prepared by adding 200 mg of glycerol to 2 g of a 5% wt hydroxyethyl cellulose (HEC) aqueous solution, to which 20 mg of P25 TiO_2 and 5 mg of the redox indicator indigotetrasulfonate (ITS) had been added. The resulting mixture was stirred magnetically for 15 minutes, followed by 15 minutes sonication to disperse the usually aggregated titania particles, followed by a further 15 minutes stirring. Typically, an oxygen indicator film was prepared by placing 3-4 drops (*ca*. 0.4 ml) of this ink onto a cut-glass microscope slide (0.8×3.8 cm), which was subsequently spun at 2500 rpm for 15 seconds. The resulting blue, transparent film was allowed to dry in the dark for 30 minutes before use.

2.3. Methods

All UV/V is spectra and absorbance versus time profiles were recorded using a Cary 50 BioVarian spectrophotometer. Luminescence spectra and luminescence intensity versus time profiles were recorded using a PerkinElmer LS50 fluorimeter and lifetime measurements were made with an IBH Fluorocube time-correlated single-photon counting system, using a NanoLed-03 source, which has its excitation peak wavelength at 370 nm. All UV irradiations were conducted using a 2×4 W BLB handheld UVA light source (typical irradiance = 4 mW cm^{-2}).

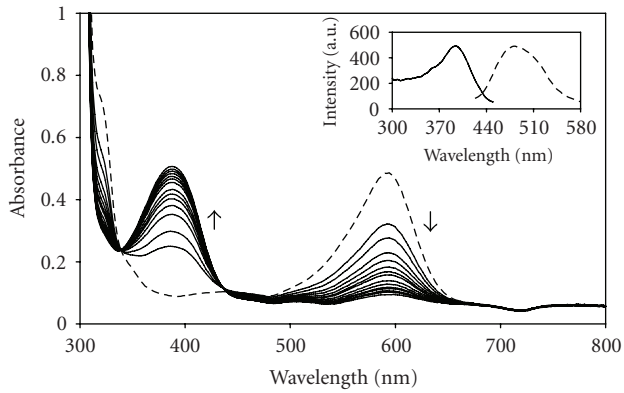

Figure 2: UV/Vis spectra recorded for an indigotetrasulfonate (ITS) deoxygenated aqueous solution 2.8×10^{-5} mol dm^{-3}, pH4): broken line. Upon reaction with a zinc amalgam pellet, the blue ITS solution is reduced to *leuco*-indigotetrasulfonate (*leuco*-ITS), signalled by the decrease in absorbance at 590 nm and the increase at 390 nm (spectra were recorded every 30 minutes). The insert diagram illustrates the excitation spectrum (solid line; λ_{em} = 485 nm) and emission spectrum broken line; λ_{ex} = 390 nm) of a 2.8×10^{-5} mol dm^{-3} *leuco*-ITS deoxygenated aqueous solution, at pH4.

3. RESULTS AND DISCUSSION

3.1. Chemical reduction of an ITS solution

An aqueous solution of *leuco*-ITS can be readily prepared from an ITS solution *via* the addition of a reductant, such as zinc amalgam. However, *leuco*-ITS is very oxygen-sensitive and readily oxidized back to ITS by ambient oxygen and so, in order to prevent this re-oxidation step occurring whilst recording the spectral properties of the reduced redox dye in solution, any oxygen needs to be removed. Thus, in a typical experiment, a dilute solution of ITS (2.8×10^{-5}), at pH4, was prepared and the absorbance spectra recorded, as illustrated in Figure 2 (broken line). ITS absorbs in the blue region of the visible spectrum, with a wavelength of maximum absorbance, λ_{max}, at 590 nm, which is typical for this dye [14]. This solution was then deoxygenated *via* 5 cycles of a freeze-thaw process. Addition of a zinc-amalgam pellet to the deoxygenated ITS solution reduced the highly coloured ITS solution to its very pale yellow *leuco*-ITS form, as shown by the decrease in absorbance at 590 nm and the increase in absorbance at 385 nm in Figure 2 (spectra were recorded every 30 minutes). Excitation of *leuco*-ITS at this wavelength (385 nm) revealed a blue luminescence with an emission maximum at 485 nm. The uncorrected excitation (λ_{em} = 485 nm) and emission spectrum (λ_{excit} = 390 nm) of the *leuco*-ITS aqueous solution are illustrated in the insert diagram of Figure 2. Single-photon counting revealed the lifetime of luminescence of *leuco*-ITS in aqueous solution, at pH4, to be 0.24 ± 0.02 microseconds.

3.2. Photobleaching of an ITS oxygen indicator film

A parallel study, to that above, was carried out on a typical ITS oxygen indicator film, with one set of experiments carried out under vacuum (10^{-3} mbar), that is, O_2 free, and the other under ambient conditions, that is, 21% O_2. A typical absorbance spectrum of a blue-coloured indicator film under vacuum before (broken line) and after activation with UVA light is illustrated in Figure 3(a). From these results it can be seen that the initially blue-coloured ITS film is activated, that is, converted from ITS to *leuco*-ITS via the photoreduction of ITS by the UV-excited titania particles (see Figure 1) in under 3 minutes of UVA irradiation. This photoreduction process (step 1, Figure 1) produces a fall in absorbance of the film at 600 nm as a function of UVA irradiation time as indicated by the data in Figure 3(a) insert diagram. In contrast, under otherwise the same conditions, a typical oxygen indicator in an ambient environment takes twice as long to activate using the same UVA light source (I = 4 mW cm^{-2}). The lower rate of photobleaching in the latter system is due to the presence of oxygen in the ambient environment which is able to reoxidise the reduced form of the dye *via* a dark reaction, that is step 2 in Figure 1.

Figure 3(b) contains photographs of a typical TiO_2/ITS/glycerol/HEC ink spun coated onto a coverslip (i) before and (ii) after photobleaching by UV irradiation (30 seconds, I = 7 mW cm^{-2}) in air. Photograph (iii), in Figure 3(b), is after *ca*. 15 minutes in the dark under ambient conditions, during which time the ITS film regains its original colour (and loses its luminescence), due to the reoxidation of *leuco*-ITS to ITS by oxygen. Photographs (i)–(v) confirm that the ITS indicator films can be photoactivated under ambient conditions to produce a luminescent yellow, *leuco*-ITS film that is oxygen-sensitive.

The UV activation of a typical ITS oxygen indicator film can also be monitored by luminescence, given that *leuco*-ITS luminesces at 470 nm in the film (see Figure 3(b), photographs (iv) and (v)). The observed change in the emission spectrum of an ITS oxygen indicator film, under vacuum, upon exposure to UVA light as a function of time is illustrated in Figure 4. The insert diagram illustrates a plot of the variation in a film's luminescence intensity as a function of UVA irradiation time, and, as in the absorption spectral changes in Figure 2, shows that in the absence of oxygen the film is activated in less than 3 minutes, in comparison to an oxygen indicator film in an ambient environment, which takes *ca*. 6 minutes due to the dark back reaction, that is, step 2 in Figure 1.

3.3. Dark oxidation of an activated ITS film

Once activated, that is, photobleached, via step 1 in the reaction scheme in Figure 1, the stability of the photobleached oxygen indicator film depends on the level of oxygen present in the environment in which it finds itself. Thus, in the dark and in the absence of oxygen, the UV-activated oxygen indicator remains bleached indefinitely, whereas in the presence of oxygen, its colour is restored within seconds and the luminescence associated with the reduced form of ITS is quenched. This is nicely illustrated by the data in Figures 5 and 6 (broken lines), which depict the recorded change in absorbance at 600 nm and luminescence intensity at 470 nm, respectively, as a function of time, of an

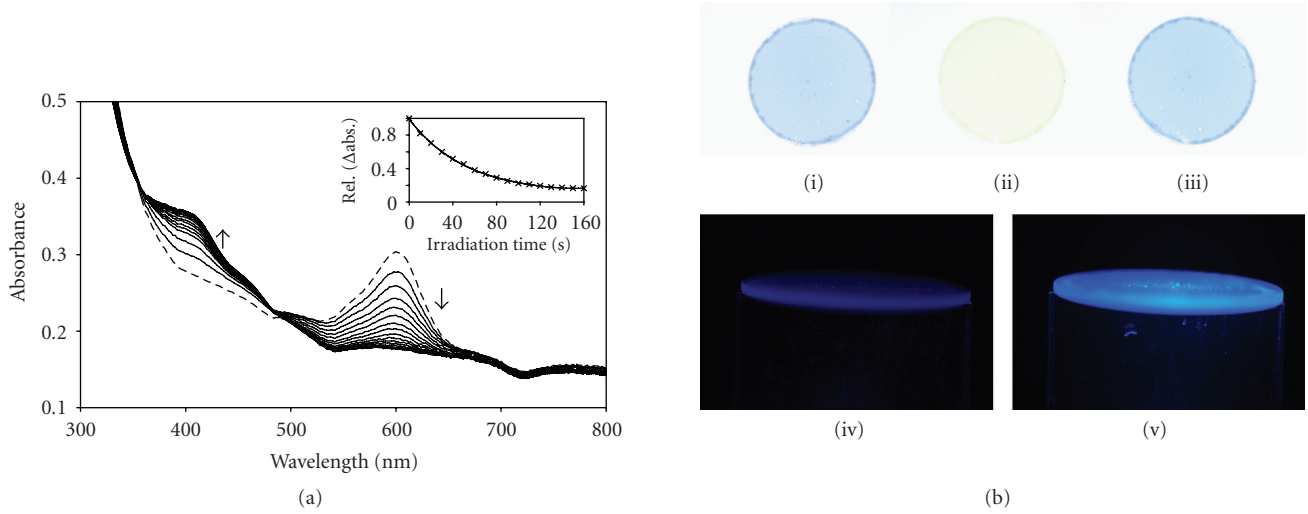

Figure 3: (a) Recorded change in the UV/Vis spectrum of an ITS oxygen indicator film (broken line), in the absence of oxygen, upon exposure to UVA light (intensity: 4 mW cm^{-2}) as a function of time. The spectra illustrated were irradiated (from top to bottom at 600 nm) for 0 second up to 160 seconds, in 10-second intervals. The insert diagram illustrates the change in absorbance of the indicator film at 600 nm as a function of irradiation time, derived from the data in the main diagram. (b) Photographs of an oxygen indicator film on a coverslip. (i) TO_2/ITS/glycerol/HEC film before and (ii) after 30 seconds UVA irradiation (I = 7 mW cm^{-2}), and (iii) film in photograph (ii) allowed to recover after 15 minutes in air. (iv) Photograph of film (i) under very low UV-light illumination in the presence of oxygen. (v) Photograph of film (ii) also under very low UV-light illumination.

ITS-based oxygen indicator film that has been UV irradiated in a vacuum and subsequently exposed to an ambient atmosphere by opening up the system to air. In contrast to this data, the solid lines in Figures 5 and 6 correspond to the recovery of an UV-activated oxygen indicator film, irradiated under ambient conditions (i.e., 21% O_2) and maintained in this environment once the photobleaching process was stopped. Not surprisingly, the oxygen indicator film in an evacuated environment recovered its original blue colour when exposed subsequently to oxygen in the dark. However, the ITS indicator film which was initially photobleached in air recovered only *ca*. 50% of its original colour, possibly due to some photodegradation of the redox dye, presumably caused by the longer exposure to UVA light in air needed to photobleach the film, which probably promotes dye degradation via singlet oxygen production.

The insert diagrams in Figures 5 and 6 show that the dark process (step 2, Figure 1) gives a good fit to first-order kinetics for a UV-activated oxygen indicator film when photobleached and left to recover in an ambient atmosphere, or when photobleached in a vacuum and subsequently exposed to air. Such first-order kinetics are typical for UV-activated oxygen film indicators and provide support for the proposed scheme, that the kinetics of step 2 in the reaction scheme in Figure 1 depend directly upon the rate of diffusion of O_2 through the film. Other work indicates that the rate of this dark recovery process is first order with respect to the partial pressure of oxygen in the ambient atmosphere as with similar UV-activated, oxygen-sensitive film indicators. The first-order rate constants for the recovery of a typical UV-activated oxygen indicator film in an ambient environment and in a vacuum are given in Table 1. It remains

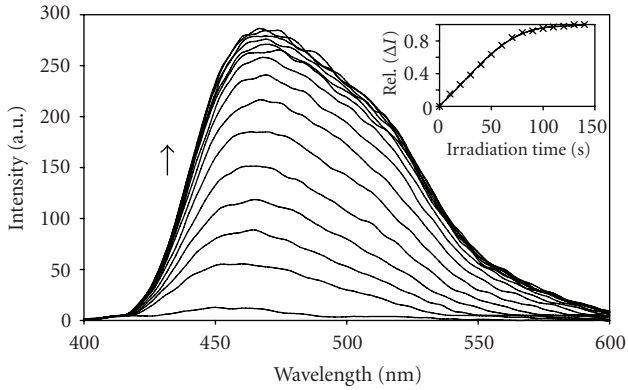

Figure 4: Recorded change in the emission spectrum of an ITS oxygen indicator film (broken line), under vacuum, upon exposure to UVA light as a function of time. The spectra illustrated were irradiated (from bottom to top) for 0 second up to 140 seconds, in 10-second intervals. The insert diagram illustrates the change in luminescence intensity of the indicator film at 470 nm as a function of irradiation time, derived from the data in the main diagram.

unclear why the kinetics of step 2, the dye recovery step, are slower for an ITS film irradiated in air, compared to that for films irradiated in a vacuum, although an appreciable degree of dye degradation is observed for the latter process (*vide supra*). The above results stress the need for oxygen-free conditions when UV-activating these ITS-based indicators.

4. CONCLUSION

A novel, fast acting luminescent and colourimetric oxygen indicator ink is described, containing a sacrificial electron

Table 1: Photobleaching and recovery kinetics of a typical UV-activated oxygen indicator.

	Photobleaching kinetics				Recovery kinetics			
Environment	Abs·k_1(s^{-1})	r^2	Int·k_1(s^{-1})	r^2	Abs·k_1(s^{-1})	r^2	Int·k_1(s^{-1})	r^2
Ambient	0.0063	0.99	0.0075	0.96	0.0062	0.99	0.0091	0.99
Vacuum	0.013	0.99	0.015	0.97	0.033	0.99	0.027	0.98

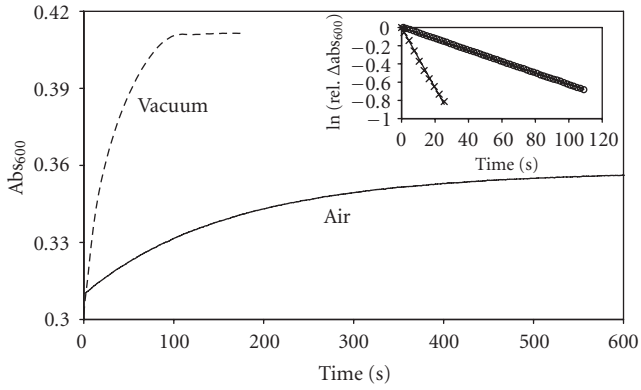

Figure 5: Change in the absorbance, at 600 nm, of a typical UV-activated ITS oxygen indicator film as a function of time, under an ambient atmosphere (solid line) and an ITS film UV-activated under vacuum and subsequently exposed to air (broken line). Each film was fully photobleached, using UVA light, before being allowed to recover. The insert diagram is a first-order plot (natural log of the change in the absorbance, that is, ln (ΔAbs), at 600 nm versus time), over one half life, derived from the data in the main diagram. The rate constants for this recovery step are given in Table 1.

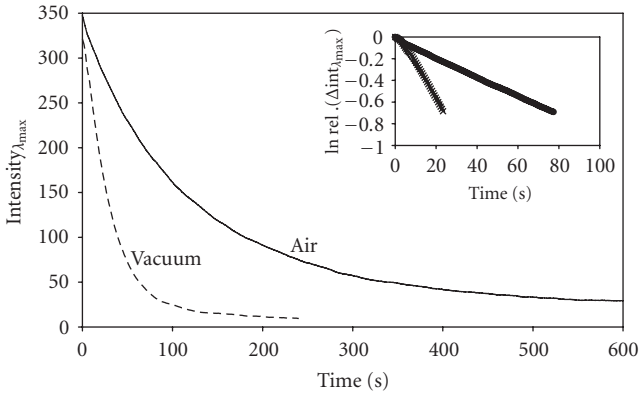

Figure 6: Change in the luminescence intensity, at 470 nm, of a typical, UV-activated ITS oxygen indicator film as a function of time, under an ambient atmosphere (solid line) and when exposed to air (broken line), having been first UV-activated under vacuum. Each film was fully photobleached, using UVA irradiation, before being allowed to recover in air. The insert diagram is a first-order plot, over one half life, derived from the data in the main diagram.

donor (glycerol) and the redox indicator (indigotetrasulfonate). The indicator is blue coloured in the absence of UV light, however, upon exposure to UV light it not only loses its colour but also luminesces, unless and until it is exposed to oxygen, whereupon, under dark conditions, its colour is restored. The initial photobleaching spectral (absorbance and luminescence) response characteristics in air and in vacuum are described and discussed in terms of a simple reaction scheme involving UV activation of the titania photocatalyst particles, which are used to reduce the redox dye, ITS, to its *leuco* form. The response characteristics of the activated, that is, UV-photobleached form of the indicator, to oxygen are also reported. This indicator appears more sensitive towards oxygen than previous UV-activated indicators, based on methylene blue, probably due to the lower redox potential [14] of ITS (−0.046 V versus SHE) compared to that of methylene blue (+0.028 V versus SHE) at pH7. This indicator appears susceptible to appreciable photodegradation when UV-activated under ambient (21% O_2) conditions. In the absence of oxygen, however, UV activation is not only more rapid, but also does not produce any significant photodegradation. Thus, the ink appears particularly suited for use in systems that are usually oxygen free, before UV activation, as a means of indicating any subsequent leak or tampering.

ACKNOWLEDGMENTS

The authors are pleased to acknowledge a grant to C. Tommons from Bell College Research Grants Committee and M. C. Tedford thanks the Royal Society of Chemistry Research Fund.

REFERENCES

[1] M. L. Rooney, *Active Food Packaging*, Blackie, London, UK, 1995.
[2] A. L. Brody, B. R. Strupinsky, and L. R. Kline, *Active Packaging for Food Applications*, Technomic Publishing, Lancaster, Pa, USA, 2001.
[3] M. L. Hitchman, *Measurement of Dissolved Oxygen*, John Wiley & Sons, New York, NY, USA, 1978.
[4] S. J. Valenty, "Gas chromatographic determination of dissolved hydrogen and oxygen in photolysis of water," *Analytical Chemistry*, vol. 50, no. 4, pp. 669–671, 1978.
[5] O. S. Wolbeis, *Fibre Optic Chemical Sensors*, CRC Press, Boca Raton, Fla, USA, 1991.
[6] OxySense, Inc., March 2007, http://www.oxysense.com/.
[7] M. Goto, "Oxygen Indicator," 1987, JP Patent 62259059.
[8] Y. Yoshikawa, T. Nawata, M. Otto, and Y. Fujii, "Oxygen indicator," 1979, US Patent 4169811.
[9] E. S. Davis and C. D. Garner, "Oxygen indicating composition," 1996, UK Patent 2298273.
[10] K. C. Krumhar and M. Karel, "Visual indicator system," 1992, US Patent 5096813.
[11] Mitsubushi Gas Chemical Company, Inc., March 2007, http://www.mgc.co.jp/eng/company/materials/products/ageless/related/index.html.

[12] S.-K. Lee, A. Mills, and A. Lepre, "An intelligence ink for oxygen," *Chemical Communications*, no. 17, pp. 1912–1913, 2004.
[13] S.-K. Lee, M. Sheridan, and A. Mills, "Novel UV-activated colorimetric oxygen indicator," *Chemistry of Materials*, vol. 17, no. 10, pp. 2744–2751, 2005.
[14] E. Bishop, *Indicators*, Pergamon Press, Oxford, UK, 1972.

Hindawi Publishing Corporation
International Journal of Photoenergy
Volume 2008, Article ID 827605, 7 pages
doi:10.1155/2008/827605

Research Article

Studies of Dye Sensitisation Kinetics and Sorption Isotherms of Direct Red 23 on Titania

Peter J. Holliman,[1] Beatriz Vaca Velasco,[1] Ian Butler,[1] Maarten Wijdekop,[2] and David A. Worsley[3]

[1] *School of Chemistry, Bangor University, Gwynedd LL57 2UW, UK*
[2] *Corus Colors, Shotton Works, Flintshire CH5 2 NH, UK*
[3] *School of Engineering, Swansea University, Swansea SA2 8PP, UK*

Correspondence should be addressed to Peter J. Holliman, p.j.holliman@bangor.ac.uk

Received 27 March 2008; Revised 27 March 2008; Accepted 19 May 2008

Recommended by Russell Howe

Sorption kinetics and isotherms have been measured for a commercial dye (Direct Red 23) on different samples of powdered Titania, and the data were analysed to better understand the dye sensitization process for dye sensitised solar cells (DSSCs). For the sorption kinetics, the data show rapid initial sorption (<1 hour) followed by slower rate of increasing uptake between 1 and 24 hours. While higher initial concentrations of dye correspond to higher sorption overall, less dye is absorbed from higher initial dye concentrations when considered as percentage uptake. The correlation between the sorption data and model isotherms has been considered with time. The Langmuir model shows better correlations compared to the Freundlich isotherm. The dye uptake data has also been correlated with Titania characterization data (X-ray diffraction, scanning electron microscopy, BET and zero point charge analysis). Kinetic data show significantly better fits to second-order models compared to first order. This suggests that chemisorption is taking place and that the interaction between the dye sorbate and the Titania sorbent involves electron sharing to form an ester bond.

1. INTRODUCTION

The need for commercially viable renewable energy sources such as photovoltaic (solar cell) devices is increasing in line with concerns over climate change resulting from fossil fuel combustion [1]. Dye sensitised solar cells (DSSCs) have the advantage that this is a relatively low-cost photovoltaic technology [2]. A DSSC device uses a dye chemisorbed to an oxide semiconductor such as Titania and operates by the dye reaching an excited state by absorbing photons in the visible region and injecting these electrons into the oxide. The electrons then pass between TiO_2 particles to an electrode and around a circuit to a second electrode finally passing via an electrolyte back to the dye to continue the cycle.

A major breakthrough in DSSC technology (solar efficiency 7%) was achieved by O'Regan and Grätzel in 1991 [3] using a Ru bipyridyl complex (the N3 dye) as the dye sensitizer along with high-surface area nanoparticulate Titania. Subsequent work by Grätzel and coworkers to develop new dyes has resulted in increased solar efficiencies for DSSC (up to 10.4%) using N719 [4] and Ru terpyridyl "black dye" [5]. Since 1991, a great deal of work has been carried out on studying new dyes as sensitizers to optimise extinction coefficient, rates of electron injection into TiO_2, and rates of regeneration of the ground state dye by interaction with the electrolyte [6, 7]. While ruthenium(II)bipy complexes have by far been the most widely studied dyes for DSSC, more recently, indoline [8], unsymmetrical phthalocyanines [9], and squaraine dyes [10] have also been reported as showing promise.

Typically, Titania is sensitized by soaking the oxide in a dye solution for either a period of hours or even overnight. However, to scale up the manufacture of DSSC, dyes must meet materials processing criteria, one of which is that the dye sensitisation process needs to take place more rapidly. In this context, the adsorption and desorption behavior of the Ru dye N3 has been studied stressing that dye coverage above 0.3 of a monolayer is necessary to increase current efficiency [11]. Also working on Ru dyes, Nazeeruddin et al. have reported a swift uptake procedure for the N719 dye [12]. More recently, it has been reported that electron injection rates into the metal oxide are an order of magnitude slower

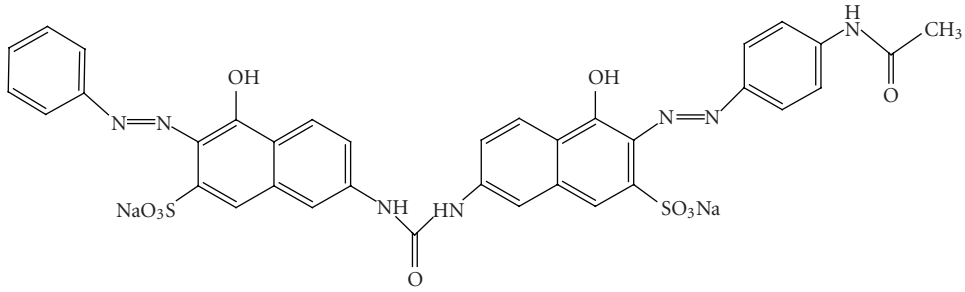

Figure 1: Chemical structure of the commercial diazo dye Direct Red 23 (C.I. 29160).

for aggregated dye compared with monomeric sensitizer dye emphasising the need for efficient monolayer sensitization [13].

This paper investigates the sorption isotherms and kinetics for the commercially available azo dye Direct Red 23 on different samples of Titania and correlates these data with both model isotherms and the physicochemical characteristics for the Titania samples. These data have been used to develop a clearer understanding of the dye sensitization process when considering time and dye concentration as two key variables.

2. EXPERIMENTAL

Three variables were explored using the commercial azo dye Direct Red 23, C.I. 29160 (Aldrich); TiO_2 grade (four samples labelled A to D were used), dye concentration (from 163 mg l^{-1} to 650 mg l^{-1}), and time (up to 24 hours).

Sorption experiments were carried out using two replicates. The data were averaged and the standard errors are shown in Figures 2(b) and 2(c). In a typical experiment, methanol (50 mL, HPLC grade, Aldrich) containing the appropriate dye concentration was added to titanium dioxide powder (1 g) in a 50 mL flask, shaken for 1 minute and left to stand. Aliquots (1.5 mL) were taken after 15, 30, and 60 minutes, then every 1 hour up to 8 hours and then at 23 and 24 hours. These were centrifuged for 10 minutes at 8000 rpm before the solution dye concentration was measured by UV-visible spectroscopy at $\lambda = 500$ nm. If necessary, dilution was carried out (1 mL in 10 mL of methanol). The amount of sorption (mg kg^{-1}) was calculated as the difference between the amount of dye initially added and that measured at each measurement time. Langmuir (1) and Freundlich (2) and (3) sorption isotherm equations were fitted to the experimental data by a computerized least-squares optimization routine, where

$$\frac{C_e}{q_e} = \frac{1}{Q_0 b} + \frac{C_e}{Q_0} \quad \text{(see, [14])} \tag{1}$$

$$q_e = k_f \times C_e^{1/n} \tag{2}$$

$$\log_{10} q_e = \log_{10} k_F + \frac{1}{n}\log_{10} C_e, \quad \text{(see, [15])}, \tag{3}$$

where C_e is the concentration of dye in the solution (mg l^{-1}) at equilibrium, q_e is the dye concentration adsorbed onto the TiO_2 (mg g^{-1}) at equilibrium, and Q_0 (mg g^{-1}) and b (l mg^{-1}) are constants related to the adsorption capacity and to the energy of adsorption, respectively [14]. For the Freundlich isotherm, k_F is a constant which measures the adsorption capacity and $1/n$ is a measure of the adsorption intensity [15]. The values for k_F and n were calculated from the intercept and slope of the plots. The solid-to-solution partition coefficient (K_d) was determined from the following equation

$$K_d = \frac{C_{\text{tot}}}{C_e}, \tag{4}$$

where C_{tot} is the total dye ($C_e + q_e$).

For TiO_2 samples A and C, first- and second-order kinetic equations were fitted to the data according to the equations proposed by Kannan and Sundaram (5) [16] and Ho and McKay (6) [17], respectively,

$$\frac{1}{q_t} = \left(\frac{k}{q_{\max}}\right)\left(\frac{1}{t}\right) + \frac{1}{q_{\max}} \quad \text{(see, [16])} \tag{5}$$

$$\frac{t}{q} = \frac{1}{k_2 q_e^2} + \frac{t}{q_e} \quad \text{(see, [17])}. \tag{6}$$

For the first-order model (5), q_t is the amount of dye adsorbed in mg g^{-1} at various times (t), $q_{\max}$ is the maximum adsorption capacity, and k is the first-order rate constant in min^{-1} [16]. Linear correlation of $1/q_t$ versus $1/t$ was made to samples A and C at 3 different dye concentrations. For the second-order model, the initial adsorption rate h in mg g^{-1} min^{-1} can be defined as $h = k_2 q_e^2$, where q_e is the equilibrium adsorption capacity in mg g^{-1} and k_2 is the second-order constant in g mg^{-1} min [17]. Both variables were calculated from the slope and intercept, respectively.

2.1. Characterisation techniques

X-ray powder diffraction (XRD) data was measured between 5 and 75 degrees two theta using Ni-filtered Cu Kα1 radiation ($\lambda = 1.54051$ Å) on an X'Pert PRO theta-theta diffractometer (PANalytical Ltd) at 45 kV and 35 mA.

Gold sputtered samples were analyzed by scanning electron microscopy (SEM) at 11 kV on a Hitachi S-520 SEM. EDAX was measured on the same instrument at 14 kV with an Oxford Instruments 7497 EDAX with Link ISIS computer software.

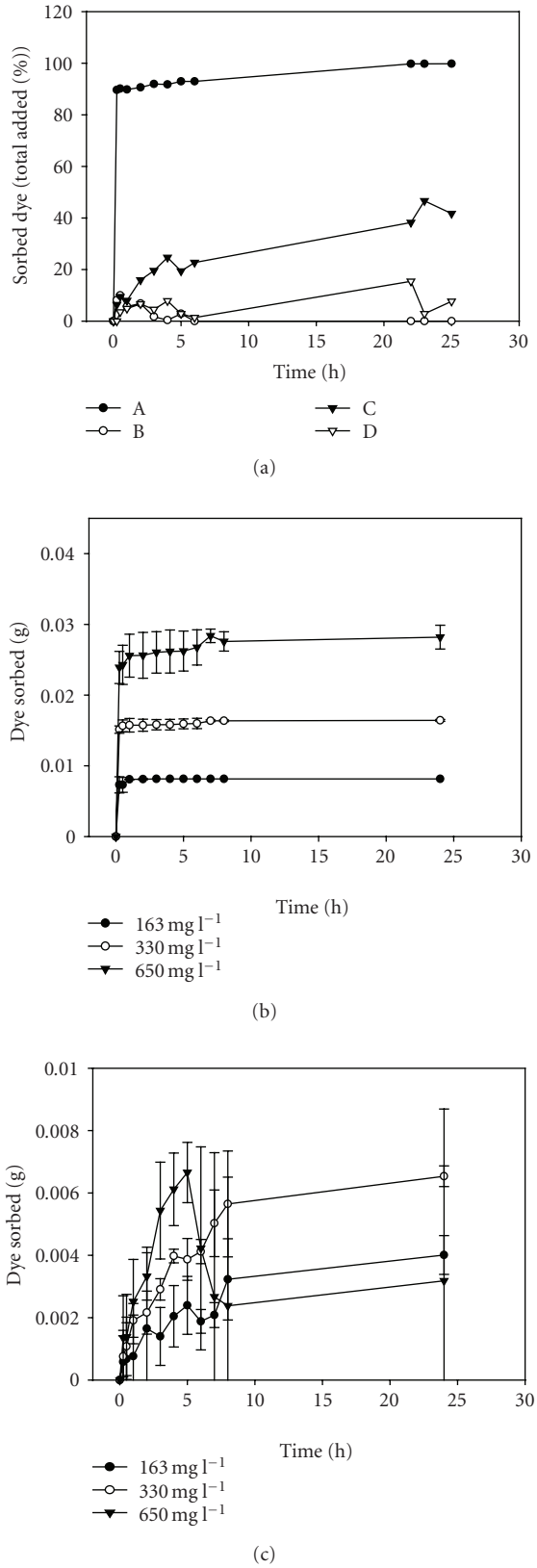

Figure 2: Sorption kinetics of (a) 330 mg l^{-1} of Direct Red 23 onto four different samples of TiO_2; (b) varying concentrations of Direct Red 23 onto TiO_2 sample A; (c) varying concentrations of Direct Red 23 onto TiO_2 sample C. Error bars are omitted from (a) for clarity.

The surface areas of the TiO_2 powders were measured at 77 K on a Micrometrics Gemini III 2375 and the data analyzed using BET (Braumer, Emmet, and Teller) isotherms.

Zero point charge (ZPC) was determined by the salt-addition method [18] using three replicates. In the procedure, ten aliquots of 0.1 M $NaNO_{3(aq)}$ (40 mL, Aldrich) were adjusted to varying pH between 2 and 11 using $NaOH_{(aq)}$ (99.99%, Aldrich) or $HNO_{3(aq)}$ (Aldrich). TiO_2 (0.2 g) was added to each aliquot, thoroughly mixed, and the pH measured after 24 hours. The difference between final pH and initial pH (ΔpH) was plotted against initial pH. ZPC was then calculated from this graph at the point where ΔpH = 0.

UV-visible spectroscopy was measured in silica cuvettes (1 cm path length) on an ATI UNICAM UV4 spectrometer and the data analyzed using VisionScan software. The instrument was calibrated using inhouse standards from 0 to 200 mg l^{-1} (typical equation was $y = 37200x - 0.004$ with $R^2 > 0.99$).

3. RESULTS AND DISCUSSION

3.1. TiO_2 powder characterisation

Four commercial samples of Titania powder have been investigated. Sample A is Degussa P25, an uncoated nanoparticulate Titania; sample B is Kronos 1001 an uncoated, anatase pigment grade Titania; sample C is Kronos 2063; and sample D is Kronos 2220, a coated rutile pigment grade Titania.

X-ray powder diffraction data (Table 1) show that Sample A is a mixture of *ca.* 80% anatase [19] and 20% rutile [20].The diffraction peaks are broader than the other samples reflecting the smaller particle size range which is confirmed by electron microscopy. Sample B shows only anatase along with narrower diffraction lines suggesting larger particles. Samples C and D also exhibit narrower diffraction peaks more characteristic of larger particles. However, for both samples, rutile is the major phase.

Scanning electron microscopy shows that all the samples are made up of spherical particles with the main morphological difference between samples being particle size. Thus, sample A has the smallest particles (20–50 nm), the particles in samples B and C are 200–300 nm while those in D are 300–500 nm. Table 1 shows that the surface areas of samples B, C, and D are all broadly similar at 11 to 15 $m^2\,g^{-1}$ while sample A has a much higher surface area at *ca.* 50 $m^2\,g^{-1}$. Similarly, sample A differs from the others with a value for the zero point charge (ZPC) of 4.50 compared to samples B and C (both *ca.* 6.50) while sample D could not be measured due to problems dispersing this powder in water.

3.2. Sorption kinetics and Isotherms

Direct Red 23 is a commercial, azo dye containing two sulfonate groups (Figure 1) which can interact with O–H groups on the surface of Titania. The % sorption against time for an initial concentration of 330 mg l^{-1} of Direct Red 23 onto four samples of Titania are shown in Figure 2(a). For sample A, the data show very fast uptake of the majority of

Table 1: Selected characteristics of titania samples.

	Titania samples			
	A	B	C	D
Surface area ($m^2\ g^{-1}$)*	49.8 (1.5)	11.1 (0.7)	14.9 (0.3)	11.1 (0.4)
Particle size† (nm)	20–50	200–300	200–300	300–500
Zero point charge (ZPC)	4.50 (0.00)	6.50 (0.15)	6.40 (0.15)	Not measured
X-ray diffraction data	Anatase (80%) + Rutile (20%)	Anatase	Rutile	Rutile

*Standard deviation shown in parentheses.
†Average particle size measured by scanning electron microscopy.

Table 2: Langmuir and Freundlich isotherm data and partition coefficients for TiO_2 samples A and C at 1, 5, and 24 hours. For R^2, the range of values is shown from the replicate experiments. For other parameters, the data shown are averages with standard errors in parentheses.

		TiO_2 Sample A			TiO_2 Sample C		
		1 h	5 h	24 h	1 h	5 h	24 h
Langmuir	R^2	0.94–0.99	0.99	0.94–0.99	0.73-0.74	0.17–0.24	0.97-0.98
	Q_o	28.4 (2.8)	27.5 (4.9)	35.2 (5.3)	2.2 (0.0)	9.4 (1.5)	8.0 (0.2)
	b	0.37 (0.30)	0.37 (0.16)	0.91 (0.44)	−0.06 (0.01)	0.01 (0.00)	0.04 (0.01)
Freundlich	R^2	0.87–0.91	0.55–0.77	0.91–0.93	0.64–0.87	0.55–0.61	0.77–0.91
	K_f	11.5 (2.8)	13.5 (1.0)	15.3 (1.8)	0.5 (0.0)	0.6 (0.2)	1.0 (0.1)
	n	4.55 (0.51)	6.53 (2.48)	3.91 (1.72)	3.35 (0.12)	2.43 (0.50)	2.72 (0.00)
Dye conc.							
K_d	A:−200 mg l^{-1} C:−240 mg l^{-1}	278	423	1085	1.3	1.3	2.7
	640 mg l^{-1}	13	12	51	1.0	2.4	1.3

the dye during the first 15–30 minutes. This is followed by a much more gradual uptake of dye between 0.5 and 24 hours. Sample C shows the next fastest and highest dye uptake but this is much more gradual. However, there is more rapid dye uptake initially (in this case, 0–5 hours) and then a slower rate up to 24 hours. Finally, Samples B and D show little dye uptake (< 20%) with sample B showing evidence of sorption in the first few hours followed by desorption between 3 and 24 hours.

Figure 2(b) shows the effect on the rate of dye uptake of changing the initial dye concentration for Titania sample A. For 163 mg l^{-1}, almost all the dye is sorbed after 1 hours whilst for 330 mg l^{-1} and 650 mg l^{-1} dye uptake is still increasing up to *ca.* 8 hours. By comparison, Figure 2(c) shows the corresponding data for sample C. Here, the larger errors reflect the lower dye uptake compared to sample A and indeed the low uptake and large errors make further analysis of samples B and D impossible. However, for sample C, the data do show similar trends to sample A of slower and proportionally lower uptake of dye with increasing initial dye concentration. These data would seem to indicate that dye uptake becomes less favourable as the oxide surface becomes increasingly populated with sorbed dye molecules and solution dye concentrations decrease as might be expected.

Table 2 shows the results of fitting the sorption data to the Langmuir and Freundlich isotherm models after 1, 5, and 24 hours of sorption. The calculations are only shown for samples A and C because, as mentioned above, the dye uptake on samples B and D is so low. For both samples A and C, the R^2 values are generally better after 1 hour and then 24 hours; the increased scatter observed after 5 hours suggesting some surface reorganisation after initial dye sorption. For sample A, in all cases, there is a closer fit from the regression lines to the Langmuir isotherm (e.g., R^2 ranges from 0.94 to 0.99 for Langmuir but from 0.55 to 0.93 for the Freundlich isotherm). By comparison, sample C shows slightly better fits to the Freundlich isotherm at 1 and 5 hours (R^2 ranging from 0.55 to 0.87 compared to 0.17 to 0.74 for Langmuir) but, conversely, a better fit to Langmuir at 24 hours (R^2 is 0.97 to 0.98 compared to 0.77 to 0.91 for Freundlich). The Langmuir isotherm assumes monolayer coverage of sorbent but also that all the sorption sites are identical and that there is no interaction between sorbent molecules [21]. By comparison, the Freundlich isotherm assumes that the enthalpy of adsorption decreases exponentially with coverage [22]. The data show that the Langmuir model fits much more closely to the experimental data for this dye for sample A and sample C at equilibrium.

Thus a mechanism of sorption can be envisaged whereby, for the pristine oxide surface, the largest number of vacant sorption sites are available and the initial rate of dye uptake is quite rapid (Figure 2). For sample A, this results in almost quantitative dye sorption in equilibrium with very low dye concentration in the surrounding solution. However, as the sorption sites are filled, fewer vacant sorption sites remain and relatively more dye molecules remain in solution. This can be represented quite clearly when considering how the partition coefficient (K_d) varies with time. For instance, at lower dye concentrations, there is a trend towards increasing

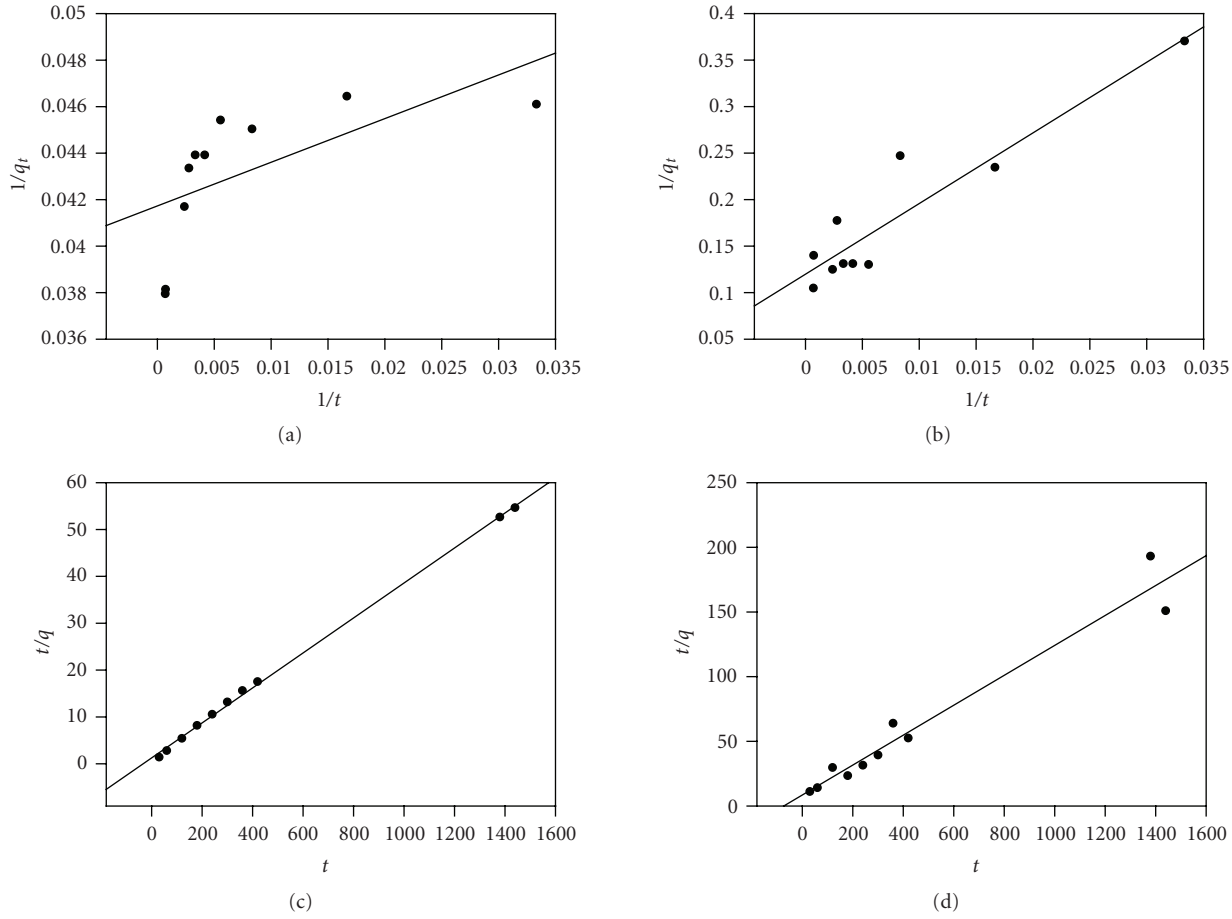

FIGURE 3: Kinetic plots at initial dye concentration of 650 mg l^{-1}. First-order plots for (a) sample A and (b) sample C. Second order plots for (c) sample A and (d) sample C.

K_d with time. Thus, for sample A, at 200 mg l^{-1}, K_d increases from 278 to 423 to 1085. This corresponds to an increasing proportion of dye sorbing to Titania compared to that remaining in solution. By comparison, although there is still an increase, K_d remains more constant at the higher dye concentrations (640 mg l^{-1}) for sample A. Overall, comparing samples A and C after 24-hour equilibration time, K_d ranges from 51 to 1085 for sample A but from 1 to 2.7 for sample C emphasizing that the equilibrium between sorbed and dissolved dye is hugely in favor of sorption for sample A across a range of dye concentrations but is much more evenly balanced for sample C (particularly at higher initial dye concentrations). Table 2 also shows that the Langmuir coefficients (Q_o and b) are larger for samples A compared with sample C which corresponds with the much greater dye uptake for the former over the latter.

Comparing all the sorption data with the characterisation data for the different Titania samples (Table 1) suggests that dye uptake is strongly influenced by metal oxide surface area and zero point charge. Most importantly, the higher surface area of sample A appears directly related to the increased uptake of this oxide because this presents a larger number of sorption sites which would be expected to lead to increased dye uptake. In addition, although the number of samples is relatively small, the data suggest that a lower value of zero point charge (ZPC) such as in sample A is an advantage. This implies that Titania sample A has a deprotonated surface at lower pH than Titania samples B and C. This is important if the mechanism of dye uptake is ascribed to chemisorption of the dyes to the Titania via the formation of sulfonate ester linkages between dye and surface O–H groups on the oxide with associated loss of water. Thus, the chemisorption process can be envisaged as occurring by nucleophilic attack of O–H groups from the Titania at the sulphur atom of the sulfonate group of the dye to forming the ester linkage. This suggests that deprotonation of the surface would lead to stronger nucleophiles which would enhance this process leading to more favourable uptake for sample A.

4. DYE SORPTION KINETICS

The results of the modelling of the kinetic data are shown in Table 3 with selected graphs in Figure 3. The data show that the linear regressions are poorer for the first-order kinetic model compared to the second-order data particularly for sample A (first-order R^2 ranges from 0.09 to 0.90 compared to 0.99 to 1.00 for second order) across the three different concentrations studied. This suggests a second-order kinetic

Table 3: Kinetic parameters for Direct Red 23 uptake onto TiO_2 samples A and C. For R^2, the range of values is shown from the replicate experiments. For other parameters, the data shown are averages with standard errors in parentheses.

		A			C		
C_o (mg l^{-1})		163	330	650	163	330	650
1st order	R^2	0.09–0.91	0.33–0.74	0.39–0.90	0.65–0.78	0.47–0.93	0.87–0.98
	K	2.42 (2.41)	1.15 (0.55)	2.97 (1.29)	19.1 (19.1)	91.4 (47.9)	295 (470)
	q_{max}	8.2 (0.1)	16.0 (0.6)	26.8 (2.8)	3.7 (3.7)	4.6 (0.3)	12.1 (9.5)
2nd order	R^2	0.99-1.00	0.99-1.00	0.99	0.07–0.99	0.90–0.97	0.60–0.95
	K_2	1.14 (1.75)	0.03 (0.03)	0.003 (0.002)	0.06 (0.06)	0.002 (0.002)	0.001 (0.001)
	q_e	8.1 (0.1)	16.5 (0.1)	28.3 (1.6)	5.5 (6.0)	7.9 (0.7)	12.9 (4.3)
	h	73 (112)	8 (10)	3 (2)	0.02 (0.04)	0.03 (0.01)	0.08 (0.05)

process dominates Direct Red 23 adsorption onto these Titania samples. This suggests that the rate-limiting step is a chemisorption process where sharing or exchange electrons between sorbent and sorbate takes place. In this case, the likelihood is that a sulfonate ester bond forms between the sulfonate groups on the dye and surface hydroxyl groups in the Titania.

Sample A produced the highest values for the parameters in the second-order kinetics equation (Table 3). Comparing the data for the initial adsorption rate (hour), these are the highest at the lowest dye concentration, decreasing dramatically as the initial dye concentration increases. This suggests that the kinetics of adsorption to the most energetically available adsorption sites are much faster and that as coverage increases, the rate of adsorption slows when only less energetically favorable sites remain. This gives a different insight into the adsorption process compared to the sorption isotherms (Langmuir) which reflect much more an equilibrium situation.

5. CONCLUSIONS

Dye sensitization is a key process in the manufacture of dye sensitized solar cell devices with very rapid dyeing uptake leading to full-monolayer coverage representing optimum objectives. Closely linked to these are the requirements for large amounts of dye uptake to maximize light absorption allowing for thinner devices along with a need for strongly chemisorbed dye molecules which do not desorb under device working conditions. The data presented for sorption of Direct Red 23 onto Titania sample A (Degussa P25) do show some of these characteristics and this is believed to be related to the higher surface area of this material along with a lower value of ZPC which offer a greater number of sorption sites and a more favourable sites for chemisorption of the dye, respectively.

Finally, whilse Direct Red 23 is not used in the currently, most efficient dye sensitized solar cells, this commercially available dye does possess similar anionic groups for adsorption onto Titania compared to Ru complexes and organic dyes. Thus, the data presented have important implications for dye sensitisation especially in the context of growing interest in organic dyes for DSSC.

ACKNOWLEDGMENTS

We gratefully acknowledge EU (ESF) Objective One funding and Corus support for BVV, Dr. Callum Hill for BET data, and Steve Jones for collecting the XRD data.

REFERENCES

[1] S. S. Hegedus and A. Luque, "Status, trends, challenges and the bright future of solar electricity from photovoltaics," in *Handbook of Photovoltaic Science and Engineering*, A. Luque and S. S. Hegedus, Eds., p. 177, John Wiley & Sons, Chichester, UK, 2003.

[2] K. Hara and H. Arakawa, "Dye-sensitized solar cells," in *Handbook of Photovoltaic Science and Engineering*, A. Luque and S. S. Hegedus, Eds., John Wiley & Sons, Chichester, UK, 2003.

[3] B. O'Regan and M. Grätzel, "A low-cost, high-efficiency solar cell based on dye-sensitized colloidal TiO_2 films," *Nature*, vol. 353, no. 6346, pp. 737–740, 1991.

[4] M. K. Nazeeruddin, A. Kay, I. Rodicio, et al., "Conversion of light to electricity by *cis*-X_2bis(2,2′-bipyridyl-4,4′-dicarboxylate)ruthenium(II) charge-transfer sensitizers (X = Cl^-, Br^-, I^-, CN^-, and SCN^-) on nanocrystalline TiO_2 electrodes," *Journal of the American Chemical Society*, vol. 115, no. 14, pp. 6382–6390, 1993.

[5] M. K. Nazeeruddin, P. Péchy, and M. Grätzel, "Efficient panchromatic sensitization of nanocrystalline TiO_2 films by a black dye based on a trithiocyanato-ruthenium complex," *Chemical Communications*, no. 18, pp. 1705–1706, 1997.

[6] N. Robertson, "Optimizing dyes for dye-sensitized solar cells," *Angewandte Chemie International Edition*, vol. 45, no. 15, pp. 2338–2345, 2006.

[7] R. Katoh, A. Furube, A. V. Barzykin, H. Arakawa, and M. Tachiya, "Kinetics and mechanism of electron injection and charge recombination in dye-sensitized nanocrystalline semiconductors," *Coordination Chemistry Reviews*, vol. 248, no. 13-14, pp. 1195–1213, 2004.

[8] T. Horiuchi, H. Miura, and S. Uchida, "Highly-efficient metal-free organic dyes for dye-sensitized solar cells," *Chemical Communications*, vol. 9, no. 24, pp. 3036–3037, 2003.

[9] P. Y. Reddy, L. Giribabu, C. Lyness, et al., "Efficient sensitization of nanocrystalline TiO_2 films by near-IR-absorbing unsymmetrical zinc phthalocyanine," *Angewandte Chemie*, vol. 119, no. 3, pp. 377–380, 2007.

[10] A. Burke, L. Schmidt-Mende, S. Ito, and M. Grätzel, "A novel blue dye for near-IR 'dye-sensitised' solar cell applications," *Chemical Communications*, no. 3, pp. 234–236, 2007.

[11] A. Fillinger and B. A. Parkinson, "The adsorption behavior of a ruthenium-based sensitizing dye to nanocrystalline TiO_2 coverage effects on the external and internal sensitization quantum yields," *Journal of the Electrochemical Society*, vol. 146, no. 12, pp. 4559–4564, 1999.

[12] M. K. Nazeeruddin, R. Splivallo, P. Liska, P. Comte, and M. Grätzel, "A swift dye uptake procedure for dye sensitized solar cells," *Chemical Communications*, vol. 9, no. 12, pp. 1456–1457, 2003.

[13] S. Tatay, S. A. Haque, B. O'Regan, et al., "Kinetic competition in liquid electrolyte and solid-state cyanine dye sensitized solar cells," *Journal of Materials Chemistry*, vol. 17, no. 29, pp. 3037–3044, 2007.

[14] D. Kavitha and C. Namasivayam, "Experimental and kinetic studies on methylene blue adsorption by coir pith carbon," *Bioresource Technology*, vol. 98, no. 1, pp. 14–21, 2007.

[15] M. Doğan, M. Alkan, Ö. Demirbaş, Y. Özdemir, and C. Özmetin, "Adsorption kinetics of maxilon blue GRL onto sepiolite from aqueous solutions," *Chemical Engineering Journal*, vol. 124, no. 1–3, pp. 89–101, 2006.

[16] N. Kannan and M. M. Sundaram, "Kinetics and mechanism of removal of methylene blue by adsorption on various carbons—a comparative study," *Dyes and Pigments*, vol. 51, no. 1, pp. 25–40, 2001.

[17] Y. S. Ho and G. McKay, "Pseudo-second order model for sorption processes," *Process Biochemistry*, vol. 34, no. 5, pp. 451–465, 1999.

[18] S. Mustafa, B. Dilara, K. Nargis, A. Naeem, and P. Shahida, "Surface properties of the mixed oxides of iron and silica," *Colloids and Surfaces A*, vol. 205, no. 3, pp. 273–282, 2002.

[19] JCPDS 01-071-1166 (Anatase).

[20] JCPDS 00-021-1276 (Rutile).

[21] E. M. McCash, "Adsorption and desorption," in *Surface Chemistry*, Oxford University Press, Oxford, UK, 2001.

[22] P. V. Messina and P. C. Schulz, "Adsorption of reactive dyes on titania-silica mesoporous materials," *Journal of Colloid and Interface Science*, vol. 299, no. 1, pp. 305–320, 2006.

Hindawi Publishing Corporation
International Journal of Photoenergy
Volume 2008, Article ID 504945, 6 pages
doi:10.1155/2008/504945

Research Article

A Rapid Method of Assessing the Photocatalytic Activity of Thin TiO_2 Films Using an Ink Based on the Redox Dye 2,6-Dichloroindophenol

Andrew Mills, Mark McGrady, Jishun Wang, and James Hepburn

WestCHEM, Department of Pure and Applied Chemistry, University of Strathclyde, 295 Cathedral Street, Glasgow G1 1XL, Scotland

Correspondence should be addressed to Andrew Mills, a.mills@strath.ac.uk

Received 24 July 2007; Accepted 1 November 2007

Recommended by Russell Howe

An indicator ink based on the redox dye 2,6-dichloroindophenol (DCIP) is described, which allows the rapid assessment of the activity of thin, commercial photocatalytic films, such as Activ. The ink works via a photoreductive mechanism, DCIP being reduced to dihydro-DCIP within ca. 7.5 minutes exposure to UVA irradiation of moderate intensity (ca. 4.8 mW cm^{-2}). The kinetics of photoreduction are found to be independent of the level of dye present in the ink formulation, but are highly sensitive to the level of glycerol. This latter observation may be associated with a solvatochromic effect, whereby the microenvironment in which the dye finds itself and, as a consequence, its reactivity is altered significantly by small changes in the glycerol content. The kinetics of photoreduction also appear linearly dependent on the UVA light intensity with an observed quantum efficiency of ca. 1.8×10^{-3}.

1. INTRODUCTION

Semiconductor photocatalysis (SPC) has progressed significantly since the early research into the possible use of semiconductor photochemistry to split water 30 years ago [1], such that it is now one of the most actively researched areas in photochemistry and is associated with several, major commercial products [2]. Its potential use in environmental remediation, based on the following reaction:

$$\text{Organic material} + O_2 \xrightarrow[\text{UVA light}]{TiO_2} \text{Mineral acids} + H_2O + CO_2, \quad (1)$$

has been the main reason for much of the interest and the semiconductor which has been the most heavily exploited for this purpose is titania (TiO_2). Despite having a relatively large band gap (ca. 3.2 eV), thus necessitating the use of ultraviolet light (UV) to initiate the photocatalytic process, titania is chemically and biologically inert, mechanically robust, inexpensive, and highly active. Of the three known forms of titania (anatase, rutile, and brookite), it is generally accepted that anatase TiO_2 is the most active form for SPC applications.

Upon activation of the titania with UV light, an electron-hole pair is produced within the bulk of the material. These species usually recombine rapidly; however, for reaction (1) to occur, the electron-hole pair must migrate to the surface of the semiconductor, whereupon the photogenerated electron reduces atmospheric O_2 to superoxide, O_2^-, which can be reduced further to water through a number of highly active intermediates, one of which is believed to be the strongly oxidising hydroxyl radical, $OH^\bullet$. Conversely, the photogenerated hole is capable of oxidising surface TiOH groups to radicals, that is, $TiOH^\bullet$, that are capable of oxidising many organic materials/pollutants into mineral acids and CO_2.

One of the reasons why titania has proved successful in the removal of both aqueous and atmospheric contaminants is that it is easily adhered to a suitable supporting substrate, which can subsequently be exposed to either an aqueous or airborne pollutant. Suitable methods for preparing titania films on the surface of a substrate include using a sol-gel method [3, 4], physical vapour deposition (i.e., sputtering) [5, 6], and chemical vapour deposition (CVD) [7, 8]. All of these techniques have been exploited in the research laboratories, but the method which has met with the most

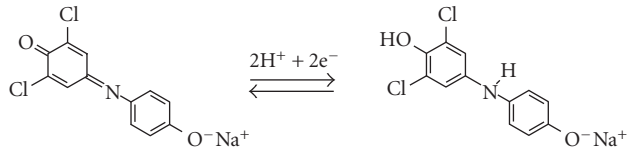

DCIP Leuco-DCIP

Figure 1: The structures of the sodium salt of DCIP (left) and its reduced product, dihydro-DCIP.

commercial success is CVD. Indeed, the world first self-cleaning glass, Activ [9], formulated by Pilkington Glass (Lathom, UK), is manufactured using an atmospheric pressure CVD (APCVD) technique [10]. Many of the World's other major glass manufacturers have followed the lead of Pilkington Glass and now manufacture their own self-cleaning product [11, 12]. More recently, there has also been the emergence of self-cleaning tiles [13], paints [14], and concrete [15] products, particularly from Japan.

With so many photocatalytic materials appearing on the market, there is an increasing interest in the development of one or more standard methods for assessing the activity of both laboratory and commercial samples. To date, there are many tests which have been used in the research laboratories to elucidate film activity, including the destruction of nitrogen oxides [16–18], the mineralization/degradation of dyes [19, 20] (particularly methylene blue [21, 22]), and the destruction of stearic acid [23, 24]. However, with all the methods outlined above, whilst suitable for use in the research laboratories, the prospect of using them in the field, for example, to demonstrate the efficacy of the photocatalytic film to potential customers, or test samples in situ, is limited, since each involves some degree of sample preparation, use of expensive, often bulky, analytical equipment, and technical skill to run the method and assess the results. From an industrial perspective at least, what is needed is a rapid, semiquantitative (if not quantitative) method of demonstrating and assessing rapidly the activity of any photocatalytic coating.

One possible route is to use a photocatalyst indicator ink which, when deposited onto a photocatalytic coating, changes colour upon UV activation of the coating. Such an ink has been proposed recently based on the blue redox dye, 2,6-dichloroindophenol (DCIP) [25], the structure of which is illustrated in Figure 1. The overall process involving the ink is as follows:

$$\underset{\text{(blue)}}{\text{DCIP}} + \text{glycerol} \xrightarrow[\text{UVA light}]{\text{TiO}_2} \underset{\text{(colourless)}}{\text{leuco-DCIP}} + \text{glyceraldehyde}. \quad (2)$$

The DCIP ink has the striking feature that it is blue before UV irradiation, but colourless, due to the formation of leuco-DCIP (the structure of which is also shown in Figure 1), afterwards. The photocatalytic process is very rapid, that is, within 7 minutes using typical solar UVA levels (ca. 4.5 mW cm^{-2}) on a commercial self-cleaning glass, such as Activ. In addition, the photoreduction of the dye has also been shown to be unaffected by both the level of O_2 and the humidity of the environment under which the ink is being used. This article reports the characterisation of a DCIP photocatalyst indicator ink when used on a typical, commercial self-cleaning glass (Activ).

2. EXPERIMENTAL

Unless stated otherwise, all reagents were Analar grade and used, as received, from Sigma-Aldrich. The conditions referred to as "ambient atmospheric conditions" are on the open bench at room temperature (ca. 20°C) and a relative humidity of ca. 60%.

A typical DCIP ink was prepared as follows: 3 g of a 1.5 wt% hydroxyethylcellulose (Fluka, medium viscosity) solution in water were placed in a sample bottle and to it were added 0.3 g of glycerol. The resulting solution was gently stirred whilst 5 mg of 2,6-dichloroindophenol (supplied by Alfa-Aesar, sodium salt hydrate, 98%) were added slowly. The solution was placed in an ultrasound bath and sonicated for 5 minutes in order to ensure complete dissolution of the dye, before being subjected to further gentle stirring for 30 minutes. Ink produced in this manner appeared stable and unchanged for at least 1month, and was used as required. In terms of parts per hundred resin (pphr), the level of polymer/SED/dye in the ink formulation is equivalent to a ratio of 100/667/11. Such a DCIP ink is referred to henceforth as the standard formulation.

The photocatalyst substrate used in this work was Activ^{TM}, kindly supplied by Pilkington Glass. Full details on its preparation can be found elsewhere [10]. The bulk Activ^{TM} samples received were cut into 25 mm × 25 mm × 4 mm thick samples so that it was possible to place them in a home-made cell holder for making spectral measurements using a UV-vis spectrophotometer. Coating of a typical glass sample was achieved by smearing approximately 1 mL of the ink under test over the sample surface and spinning the sample, using an Electronic Micro Systems Model 4000-1 spin coater, at 500 rpm for 15 s, which generates a film ca. 900 nm thick on the photocatalyst surface. The ink was then further dried by placing the spun-coated Activ^{TM} substrate in an oven at 70°C for 10 minutes, although similar kinetic results were also observed when the ink-coated substrate was simply allowed to dry in air in the absence of light for 1 hour.

The UV-driven reduction of the dye on the photocatalyst surface was monitored via UV-visible spectroscopy, using a Cary 50 Bio UV-visible spectrophotometer. The instrument was configured to scan in the wavelength range 300–800 nm, with scans taken at time intervals between UV irradiations typically ranging from 10 s to 10 minutes depending upon the observed rate of photoreduction (i.e., photobleaching). UV irradiations were conducted using a hand-held, 2 × 4 W Black Light Blue (BLB) UVA source (peak wavelength 365 ± 20 nm). Unless stated otherwise, the UVA irradiance used for all irradiations was ca. 4.8 mW cm^{-2}, which is comparable to the standard UVA irradiance on a sunny day (ca. 4.5 mW cm^{-2}) [26].

3. RESULTS AND DISCUSSION

Both the DCIP ink and the resulting dried ink film on the desired substrate are blue in colour, and this blue colour persists when the ink is cast on plain glass, or indeed any substrate with nil photocatalyst, and irradiated with UVA light for an extended (ca. 1 hour) time period. With such films, no significant change in the absorbance was noted over this time period at the wavelength of maximum absorbance, λ_{max} (ca. 629 nm and HPBW ca. 100 nm). In aqueous solution, a dilute (i.e., 10^{-4} M) solution of DCIP has a λ_{max} at 600 nm and a half peak band width (HPBW) of ca. 130 nm (measured in house). Therefore, in the ink it is observed that the λ_{max} is slightly red shifted compared to what is observed in solution. However, a similar HPBW is observed with the dried ink film, which is indicative of multimer (dimer, trimer, etc.) formation. The formation of said multimers in the dried film is not surprising given the effective dye concentration of 0.064 M.

In contrast, when cast on Activ, the blue ink film is observed to be rapidly photobleached upon irradiation with UVA light. Figure 2(a) shows the observed absorption spectra obtained for a DCIP ink cast as a film on the surface of Activ and subsequently irradiated with UVA light. Thus, upon UV irradiation of a typical DCIP film on Activ, the absorbance of the film decreases with time (as indicated by the arrow) and the ink is completely bleached, that is, the dye is fully reduced to dihydro-DCIP, after ca. 7.5 minutes. The change in the absorbance ($\Delta Abs = Abs_t - Abs_\infty$, where Abs_t and Abs_∞ are the absorbance of the film at UV irradiance times t and after complete photobleaching, resp.) at λ_{max} is shown more explicitly in Figure 2(b). The initial rate of reduction of the ink, r_i, is derived from the absorbance data recorded over the time necessary for the initial absorbance of the ink to decrease by ca. 20% of its initial value. Based upon the data presented in Figures 2(a) and 2(b), the initial rate of reduction of a typical DCIP ink under ambient atmospheric conditions using 4.8 mW cm^{-2} UVA light is ca. 4.5×10^{-4} AbsU s^{-1}, where AbsU is used to denote absorbance units, thus avoiding confusion that the value quoted is a rate constant.

Since DCIP is a redox dye (E°(DCIP/dihydroDCIP) = + 0.228 V at pH 7 versus SHE [27]), it is possible that, once DCIP has been reduced on the surface of Activ to dihydro-DCIP, the latter may be reoxidised by atmospheric O_2, regenerating the initial level of DCIP, and thus restoring the original blue colour of the ink film. However, monitoring the absorbance at λ_{max} of a typical DCIP film on Activ before and after UV bleaching revealed that the photobleached DCIP only partially (ca. 38%) recovers its original colour over a period of many hours (see Figure 2(c)).

The initial rate of recovery in absorbance at 629 nm of the ink, from Figure 2(c), is typically 1.8×10^{-6} AbsU s^{-1}, a rate which is more than 100 times slower than its initial rate of reduction, thus allaying any concerns that the "dark" reoxidation of dihydro-DCIP by ambient O_2 would compete with the reduction of the dye during irradiation, that is, effectively, the photobleaching of the DCIP ink on Activ appears an irreversible process. This observation supports

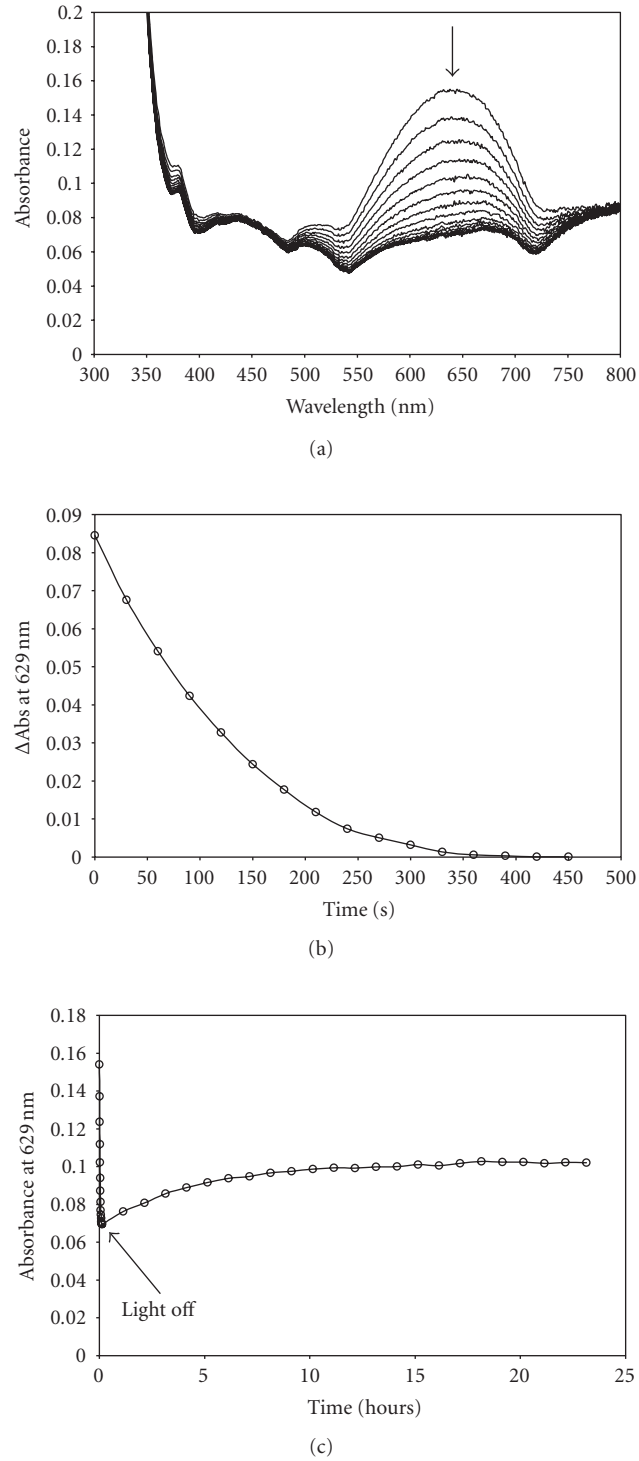

FIGURE 2: (a) The spectral shape obtained for a standard DCIP ink cast on the surface of Activ, and the subsequent changes (from top to bottom) in this spectral shape as the sample is irradiated with UVA light at an intensity of ca. 4.8 mW cm^{-2}. Spectra were recorded at 30-second intervals. (b) The change in the absorbance (ΔAbs) at λ_{max} (629 nm) with UVA irradiation of a DCIP ink, based on the data presented in Figure 2(a). (c) The reduction, and subsequent recovery, of a DCIP ink on the surface of Activ at 629 nm. The reduction conditions were similar to those detailed previously in Figure 2(a), whereas the ink recovery was monitored in the dark with spectra recorded at 1 hour intervals.

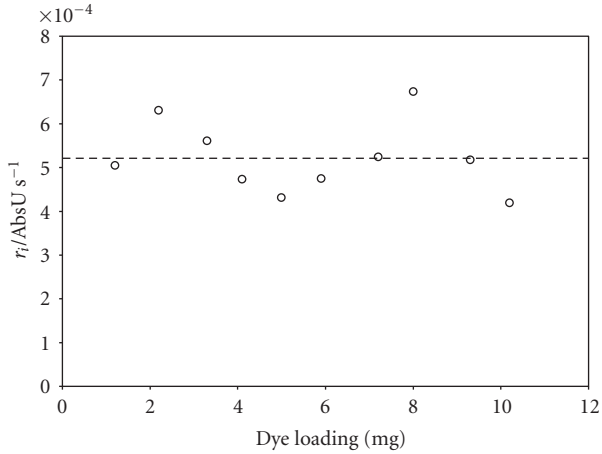

Figure 3: The variation in the initial rate of reduction (r_i) of a DCIP ink on Activ as the level of dye in the ink formulation is altered between 1 and 10 mg. The dotted line indicates the calculated average r_i of 5.21×10^{-4} AbsU s^{-1}.

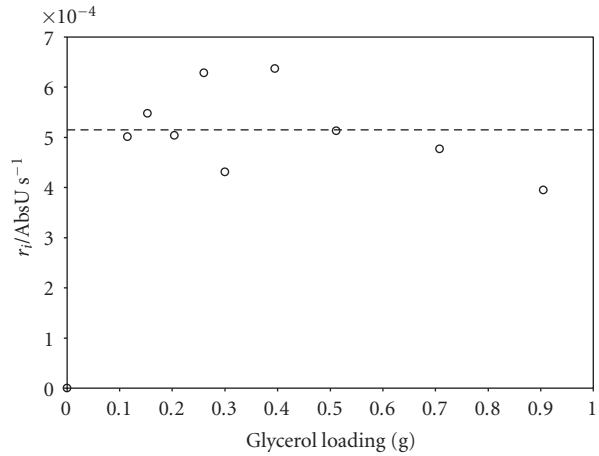

Figure 4: The variation in r_i as the level of glycerol in the ink formulation is altered between 0.1 and 0.9 g. As in Figure 3, the dotted line in the plot indicates the average r_i of 5.15×10^{-4} AbsU s^{-1} .

the results of previous work on the ink, where the kinetics of photoreduction by Activ were assessed under varying levels of oxygen and noted to be the same under both anaerobic and O_2-saturated conditions [25].

3.1. The effect of dye loading on the initial rate of photoreduction of a typical DCIP film on Activ

The variation of r_i as a function of dye loading (5 mg dye per 45 mg polymer in a typical ink formulation) was studied over the range 1–10 mg (equivalent to 2.2–22 pphr) and the results of this work are illustrated in Figure 3. From these results, it appears that r_i is approximately independent of dye loading, with an observed average r_i of 5.2×10^{-4} AbsU s^{-1} . This result is in stark contrast to the behaviour of the Rz photocatalyst indicator ink reported previously [28] over a similar dye loading range, where the initial rate of reduction was observed to decrease by a factor of 4 as the dye level was increased from 1 to 8 mg. This latter effect was attributed to an increasing level of less reactive Rz dimers with increasing dye loading, supported by spectral changes showing a shoulder peak emerging at 570 nm as the dye loading was increased up to 40 mg. In contrast, the shape of the absorption spectrum of the DCIP ink did not change as a function of dye loading. The invariance of r_i as a function of [substrate] is not unusual in semiconductor photochemistry and implies that either all the reactive sites associated with dye reduction are occupied by molecules of DCIP; or that the rate-determining step in reaction (2) does not involve the reduction of DCIP.

3.2. Effect of glycerol level on the initial rate of photoreduction

In the standard ink formulation, glycerol is present to act as a sacrificial electron donor (SED); essentially, the glycerol molecules act as "hole traps," preventing recombination of the photogenerated electron-hole pair by undergoing oxidation, thus allowing any photogenerated electrons to reduce the dye molecules in the ink at the photocatalyst surface. If an ink formulation is prepared with no glycerol present, cast on the surface of Activ, and irradiated with UVA light over a prolonged irradiation period (ca. 1 hour), there is no observed photobleaching/reduction of the dye on the photocatalyst surface, indicating that the removal of the SED from the DCIP ink results simply in electron-hole recombination becoming the predominant process.

Experiments show that r_i is independent of glycerol loading over the range 0.1–0.9 g (typically, 0.3 g glycerol is present in the formulation), as demonstrated in Figure 4. However, r_i does vary markedly from 0–0.1 g (0–222 pphr) glycerol loading, as illustrated by the results in Figure 5. The initial rate of reduction, r_i, is observed to increase steadily as the glycerol level is increased from 0 to ca. 0.03 g (0–66 pphr), after which point a plateau value is achieved. In addition to the above kinetic data, Figure 5 also charts the observed variation in the λ_{max} of the resulting DCIP ink as the glycerol level is varied over the same range. It would appear from this plot that the variations in λ_{max} and r_i are linked in some way, with λ_{max} being blue-shifted as the glycerol level is increased. The likely cause of this shift in the peak wavelength is a solvatochromic effect, brought about by a change in the solvation shell of the dye molecules in the ink formulation and subsequent ink film as the glycerol level is increased. Such a change in the solvation shell is likely to alter the reactivity of the DCIP and may be responsible for the variation in r_i with glycerol loading illustrated in Figure 5.

However, there may be other effects working here since the work by Van Keuren and Schrof [29] showed that in a PVA/glycerol solution, where the glycerol content was varied between 10 and 40 wt%, the diffusion coefficient for

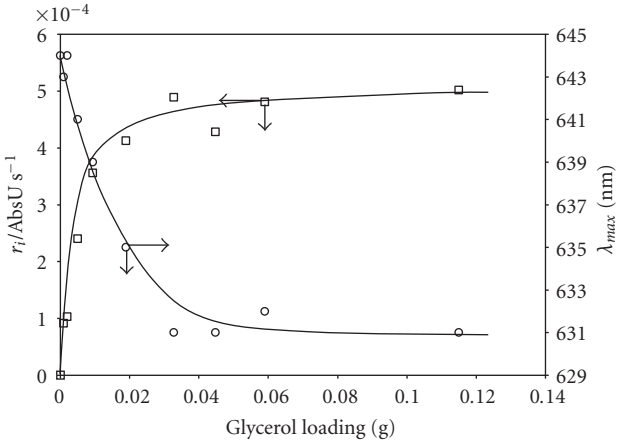

FIGURE 5: The variation in r_i(□) and the λ_{max}(○) as the level of glycerol in the ink formulation is altered between 0 and 0.1 g.

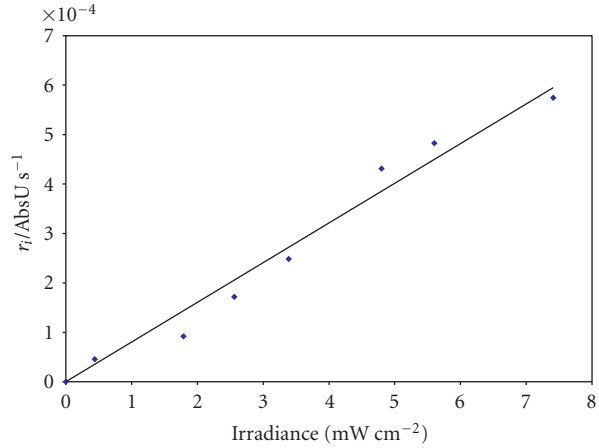

FIGURE 6: The variation in r_i with UVA irradiance.

a dye, rhodamine B, increased by a factor of 10^4. Beyond 40 wt% glycerol, the dye exhibited a diffusion coefficient similar to that observed for the dye in neat glycerol. In the DCIP ink formulations presented here, with a 0.1 g glycerol loading, the glycerol wt% is 66 wt%, and thus the variation in r_i as a function of glycerol loading illustrated in Figure 5 could be simply due to the variation in the diffusion coefficient of the dye from the bulk film to the surface of Activ, assuming that this is the rate determining step for the photoreduction/bleaching process. In this instance, the maximum rate observed at glycerol loading ≥0.1 g is due to the diffusion coefficient for DCIP in the film (HEC/glycerol) reaching a limiting value, as was observed by Van Keuren for rhodamine B in PVA/glycerol.

3.3. *The effect of UVA light irradiance on the initial rate of photoreduction*

In a final set of experiments, the initial rate of reduction of a typical DCIP film was determined as a function of UVA light irradiance, varied from 0.44 to 7.41 mW cm^{-2}, and the results are illustrated in Figure 6. Not surprisingly, r_i increases with increasing light irradiance, since the number of photons reaching the photocatalyst surface, and hence the number of photogenerated electrons produced, will increase. The strong linear dependence of r_i on the UV light irradiance is attributed to the relatively low light intensities used here to reduce the dye, the low absorbance of the underlying Activ photocatalyst layer, and the fact that, at such low UV irradiance levels, the reduction reaction will be controlled by the reactions at the ink/photocatalyst interface of the photogenerated electron-hole pairs, as opposed to their recombination (which is expected at high irradiance levels). A similar linear dependence of r_i on the UV irradiance was observed for the Rz-based photocatalyst indicator ink [28].

Since ΔAbs_t for the reduction of DCIP is ca. 0.085 AbsU, as illustrated earlier in Figure 2(b), for the standard ink formulation, and since it is known that 1 mW cm^{-2} of 365 nm light is equivalent to 1.1×10^{17} photons per cm^2 per minute, the quantum efficiency for the process can be estimated to be 0.0018 molecules per photon. It is also known from spectral studies conducted elsewhere that Activ only absorbs ca. 7.2% of the incident UVA irradiation from black light blue lamps [30], thus the quantum yield for the reduction of DCIP on the substrate can be estimated to be 2.5%. Both of these estimated values are greater than those observed for the Rz ink (2.5×10^{-4} molecules per photon and 0.35%, resp.) [28], although in practice the initial rate of photoreduction of DCIP is slower than that of Rz in the ink formulation under ambient atmospheric conditions [25].

4. CONCLUSIONS

A characterisation study of an indicator ink based on the redox dye 2,6-dichloroindophenol for assessing the photocatalytic activity of thin photocatalytic films of titania has been conducted. The initial rate of photoreduction of the dye in the ink formulation is independent of the dye loading level but highly sensitive to the level of glycerol present, reaching a plateau above a loading of 0.1 g glycerol. Accompanying this trend in the reduction rate is an inverse shift in the λ_{max} of the dye, believed to be due to changes to the solvent shell surrounding the dye with changing glycerol content. As anticipated, the rate of photoreduction increased with increasing UV irradiation intensity, similar to what has been reported for an Rz ink. The quantum yield for the photoreduction of DCIP by an Activ film was estimated to be 2.5%, which is greater than that observed for the Rz-based ink communicated previously.

ACKNOWLEDGMENTS

The authors wish to thank Pilkington Glass for supplying the Activ samples used in this work. Mark McGrady is grateful to The Carnegie Trust for the Universities of Scotland for funding.

REFERENCES

[1] A. Fujishima and K. Honda, "Electrochemical photolysis of water at a semiconductor electrode," *Nature*, vol. 238, no. 5358, pp. 37–38, 1972.

[2] A. Mills and S.-K. Lee, "A web-based overview of semiconductor photochemistry-based current commercial applications," *Journal of Photochemistry and Photobiology A*, vol. 152, no. 1–3, pp. 233–247, 2002.

[3] W. Ho, J. C. Yu, and S. Lee, "Photocatalytic activity and photo-induced hydrophilicity of mesoporous TiO_2 thin films coated on aluminum substrate," *Applied Catalysis B*, vol. 73, no. 1-2, pp. 135–143, 2007.

[4] L. Ge, M. Xu, M. Sun, and H. Fang, "Fabrication and characterization of nano TiO_2 thin films at low temperature," *Materials Research Bulletin*, vol. 41, no. 9, pp. 1596–1603, 2006.

[5] A. Karuppasamy and A. Subrahmanyam, "Studies on the room temperature growth of nanoanatase phase TiO_2 thin films by pulsed dc magnetron with oxygen as sputter gas," *Journal of Applied Physics*, vol. 101, no. 6, Article ID 064318, 7 pages, 2007.

[6] Q. Ye, P. Y. Liu, Z. F. Tang, and L. Zhai, "Hydrophilic properties of nano-TiO_2 thin films deposited by RF magnetron sputtering," *Vacuum*, vol. 81, no. 5, pp. 627–631, 2007.

[7] P. Evans, M. E. Pemble, and D. W. Sheel, "Precursor-directed control of crystalline type in atmospheric pressure CVD growth of TiO_2 on stainless steel," *Chemistry of Materials*, vol. 18, no. 24, pp. 5750–5755, 2006.

[8] S. A. O'Neill, R. J. H. Clark, I. P. Parkin, N. Elliott, and A. Mills, "Anatase thin films on glass from the chemical vapor deposition of titanium(IV) chloride and ethyl acetate," *Chemistry of Materials*, vol. 15, no. 1, pp. 46–50, 2003.

[9] 2007, http://www.pilkington.com/international+products/activ/default1.htm.

[10] D. W. Sheel, R. J. McCurdy, and S. J. Hurst, "Method of depositing tin oxide and titanium oxide coatings on flat glass and the resulting coated glass," Patent Application WO/1998/006675.

[11] 2007, http://www.selfcleaningglass.com/.

[12] 2007, http://corporateportal.ppg.com/NA/Glass/Residential Glass/Homeowners/ ProductInformation/SunClean/.

[13] 2007, http://www.toto.co.jp/products/hydro/genri_en.htm.

[14] 2007, http://www.stocorp.com/allweb.nsf/lotusanpage.

[15] 2007, http://www.mmc.co.jp/english/csr/csr2006.pdf.

[16] F.-L. Toma, G. Bertrand, S. O. Chwa, C. Meunier, D. Klein, and C. Coddet, "Comparative study on the photocatalytic decomposition of nitrogen oxides using TiO_2 coatings prepared by conventional plasma spraying and suspension plasma spraying," *Surface and Coatings Technology*, vol. 200, no. 20-21, pp. 5855–5862, 2006.

[17] F.-L. Toma, G. Bertrand, S. O. Chwa, et al., "Microstructure and photocatalytic properties of nanostructured TiO_2 and TiO_2-Al coatings elaborated by HVOF spraying for the nitrogen oxides removal," *Materials Science and Engineering A*, vol. 417, no. 1-2, pp. 56–62, 2006.

[18] N. Negishi, K. Takeuchi, and T. Ibusuki, "The surface structure of titanium dioxide thin film photocatalyst," *Applied Surface Science*, vol. 121-122, pp. 417–420, 1997.

[19] L. Andronic and A. Duta, "TiO_2 thin films for dyes photodegradation," *Thin Solid Films*, vol. 515, no. 16, pp. 6294–6297, 2007.

[20] J. Yu, X. Zhao, and Q. Zhao, "Effect of surface structure on photocatalytic activity of TiO_2 thin films prepared by sol-gel method," *Thin Solid Films*, vol. 379, no. 1-2, pp. 7–14, 2000.

[21] M. Wark, J. Tschirch, O. Bartels, D. Bahnemann, and J. Rathouský, "Photocatalytic activity of hydrophobized mesoporous thin films of TiO_2," *Microporous and Mesoporous Materials*, vol. 84, no. 1–3, pp. 247–253, 2005.

[22] C. H. Kwon, H. Shin, J. H. Kim, W. S. Choi, and K. H. Yoon, "Degradation of methylene blue via photocatalysis of titanium dioxide," *Materials Chemistry and Physics*, vol. 86, no. 1, pp. 78–82, 2004.

[23] A. Mills, G. Hill, S. Bhopal, I. P. Parkin, and S. A. O'Neill, "Thick titanium dioxide films for semiconductor photocatalysis," *Journal of Photochemistry and Photobiology A*, vol. 160, no. 3, pp. 185–194, 2003.

[24] R. Fretwell and P. Douglas, "An active, robust and transparent nanocrystalline anatase TiO_2 thin film—preparation, characterisation and the kinetics of photodegradation of model pollutants," *Journal of Photochemistry and Photobiology A*, vol. 143, no. 2-3, pp. 229–240, 2001.

[25] A. Mills and M. McGrady, "A study of new photocatalyst indicator inks," *Journal of Photochemistry and Photobiology A*, vol. 193, no. 2-3, pp. 228–236, 2008.

[26] A. Mills, M. McFarlane, and S. Schneider, "A viologen-based UV indicator and dosimeter," *Analytical and Bioanalytical Chemistry*, vol. 386, no. 2, pp. 299–305, 2006.

[27] P. G. Tratnyek, T. E. Reilkoff, A. W. Lemon, et al., "Visualizing redox chemistry: probing environmental oxidation-reduction reactions with indicator dyes," *The Chemical Educator*, vol. 6, no. 3, pp. 172–179, 2001.

[28] A. Mills, J. Wang, and M. McGrady, "Method of rapid assessment of photocatalytic activities of self-cleaning films," *Journal of Physical Chemistry B*, vol. 110, no. 37, pp. 18324–18331, 2006.

[29] E. Van Keuren and W. Schrof, "Fluorescence recovery after two-photon bleaching for the study of dye diffusion in polymer systems," *Macromolecules*, vol. 36, no. 13, pp. 5002–5007, 2003.

[30] A. Mills, A. Lepre, N. Elliott, S. Bhopal, I. P. Parkin, and S. A. O'Neill, "Characterisation of the photocatalyst Pilkington Activ^{TM}: a reference film photocatalyst?" *Journal of Photochemistry and Photobiology A*, vol. 160, no. 3, pp. 213–224, 2003.

Hindawi Publishing Corporation
International Journal of Photoenergy
Volume 2008, Article ID 964721, 9 pages
doi:10.1155/2008/964721

Research Article

Gas-Phase Photodegradation of Decane and Methanol on TiO_2: Dynamic Surface Chemistry Characterized by Diffuse Reflectance FTIR

William Balcerski, Su Young Ryu, and Michael R. Hoffmann

W. M. Keck Laboratories, California Institute of Technology, Pasadena, CA 91125, USA

Correspondence should be addressed to Michael R. Hoffmann, mrh@caltech.edu

Received 24 July 2007; Accepted 4 January 2008

Recommended by Russell Howe

Diffuse reflectance infrared Fourier transform spectroscopy (DRIFTS) was used to study illuminated TiO_2 surfaces under both vacuum conditions, and in the presence of organic molecules (decane and methanol). In the presence of hole scavengers, electrons are trapped at Ti(III)–OH sites, and free electrons are generated. These free electrons are seen to decay by exposure either to oxygen or to heat; in the case of heating, reinjection of holes into the lattice by loss of sorbed hole scavenger leads to a decrease in Ti(III)–OH centers. Decane adsorption experiments lend support to the theory that removal of surficial hydrocarbon contaminants is responsible for superhydrophilic TiO_2 surfaces. Oxidation of decane led to a mixture of surface-bound organics, while oxidation of methanol leads to the formation of surface-bound formic acid.

1. INTRODUCTION

TiO_2 is of great interest in the field of heterogeneous photo-oxidation catalysis, especially in the area of environmental cleanup. TiO_2 has the advantage of being relatively cheap, nontoxic, and stable, all of which make it attractive for remediation of environmental organic pollutants [1]. Studies on the surface chemistry of TiO_2 help to answer important questions such as the active species for photo-oxidation, the fate of charge carriers, and the mechanism for transfer of charge to species bound to the surface [2]. Previously, we used FTIR (DRIFT) spectroscopy to monitor surface species, surface electron, and hole traps on TiO_2 powders [3–5]; and to attribute broad spectral features to free conduction band electrons [3].

Representative hydrocarbon species (e.g., decane and methanol) were chosen for further investigation of hydrocarbon adsorption and photo-oxidation on the surface of illuminated TiO_2. The primary objective of these studies is to gain insight into the gas-phase and surface-bound photo-oxidation products.

2. EXPERIMENTAL PROCEDURES

TiO_2 (Degussa P25; 25% rutile, and 75% anatase), decane (99.9%, Aldrich), methanol (99.9%, Aldrich), methanol-d4 (CD_3OD, 99% isotopic purity, Aldrich), and formic acid (88%, Aldrich) were used as received. Oxygen gas (99.9%) was passed through a water trap before use in FTIR experiments.

DRIFT spectra were acquired using a Bio-Rad FTS-45 spectrometer with a liquid N_2-cooled MCT detector. Spectra were collected at $8\,cm^{-1}$ resolution using a Spectra-Tech Collector diffuse-reflectance accessory. The solid samples were held in the sample cup of a Spectra-Tech high-temperature environmental chamber (HTEC) that could be resistively heated to 1000 K (± 1 K), and the chamber evacuated to $10\,\mu$Torr. A gas manifold connected to the sample chamber allowed for pure gas samples (e.g., O_2) or organic vapors (e.g., decane and methanol vapor) to be introduced and removed as needed. The organic samples were attached to the system via a glass bulb, and these samples underwent several freeze-thaw cycles to remove dissolved gases. UV radiation from a 1 kW Oriel Xe lamp was

focused into the HTEC chamber through a moveable mirror and lens system that allowed for photolysis experiments to be conducted without breaking system purge.

3. RESULTS AND DISCUSSION

3.1. Hole and electron trapping on TiO_2 surfaces

One of the primary results of our previous work [3] was an observed rise in the DRIFT spectrum baseline when TiO_2 is irradiated in vacuo, which was caused by the generation of free electrons. The baseline gradually decayed over the course of several hours, leading to a stable trapped electron in a Ti(III)–OH group at 3714 cm^{-1}. We now believe that the impurities seen in previously C–H bands found at 2927 and 2859 cm^{-1} are indicative of surface-bound species responsible for hole trapping. To test this hypothesis, a small amount of methanol vapor was added to the system, followed by the normal vacuum pumping on the system to remove as much methanol as possible. Experiments conducted in the weeks following the methanol exposure led to a background C–H signal, which had been observed previously, but more importantly led to the expected baseline increase and Ti(III)–OH formation upon irradiation.

Figure 1 shows the DRIFT spectra for TiO_2 powder in vacuo under different conditions. In the untreated powder, bridging hydroxyl groups are seen at 3414 cm^{-1} and Ti(IV)–OH stretches are seen around 3645 cm^{-1}. There is also a broad adsorption between 3000 and 3600 cm^{-1} due to surface-bound water molecules. Upon heating to 200°C, surface water is lost, allowing the bridging hydroxyl groups to be more clearly seen in the spectrum. Furthermore, the Ti(IV)–OH peak becomes more clearly defined as a single peak at around 3645 cm^{-1}. Upon irradiation, bridging hydroxyl groups are completely lost, the Ti(IV)–OH peak is reduced in intensity, and a new peak at 3714 cm^{-1} is seen, which corresponds to trapped electrons in Ti(III)–OH groups. These results are consistent with our earlier work [3].

Alcohols are known to chemisorb to TiO_2 surfaces, [6–8] thus the expected surface species in the case of methanol vapor would be Ti–OCH_3. This adsorbed species provides a viable hole trap, by either direction hole transfer or through a chemical reaction to form formate:

$$\text{Ti(IV)–OCH}_3 + h^+ \longrightarrow \text{Ti(IV)–O}^+\text{CH}_3, \quad (1)$$

$$\begin{aligned}\text{Ti(IV)–OCH}_3 + h^+ &\longrightarrow \text{Ti(IV)–OCH}_2{}^* + \text{H}^+ \\ &\longrightarrow \text{CH}_2\text{O(abs, g)} + \text{e}^-_{\text{bulk}} + \text{H}^+.\end{aligned} \quad (2)$$

In either case, free electrons are present in the conduction band, leading to the aforementioned rise in baseline and a change in the color of the powder from white to blue as a result of Ti(III) atoms.

In the reaction described by (2), the injection of an electron into the lattice would create a current-doubling effect, which is well known for the case of organic photo-oxidation by TiO_2 [9–12]. Thus, some of the free electrons observed after photolysis may be a result of such an effect.

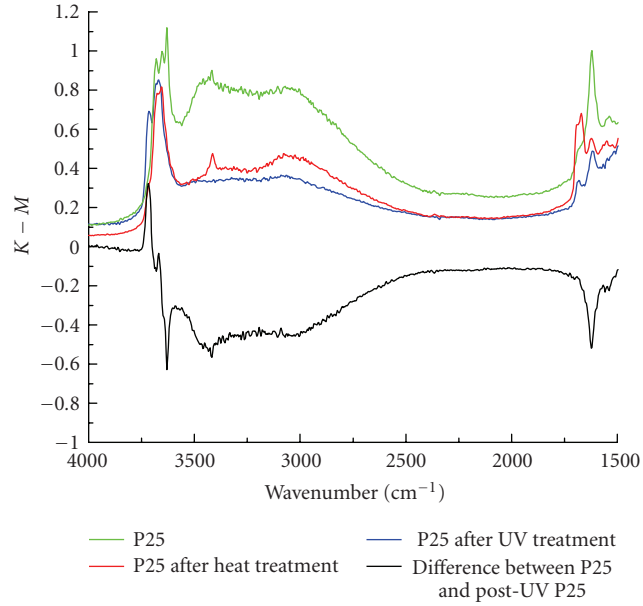

Figure 1: DRIFT spectra showing the effect of heating (to 200°C) and UV irradiation on P25 TiO_2 powder in vacuoin presence of hole scavenger contaminants.

The electron-generating reaction would have to proceed under anoxic conditions, and would likely be initiated by the loss of a proton. Figure 2 shows the effect of sequential heat treatment (523 K) and UV treatment in vacuoon a TiO_2 surface which had been exposed to methanol vapor. The heat treatment effectively removed all the water and some of the methanol, but the UV treatment led to an additional decrease in C–H intensity, as seen in the difference spectrum. Thus, there is a photochemical methanol loss pathway, even in vacuo, which supports the mechanism postulated in (2).

When the system was under a constant 1.0 atm N_2 and the fresh TiO_2 sample was not exposed to a vacuum, the baseline did not increase upon irradiation. This was most likely due to the inability of methanol molecules to desorb or detach from the walls and diffuse to the powder surface. The background methanol persisted in the system on the order of weeks and months, unless vigorous cleaning methods (frequent purging of the gas manifold with N_2 or O_2) were taken. Given the well-known affinity for TiO_2 to sorb hydrocarbons, [2] it is not unlikely that a small amount of impurity in the system could transfer from the walls to the TiO_2 powder, especially given that the amount of manifold surface area is several thousand times larger than the surface area of the powder in the sample compartment. Indeed, work with other organic samples such as methoxychlor and lindane led to a several-month contamination of the experimental setup, as new TiO_2 samples would continually turn orange from picking up these long-lived residual pesticide molecules. The problem of reproducing clean TiO_2 systems is not unique, as seen by the debate over the cause of UV-induced hydrophilicity on TiO_2 crystal surfaces, which has only recently been shown to be a result of the removal of surface hydrocarbon contaminants [13].

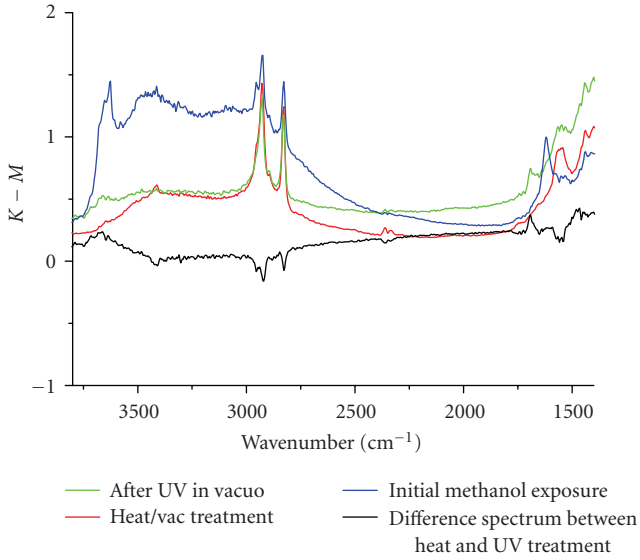

FIGURE 2: DRIFT spectra of TiO_2 powder heated and irradiated in vacuo after absorbing methanol vapor, and the difference spectrum showing the effect of irradiation on the surface which had already undergone heat treatment.

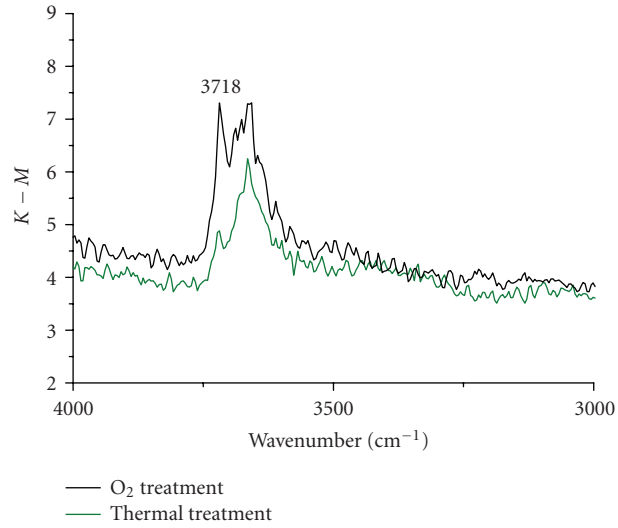

FIGURE 3: DRIFT spectra of TiO_2 powder irradiated in the presence of methanol vapor, followed by either thermal or O_2 treatment.

Given this new information, some of the previous conclusions need to be refined, especially in regards to postirradiation baseline relaxation. As reported earlier, both thermal treatment at 423 K as well as exposure to O_2 at 300 K led to a rapid relaxation of the baseline, as opposed to slow relaxation if the system was left alone [3]. These experiments were repeated, and in the case of relaxation by O_2, the resulting peak at 3714 cm^{-1} is much larger, as seen in Figure 3. This can be explained as follows. The slow relaxation is a result of charge recombination, and has been studied previously [5]. The rapid relaxation from exposure to oxygen is due to electron scavenging by oxygen, as it is a well-known electron acceptor:

$$O_2 + e^-_{bulk} \longrightarrow O_2{}^-. \quad (3)$$

The relaxation from thermal treatment is due to injection of trapped holes back into TiO_2 upon methanol desorption, which begins to occur at 400 K under vacuum conditions [6]. Not all methanol will be removed by this pathway though, as even at 475 K, the TiO_2 surfaces can contain alkoxides [7]:

$$\begin{aligned} &\text{Ti(IV)–O}^+\text{CH}_3 + \text{Ti(IV)–OH} \\ &\quad\longrightarrow \text{Ti(IV)–O–Ti(IV)} + \text{CH}_3\text{OH(g)} + h^+. \end{aligned} \quad (4)$$

The injected holes can then recombine with bulk electrons, that is, annihilation, but they can also combine with the trapped electrons in the form of Ti(III)–OH groups:

$$h^+ + \text{Ti(III)–OH} \longrightarrow \text{Ti(IV)–OH}. \quad (5)$$

Thus, since the O_2 treatment does not remove the surface methanol, there are both less holes injected into the lattice and more hole traps, leading to an increased intensity of the Ti(III)–OH peak at 3714 cm^{-1}.

It was observed that the Ti(III)–OH groups could be removed by illumination under O_2, but only after being partially rehydrated under H_2O vapor [3]. This result is consistent with loss of chemisorbed methanol (and thus hole injection) upon rehydration as reported elsewhere [14]. Thus, the previous explanation for this observed behavior, which stated that defects were stabilized by surface reconstruction involving OH groups, needs to include the possibility of the methanol loss pathway. Likewise, the role of lattice O-vacancies in the mechanism of hole-trapping, while not completely disproved, cannot account for all the experimental results.

3.2. Decane adsorption and degradation on TiO_2 surfaces

A potential practical application of TiO_2 is in the remediation of oil spills by coated glass beads [15]. In order to gain insight into alkane photocatalysis by TiO_2, decane was chosen as a sample hydrocarbon for a series of photoexperiments. The primary reasons for choosing decane were its simplicity (straight-chain alkane) and its vapor pressure (~1 Torr at room temperature, ideal for dosing samples via the gas manifold).

Hydrocarbon oxidation on TiO_2 has been studied extensively. Several decades ago, Djeghri et al. [16] used a flow-through reactor to study the UV-illuminated photocatalysis of alkanes (methane through octane) in the vapor phase. They found that the alkanes are oxidized to ketones, aldehydes, and CO_2, and that steady-state product concentrations are reached within minutes [16]. More recently, Minabe et al. have studied the photo-oxidation of long-chain organics on TiO_2 thin film, and observed that only CO_2 and H_2O were produced in the gas phase [17]. They suggest that the initial reactants as well as all intermediates were continuously

attached to the TiO_2 surface; however, they offered no insight into how the organics were oriented on the surface, or on the nature of the intermediates. The authors prepared their samples by melting their organics, then spreading the liquid on the TiO_2 thin-film surface, whereas Teichner et al. introduced the organics in the gas phase over nonporous anatase particles. These differences in catalyst and sample introduction, as well as the long exposure time of Fujishima's physisorbed organics compared to the gas-phase organics in Teichner's experimental setup, likely account for Fujishima and coworkers inability to detect any intermediates.

In the first set of experiments, decane vapor was introduced to TiO_2 surfaces that had been pretreated by UV irradiation in vacuo, and surface coverage was compared to the nonirradiated case. It was known at the time that UV treatment makes TiO_2 surfaces superhydrophilic, and we believed that the UV pretreatment would affect the ability for decane to absorb to the surface. Decane dosing was performed by opening a glass bulb containing decane, which was attached to a section of the gas manifold, for 2 minutes. The bulb was then closed, and that segment of the manifold was then opened to the sample chamber. The decane vapor was allowed to equilibrate with the sample for 10 minutes, and an initial FTIR spectrum was taken. The system was then opened to vacuum, and a series of scans were taken as the system was pumping down. Figure 4 shows the results of these experiments. Although initial decane concentrations were different ($t = 0$, while sample was sitting nonevacuated under decane vapor), after exposure to vacuum, both samples had near identical decane desorption profiles. Nearly all decane was lost from both the nonirradiated and irradiated surfaces during vacuum treatment, indicating that the decane was weakly bound, that is, physically absorbed to the surface. These experiments provide support for the theory that hydrocarbon contaminants [13], not UV-induced defects [18] or UV-induced rupture of Ti–OH bonds [19], are responsible for surface hydrophilicity. The experiments suggest that the UV pretreated surface, once exposed to decane vapor, lost its super-hydrophilic character and behaved similarly to the nontreated surface in regards to the amount of decane adsorbed on the surface.

In the next series of experiments, the oxidation of decane on TiO_2 was studied. After dosing the sample with decane, the system was immediately exposed to 1 atm O_2, so as to prevent the decane from desorbing from the surface. The sample was then irradiated for 5–10-minute intervals, at which point the lamp was turned off and a spectrum was recorded. Total time spent undergoing irradiation was 1 hour. Figure 5 shows the resulting spectra over 2000–4000 cm^{-1}. As expected, both water (broad adsorption between 3000 and 3600 cm^{-1}) and CO_2 (2320 cm^{-1}) are produced, with a loss in hydrocarbon intensity (C–H stretches between 2800 and 3000 cm^{-1}). To further probe the reaction products, a series of difference spectra are used, as shown in Figure 6. After one minute of irradiation, water (but not CO_2) is seen to form, and peaks are seen in the 1350–1750 cm^{-1} region, which are indicative of C–O bonds. The initial formation of water indicates that hydrogen abstraction is the first step in decane oxidation [20]. As the oxidation progressed, these C–O stretches eventually gave way to the C=O stretch at 1737 cm^{-1}, simultaneously accompanied by the formation of CO_2, as seen in the difference spectrum between 5 and 20 minutes of irradiation. At the end of the photoreaction, the system was exposed to vacuum, and some, but not all, of the reaction products were removed. Further oxidation in vacuo was used to remove the more strongly bound surface species.

Two possible mechanisms for the reaction are as follows. The active species for oxidation could be a surface-bound hydroxyl radical, which abstracts a hydrogen atom from a surface decane molecule, forming an alkyl radical. The alkyl radical could then react in any number of ways, such as attachment to a Ti–O–Ti group to form an alkoxy species, which would then undergo further oxidation to ketones and eventually CO_2:

$$\begin{aligned}
&h^+ + \mathrm{Ti(IV)O{-}H} \longrightarrow [\mathrm{Ti(IV)O^{\bullet}{-}H}]^+(\mathrm{Y}),\\
&\mathrm{Y} + \mathrm{CH_3(CH_2)_nCH_3}\\
&\quad \longrightarrow \mathrm{CH_3(CH_2)_{n-1}CH^{\bullet}CH_3} + \mathrm{Ti(IV){-}OH_2}^+,\\
&\mathrm{CH_3(CH_2)_{n-1}CH^{\bullet}CH_3} + \mathrm{Ti{-}O{-}Ti} \longrightarrow \mathrm{Ti{-}O(CHR){-}Ti},\\
&\mathrm{Ti(IV){-}OCHR} + h^+ + \mathrm{O_2} \longrightarrow \text{ketones + further products.}
\end{aligned} \tag{6}$$

Another possible mechanism involves superoxide formation, which leads to a free-radical-chain mechanism as outlined below:

$$\begin{aligned}
&\mathrm{O_2} + \mathrm{e^-O_{2,s^-}},\\
&\mathrm{O_{2,s^-}} + \mathrm{RCH_2R} \longrightarrow \mathrm{RCH^{\bullet}R} + \mathrm{HO_2}^-,\\
&\mathrm{RCH^{\bullet}R} + \mathrm{O_2} \longrightarrow \mathrm{RCH^{\bullet}(O_2)R},\\
&\mathrm{RCH^{\bullet}(O_2)R} + \mathrm{RCH_2R} \longrightarrow \mathrm{RCH(O_2H)R} + \mathrm{RCH^{\bullet}R},\\
&\mathrm{RCH(O_2H)R} \longrightarrow \mathrm{RC(=O)R} + \mathrm{H_2O}.
\end{aligned} \tag{7}$$

On the basis of the FTIR data alone, neither mechanism can be proved nor disproved, although ketones are clearly an intermediate product. The spectra are especially complex between 1300 and 1700 cm^{-1}, likely due to peak overlap from ethers and ketones of various carbon-chain lengths, making absolute product assignment impossible.

3.3. Methanol adsorption and degradation on TiO_2 surfaces

Methanol was chosen as the next molecule to examine, due to the simplicity of possible photo-oxidation products (no long-chain carbon products) as well as the ability for methanol to chemisorb to the TiO_2 surface [6–8]. Samples were dosed with methanol vapor in a similar manner to decane, but unlike decane, the methanol species remained behind on the surface after complete evacuation of the sample chamber. Figure 7 shows the difference spectra before and after methanol and d4-methanol adsorption onto the TiO_2 sample. Both samples show a loss of Ti–OH groups, as methanol molecules can displace surface OH groups during chemisorption as seen below:

$$\mathrm{R{-}OH(g)} + \mathrm{OH(ad)} \longrightarrow \mathrm{R{-}O(ad)} + \mathrm{H_2O}\ (\text{g or ad}). \tag{8}$$

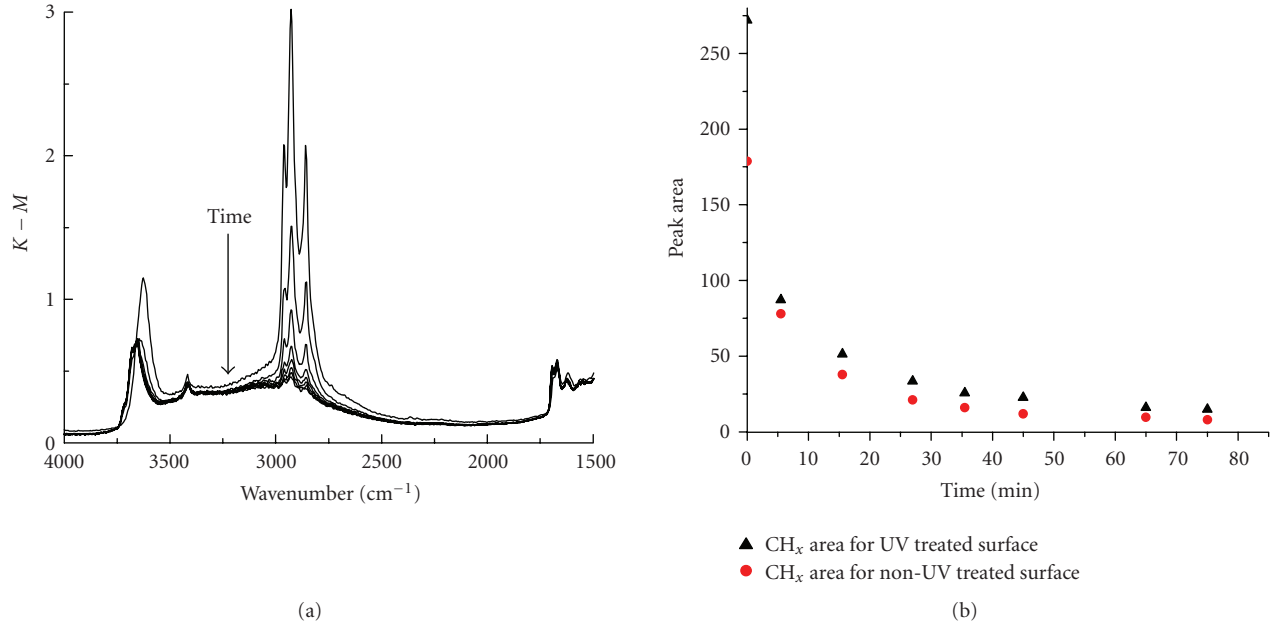

FIGURE 4: Typical time series of decane desorption on TiO_2 in vacuo (a), and hydrocarbon peak intensity of decane absorbed to UV versus non-UV-treated TiO_2 (b).

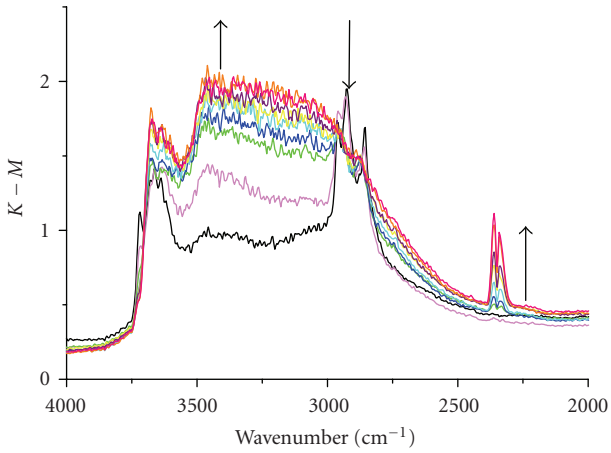

FIGURE 5: DRIFT spectra taken during the course of 1-hour UV oxidation of decane on TiO_2 under 1 atm O_2. Arrows indicate increase in surface-bound water and CO_2 vapor, and a decrease in hydrocarbon intensity.

For d4-methanol, CD_3 stretches are seen at 2072 and 2226 cm^{-1}, and the methanol OD stretch is seen as a broad peak centered at 2470 cm^{-1}. An OD stretch corresponding to Ti–OD is also seen at 2716 cm^{-1}, indicating scrambling of surface OH groups with methanol [3].

Figure 8 shows a series of difference spectra taken during the course of methanol oxidation under 1 atm O_2. Within the first 5 minutes, both water and CO_2 are seen to form. There is a decrease in CH_3 stretches at 2916 and 2816 cm^{-1}, and a new peak assigned to a CH_2 stretch at 2862 cm^{-1}. There are also 2 new peaks at 1583 and 1361 cm^{-1}, which are assigned to the asymmetrical and symmetrical stretching bands of carboxylate anion, respectively [21]. These products were also seen in the case of d4-methanol (Figure 9). To further validate that formic acid is indeed the intermediate species identified in the difference spectra, a drop of formic acid was placed directly on a fresh TiO_2 surface, and the resulting DRIFT spectrum is shown in Figure 10. Carboxylate peaks are observed in the same location as the peaks from the difference spectra, confirming the assignment.

After 15 more minutes of irradiation, there is a decrease in the carboxylate species, and an increase in CO_2 occurs. Upon evacuation, surface water and CO_2 are lost, but an increase is seen in carboxylate, indicating that it is a surface-bound species which now has increased signal strength, possibly due to readsorption of gas-phase carboxylic acid molecules once surface water was removed. A possible mechanism for the reaction, which is consistent with the spectral evidence presented above, is as follows. The initiating step is hydrogen abstraction, either by direct hole transfer or superoxide. A hydroperoxy species is formed, which rearranges to a surface-bound formic acid, which can then be released as CO_2:

$$\begin{aligned}
&\text{Ti(IV)–OCH}_3 + h^+ \longrightarrow \text{Ti(IV)–OCH}_2{}^* + \text{H}^+,\\
&\text{O}_{2,s-} + \text{Ti(IV)–OCH}_3 \longrightarrow \text{Ti(IV)–OCH}_2{}^* + \text{HO}_2{}^-,\\
&\text{Ti(IV)–OCH}_2{}^* + \text{O}_2 \longrightarrow \text{Ti(IV)–OCH}_2\text{OO}^*,\\
&\text{Ti(IV)–OCH}_2\text{OO}^* + (\text{R–H or Ti–OH})\\
&\qquad \longrightarrow \text{Ti(IV)–OCH}_2\text{OOH},\\
&\text{Ti(IV)–OCH}_2\text{OOH} \longrightarrow \text{Ti(IV)–OC(=O)H} + \text{H}_2\text{O},\\
&\text{Ti(IV)–OC(=O)H} + h^+ \longrightarrow \text{Ti(IV)} + \text{CO}_2 + \text{H}^+.
\end{aligned} \tag{9}$$

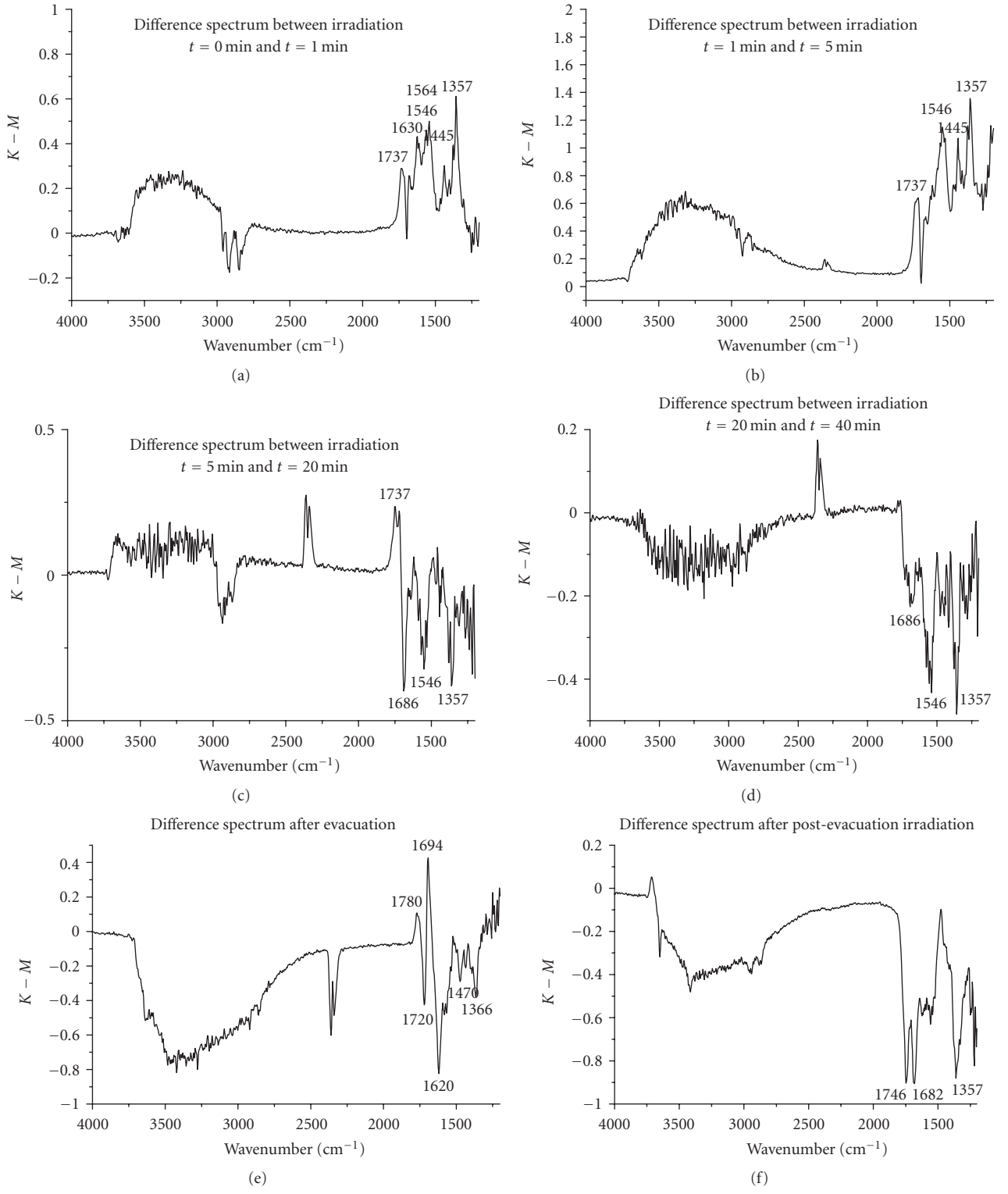

Figure 6: Time series DRIFT difference spectra following course of decane oxidation.

4. CONCLUSIONS

Only when TiO_2 is irradiated in the presence of a hole scavenger, even at very low surficial concentrations, electrons are trapped at Ti(III)–OH sites, and free electrons are also generated. Upon heating, the hole scavengers are desorbed and with the consequent reinjection of previously trapped holes. This leads to a decrease in detectable Ti(III)–OH centers. Decane adsorption experiments lend support to the theory that removal of hydrocarbon contaminants is

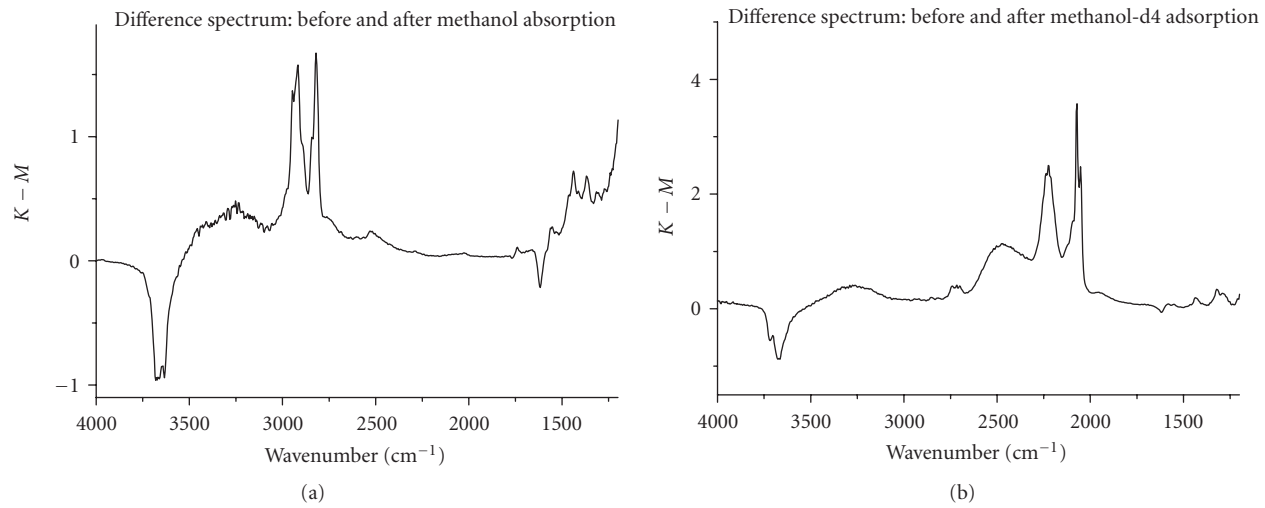

Figure 7: DRIFT spectra showing surface coverage of methanol and methanol-d4.

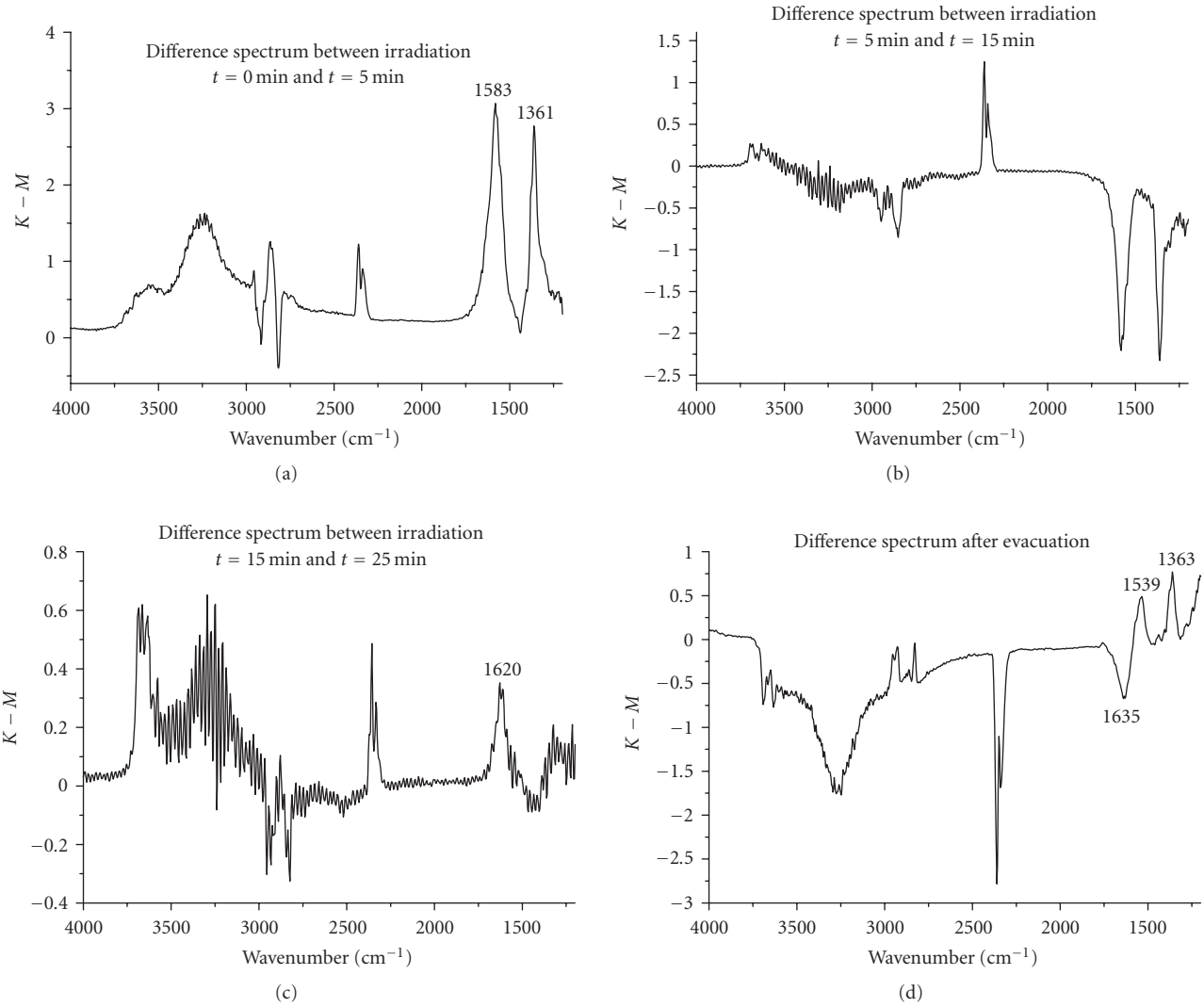

Figure 8: Time series DRIFT difference spectra following course of methanol oxidation.

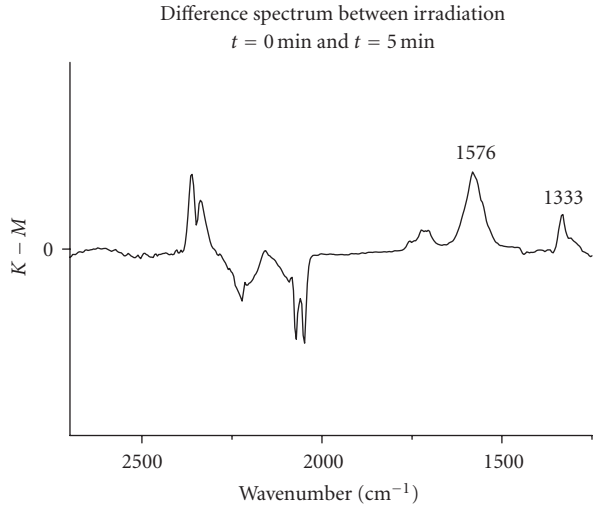

Figure 9: Initial products of d4-methanol oxidation.

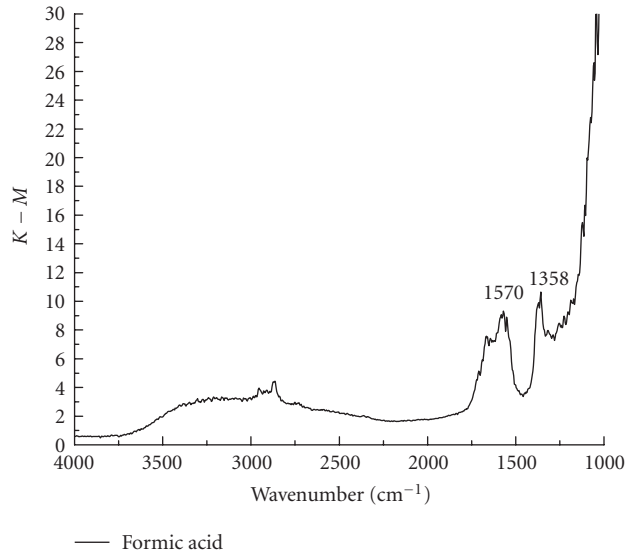

Figure 10: Formic acid absorbed on TiO_2.

responsible for the appearance of super-hydrophilic TiO_2 surfaces. While the oxidation of decane did not lead to any definitive product assignments, the oxidation of methanol led to identification of surface-bound formic acid.

ACKNOWLEDGMENTS

We are grateful to the Hydrogen Energy Research & Development Center and 21st Century Frontier Research and Development Program of the Ministry of Science and Technology of Korea for research support. Supplementary support was generously provided by the Northrop-Grumman Corporation. Special issue dedicated to the second international conference on semiconductor photochemistry.

REFERENCES

[1] M. R. Hoffmann, S. T. Martin, W. Choi, and D. W. Bahnemann, "Environmental applications of semiconductor photocatalysis," *Chemical Reviews*, vol. 95, no. 1, pp. 69–96, 1995.

[2] T. L. Thompson and J. T. Yates Jr., "Surface science studies of the photoactivation of TiO_2-new photochemical processes," *Chemical Reviews*, vol. 106, no. 10, pp. 4428–4453, 2006.

[3] S. H. Szczepankiewicz, A. J. Colussi, and M. R. Hoffmann, "Infrared spectra of photoinduced species on hydroxylated titania surfaces," *Journal of Physical Chemistry B*, vol. 104, no. 42, pp. 9842–9850, 2000.

[4] S. H. Szczepankiewicz, J. A. Moss, and M. R. Hoffmann, "Electron traps and the stark effect on hydroxylated titania photocatalysts," *Journal of Physical Chemistry B*, vol. 106, no. 31, pp. 7654–7658, 2002.

[5] S. H. Szczepankiewicz, J. A. Moss, and M. R. Hoffmann, "Slow surface charge trapping kinetics on irradiated TiO_2," *Journal of Physical Chemistry B*, vol. 106, no. 11, pp. 2922–2927, 2002.

[6] V. S. Lusvardi, M. A. Barteau, and W. E. Farneth, "The effects of bulk titania crystal-structure on the adsorption and reaction of aliphatic-alcohols," *Journal of Catalysis*, vol. 153, no. 1, pp. 41–53, 1995.

[7] G. A. M. Hussein, N. Sheppard, M. I. Zaki, and R. B. Fahim, "Infrared spectroscopic studies of the reactions of alcohols over group IVB metal oxide catalysts—part 3: ethanol over TiO_2, ZrO_2 and HfO_2, and general conclusions from parts 1 to 3," *Journal of the Chemical Society, Faraday Transactions*, vol. 87, no. 16, pp. 2661–2668, 1991.

[8] E. Farfan-Arribas and R. J. Madix, "Role of defects in the adsorption of aliphatic alcohols on the $TiO_2(110)$ surface," *Journal of Physical Chemistry B*, vol. 106, no. 41, pp. 10680–10692, 2002.

[9] S. R. Morrison and T. Freund, "Chemical role of holes and electrons in ZnO photocatalysis," *Journal of Chemical Physics*, vol. 47, no. 4, pp. 1543–1551, 1967.

[10] M. Miyake, H. Yoneyama, and H. Tamura, "Two step oxidation reactions of alcohols on an illuminated rutile electrode," *Chemistry Letters*, vol. 5, no. 6, pp. 635–640, 1976.

[11] B. Kraeutler and A. J. Bard, "Heterogeneous photocatalytic decomposition of saturated carboxylic acids on TiO_2 powder. Decarboxylative route to alkanes," *Journal of the American Chemical Society*, vol. 100, no. 19, pp. 5985–5992, 1978.

[12] T. Ohno, S. Izumi, K. Fujihara, Y. Masaki, and M. Matsumura, "Vanishing of current-doubling effect in photooxidation of 2-propanol on TiO_2 in solutions containing Fe(III) ions," *Journal of Physical Chemistry B*, vol. 104, no. 29, pp. 6801–6803, 2000.

[13] T. Zubko, D. Stahl, T. L. Thompson, D. Panayotov, O. Diwald, and J. T. Yates Jr., "Ultraviolet light-induced hydrophilicity effect on $TiO_2(110)(1 \times 1)$. Dominant role of the photooxidation of adsorbed hydrocarbons causing wetting by water droplets," *Journal of Physical Chemistry B*, vol. 109, no. 32, pp. 15454–15462, 2005.

[14] A. Y. Nosaka, T. Fujiwara, H. Yagi, H. Akutsu, and Y. Nosaka, "Photocatalytic reaction sites at the TiO_2 surface as studied by solid-state ^{1}H NMR spectroscopy," *Langmuir*, vol. 19, no. 6, pp. 1935–1937, 2003.

[15] I. Rosenberg, J. R. Brock, and A. Heller, "Collection optics of TiO_2 photocatalyst on hollow glass microbeads floating on oil slicks," *Journal of Physical Chemistry*, vol. 96, no. 8, pp. 3423–3428, 1992.

[16] N. Djeghri, M. Formenti, F. Juillet, and S. J. Teichner, "Photointeraction on the surface of titanium dioxide between oxygen and alkanes," *Faraday Discussions of the Chemical Society*, vol. 58, pp. 185–193, 1974.

[17] T. Minabe, D. A. Tryk, P. Sawunyama, Y. Kikuchi, K. Hashimoto, and A. Fujishima, "TiO_2-mediated photodegradation of liquid and solid organic compounds," *Journal of Photochemistry and Photobiology A*, vol. 137, no. 1, pp. 53–62, 2000.

[18] R. Wang, K. Hashimoto, A. Fujishima, et al., "Light-induced amphiphilic surfaces," *Nature*, vol. 388, no. 6641, pp. 431–432, 1997.

[19] N. Sakai, A. Fujishima, T. Watanabe, and K. Hashimoto, "Quantitative evaluation of the photoinduced hydrophilic conversion properties of TiO_2 thin film surfaces by the reciprocal of contact angle," *Journal of Physical Chemistry B*, vol. 107, no. 4, pp. 1028–1035, 2003.

[20] R. Nakamura and S. Sato, "Oxygen species active for photooxidation of *n*-decane over TiO_2 surfaces," *Journal of Physical Chemistry B*, vol. 106, no. 23, pp. 5893–5896, 2002.

[21] R. Silverstein and F. Webster, *Spectrometric Identification of Organic Compounds*, John Wiley & Sons, New York, NY, USA, 6th edition, 1998.

Hindawi Publishing Corporation
International Journal of Photoenergy
Volume 2008, Article ID 759736, 7 pages
doi:10.1155/2008/759736

Research Article

A Photocatalytic Active Adsorbent for Gas Cleaning in a Fixed Bed Reactor

Peter Pucher,[1] Rabah Azouani,[2] Andrei Kanaev,[2] and Gernot Krammer[3]

[1] *Department of Chemical Apparatus Design, Particle Technology and Combustion, Graz University of Technology, Inffeldgasse 25/B, 8010 Graz, Austria*
[2] *Laboratoire d'Ingénierie des Matériaux et des Hautes Pressions, CNRS, Institut Galilée, Université Paris-Nord, 93430 Villetaneuse, France*
[3] *Department of Energy and Process Engineering, Norwegian University of Science and Technology, Kolbjørn Hejes vei 1, 7491 Trondheim, Norway*

Correspondence should be addressed to Peter Pucher, peter.pucher@tugraz.at

Received 24 July 2007; Accepted 27 February 2008

Recommended by Russell Howe

Efficient photocatalysis for gas cleaning purposes requires a large accessible, illuminated active surface in a simple and compact reactor. Conventional concepts use powdered catalysts, which are nontransparent. Hence a uniform distribution of light is difficult to be attained. Our approach is based on a coarse granular, UV-A light transparent, and highly porous adsorbent that can be used in a simple fixed bed reactor. A novel sol-gel process with rapid micro mixing is used to coat a porous silica substrate with TiO_2-based nanoparticles. The resulting material posses a high adsorption capacity and a photocatalytic activity under UV-A illumination (PCAA = photocatalytic active adsorbent). Its photocatalytic performance was studied on the oxidation of trichloroethylene (TCE) in a fixed bed reactor setup in continuous and discontinuous operation modes. Continuous operation resulted in a higher conversion rate due to less slip while discontinuous operation is superior for a total oxidation to CO_2 due to a user-defined longer residence time.

1. INTRODUCTION

Many pollutants, smells, and odors as well as bacteria and pathogens exist in the atmosphere. They influence the quality of life and they are sources of illnesses and allergies even if they are at very low concentrations. An abatement of these unwanted substances with state-of-the-art technology is either technically complex or energetically expensive. The photocatalytic oxidation technique represents a new and promising method for gas cleaning. Hence, the interest in photocatalytic chemistry is rising worldwide as demonstrated by high numbers of citations and patents [1]. However, upscaling and technical implementation of photocatalysis are difficult, which is one of the reasons why industrial realizations are still limited.

The basic problem of the photocatalytic processes scale-up for commercial utilization is to provide sufficient illuminated active surface area. A uniform distribution of light inside the reactor and provision of a high number of active surface sites per reactor volume unit are key parameters of a successful reactor design [2]. One approach to meet these requirements is based on a fixed bed reactor with an irradiated nanocoated fill. The used material should possess optimal optical properties and a large inner surface with unhindered access by pollutant to catalyst layer. Coarse-granular wide-pore silica is an excellent candidate because it has open porous structure and high-specific surface area, and it satisfies UV-light transmission [3].

In the present communication we report on a new photocatalytic active adsorbent (PCAA) as a combination of TiO_2-sol nanoparticles immobilized on a UV-transparent coarse-granular porous silica support. The UV-light-triggered degradation of trichloroethylene is investigated and its kinetics is discussed.

2. EXPERIMENTAL

2.1. Preparation and immobilization of nanoparticles

The sol nanoparticles are prepared in a sol-gel reactor using titanium tetraisopropoxide (TTIP) as a precursor. This

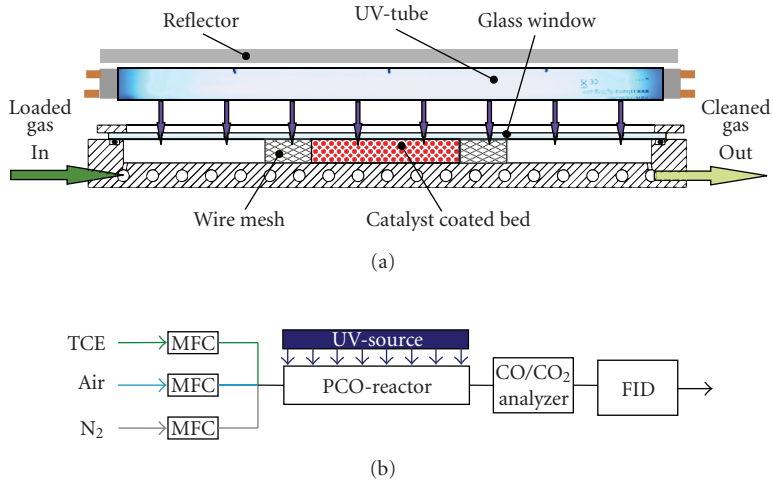

Figure 1: (a) Cut section of the photocatalytic reactor and (b) simplified flow sheet of the setup.

Table 1: BET surface and pore characteristics of PCAA.

Substrate	Mean grain size (mm)	BET surface (m^2/g)	Most abundant pore diameter (nm)	Pore volume (mm^3/g)
Porous silica granulate	3-4	330 ± 30	6 ± 0.7	810 ± 70

reactor has been described in [4]. In present experiments, the standard operation conditions were conserved: two stock solutions of TTIP/propan-2-ol and H_2O/propan-2-ol (C_{Ti} = 0.146 M, H = C_{H_2O}/C_{Ti} = 2.46) were synchronously injected at high Reynolds numbers into the reactor container through the static Hartridge-Roughton-type T-mixer by applying a dry nitrogen gas pressure. The reactor temperature was maintained at 20.0°C. As a result, metastable sol particles of size 2R = 6.0 nm with a narrow size distribution were generated in the reactor. The sols slowly grow in size during the so-called induction period that amounts for t_{ind} = 55 minutes. Particle immobilization was achieved during the period of their relative stability: $t < t_{ind}/2$. The support was immersed into the reactive colloid for ~25 minutes, then withdrawn, cleaned, and dried. The TiO_2 nanoparticles are involved into their bulk by capillary forces, then reacting on the internal surface of pores. Hence, they are immobilized on the support surface. After the drying stage in a glove box and then in an oven (80°C), a calcination at 450°C was performed typically during 4 hours. The deposited catalyst mass on the porous substrate was measured as described in [5]. A mean value of 0.55 wt.% has been obtained.

2.2. Photocatalytic reactor

The photocatalytic performance of the prepared PCAA was studied in a fixed bed plug flow reactor setup, depicted in Figure 1. Trichloroethylene (C_2HCI_3, TCE) was used as a model pollutant at an inlet concentration varied from 25 to 300 ppmv. Purified-compressed air and N_2 acted as carrier gas, free of oil, CO/CO_2, and humidity. The overall gas flow of 1 l/min s.t.p. was controlled by mass flow controllers. All experiments were carried out at ambient pressure and temperature (~1 bar, 23 ± 3°C) with dry gas. The inlet and outlet gas temperatures were monitored by two type-K thermocouples. The coated material was filled in the stainless steel reactor of a rectangular shape (fill size 50×76×11 mm^3) covered by a UV-A transparent glass window. One UV-A fluorescent tube (Sylvania BL350 8W, peak emission at 350 ± 15 nm) illuminated the material. Its performance was adjusted from 25% to 100% by an electronic ballast (Philips EVG HF-R 114 TL5). This corresponds to the integral intensity I varied from 0.68 to 5.35 mW/cm^2, measured with a Solatell Sola-Scope 2000 setup. The TCE concentration was measured by a flame-ionization detector (FID TESTA 123), which was calibrated with TCE gas before the measurements. A CO/CO_2 gas analyzer (NDIR Hartmann&Braun URAS 14) measured the final products of the photocatalytic TCE oxidation. The reactor could be bypassed to measure the inlet concentrations.

3. RESULTS AND DISCUSSION

3.1. Surface area and pore size

The uncoated substrate and impregnated PCAA grains were analyzed for their total pore volume and pore size distribution with Hg-intrusion method (Porotec Inc., Niederhofheimer Str. 55a, 65719 Hofheim, Germany), and their internal surface area with BET method (STRÖHLEIN AREA-meter II). The nanoparticle coating process appears to have no significant influence on both pore volume and surface area. Table 1 summarizes the results for PCAA. The measured properties for coated and uncoated materials were found to be within the range of deviation due to inhomogeneities in the raw material. Thus, it can be concluded that

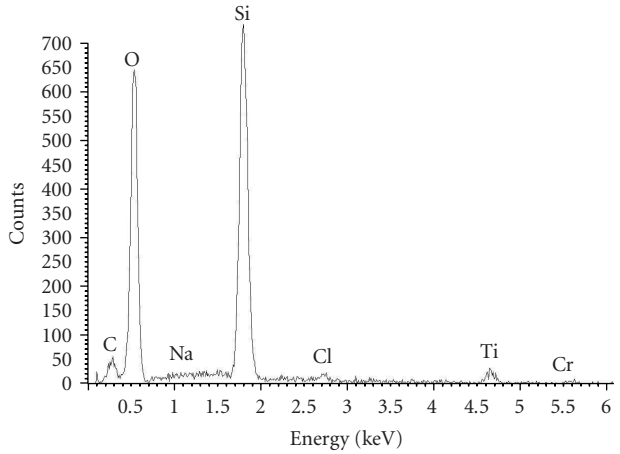

Figure 2: Electron microscope EDX spectrum of nano-TiO_2 impregnated silica substrate PCAA (FELMI Graz).

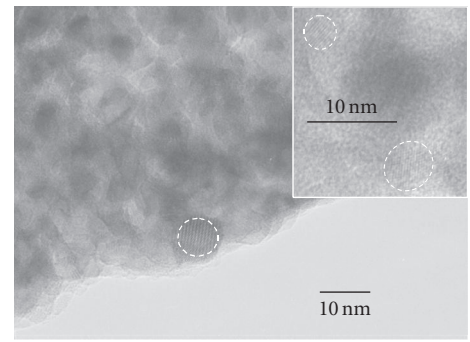

Figure 3: High-resolution TEM image of the TiO_2 nanoparticles immobilized into the nanoporous silica substrate (LIMHP Paris).

hardly any pores are blocked by incorporated TiO_2 particles. The pore size distribution of the substrate is broad enough to give sufficient room for nanoparticles already at wide pore diameters. On the other hand, an increase of the surface area due to the nanoparticles is low because of their low-mass load (~0.55 wt.%). Benmami et al. [5] have reported the specific surface of the noncrystalline TiO_2 nanoparticles in the range of 480 m^2/g correlated to their own mass. Being normalized on the total PCAA mass, this corresponds to an active surface area of about 2.7 m^2/g or just 0.8% of the substrate surface.

3.2. Morphology analysis of PCAA

EDX (Zeiss DSM 982 GEMINI), XRD (XRG 3000 INEL), and TEM (JEOL 200 keV) measurements were carried out to characterize the immobilized catalyst nanoparticles on the inner substrate surface. Beneath the typical peaks for the silica substrate (Si, O), the EDX spectrum (Figure 2) shows a small peak for titanium at about 4.5 keV. Because of a low-mass loading of TiO_2 nanoparticles embedded in amorphous silica, the XRD patterns of PCAA showed no characteristic peaks. It was not possible to identify the crystalline phase of TiO_2 with this method. High-resolution TEM measurements of PCAA bulk material have been performed to investigate particle size and distribution of the nanoparticular TiO_2 mater. Figure 3 evidences rare nonagglomerated crystalline domains of size in the range between 5 and 10 nm. These rare crystallites are surrounded by amorphous silica matrix visualized by low-contrast gray slabs and spots. A first approximation of their crystalline layer distances indicates the anatase phase.

3.3. UV-absorption of the nanocoated substrates

The UV transmission of a substrate is one important property, since a large active area has to be illuminated in practical applications. The substrate must not absorb photons at energies sufficient to elevate an electron from the valence band to the conduction band of the semiconductor. A custom-made setup consisting of a big volume quartz cell ($55 \times 35\,mm^2$ window size) with adjustable spacing and an 8W UV-A tube (Sylvania BL350) light source was used to measure the optical transparency dependence on the fill thickness (10–30 mm). The penetrating light was detected by a Chromex 250IS monochromator (grating 150 l/mm, f = 30 cm, slit 20 μm) equipped with a CCD detector (Princeton). Figure 4(a) shows the spectral dependence on the absorption shows a plateau with no particular band structure. Because the silica band gap is large, we assign this opacity to the light scattering on silica pores. On the other hand, the opacity of TiO_2-coated PCAA exhibits a characteristic onset below ~400 nm, which corresponds to the bulk TiO_2 anatase absorption [6]. Short-wave UV-light is thereby scattered and absorbed inside PCAA, while long-wave UV/VIS light is transmitted through a fill of PCAA. This finding is documented by Figure 4(b)) which clearly shows a red shift of the normalized absorbance with increasing fill thickness.

3.4. Photocatalytic oxidation in continuous mode

First experiments were carried out under continuous gas feed and UV-A illumination. The photocatalytic performance of PCAA was studied by the TCE degradation rate (r_{TCE}) based on the volume of the fixed bed (V_{FB}). The experimental data of pollutant concentration (in ppmv) at inlet (Y_{IN}) and outlet (Y_{OUT}) and the total molar gaseous flow $\dot{N}_g$ (in mol/s) were used to calculate the experimental rate $r_{TCE,exp}$ as presented in

$$r_{TCE,exp}(\overline{Y}) = \frac{\dot{N}_g}{V_{FB}} \cdot (Y_{IN} - Y_{OUT}) \left(\frac{mol}{m^3 \cdot s}\right). \quad (1)$$

Due to reactions, the TCE concentration decreases downstream of the gas flow. Thus assuming Langmuir-Hinshelwood reaction kinetics, this experimental rate is related to the logarithmic mean concentration $\overline{Y}$ between inlet and outlet:

$$\overline{Y} = \frac{(Y_{IN} - Y_{OUT})}{\ln(Y_{IN}/Y_{OUT})}\ (ppmv). \quad (2)$$

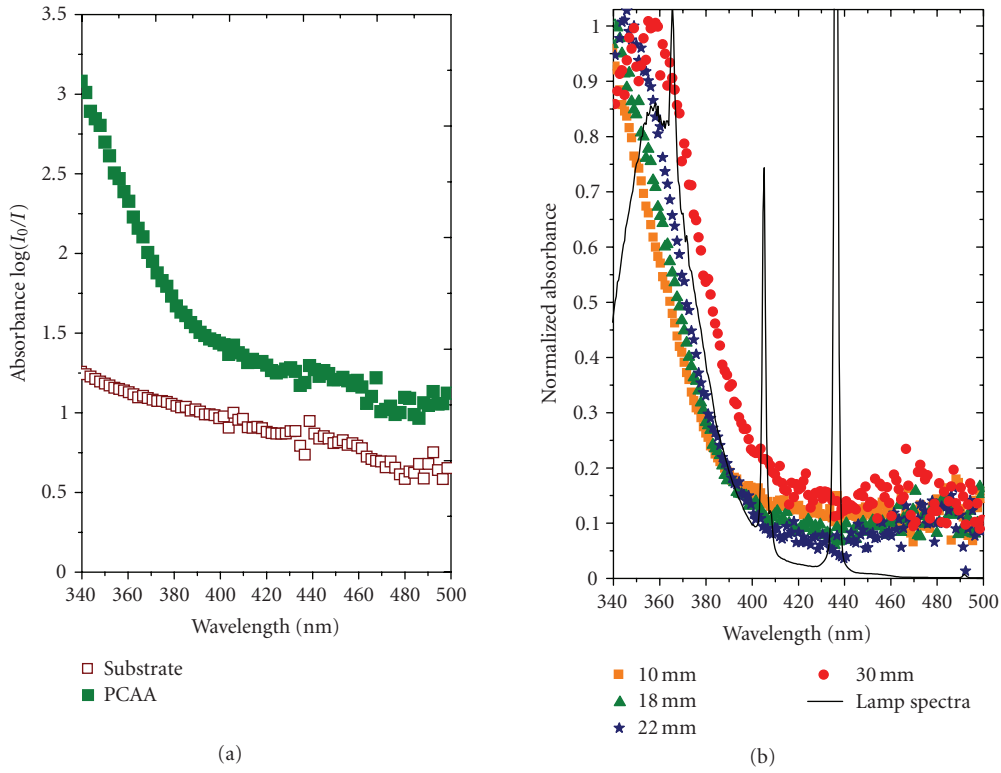

Figure 4: (a) Spectral dependence of the absorbance of pure and nano-TiO_2 impregnated silica substrate. (b) Red-shift of the normalized absorbance with increasing fill thickness of PCAA.

Among different kinetic studies concerning the photocatalytic oxidation of TCE reported in literature (see, e.g., Anderson et al. [7], Demeestere et al. [8], Doucet et al. [9]), we found that none of them provided sufficient information about the reaction rate dependence on light intensity over a wide range of concentrations. Our experimental kinetic study was performed in continuous operation mode for different inlet concentrations and varying light intensity I. We developed a modified Langmuir-Hinshelwood kinetic model to accommodate the influence of the concentration and light intensity on the TCE decomposition rate r_{TCE}:

$$r_{TCE}(Y,I) = \frac{k_I \cdot K_{Ad} \cdot Y}{1 + K_{Ad} \cdot Y} \cdot \left(1 - e^{-C \cdot (I/I_{max})}\right) \left(\frac{\text{mol}}{\text{m}^3 \cdot \text{s}}\right). \quad (3)$$

The influence of the light intensity I is expressed by the exponential term of (3). Thereby, the intrinsic light intensity I was related to the maximal intensity I_{max} (5.36 mW/cm^2). A dimensionless adjustable parameter C, with no further physical meaning, was used as a fit parameter. This exponential term was suggested to describe best the observed saturation behavior over the applied concentration range. Figure 5 illustrates this behavior in a 3D surface fit. The points set for the experimental data obtained with (1) and (2), while the surface presents the calculated model according to (3), computed with the kinetic parameters of Table 2. The model satisfactorily describes the measured data with a high-correlation coefficient r^2 of 0.976.

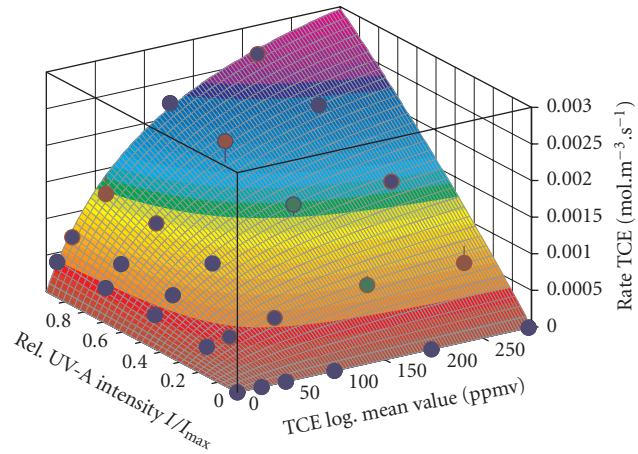

Figure 5: Experimental results (dots) and kinetic fit for the photocatalytic oxidation of TCE on PCAA in dependence of concentration and light intensity.

3.5. Photocatalytic oxidation in discontinuous mode

PCAA possesses a large inner surface and hence a high capacity for the adsorption of polar pollutant molecules. In case of TCE, experiments resulted in the adsorption of about 1.4 mg/g at 100 ppmv (23°C) and no UV-A illumination. This adsorption capacity combined with the photocatalytic

Table 2: Calculated kinetic parameters for the photocatalytic oxidation of TCE (25–300 ppm) on PCAA in dependence of UV-A light intensity (0–5.35 mW/cm^2, 11 mm fill thickness).

Catalyst	Rate k_I (mol·m^{-3}·s^{-1})	Adsorption constant K_{Ad} (ppm^{-1})	Light constant C (1)	Correlation r^2 (1)
PCAA	0.0149	0.0085	0.325	0.9769

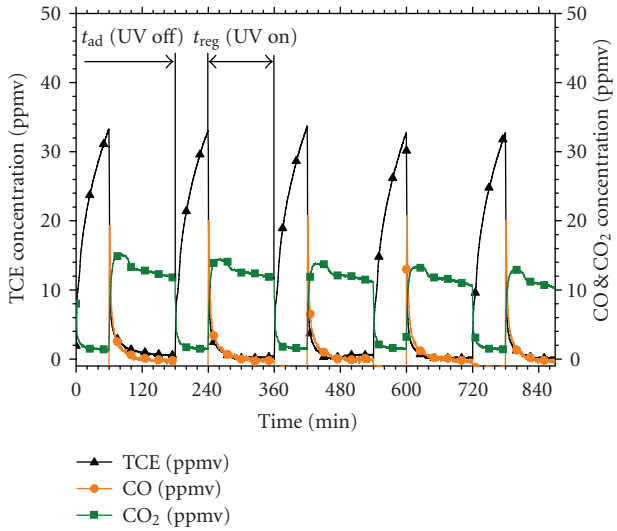

Figure 6: Transient TCE, CO, and CO_2 concentration at reactor outlet for the discontinuous oxidation of TCE on PCAA (50 ppm TCE inlet concentration, mode B: $t_{reg} = 2 \cdot t_{ad} = 120$ minutes).

activity can be used to run a reactor unit equipped with PCAA in a discontinuous mode for gas cleaning purposes. In this regime, first the adsorption step occurs of a pollutant from the raw gas stream under no UV-A illumination, followed by a regeneration step with/without clean air flush under UV-A illumination. Zou et al. [10] described the photocatalytic oxidation of toluene on titania-silica pellets in alternating adsorption/regeneration mode. A higher removal efficiency is generally expected with an increased regeneration time.

To test PCAA in discontinuous operation conditions, we conducted experiments at 50 ppmv and 100 ppmv TCE inlet concentration under two different conditions. Mode A was designed with the adsorption time t_{ad} = 60 minutes and equal regeneration time $t_{reg} = t_{ad}$. Mode B was designed with a twice longer regeneration time $t_{reg} = 2 \cdot t_{ad}$ (120 minutes). During regeneration, the reactor was flushed with 1 l/min s.t.p. clean air and UV-A light was on with the maximum lamp performance (5.36 mW/cm^2). Figure 6 shows the transient analyzer signals for Mode B at 50 ppmv TCE inlet concentration. Since the fill volume was small (42 cm^3), a certain amount of TCE passed as slip the fixed bed reactor during the adsorption step (UV-A lamps off). Around 50% of the incoming TCE molecules were emitted on this stage. During the regeneration step only a very low TCE quantities were emitted and the adsorbed TCE was stored in PCAA, being slowly oxidized by the photocatalytic process until the next adsorption step.

3.6. CO and CO_2 products formation during continuous and discontinuous operation modes

A complimentary possibility in evaluation of the material photocatalytic performance is to follow the reaction products formation. CO_2 is the most desired final product of this process. Table 3 compares the main figures of overall conversion efficiency, oxidation rate C_{OX}/C_{TCE}, and ratio of produced CO_2 versus CO in discontinuous and continuous operation modes. This comparison shows a much higher conversion efficiency in the continuous mode compared to the discontinuous one. This is well supported by the high slip of our setup during the adsorption step, as we defined conversion efficiency as $(TCE_{IN} - TCE_{OUT})/TCE_{IN}$. The main advantage of the discontinuous operation mode is the longer residence time of the pollutant in PCAA. Hence, a much higher conversion of TCE to CO and CO_2 can be achieved. This is illustrated by the C_{OX}/C_{TCE} ratio, which is computed out of a carbon balance for adsorbed/reacted TCE to produced CO and CO_2. Furthermore, a full oxidation to CO_2 is preferred with longer regeneration time, which is illustrated by a higher CO_2/CO ratio for mode B. For all discontinuous tests, the computed oxidation rate was smaller than 1 which implies that a larger-quantity pollutant was adsorbed than oxidized at the regeneration steps. Hence, the regeneration time was too short and the system was still in an unsteady regime after ~15 hours operation in mode B. Out of this finding, it can be concluded that TCE is to be converted into chlorinated intermediates (e.g., DCAC [11, 12], Phosgene [11–13], etc.) in a first fast reaction step. FTIR measurements proved the presence of DCAC and phosgene in the off-gas stream of the photo-reactor. Since their high polarity, these chlorinated intermediates can remain adsorbed onto the polar PCAA surface and oxidized slowly to the final oxidation products including CO and CO_2. We assume a first-order kinetic reaction with the molar load of hydrocarbon in PCAA as determining concentration. Figure 7 shows the transient outlet concentration of CO/CO_2 during a long-term regeneration step. Thereby, the plotted lines were calculated with a first-order reaction scheme. A detailed analysis of the reaction pathways was not subject of the present communication.

4. CONCLUSION

A photocatalytic active adsorbent (PCAA) was prepared by coating a coarse granular porous silica with TiO_2 nanoparticles in a sol-gel reactor. The used substrate acts as adsorbent possessing a high inner surface (BET = 330 m^2/g) with an open wide pore structure. A high-resolution TEM image revealed a particle size of 5–10 nm. The crystalline

Table 3: Conversion efficiency, slip during adsorption, oxidation ratio, and CO_2-to-CO ratio for regeneration time equals adsorption time ($t_{reg} = t_{ad}$, mode A), regeneration time twice adsorption time ($t_{reg} = 2 \cdot t_{ad}$, mode B), and continuous operation (mode C).

TCE inlet ppm	Mode	Total TCE conversion (%)	Slip during adsorption (%)	C_{OX}/C_{TCE} (%)	CO_2/CO (1)
50	A	45	51	32	2.73
	B	44	49	65	3.43
	C	89	—	25	1.75
100	A	38	55	30	2.04
	B	40	53	48	3.05
	C	73	—	28	1.61

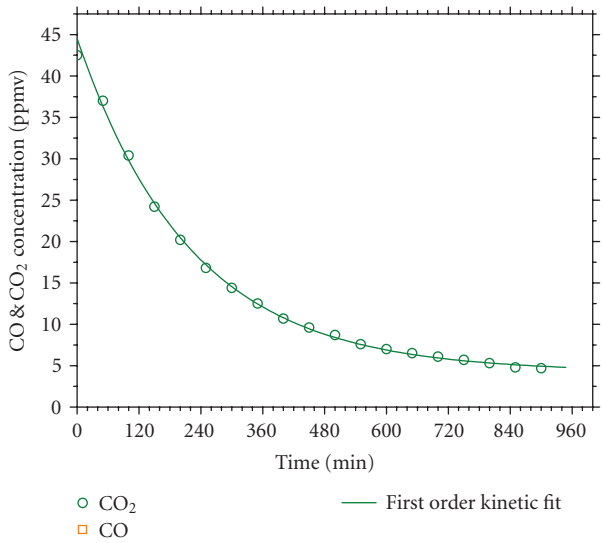

Figure 7: Transient CO, CO_2 concentration at reactor outlet for a long-term regeneration run. The measured data points were fitted with a first-order kinetic fit (line).

particles are isolated embedded in the amorphous silica matrix. Experimental test for the photocatalytic oxidation of trichloroethylene (TCE) was conducted in a fixed-bed reactor setup under dry conditions. A study of influence of the pollutant concentration and UV-A light intensity was performed in a continuous operation mode. An adapted Langmuir-Hinshelwood kinetic model was found to satisfactorily describe the measured TCE destruction rate. The continuous operation mode resulted in a higher TCE conversion efficiency but a lower oxidation ratio to CO and CO_2 than the discontinuous operation mode. The main problem of a discontinuous operation was the slip of pollutant during the adsorption step. This problem can be solved by a longer length of the PCAA fill. The CO and CO_2 production rates were found to be directly dependent on the amount of pollutant or intermediate adsorbed in PCAA rather than on the inlet concentration.

PCAA can be regenerated by the photocatalytic oxidation process. This opens up new and alternative ways in photocatalytic reactor design and gas cleaning technology. Our results indicate a large material potential for applications at low pollutant concentrations and small to medium gas flow rates. Recent experiments indicate a photo-induced activity of the uncoated substrate for the destruction of TCE developed after some UV-A illumination time. This currently unknown process maybe driven by a chlorine radical reaction. Further experiments with photocatalytic oxidation of methanol on PCAA are under way.

ACKNOWLEDGMENTS

This work is supported by the COST D41 Actions of the European Commission and Franco-Norwegian cooperation program AURORA. One of the authors gratefully acknowledges the experimental support by the Research Institute for Electron Microscopy at Graz University of Technology.

REFERENCES

[1] D. M. Blake, "Bibliography of work on the heterogeneous photocatalytic removal of hazardous compounds from water and air," Tech. Rep. NREL/TP-510-31319, NREL, Golden, Colo, USA, 2001.

[2] D. Bahnemann, "Photocatalytic water treatment: solar energy applications," *Solar Energy*, vol. 77, no. 5, pp. 445–459, 2004.

[3] P. Pucher, M. Benmami, G. Krammer, K. Chhor, J.-F. Bocquet, and A. Kanaev, "Photocatalytic activity of sol-gel derived TiO_2 nanocoatings toward trichloroethylene decomposition in the gas phase," in *Proceedings of the International Congress on Particle Technology (PARTEC '07)*, Nuremberg, Germany, March 2007.

[4] M. Rivallin, M. Benmami, A. Kanaev, and A. Gaunand, "Sol-gel reactor with rapid micromixing: modelling and measurements of titanium oxide nano-particle growth," *Chemical Engineering Research and Design*, vol. 83, no. A1, pp. 67–74, 2005.

[5] M. Benmami, K. Chhor, and A. V. Kanaev, "Supported nanometric titanium oxide sols as a new efficient photocatalyst," *Journal of Physical Chemistry B*, vol. 109, no. 42, pp. 19766–19771, 2005.

[6] M. R. Hoffmann, S. T. Martin, W. Choi, and D. W. Bahnemann, "Environmental applications of semiconductor photocatalysis," *Chemical Reviews*, vol. 95, no. 1, pp. 69–96, 1995.

[7] M. A. Anderson, S. Yamazaki-Nishida, and S. Cervera-March, "Photodegradation of trichloroethylene in the gas phase using TiO_2 porous ceramic membrane," in *Photocatalytic Purification and Treatment of Water and Air*, D. F. Ollis and H. Al-Ekabi, Eds., pp. 405–420, Elsevier, Amsterdam, The Netherlands, 1993.

[8] K. Demeestere, A. De Visscher, J. Dewulf, M. Van Leeuwen, and H. Van Langenhove, "A new kinetic model for titanium dioxide mediated heterogeneous photocatalytic degradation of trichloroethylene in gas-phase," *Applied Catalysis B*, vol. 54, no. 4, pp. 261–274, 2004.

[9] N. Doucet, F. Bocquillon, O. Zahraa, and M. Bouchy, "Kinetics of photocatalytic VOCs abatement in a standardized reactor," *Chemosphere*, vol. 65, no. 7, pp. 1188–1196, 2006.

[10] L. Zou, Y. Luo, M. Hooper, and E. Hu, "Removal of VOCs by photocatalysis process using adsorption enhanced TiO_2-SiO_2 catalyst," *Chemical Engineering and Processing*, vol. 45, no. 11, pp. 959–964, 2006.

[11] S.-J. Hwang, C. Petucci, and D. Raftery, "*In situ* solid-state NMR studies of trichloroethylene photocatalysis: formation and characterization of surface-bound intermediates," *Journal of the American Chemical Society*, vol. 120, no. 18, pp. 4388–4397, 1998.

[12] P. B. Amama, K. Itoh, and M. Murabayashi, "Photocatalytic oxidation of trichloroethylene in humidified atmosphere," *Journal of Molecular Catalysis A*, vol. 176, no. 1-2, pp. 165–172, 2001.

[13] K.-H. Wang, H.-H. Tsai, and Y.-H. Hsieh, "The kinetics of photocatalytic degradation of trichloroethylene in gas phase over TiO_2 supported on glass bead," *Applied Catalysis B*, vol. 17, no. 4, pp. 313–320, 1998.

Hindawi Publishing Corporation
International Journal of Photoenergy
Volume 2008, Article ID 280513, 11 pages
doi:10.1155/2008/280513

Research Article

Durability of Ag-TiO_2 Photocatalysts Assessed for the Degradation of Dichloroacetic Acid

Víctor M. Menéndez-Flores,[1] Donia Friedmann,[2] and Detlef W. Bahnemann[1]

[1] *Institut für Technische Chemie, Leibniz Universität Hannover, Callinstraße 3, D-30167 Hannover, Germany*
[2] *Interdisciplinary Nanoscience Center, University of Aarhus, Building 520, 8000 Aarhus C, Denmark*

Correspondence should be addressed to Detlef W. Bahnemann, bahnemann@iftc.uni-hannover.de

Received 31 March 2008; Revised 21 July 2008; Accepted 13 August 2008

Recommended by Russell Howe

The stability of Ag-TiO_2 photocatalysts was examined for the photocatalytic degradation of dichloroacetic acid (DCA) as a function of the recycling times. The photocatalytic activity was investigated by measuring the rate of H^+ ions released during the photodegradation of DCA and confirmed by measuring the total organic carbon removal. The photodegradation reactions were studied at pH 3 and pH 10 for a series of Ag-TiO_2 photocatalysts as different with Ag loadings . All the Ag-TiO_2 and bare TiO_2 photocatalysts showed a decrease in photocatalytic activity on recycling for the DCA photodegradation reaction. The decrease in activity can be attributed to poisoning of active sites by Cl^- anions formed during the photocatalytic DCA degradation. The photocatalytic activity was, however, easily recovered by a simple washing technique. The reversibility of the poisoning is taken as evidence to support the idea that the recycling of Ag-P25 TiO_2 photocatalysts does not have a permanent negative effect on their photocatalytic performance for the degradation of DCA. The choice of the preparation procedure for the Ag-TiO_2 photocatalysts is shown to be of significant importance for the observed changes in the photocatalytic activity of the Ag-TiO_2 particles.

1. INTRODUCTION

The presence of cocatalytic noble metal deposits on metal oxide particles is often employed to enhance the photocatalytic oxidation efficiency of processes through achieving a more efficient charge separation [1]. Considerable work has been done on Ag-TiO_2 modified photocatalysts and their potential applications as enhanced photocatalysts. The presence of Ag deposits on the TiO_2 surface can help to efficiently separate the electron hole pairs by attracting the conduction band photoelectrons. This process has been shown to improve the overall efficiency for a number of photocatalytic reactions [2]. Ag-TiO_2 particles are typically prepared by photodeposition with the titanium dioxide particles being suspended in an aqueous solution containing the metal salt. When the suspension is illuminated, metal ions are reduced by conduction band electrons to form the metal deposits on the TiO_2 surface. This process is described by the series of reactions (1)–(3). Depending on the preparation conditions, this photodeposition procedure typically yields small metal deposits ranging from a few nanometers to tens of nanometers [2]

$$TiO_2 + h\nu \longrightarrow TiO_2(e^-, h^+), \tag{1}$$

$$(TiO_2)OH + h^+ \longrightarrow (TiO_2)OH^{\bullet +}, \tag{2}$$

$$Ag^+ + e^- \longrightarrow Ag^0. \tag{3}$$

The size and dispersion of metal deposits on TiO_2 particles are critical in controlling their photocatalytic activity. Given the strong effect of deposit size and dispersion, the development of preparation methods which provide such close control over deposit size is essential [3, 4]. An issue that is not often addressed is the stability of these metal-doped particles and hence the effects, if any, on the longer-term application potential and shelf-life stability of these particles. This is particularly true for applications as photocatalysts, where these particles are subjected to irradiation with UV(A) light. Reformation of surficial metal clusters when the semiconductor particles are exposed to ultrabandgap irradiation has often been reported [5, 6]. For example, while

cluster stabilization can be achieved by adsorption of metal clusters onto a solid surface, it has been shown that the rate of cluster growth on a quartz surface is accelerated by UV light [5].

The stability of metal deposits on photocatalysts under illumination may depend on a number of factors, such as, for example, the type of metal, the deposit size, the photocatalytic reactions taking place, and the reaction conditions such as solution pH. Additionally, the redox potential can affect the reduction state of the supporting oxide. For example, the efficiency of the cluster-oxide coupling has been found to strongly depend on the band bending in TiO_2 after silver deposition which in turn varies with the reduction state of the oxide [7].

Despite the large volume of studies focusing on metal-deposited TiO_2 photocatalysts, particularly Ag-TiO_2, the photocatalyst stability and recycling has been addressed only in a few studies. Reproducibility tests were carried out on Ag-doped TiO_2 films prepared through a 2-step dipping and illumination process using Degussa P25 as the photocatalyst. These tests proved that the photocatalytic activity of the silver-modified films for the degradation of methyl orange remains unchanged even after six consecutive experiments with newly added pollutant quantities [8]. Xu et al. [9] have studied recycled 0.5 atom% Ag-deposited magnetic TiO_2-SiO_2-Fe_3O_4 photocatalysts and have also found that the photoreactivity for the degradation of orange (II) was maintained after 3 recycles. However, the total irradiation time was only 20 minutes which is relatively short.

In a study by Zhang, Ag-TiO_2 photocatalysts were in fact deactivated during the photocatalytic degradation of acetone in air [10], with a 73% reduction in activity during the fourth hour of reaction. The deactivation was explained as being due to interactions between partially oxidized organics and the Ag deposits, and possibly by the aggregation of the silver nanoparticles, which was reflected in changes in the absorption spectra of these particles. Regeneration was achieved by visible light illumination and was attributed to the oxidation of Ag deposits to Ag^+ ions, in the form of Ag_2O, which were reduced to Ag^0 upon UV illumination. This study raised the issue of the nanometre level control of feature size and interfeature spacing and the long-term stability of such structures, hindering their full exploitation for device applications [11].

Apart from photocatalytic applications, Sun et al. [12] have studied Ag-TiO_2 cyanide sensors prepared by the photodeposition method which were tested under mild conditions and found to give good results using 0.1–10 μmol/L cyanide at pH 9–12. The Ag-TiO_2 sensors were found to be effective, without the need for regeneration for up to one month. It must be said that the available silver content was greater than the amount of cyanide to be detected.

In this study, we have examined the durability of Ag-TiO_2 photocatalysts under practically relevant conditions. The model reaction was the photodegradation of dichloroacetic acid (DCA). DCA is a known industrial pollutant the photodegradation of which has been studied extensively, for example, by Bahnemann et al. [13]. Important parameters selected for an initial exploration were the duration of illumination and the silver content. The poisoning of the photocatalyst surface by chloride ions was explored and reactivation was investigated using a simple washing technique. The deactivation of self-prepared colloidal TiO_2 was compared to that of the commercially available P25 TiO_2 photocatalysts.

2. EXPERIMENTAL

2.1. Preparation of Ag-TiO_2 and colloidal TiO_2 photocatalysts

The Ag-TiO_2 photocatalysts were prepared by a photodeposition process. Degussa P25 was used as the TiO_2 photocatalyst. P25 TiO_2 consists of 70% anatase and 30% rutile with an average primary particle diameter of 55 ± 5 nm and a BET surface area of 48 m^2/g. The photochemical experiments were performed in a reactor (50 mL) with a plain quartz window on which the light beam ($\lambda \geq 320$ nm) was focused. Figure 1 provides a schematic of the photocatalytic reactor setup. The reactor was equipped with a magnetic stirring bar, a water-circulating jacket and three openings for pH electrode, gas supply, and sample withdrawing. The photoreactor was filled with 50 mL of the aqueous suspension containing the TiO_2 photocatalyst at a loading of 0.5 g/L. The photocatalyst slurry was illuminated with UV(A) light for 20 minutes to oxidize any possible organic carbon impurities on the TiO_2 surface.

Silver ions in the form of $AgClO_4$ were then added to the TiO_2 slurry at an initial pH of approximately 6 to obtain the desired Ag^+:Ti ratio. The suspension was illuminated for 24 hours. A series of Ag-TiO_2 photocatalysts with a respective Ag loading of 0.1, 0.2, 0.35, 0.5, 1, and 2 atom% was prepared. The samples were labelled as xAg-TiO_2, where x is the amount of Ag^+ added given in atom%.

The prepared particles were characterized by electron microscopy (emission transmission electron microscope JEOL JEM-2100F-UHR and emission scanning electron microscope JEOL JSM-6700F). The STEM was supported by an energy dispersive spectroscopic analysis (EDX) and elemental X-ray mapping images provided information regarding the distribution of the various components (TiO_2 and Ag) and ions (Ti, Ag, Cl) before and after the photoreaction.

Colloidal TiO_2 was prepared by a method described by Bahnemann [14] that involved the dropwise addition of titanium tetraisopropoxide dissolved in 99.99% 2-propanol to an aqueous hydrochloric acid solution of pH 1.5. The final concentrations of TiO_2 and 2-propanol were 1.5×10^{-2} and 1.2 M, respectively. The reaction volume was 1 L. This mixture was stirred overnight employing a magnetic stirrer. The final solution was optically transparent. Evaporation under vacuum was used to collect the TiO_2 powder which can be resuspended in water and other polar solvents (e.g., alcohols) to form transparent colloidal suspensions. UV-Vis absorbance measurements in the wavelength range 200–700 nm showed the steep increase in absorption below approximately 350 nm which is typical for nanosized TiO_2. The final TiO_2 solution, whose photoactivity was tested, was

prepared by suspending 500 mg of this powder in 1 L of water.

2.2. Photocatalytic degradation of DCA

After the photodeposition reaction, the Ag-TiO_2 photocatalysts were collected and sonicated for 15 minutes before the addition of 1 mM DCA into the slurry. The pH was then adjusted to either 3 or 10, by addition of 0.1 M $HClO_4$ or 0.1 M NaOH, respectively. The temperature of the suspension was maintained at 25°C. The suspension was vigorously stirred without illumination for 30 minutes to attain adsorption equilibrium of the DCA molecules on the photocatalyst surface and continuously purged with air to ensure a constant O_2 concentration throughout the experiment. After this adsorption period, UV illumination was provided by a high-pressure Xe-lamp (OSRAM HBO-500W). A UV(A)/Vis illumination was achieved employing a band-pass filter (WG 320) which eliminates UV-radiation below $\lambda = 320$ nm. The intensity of UV(A) illumination was 20 mW/cm^2 at the entrance window of the photoreactor as measured by a UV light meter (ultraviolet radiometer LT Lutron UVA-365).

The pK_a of DCA is 1.29 [15] and it thus exists in its anionic form in aqueous solutions at pH > 2. The photocatalytic oxidation of one DCA anion results in the formation of one proton, two CO_2 molecules, and 2 Cl^- ions (4). The reaction pH was maintained constant using a pH-stat setup with the addition of $HClO_4$ or NaOH as needed.

$$CHCl_2COO^- + O_2 \xrightarrow{h\nu,TiO_2} 2CO_2 + H^+ + 2Cl^-. \quad (4)$$

The rate of the photodegradation of DCA was followed by measuring the amount of OH^- added to keep the pH constant and thus the amount of H^+ formed using the pH-stat technique as described by Bahnemann et al., 1993 [16]. Samples were taken at the beginning and at the end of each run for total organic carbon (TOC) analysis. The reaction time was 4 hours for each run. In total, 3 consecutive runs were preformed with the same photocatalyst. 1 mM of DCA was injected at the beginning of each run. For the third run, 4 mM Cl^- was also added to selected experiments in order to compare and investigate the effect of chloride ions on the photocatalytic reaction rate.

3. RESULTS AND DISCUSSION

For the preparation of the Ag-TiO_2 photocatalysts, the first indication of the deposition of metallic silver onto the TiO_2 surface upon irradiation of the TiO_2 and Ag^+ suspensions was a color change of the particles from white to brown. A higher concentration of silver ions corresponded to a higher intensity of this brownish color. According to the literature, the photodeposited Ag should be present in metallic form, based on XRD analysis of Ag/TiO_2 particles prepared using 20.0 atom% Ag^+ loading which confirmed the presence of metallic silver [17]. At lower Ag content, metallic silver could not be detected since the mass of silver in the sample was below the detection limit of the employed instrument [17].

In Figure 2(a), the degradation of 1 mM DCA within each run (followed as release of H^+ ions during the degradation process) using pure Degussa P25 as the photocatalyst is shown. Three runs were consecutively carried out and a third run from a second series of experiments is also presented here with 4 mM Cl^- added before the illumination to evaluate a possible poisoning effect of the photocatalyst's active sites by chloride ions. It can be clearly seen that both the reaction rate and yield are reduced during each consecutive run with the most obvious inhibition being observed upon the addition of chloride ions.

As shown in Figure 2(b), the photocatalytic activity of Degussa P25 toward the degradation of DCA is almost completely recovered once the catalyst is simply washed with pure water before the next activity test. This clearly indicates the inhibitory effect of Cl^- ions that was already obvious from the results presented in Figure 2(a).

The effect of recycling the 0.35 Ag-TiO_2 photocatalyst on the photocatalytic degradation rate of DCA is shown in Figure 3(a) and once again employing the washing technique in Figure 3(b). The reaction conditions were the same as described previously for the experiment with pure P25 TiO_2. As can be seen from Figure 3(a), the reaction rate is found to be lowered after the first run, and is lowered even more during the 3rd run. Once again, the reaction rate is further reduced when this third run is carried out after the addition of 4 mM Cl^-. Moreover, the reaction seems to stop in this case after about 20% of the initially present DCA has been degraded. This is consistent with the respective TOC results shown in Figure 6 (*vide infra*).

In the next set of experiments, the aim was to investigate whether the negative effect of recycling the Ag-TiO_2 photocatalyst can also be avoided by a simple washing technique. Washing of the photocatalysts was carried out by recovering the material by centrifugation of the reaction slurry after each run and resuspending it in distilled water, followed by the appropriate adjustment of pH. The results are shown in Figure 3(b). As in the case of pure Degussa P25, it is obvious that this simple intermittent washing technique between each reaction run leads to a remarkable improvement in activity following the first and second recycles.

The results shown in Figures 2 and 3 clearly show that a "clean" surface is a prerequisite for the photocatalyst to exhibit its full activity independent of the absence or presence of cocatalysts such as Ag-deposits. The detrimental effect of codissolved ions such as Cl^- is known since they are likely to adsorb onto the TiO_2 surface and can disturb the adsorption of the organic compounds [18].

The self-prepared colloidal TiO_2 photocatalyst was tested with the same intention as pure Degussa P25 and P25-Ag under the identical experimental conditions. Figure 4 shows the results of these experiments. Obviously, the reaction rate and yield also decrease in subsequent runs. However, this poisoning effect appears to be much less pronounced for the colloidal particles as compared with pure or Ag-deposited Degussa P25. Even with the further addition of 4 mM of Cl^- ions before the third run, no substantial difference is observed as compared with a third run without the addition of chloride ions. Thus the capacity of the self-prepared

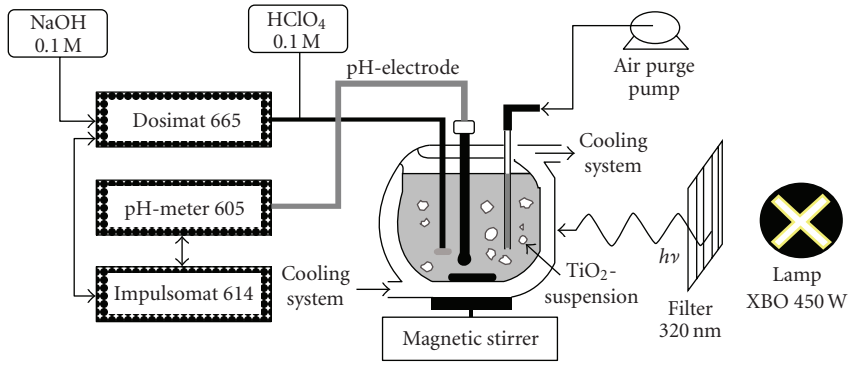

Figure 1: Schematic presentation of the photocatalytic reactor setup.

colloidal particles to accommodate chloride ions without any loss in photocatalytic activity appears to be very high.

The results of the TOC analysis performed at the end of each experimental run, that is after 4 hours of illumination, and the H^+ production efficiency in percent increase at the same time are presented in Figures 5–7. These figures provide a summary of the effect of recycling and washing of the photocatalysts with respect to the mineralization of DCA. The TOC removal results are in fact in good agreement with the results obtained following the release of H^+, evincing that the simple stoichiometry given in (4) is indeed correct.

In Figure 5, the results for pure Degussa P25 are shown. The gradual decline in photoactivity following each recycle can be seen from set A for the consecutive runs. In set B, the strong detrimental effect of chloride ion addition before run 3 can be clearly seen. In set C, the photocatalyst was collected after each run by centrifugation, resuspended in distilled water at the correct pH and placed back in the reactor. However, for the pure P25 photocatalyst, the recovery of the photoactivity was not complete. Comparing the results obtained from set A with those of set C, however, it is obvious that the photoactivity after the washing technique is slightly higher than that observed without washing.

The results for the TOC removal using the 0.35 Ag-TiO_2 photocatalyst are presented in Figure 6. These are also in agreement with the DCA degradation results shown in Figures 3(a) and 3(b). The results of set C show the successful application of this simple washing technique resulting in an almost complete recovery of the photocatalytic activity. While the amount of DCA degraded after 4 hours of illumination even seems to slightly increase after each illumination/washing cycle (Figure 6, set C), the initial rate of degradation is found to decrease (Figure 3(b)), in particular, for the second run. In comparison with the results obtained for pure Degussa P25, however, it is obvious that the photocatalytic activity of Ag-TiO_2 can be recovered much more rapidly by this simple washing procedure. As will be shown below (in Figures 13 and 14), this might be due to the fact that the chloride ions show a strong tendency to adsorb at the silver clusters from where they can obviously be removed much easily than from the bare TiO_2 surface.

For the colloidal TiO_2 particles, the analysis of the TOC removal after 4 hours of illumination also showed the durability of this photocatalyst (the results are shown in Figure 7). In fact, this photocatalyst showed a greater resilience to deactivation compared to pure Degussa P25 and to the Ag-TiO_2 photocatalysts. This is believed to be due to the greater number of active sites provided by this photocatalyst for the photocatalytic reaction, hence minimizing the observed poisoning by the chloride ions. It is important to note that due to its colloidal nature, this photocatalyst could not be separated by centrifugation and hence it could not be washed between the recycles. Both its advantages and drawbacks need to be taken into account when considering its application under real conditions.

In the next set of experiments, the effect of catalyst recycling on the photocatalytic DCA-degradation rates was examined for a series of Ag-TiO_2 photocatalysts varying the amount of deposited Ag. These degradation experiments were carried out both under acidic (pH 3) and under basic (pH 10) conditions. The aim was to identify reaction conditions or photocatalyst composition, where the observed reduction in photonic efficiency due to recycling can be minimized. Figure 8 provides a summary for the results obtained for the measured photonic efficiencies (based on the initial degradation rate of DCA as measured by the release of H^+).

The photonic efficiency ζ is defined as the ratio of the initial degradation rate and the incident photon flux (see (5)), where the initial photocatalytic rate is calculated from the slope of the individual concentration versus time profiles. This definition of the photonic efficiency was first suggested by Serpone and Salinaro [19]. The incident photon flow per volumetric unit (I varied between 3.39×10^{-2} Einstein $L^{-1}h^{-1}$ and 3.74×10^{-2} Einstein $L^{-1}h^{-1}$) was calculated based upon the UV-A light meter measurements [20], the irradiated surface area of 8.042 cm^2, and the volume of the suspension (5×10^{-2} L).

$$J_0 = \frac{I \cdot \lambda}{N_A \cdot h \cdot c},$$
$$\zeta(\%) = \frac{k \cdot c_0 \cdot V}{J_0 \cdot A} \cdot 100 \tag{5}$$

with J_0 = light flux [$mol^* s^{-1} cm^{-2}$]; I = light intensity [$J^* s^{-1} cm^{-2}$]; N_A = Avogadro's number [$6.022 \cdot 10^{23} mol^{-1}$];

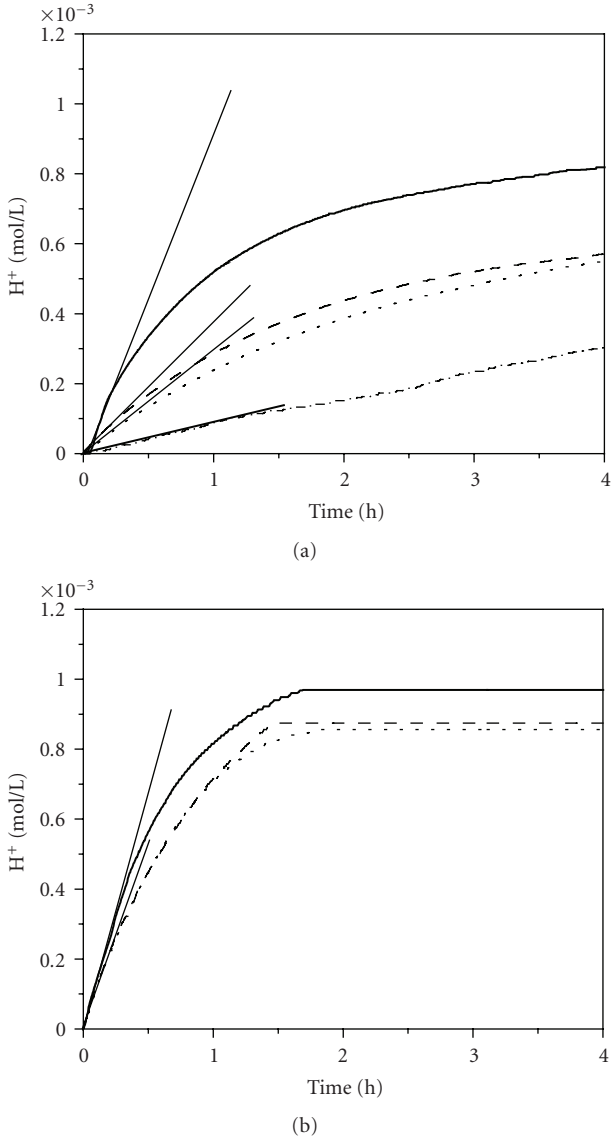

Figure 2: (a) Degradation of DCA (shown as release of H^+) using the photocatalyst Degussa P25 at pH 3 in 3 consecutive runs, 1st run (—), 2nd run (– – –), 3rd run (· · ·), a 3rd run (-·-) with addition of 4 mM Cl^- before the run started, and slope (___) used for the determination of the photonic efficiency of each run with $I \approx 3.39 \times 10^{-2}$ Einstein $L^{-1}h^{-1}$. The photocatalyst loading was 0.5 g/L. (b) Degradation of DCA (shown as release of H^+) using the photocatalyst Degussa P25at pH 3 in 3 consecutive runs with intermittent washing between the runs, 1st run (—), 2nd run (– – –), 3rd run (· · ·), and slope (___) used for the determination of the photonic efficiency of each run with $I \approx 3.39 \times 10^{-2}$ Einstein $L^{-1}h^{-1}$. The photocatalyst loading was 0.5 g/L.

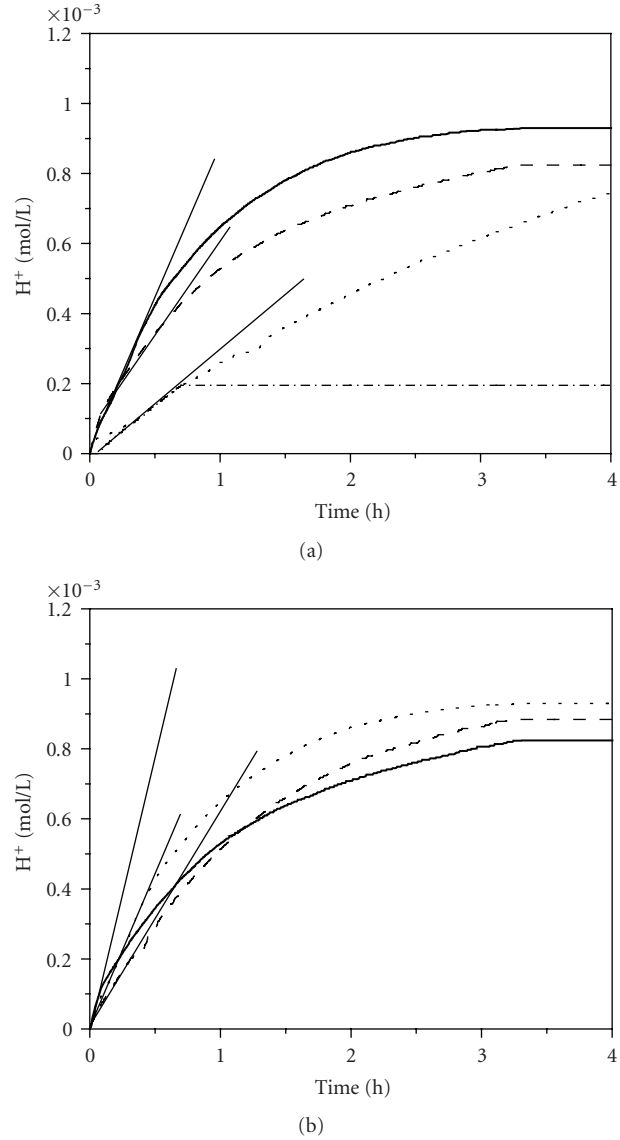

Figure 3: (a) Degradation of DCA (shown as release of H^+) using the photocatalyst 0.35 Ag-TiO_2 at pH 3 in 3 consecutive runs, 1st run (—), 2nd run (– – –), 3rd run (· · ·), a 3rd run (-·-) with addition of 4 mM Cl^- before the run started, and slope (___) used for the determination of the photonic efficiency of each run with $I \approx 3.39 \times 10^{-2}$ Einstein $L^{-1}h^{-1}$. The photocatalyst loading was 0.5 g/L. (b) Degradation of DCA (shown as release of H^+) using the photocatalyst 0.35 Ag-TiO_2 at pH 3 in 3 consecutive runs with intermittent washing between runs, 1st run (—), 2nd run (– – –), 3rd run (· · ·), and slope (___) used for the determination of the photonic efficiency with $I \approx 3.39 \times 10^{-2}$ Einstein $L^{-1}h^{-1}$. The photocatalyst loading was 0.5 g/L.

h = Planck constant [$6.63 \cdot 10^{-34}$Js]; c = light velocity [$3 \cdot 10^8 m^* s^{-1}$]; k = initial rate constant [s^{-1}]; A = area [cm^2]; C_0 = initial DCA concentration [$mol^* L^{-1}$]; λ = wavelength [nm]; V = volume [L] .

In Figure 8, the photonic efficiency measured for each run is presented, comparing the fresh photocatalyst with the recycled ones after the second and third runs. Figure 8 shows overall higher rates during the first run at pH 3 compared to pH 10 both, for pure Degussa P25 and when silver is photodeposited. This DCA degradation trend, although performed with a different photocatalyst, is in agreement with earlier studies reported by Bahnemann et al. [13], who attributed the faster rates observed under acidic conditions (pH 2.6) to the favorable DCA coordination through the

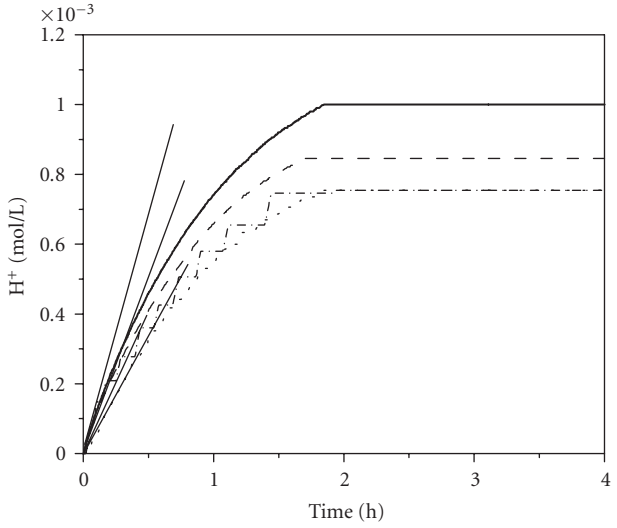

Figure 4: Degradation of DCA (shown as release of H^+) using the prepared colloidal TiO_2 photocatalyst at pH 3 in 3 consecutive runs without intermittent washing between runs, 1st run (—), 2nd run (– – –), 3rd run (· · ·), a 3rd run (-·-) with addition of 4 mM Cl^- before the run started, and slope (___) used for the determination of the photonic efficiency of each run with $I \approx 3.39 \times 10^{-2}$ Einstein $L^{-1}h^{-1}$. The photocatalyst loading was 0.5 g/L.

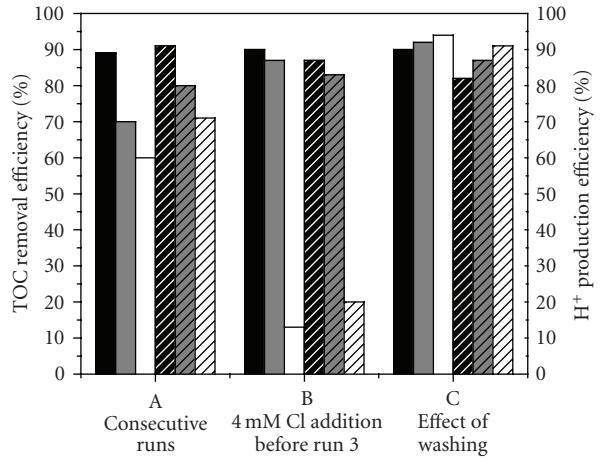

Figure 6: Removal of DCA (TOC removal) after 4 hours of illumination using the photocatalyst 0.35 Ag-TiO_2 at pH 3 in 3 consecutive runs (1st run ■, 2nd run ▒, and 3rd run □), the H^+ production efficiency after 4 hours of illumination is also shown (1st run ▨, 2nd run ▨, and 3rd run ▨) in set A, with chloride ion addition in set B before the third run and with intermittent washing between runs (set C). The photocatalyst loading was 0.5 g/L and the light intensity $I \approx 3.39 \times 10^{-2}$ Einstein $L^{-1}h^{-1}$.

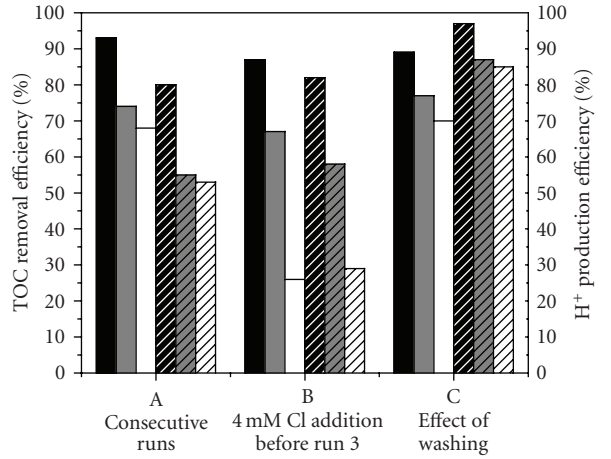

Figure 5: Removal of DCA (TOC removal) after 4 hours of illumination using the photocatalyst P25-TiO_2 at pH 3 in 3 consecutive runs (1st run ■, 2nd run ▒, and 3rd run □), the H^+ production efficiency after 4 hours of illumination is also shown (1st run ▨, 2nd run ▨, and 3rd run ▨) in set A, with chloride ion addition before the third run (set B), and with intermittent washing between runs (set C). The photocatalyst loading was 0.5 g/L and the light intensity $I \approx 3.39 \times 10^{-2}$ Einstein $L^{-1}h^{-1}$.

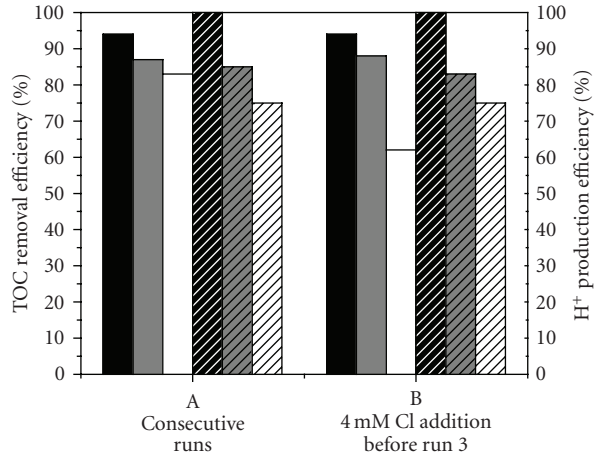

Figure 7: Removal DCA (TOC removal) after 4 hours of illumination using the colloidal-TiO_2 photocatalyst at pH 3 in 3 consecutive runs (1st run ■, 2nd run ▒, and 3rd run □) the H^+ production efficiency after 4 hours of illumination is also shown (1st run ▨, 2nd run ▨, and 3rd run ▨) in set A and with chloride ion addition before the third run (set B). The photocatalyst loading was 0.5 g/L and the light intensity $I \approx 3.39 \times 10^{-2}$ Einstein $L^{-1}h^{-1}$.

formation of bidentate complexes that could not be formed in alkaline medium at pH 11.3. The absolute value of the photonic efficiency for the pure P25 photocatalyst obtained here is slightly lower than that reported previously [21], where a photonic efficiency $\zeta = 3.9\%$ was measured at pH 3 under similar conditions. This could, for example, be explained by a variation of the activity of such a commercial product between different production batches which are well known for most catalysts. It is interesting to note the influence of the presence of chloride ions in the suspension. With the presence of 8 mM NaCl (2×2 mM for runs 1 and 2 plus 4 mM added before run 3) prior to run 3 the efficiency decreases by approximately 50%, that is, the photocatalytic activity can be considerably inhibited by the presence of

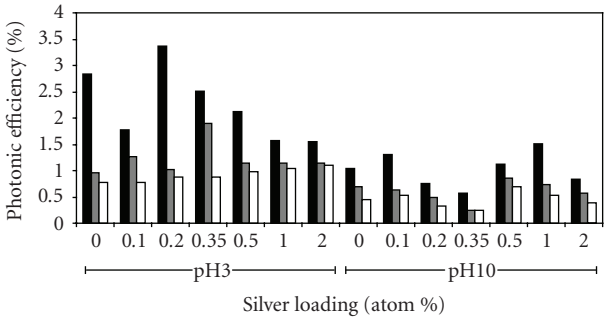

Figure 8: Effect of recycling Ag-TiO_2 photocatalysts on observed photonic efficiencies at pH 3 and pH 10 (1st run ■, 2nd run ▒, and 3rd run □), degradation of 1 mM DCA without any extra addition of chloride ions or washing technique performed. The photocatalyst concentration was 0.5 g/L with different silver loadings (atom%). The light intensity at pH 3 was $I \approx 3.39 \times 10^{-2}$ Einstein $L^{-1}h^{-1}$ and at pH 10 was $I \approx 3.74 \times 10^{-2}$ Einstein $L^{-1}h^{-1}$.

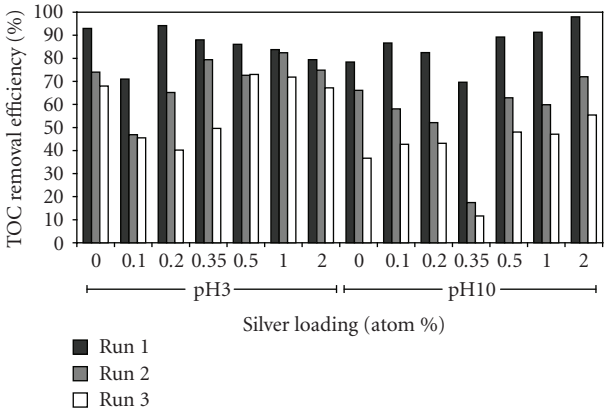

Figure 9: Effect of recycling Ag-TiO_2 photocatalysts on observed TOC removal at pH 3 and pH 10 (1st run ■, 2nd run ▒, and 3rd run □), degradation of 1 mM DCA without any extra addition of chloride ions or washing technique performed. The light intensity at pH 3 was $I \approx 3.39 \times 10^{-2}$ Einstein $L^{-1}h^{-1}$ and at pH 10 was $I \approx 3.74 \times 10^{-2}$ Einstein $L^{-1}h^{-1}$.

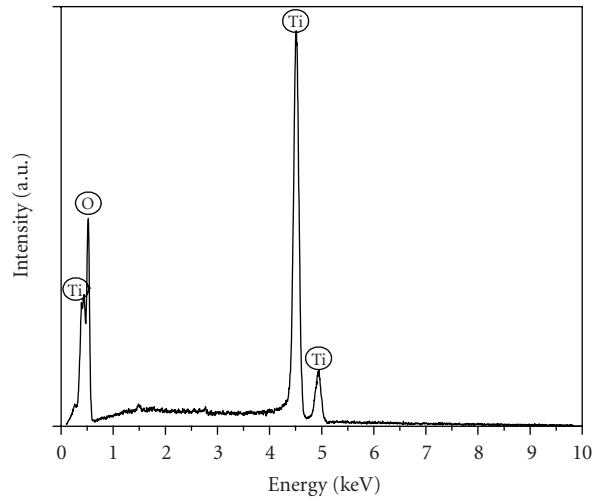

Figure 10: EDXS-spectrum of Degussa P25 prior to the photodeposition of silver or the photodegradation of DCA.

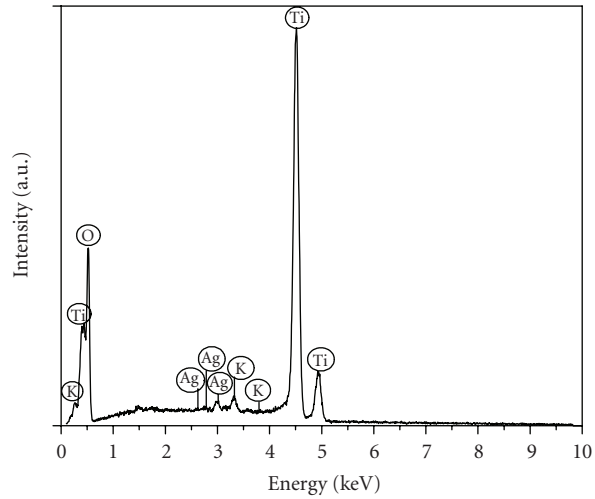

Figure 11: EDXS spectrum of 0.2 Ag-TiO_2 photocatalyst prior to the photodegradation of DCA.

anions such as chloride. A similar yet less pronounced effect has been reported previously [21].

In Table 1, all photonic efficiency values are presented that have been calculated using (5) for each experiment. Previous reports ([21], Figure 4), concerning the photonic efficiency of the degradation of DCA in the presence of P25, are consistent with the photonic efficiency values obtained in this work. Here, the photonic efficiency was found to be between 2.83 and 3.69% at pH 3 (cf. $\zeta = 3.9\%$ at pH 3 [21]). Also, a decrease of the photonic efficiency was previously noted at pH 10 (cf. $\zeta = 0.6\%$ at pH 10 [21]). The results obtained here concerning the influence of Cl^- can be compared with a set of experiments carried out previously also [21], where the efficiency was reported to decrease from $\zeta = 3.8\%$ with the number of subsequent experiments to $\zeta = 2.0\%$ during run 3 and $\zeta = 0.9\%$ during run 6. Once again, the photonic efficiency recovered after washing of the photocatalyst (reaching $\zeta = 2.2\%$ [21]) as confirmed in the present results.

A closer inspection of the results shown in Figure 8 reveals that while at pH 10 there is no clear relationship between the observed photonic efficiency and the absence or presence of Ag on the photocatalyst, at pH 3, the fresh 0.2 Ag-TiO_2 photocatalyst slightly outperforms pure Degussa P25. For the second run, however, the situation has changed with 0.35 Ag-TiO_2 now being the best photocatalyst for the DCA degradation. Finally, in the third run all tested catalysts exhibit almost the same photocatalytic activity ($\zeta \leq 1\%$). Apparently, the Cl^- ions formed during the photocatalytic oxidation of dichloroacetate are able to completely "neutralize" any enhancement in activity induced by the Ag clusters. Based on the experimental evidence given in Figures 13 and

Table 1: Photonic efficiency values of the employed photocatalysts (e.g., as given in Figures 2 and 3).

Photocatalyst [0.5 g/L]		pH 3 Rate [mol/Lh] 1.00E-04			pH 3 Intensity [mol/Lh]	pH 3 Photonic Efficiency (%)			pH 10 Rate [mol/Lh] 1.00E-04			pH 10 Intensity [mol/Lh]	pH 10 Photonic Efficiency (%)		
		Run 1	Run 2	Run 3		Run 1	Run 2	Run 3	Run 1	Run 2	Run 3		Run 1	Run 2	Run 3
P25		9.58	3.26	2.65	3.39E-02	2.83	0.96	0.78	3.90	2.60	1.70	3.74E-02	1.04	0.70	0.45
P25-Ag%	0.1	6.00	4.30	2.60	3.39E-02	1.77	1.27	0.77	4.86	2.39	1.95	3.74E-02	1.30	0.64	0.52
	0.2	11.42	3.48	3.00	3.39E-02	3.37	1.03	0.89	2.84	1.84	1.24	3.74E-02	0.76	0.49	0.33
	0.35	8.50	6.40	3.00	3.39E-02	2.51	1.89	0.89	2.16	0.95	0.95	3.74E-02	0.58	0.25	0.25
	0.5	7.22	3.88	3.33	3.39E-02	2.13	1.15	1.98	4.20	3.20	2.59	3.74E-02	1.12	0.85	0.69
	1	5.35	3.90	3.53	3.39E-02	1.58	1.15	1.04	5.61	2.78	2.00	3.74E-02	1.50	0.74	0.53
	2	5.26	3.84	3.74	3.39E-02	1.55	1.13	1.10	3.12	2.16	1.48	3.74E-02	0.83	0.58	0.40
	0.35 (4 mM Cl)	8.03	5.45	2.35	3.39E-02	2.37	1.61	0.69							
	0.35 Washed	12.50	6.17	8.54	3.39E-02	3.69	1.82	2.52							
P25 before 3rd run (4 mM Cl)		9.32	3.14	0.75	3.39E-02	2.75	0.93	0.22							
P25 Washed		12.30	9.37	9.31	3.39E-02	3.63	2.77	2.75							
TiO_2 colloid		11.40	9.07	6.73	3.39E-02	3.37	2.68	1.99							
TiO_2 colloid before 3rd run (4 mM Cl)		11.20	8.92	6.44	3.39E-02	3.31	2.63	1.90							

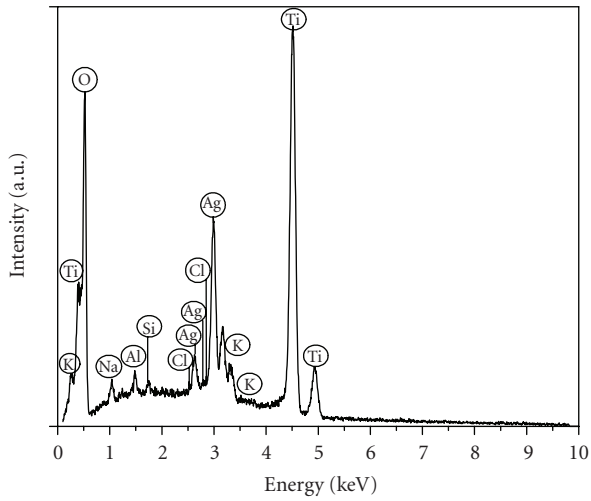

Figure 12: EDXS spectrum of 0.2 Ag-TiO_2 photocatalyst after photodegradation of DCA in three consecutive runs.

14 below, this is explained by the preferred adsorption of chloride ions at these silver clusters.

In Figure 9, a summary is provided of the results obtained for the measured TOC removal after 4 hours of illumination for the same experiments shown in Figure 8. Figure 9 shows the TOC removal measured for each run, comparing the fresh catalysts with the recycled photocatalysts after the third run. Again, the results show the decline in activity on recycling, with no particular trend with regard to the amount of silver deposited or to the reaction pH. It is clear from both, the results in Figures 8 and 9, that while there is an optimum silver loading at 0.2 atom% at pH 3, this 0.2 Ag-TiO_2 photocatalyst has no clear advantage compared to the other Ag-TiO_2 samples after recycling. Finally, it should be noted that while the initial degradation rate (used to calculate the ζ-values presented in Figure 8) seems to be rather sensitive to the presence of the Ag-clusters (at least at pH 3), there is no such dependence observed for the overall reaction yield after 4 hours of illumination (cf. Figure 9).

At pH 10, all the Ag-TiO_2 photocatalysts showed a similar performance regardless of silver content. Given that P25 TiO_2 and Ag-TiO_2 photocatalysts had a similar photoactivity after recycling, this study demonstrates that at least for the photodegradation of DCA, there was no advantage in depositing Ag on the TiO_2 surface if the intention is to recycle the photocatalyst with no intermittent washing. For practical applications, where recycling is part of a normal assumed procedure [22], this finding is of great consequence.

TEM analysis of the photocatalysts was carried out with the aim to examine if any visible morphological changes

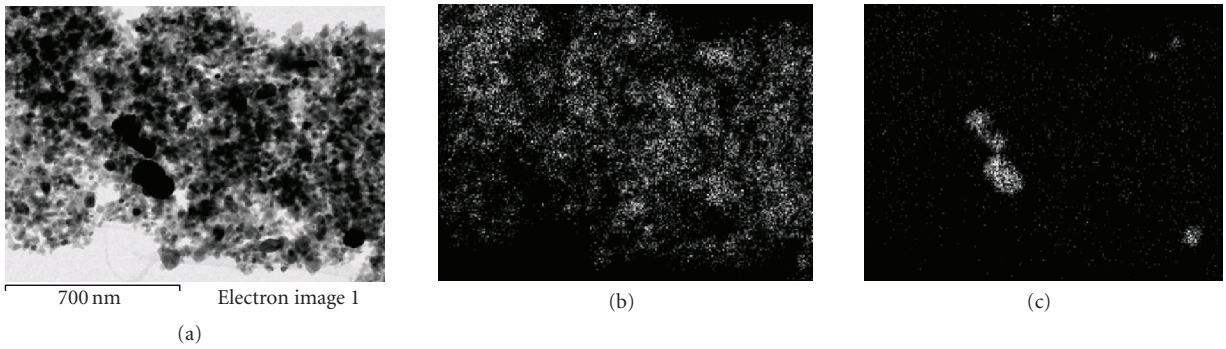

Figure 13: Electron microscopy analysis of 0.2 Ag-TiO_2 photocatalyst particles before the DCA photodegradation reaction. (a) STEM image of particles, (b) corresponding Ti X-ray map, and (c) corresponding Ag X-ray map.

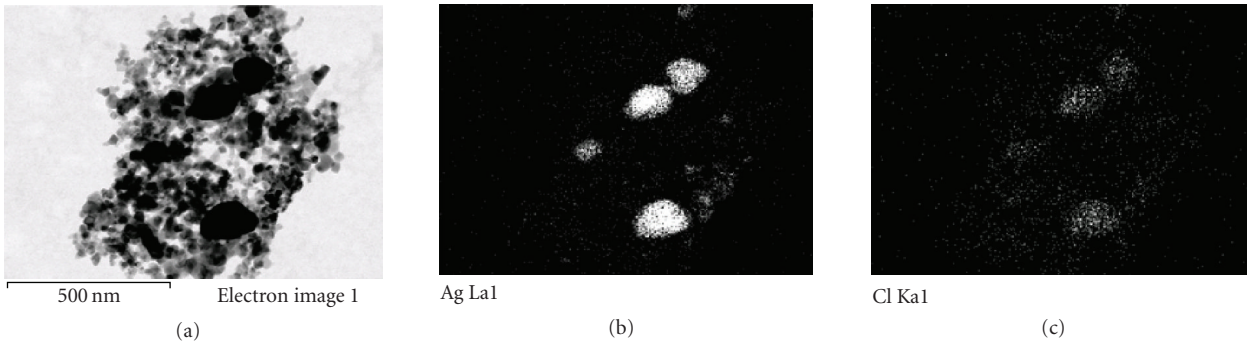

Figure 14: Electron microscopy analysis of 0.2 Ag-TiO_2 photocatalyst particles after the DCA photodegradation reaction. (a) STEM image of particles, (b) corresponding Ag X-ray map, and (c) corresponding Cl X-ray map.

had occurred to the photocatalyst samples after the second recycle. The TEM analysis was combined with an EDXS-REM from which elemental maps of Ti, Ag, and Cl were obtained to observe their distribution in the samples. As a blank comparison, Figure 10 presents an EDX spectrum of Degussa P25 before the photodeposition of silver or the photodegradation of DCA. Figure 11 shows the same sample after Ag was deposited on the surface. The results are presented for the 0.2 Ag-TiO_2 sample which showed the highest initial activity at pH 3 and the greatest decline in performance after 2 recycles. Figure 12 shows the EDX spectrum after the photodegradation of DCA in three consecutive runs. The presence of Cl^- ions detected, indicative of the poisoning of the photocatalyst surface.

In Figure 13, the STEM image and the elemental maps of Ti and Ag in the 0.2 Ag-TiO_2 are shown. These show the distinct silver deposits present in the samples. The size of the silver deposits in 0.2 Ag-TiO_2 sample is larger than that typically presented in the literature [2]. This is believed to be due to the comparatively long irradiation time of 24 hours during the photodeposition reaction. Figure 14 shows the STEM image of the same 0.2 Ag-TiO_2 photocatalyst sample after the DCA photodegradation reaction. The corresponding X-ray maps of Ag and Cl confirm the presence of the Cl^- ions and the close association of Ag with the Cl^- ions.

Based on the above electron microscopy results, it is clear that following the DCA degradation, there is a considerable amount of Cl^- ions on the photocatalysts surface.

It is believed that the chloride ions are merely physically adsorbed onto the surface of the photocatalyst rather than reacting with the silver deposits. This was supported by the fact that the photocatalysts were found to regain their activity by a simple washing procedure. When considering the preparation of the Ag-TiO_2 particles by photodeposition, the silver salt ($AgClO_4$) was added at slightly acidic pH (pH 6) and the titration to the reaction pH followed afterward. Hence at pH 10, the silver ions are expected to stay adsorbed on the surface and there will be hardly any external formation of AgOH precipitates. Similarly, at pH 3 the silver ions are expected to remain adsorbed onto the TiO_2 surface. This is believed to have minimized the reaction between Cl^- ions and Ag^+ or AgOH as the photodegradation reaction proceeded.

If, on the other hand, the titration of the titania to pH 3 or pH 10 was to be done before the silver was added, different results would have been expected. At pH 3, there would have been a lower amount of silver adsorbed onto the titania surface since both Ag^+ and the titania surface are positively charged. At pH 10, AgOH will most certainly form adjacent to the titania particles. When Cl^- anions are formed in solution, these are expected to react with the Ag^+

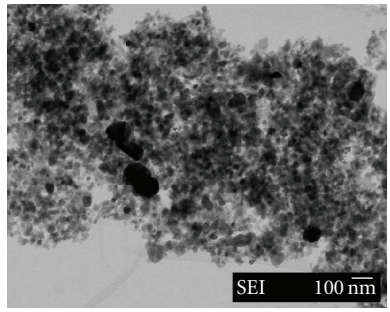

(a)

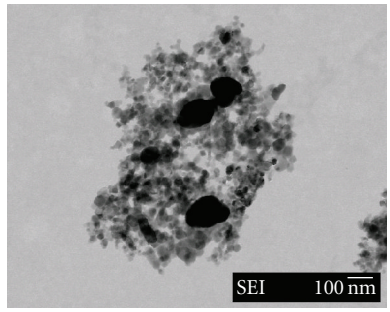

(b)

Figure 15: TEM images of 0.2 Ag-TiO_2 photocatalyst (a) before and (b) after recycle.

ions or AgOH to form the silver halides (silver chloride has a solubility of 0.8 ppm ($K_{sp}(AgCl) = 1.6 \times 10^{-10}$) which is pH independent, so most of the silver chloride would have precipitated). Upon UV exposure, the silver salts/compounds are expected to be reduced to silver atoms (as in the photographic process). This would have quite a significant impact on the photolytic formation of the silver deposits on the titania surfaces and the subsequent photocatalytic behavior of the material.

It is also often reported that small photodeposited Ag particles grow due to Oswald ripening as the photodeposition reaction proceeds. For example, at a silver loading of 0.39 wt%, after 60 seconds of irradiation, the size of the Ag deposits was 3 nm which increased as the irradiation time was doubled with some larger Ag deposits (23 nm) being formed [23]. TEM analysis was carried out on the 0.2 Ag-TiO_2 photocatalysts before and after recycling to check, if the silver deposits were in fact reforming after multiple exposures. The results presented in Figure 15 demonstrate that there was no observable change in the size of the Ag deposits. This was as expected since the preparation process allowed 24 hours of illumination for the deposition of the silver particles. As mentioned earlier, the initial Ag deposits were in fact much larger than Ag-TiO_2 photocatalysts which are typically studied. Such studies often employ much shorter irradiation times (30 minutes to few hours) [2]. For our case, the intention was to mimic real conditions which in fact can involve long periods of illumination as several pilot plant studies on photocatalysis have demonstrated [18, 22]. Hence the procedure for preparing the Ag-TiO_2 photocatalyst particles is critical in determining the nature of the Ag-TiO_2 particles that are formed and the subsequent changes and/or interactions which may occur as the photocatalytic reaction proceeds under real conditions.

4. CONCLUSIONS

In this study, it was possible to demonstrate the drop in photocatalytic activity after 3 consecutive runs for the degradation of DCA, using Ag-TiO_2 photocatalysts under both acidic and basic conditions. The aim was to test these photocatalysts under realistic process conditions which may involve photocatalyst recycle, and extended periods of illumination (up to 12 hours). Interestingly, a minimal reduction in activity was observed for high-surface area, colloidal TiO_2. This is believed to be due to the greater number of active sites in this sample which made it more resilient to poisoning by the released chloride ions during the photodegradation of DCA.

The photocatalytic activity was easily recovered by a simple washing technique, which involved the collection of the photocatalyst particles by centrifugation and their resuspension in a chloride-free solution. The reversibility of the poisoning by the chloride ions provides evidence to the assumption that the recycling of Ag-P25 TiO_2 photocatalysts (for a total 12 hours of illumination) does not have a permanent negative effect on their photocatalytic performance for the degradation of DCA. This was clearly affected by the choice of preparation procedure which minimized the interaction of the chloride ions with free Ag^+ ions or AgOH precipitates in solution, hence avoiding the formation of AgCl. The formation of AgCl in the system would have lead to complex photolytic reactions, whereby the overall performance for the photodegradation of DCA would have been difficult to predict.

ACKNOWLEDGMENTS

V. M. Meńendez-Flores thanks Deutscher Akademischer Austausch Dienst (DAAD) for their generous support of his Ph.D. Scholarship. D. Friedmann thanks the Alexander-von-Humboldt-Stiftung for a research fellowship grant supporting her work in Hannover.

REFERENCES

[1] H. Hidaka, H. Honjo, S. Horikoshi, and N. Serpone, "Photoinduced Ag_n^0 cluster deposition. Photoreduction of Ag^+ ions on a TiO_2-coated quartz crystal microbalance monitored in real time," *Sensors and Actuators B*, vol. 123, no. 2, pp. 822–828, 2007.

[2] H. Tran, J. Scott, K. Chiang, and R. Amal, "Clarifying the role of silver deposits on titania for the photocatalytic mineralisation of organic compounds," *Journal of Photochemistry and Photobiology A*, vol. 183, no. 1-2, pp. 41–52, 2006.

[3] W. Y. Teoh, L. Mädler, D. Beydoun, S. E. Pratsinis, and R. Amal, "Direct (one-step) synthesis of TiO_2 and Pt/TiO_2 nanoparticles for photocatalytic mineralisation of sucrose,"

Chemical Engineering Science, vol. 60, no. 21, pp. 5852–5861, 2005.

[4] F. Zhang, N. Guan, Y. Li, X. Zhang, J. Chen, and H. Zeng, "Control of morphology of silver clusters coated on titanium dioxide during photocatalysis," *Langmuir*, vol. 19, no. 20, pp. 8230–8234, 2003.

[5] A. V. Loginov, V. V. Gorbunova, and T. B. Boitsova, "Photochemical synthesis and properties of colloidal copper, silver and gold adsorbed on quartz," *Journal of Nanoparticle Research*, vol. 4, no. 3, pp. 193–205, 2002.

[6] B. G. Ershov, E. Janata, A. Henglein, and A. Fojtik, "Silver atoms and clusters in aqueous solution: absorption spectra and the particle growth in the absence of stabilizing Ag^+ ions," *Journal of Physical Chemistry*, vol. 97, no. 18, pp. 4589–4594, 1993.

[7] H.-J. Freund, "Clusters and islands on oxides: from catalysis via electronics and magnetism to optics," *Surface Science*, vol. 500, no. 1–3, pp. 271–299, 2002.

[8] I. M. Arabatzis, T. Stergiopoulos, M. C. Bernard, D. Labou, S. G. Neophytides, and P. Falaras, "Silver-modified titanium dioxide thin films for efficient photodegradation of methyl orange," *Applied Catalysis B*, vol. 42, no. 2, pp. 187–201, 2003.

[9] M.-W. Xu, S.-J. Bao, and X.-G. Zhang, "Enhanced photocatalytic activity of magnetic TiO_2 photocatalyst by silver deposition," *Materials Letters*, vol. 59, no. 17, pp. 2194–2198, 2005.

[10] Z. Zhang, *Size-dependent structures and properties of metallic particles and thin films*, Ph.D. dissertation, University of Notre Dame, Notre Dame, Ind, USA, December 2004.

[11] K. M. Rao, M. Pattabi, S. R. Sainkar, et al., "Preparation and characterization of silver particulate structure deposited on softened poly(4-vinylpyridine) substrates," *Journal of Physics D*, vol. 32, no. 18, pp. 2327–2336, 1999.

[12] H. Sun, Y. Y. Zhang, S. H. Si, D. R. Zhu, and Y. S. Fung, "Piezoelectric quartz crystal (PQC) with photochemically deposited nano-sized Ag particles for determining cyanide at trace levels in water," *Sensors and Actuators B*, vol. 108, no. 1-2, pp. 925–932, 2005.

[13] D. W. Bahnemann, D. Bockelmann, R. Goslich, M. Hilgendorff, and D. Weichgrebe, "Photocatalytic detoxification: novel catalysts, mechanisms and solar applications," in *Trace Metals in the Environment 3: Photocatalytic Purification and Treatment of Water and Air*, D. F. Ollis and H. Al-Ekabi, Eds., pp. 301–319, Elsevier Science, Amsterdam, The Netherlands, 1993.

[14] D. W. Bahnemann, "Ultrasmall metal oxide particles: preparation, photophysical characterization and photocatalytic properties," *Israel Journal of Chemistry*, vol. 33, pp. 115–136, 1993.

[15] D. R. Lide, *Handbook of Chemistry and Physics*, CRC Press, Boca Raton, Fla, USA, 70th edition, 1990.

[16] D. W. Bahnemann, D. Bockelmann, and R. Goslich, "Mechanistic studies of water detoxification in illuminated TiO_2 suspensions," *Solar Energy Materials*, vol. 24, no. 1–4, pp. 564–583, 1991.

[17] V. Vamathevan, *The role of silver deposits on titania in the photocatalytic oxidation of organics in aqueous media*, Ph.D. dissertation, The University of New South Wales, Sydney, Australia, 2003.

[18] D. Robert and S. Malato, "Solar photocatalysis: a clean process for water detoxification," *Science of the Total Environment*, vol. 291, no. 1–3, pp. 85–97, 2002.

[19] N. Serpone and A. Salinaro, "Terminology, relative photonic efficiencies and quantum yields in heterogeneous photocatalysis—part 1: suggested protocol," *Pure and Applied Chemistry*, vol. 71, no. 2, pp. 303–320, 1999.

[20] J. Marugán, D. Hufschmidt, G. Sagawe, V. Selzer, and D. W. Bahnemann, "Optical density and photonic efficiency of silica-supported TiO_2 photocatalysts," *Water Research*, vol. 40, no. 4, pp. 833–839, 2006.

[21] M. Lindner, D. W. Bahnemann, B. Hirthe, and W.-D. Griebler, "Solar water detoxification: novel TiO_2 powders as highly active photocatalysts," *Journal of Solar Energy Engineering*, vol. 119, no. 2, pp. 120–125, 1997.

[22] I. Muñoz, J. Peral, J. Ayllón, S. Malato, P. Passarinho, and X. Domènech, "Life cycle assessment of a coupled solar photocatalytic-biological process for wastewater treatment," *Water Research*, vol. 40, no. 19, pp. 3533–3540, 2006.

[23] S. C. Chan and M. A. Barteau, "Preparation of highly uniform Ag/TiO_2 and Au/TiO_2 supported nanoparticle catalysts by photodeposition," *Langmuir*, vol. 21, no. 12, pp. 5588–5595, 2005.

Hindawi Publishing Corporation
International Journal of Photoenergy
Volume 2008, Article ID 674537, 7 pages
doi:10.1155/2008/674537

Research Article

Novel Photocatalytic Reactor Development for Removal of Hydrocarbons from Water

Morgan Adams, Ian Campbell, and Peter K. J. Robertson

Centre for Research in Energy and the Environment, School of Engineering, The Robert Gordon University, Aberdeen AB10 1FR, UK

Correspondence should be addressed to Peter K. J. Robertson, peter.robertson@rgu.ac.uk

Received 22 July 2007; Accepted 19 August 2008

Recommended by Russell Howe

Hydrocarbons contamination of the marine environment generated by the offshore oil and gas industry is generated from a number of sources including oil contaminated drill cuttings and produced waters. The removal of hydrocarbons from both these sources is one of the most significant challenges facing this sector as it moves towards zero emissions. The application of a number of techniques which have been used to successfully destroy hydrocarbons in produced water and waste water effluents has previously been reported. This paper reports the application of semiconductor photocatalysis as a final polishing step for the removal of hydrocarbons from two waste effluent sources. Two reactor concepts were considered: a simple flat plate immobilised film unit, and a new rotating drum photocatalytic reactor. Both units proved to be effective in removing residual hydrocarbons from the effluent with the drum reactor reducing the hydrocarbon content by 90% under 10 minutes.

1. INTRODUCTION

Hydrocarbons can contaminate the aqueous environment through several routes, for example, as by-products of the oil and gas industry such as drill cuttings, or as surface run off from petrol stations and garages. Pollution resulting from hydrocarbons [1, 2] contaminating the marine environment must be addressed due to the potential toxic effects associated with these compounds can cause considerable harm to a range of targets within the environment [3–5]. Produced water presents a significant environmental problem to the oil industry internationally. In one year over 8500 tonnes of oil was discharged from oil and gas installations to the North Sea from produced water discharges [6]. This is a particular problem now as the offshore industry is moving towards zero discharges from platforms.

Drill cuttings are one of the by-products of oil exploration and recovery, with around 8000 m^3 of diesel and low toxicity oil contaminated drill cuttings deposited around the base of platforms in the North Sea [7]. Drill cuttings consist of small pieces of rock which are generated when drilling a well, which vary in size from gravel to fine silt. These cuttings are carried from down hole to the oil platform by drilling fluid which not only lubricates and cools the drill bit, but also prevents blowouts. On the platform, the cuttings are separated from the fluid with the fluid being reinjected. Most of the cuttings will also, at some point, come into contact with hydrocarbons which are difficult to remove in an environmentally friendly manner. In the past, almost all of the drill cuttings from the North Sea were dumped overboard onto the seabed.

Since the detrimental environmental impacts [8] of these cuttings were established, the government legislation has reduced the amount of drill cuttings permitted to be discharged into the sea and is moving towards banning the practice altogether [9, 10]. Consequently, the oil and gas industries have investigated alternative methods for disposing of drill cuttings. Processes that have been investigated include reinjecting the cuttings back into the well (well injection) [7] or shipping the cuttings to shore for treatment. The on-shore treatment and disposal options which include techniques such as thermal desorption, thermal distillation, solvent extraction, solidification, incineration/combustion, and landfill [11].

With thermal desorption [12], the drill cuttings are treated by heating the materials, which results in the vaporisation of water and hydrocarbons. This vapour is separated and subsequently recondensed giving an oil/water liquid and

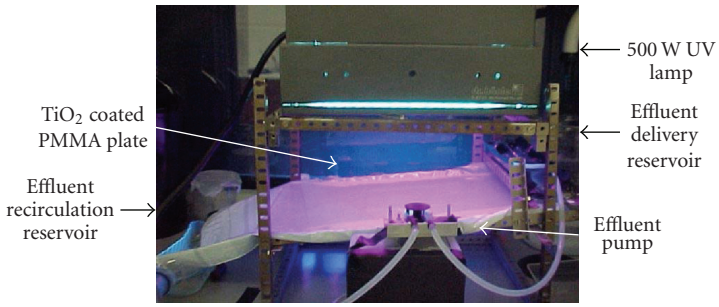

Figure 1: Prototype flat plate reactor treatment system under a UV source.

clean drill cuttings. The drill cuttings are then bagged and used for landfill whilst oil and water are separated. The recovered oil is burned in oil-fired power stations whilst the water is filtered to remove any residual hydrocarbons before being discharged into the sea. This water may still have residual hydrocarbon content.

Hydrocarbon contamination of water can also occur at the distribution stage as well as extraction. A particular example of such contamination results from "surface runoff" from Garage Forecourts. This effluent frequently contains petrol, diesel, oils, brake fluids, and also dust from brake parts and exhaust particles. The effluent is collected from drainage tanks for specialised treatment and disposal. Typically, the waste water effluent is passed through filtration systems but cannot fully remove volatile organic compounds (VOCs), and hence secondary treatment is often required.

Semiconductor photocatalysis is a rapidly developing process which may have a significant impact on the reduction and removal of these harmful and toxic compounds from produced water and waste water effluents and has even been used for potable water treatment [13–17]. This technology should be therefore a highly feasible process for the treatment of both produced waters and waste water runoff from garage forecourts. Although the use of the technology for removal of a vast range of compounds from water has been previously reported, one of the main challenges to date has been the up-scaling of the process to a size where it can practically treat large volumes of water. Many processes reported are usually treating litres per hour or even tens of litres per hour. Most practical effluent treatment processes require at least 5–10 m^3hr^{-1}, and some offshore oil and gas platforms generate up to 10^5 m^3hr^{-1}. A review by Alfano et al. [18] provides an excellent overview of many of the practical processes that have been developed for photocatalytic water treatment, particularly those utilising solar energy. In this paper, we report the development of both flat bed and drum reactor designs for the treatment of two real contaminated water samples, that is, a pretreated produced water and a waste water sample from a garage forecourt. The basic concept of these processes has been assessed and described herein.

In this paper, we describe a method of substituting the water filtration system, as an addition to the current system, to achieve very low levels of hydrocarbons in water.

2. MATERIALS AND METHODS

2.1. Multiplate thin film reactor design

There are several important parameters in the reactor design; one of the most significant of which is the active photocatalyst coating and the underlying substrate material. In addition, the coating preparation and the surface area of the catalyst available to the pollutant molecules are also crucial considerations. Two substrate materials were studied in this investigation: polymethylmethacrylate (PMMA) and titanium metal.

It is well known that certain forms of PMMA are transparent to ultraviolet radiation making the material ideally suited for an optical type chemical reactor where ultraviolet light is used to activate the photocatalyst. The other material under investigation is titanium. Although expensive, there is an important property in that when the titanium is oxidised, titanium dioxide is produced which is the photocatalyst being used in the reactor. There may also be advantages in that; there is likely to be good adhesion between the titanium and titanium dioxide.

The initial system developed for treating contaminated water was based on a thin film photocatalytic reactor. Figure 1 shows the prototype design of the photocatalytic reactor where the UV source was mounted on a support frame above the coated plate. The plate was placed on a water tight channel which had an effluent delivery tank at the head and an effluent collection reservoir at the base. The plate was mounted at an angle inducing effluent flow when introduced at the top of the unit.

The thin film plates of either PMMA or titanium were coated with TiO_2 in a 50 mL methanol suspension, containing between 200 and 250 mg of photocatalyst. This was achieved by stirring the solution for 10 minutes to obtain an evenly distributed mixture; this was then applied to the PMMA or titanium plates. The plate to be coated was placed in a shallow vessel with the TiO_2/methanol solution applied centrally, and the vessel gently tipped from side to side to produce an even coating.

In this type of unit, the plates and plate reservoirs ultimately could be jointed creating a "concertina" multiple plate reactor module for large-scale water treatment (see Figure 2).

The contaminated water sample used to assess the efficiency of this reactor was a sample of effluent taken

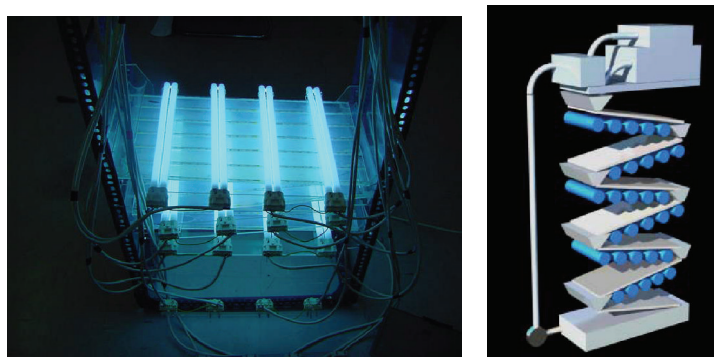

(a) (b)

Figure 2: Multiple thin film plate reactor stack (a) lab-based unit, (b) concept design for scaled-up unit.

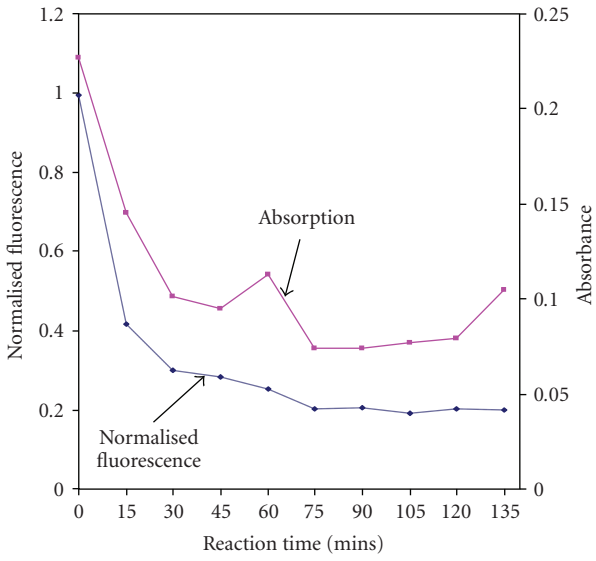

Figure 3: Demonstration of the decrease in both absorbance and fluorescence activity of produced water with reaction time.

from a thermal desorption plant used to treat drill cuttings. The water sample typically contained 100–200 ppm hydrocarbons. This is significantly higher than the permissible discharge consent level for the UK controlled waters which is currently 30 mg/L [19].

We have previously reported the use of fluorescence spectroscopy for in situ monitoring of hydrocarbons in the marine environment. As part of this study, the applicability of absorption spectroscopy as an alternative technique to fluorescence spectroscopy was assessed. Figure 3 shows the results obtained for the analysis of a produced water sample using absorption and fluorescence spectroscopy, when the sample was treated using a flat plate reactor. As can be seen from the figure for this study, a good correlation between the two techniques was obtained and hence absorption spectroscopy was used for monitoring the hydrocarbon reduction for this investigation. The analysis was performed using a Novaspec II absorption spectrometer monitoring the decrease of the broadband peaking at 335 nm.

2.2. Drum reactor design

The drum reactor was designed to be a single pass continuous flow system for produced water/effluents. If after one pass the water was still above the discharge level for hydrocarbons, the water was allowed to run into a lower reservoir. Typically, the residence time in each drum was just over 3 minutes, with a total treatment time after passing through three drum modules being around 10 minutes. If at this stage the sample was still contaminated, it was then recirculated.

The addition of hydrogen peroxide to the photocatalytic system has been previously reported to enhance photocatalytic degradation rates through the generation of additional OH radicals via the conductance band reaction with the peroxide molecule [20, 21]. This was also found to be the case for the degradation of hydrocarbons in both our systems so was introduced into the final reactor setup. The hydrogen peroxide concentration was 0.5% v/v total concentration in the effluent. This recirculation process was continued until the hydrocarbons had been removed.

The TiO_2 utilised in the reactor was a Hombikat C material supplied by Sachtleben Chemie, Duisburg, Germany. The reactor drums were irradiated using 36 W Philips PL-L sunlamp UV tubes supplied by RS Components Ltd, Northants, UK. Figures 4(a) and 4(b) show the patented photocatalytic drum reactor configuration [22]. Sampling was achieved via the open air vents at the fluid inlet side of the reactor drum.

The waste water sample was taken from an interceptor waste water collecting effluent from a Garage Forecourt. This sample contained a mixture of hydrocarbons at a total COD level of between 3500 and 4000 ppm.

The destruction of the hydrocarbons was monitored by both measuring the chemical oxygen demand of the sample and also by gas chromatography/mass spectrometry (GCMS) using a Hewlett Packard model 5890 series II GC connected to a Hewlett Packard model 5971A mass selective detector.

3. RESULTS AND DISCUSSION

3.1. Flat plate reactor

Initial experiments focused on the optimisation of the TiO_2 coating on the plate substrate were performed by preparing

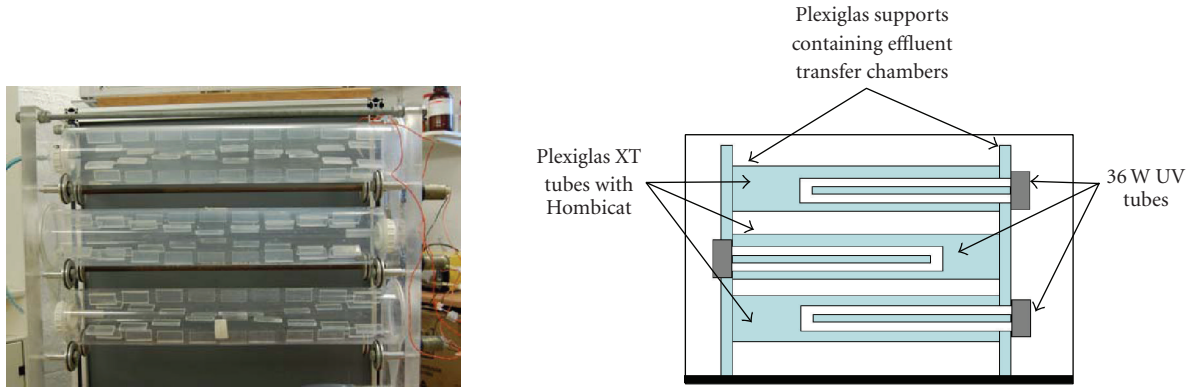

Figure 4: (a) Photocatalytic reactor drum setup with patented paddle design [20] and (b) drum reactor configuration in UV box.

different coatings using the slurry method described above. It can be seen from Figure 5 that the most effective coatings were achieved using suspensions of between 200 and 250 mg of TiO_2 (Degussa P25) in 50 mL of pure methanol followed by air drying at room temperature. Experiments were also carried out using elevated temperatures for evaporating off the methanol. As can be seen from Figure 5, the effect of catalyst loading on the system was only marginal, which would be expected in this type of unit where mass transfer kinetics would be expected to predominate [23–25].

After establishing loading parameters, the reaction rate was studied as a function of plate angle and substrate material. It can be seen from the plot that the PMMA substrate plate consistently outperformed the titanium substrate when both are coated with the optimal TiO_2 loading at a sub 15° angle. The primary reason that the shallower plate angle had greater destructive efficiency is most likely due to a greater contact time of the effluent on the catalyst plate due to the slower flow rates and hence longer residence time (see Figure 6).

To determine increase in efficiency of the reaction by the addition of an alternative electron acceptor to oxygen (air), hydrogen peroxide solution was added at an optimum initial concentration of 0.5% to the produced water sample. Figure 7 shows the results of bubbling air only through the produced water, using a combination of air and hydrogen peroxide and hydrogen peroxide only. It can be seen that a significant enhancement was obtained with the addition of the peroxide alone. In addition bubbling air through this system did not lead to any additional enhancement of the destruction of the hydrocarbons in the produced water. This supports similar observations previously reported by our own group and others [26–31] and indicates that the rate of aeration of the solution by ambient air is faster than the rate of oxygen consumption associated with the photocatalytic destruction of the hydrocarbons.

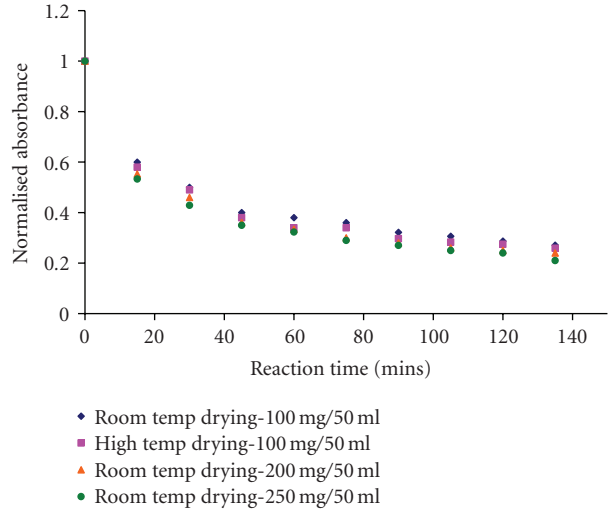

Figure 5: Comparison of TiO_2 loading and heat treatment.

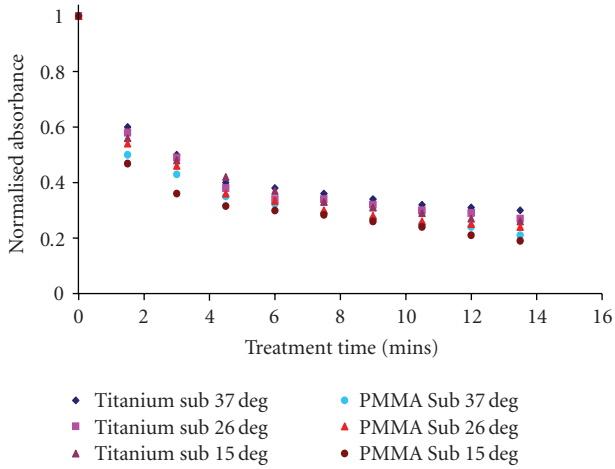

Figure 6: Comparison of substrate material with reactor plate angle at the optimum TiO_2 loading.

3.2. Drum reactor

Initial experiments using the drum reactor were configured for continuous flow effluent treatment. The photocatalyst was initially washed with distilled water to remove excess particulates TiO_2 from the surface of the pellets which

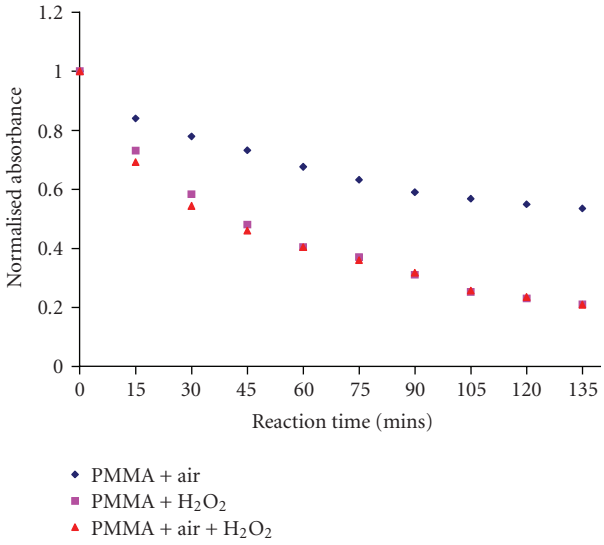

Figure 7: Effect of bubbling air and adding hydrogen peroxide on the destruction rate of produced water with the plate reactor.

Table 1: Mean COD values for pretreatment, 1st pass and 2nd pass through the drum reactor.

Sample pass	Mean COD mg/L
0 pass pretreatment	3618
1st pass through drum reactor	2166
2nd pass through drum reactor	868

could affect the photocatalytic reaction by providing a higher surface area of catalyst within the reactor drum. This would also cause secondary problems for the setup of the reactor as the excess particulates could block the effluent transfer pathways.

Figure 8 shows the GC/MS results which clearly show a 90% overall destruction over 10 minutes of VOCs present in the waste water effluent treated through a total of 600 g of the TiO_2 catalyst. This was achieved by passing the waste water effluent through three consecutive reactor drums each containing 200 g loads of photocatalyst. It can be seen that with 10 minutes and after passing through the third drum, the level of hydrocarbons in the water sample had virtually disappeared.

The chemical oxygen demand (COD) of the water samples was also measured as an indicator of the total hydrocarbon level in the untreated and treated samples. Table 1 shows the mean COD values obtained from 5 experimental runs with each point being an average of 3 samples. It can be seen that the COD value decreases very quickly during the time it takes to process through the 3 consecutive reaction drums (10-minute reaction time). As these experiments were performed on different days and the waste water effluent was decanted from a large storage drum, it is possible that the effluent content was not 100% consistent.

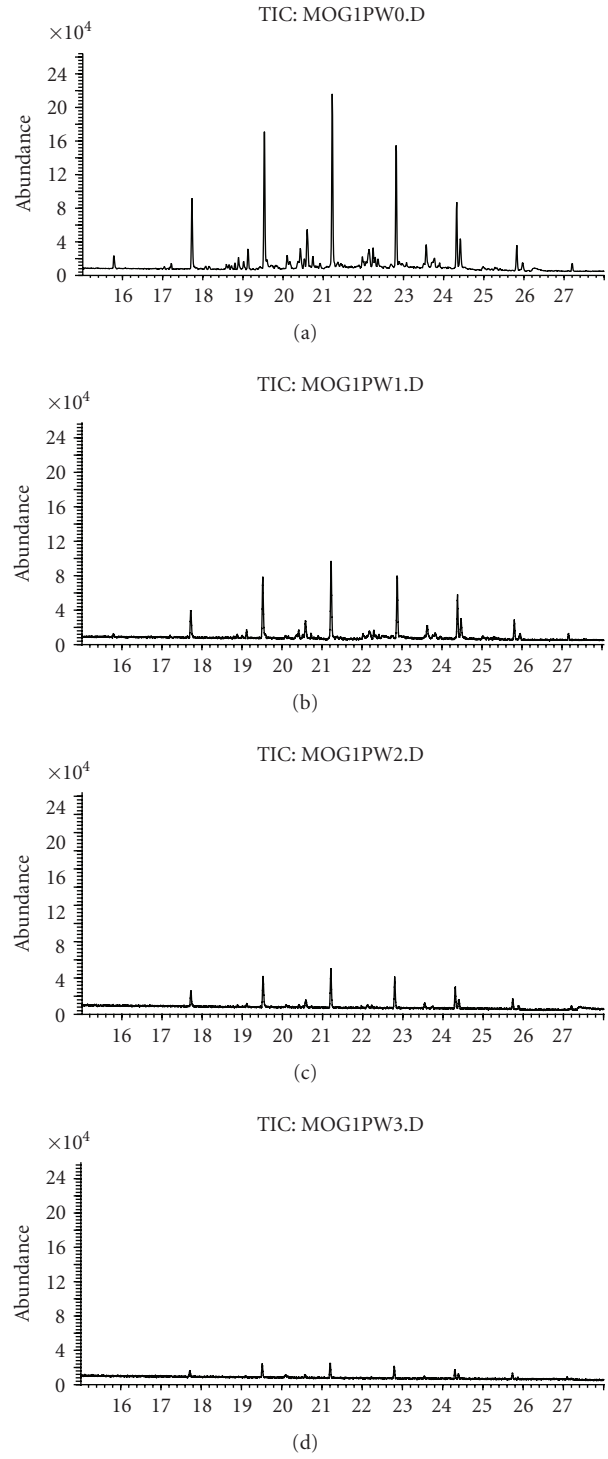

Figure 8: GC/MS chromatogram of waste water effluent, (a) pure sample with no treatment, (b) 1st pass through drum reactor, (c) 2nd pass through drum reactor, and (d) 3rd pass through drum reactor (accumulative total) catalyst treatments over a 10-minute irradiation.

4. CONCLUSION

The results of this study have demonstrated that both reactor designs proved effective for the removal of hydrocarbon

contamination from waster water effluents. With the thin film plate reactor, the assessment of PMMA and titanium metal plates as substrate materials was investigated under different conditions. By varying the mounting angle of the plates, the PMMA plate mounted at 15 degrees produced 60% destruction after 15 minutes. This demonstrated that the lower plate angle increases the retention time of the pollutant and therefore the chance of a successful catalyst–pollutant interface. An investigation into the effect of adding air and H_2O_2 to the system showed that the addition of air alone to the reactor produced 40% degradation, compared to the 80% degradation of H_2O_2, over 135 minutes.

With the development of the pelletised TiO_2, it was possible to develop an alternative reactor configuration with a smaller foot print. Conventional powder catalyst systems have traditionally posed removal problems with filtration, and settling is required to remove powder from the effluent. This limits the type of reactor design to batch, as it is impractical to provide online filtration for a continuous flow reactor system.

The drum reactor reported in this study was configured for continuous flow through 3 reactor tubes (see Figure 4(b)) each containing the same quantity of catalyst; GC/MS results showed the effective 90% removal of VOCs over 5 minutes. The mechanical mixing action of the paddle array within the reactor tubes greatly increases the pollutant-catalyst interface, enhances mass transport, and also removes the need for additional air to be added to the system. The patented paddle array also maintains an even spread of the catalyst pellet within the drum which would normally suffer from "corkscrew" effect of the turning drum. Using a standard indicator for organic compounds in water, chemical oxygen demand, the drum reactor showed an 85% reduction of organic content.

It should finally be noted that for both reactors assessed in this paper, the processes had been developed as "polishing" units and a complementary technology to existing techniques. The technique would not be viable for more heavily contaminated water samples as the kinetics of the process would require very significant reaction times and the photocatalytic process cannot compete with existing technologies, where semiconductor photocatalysis has demonstrated a particular effectiveness in such a final polishing step for removal of more resilient compounds that traditional waste water technologies are not capable of removing.

ACKNOWLEDGMENT

This project was funded under the Scottish Enterprise Proof of Concept Programme.

REFERENCES

[1] M. Russell, L. Webster, P. Walsham, et al., "The effects of oil exploration and production in the Fladen Ground: composition and concentration of hydrocarbons in sediment samples collected during 2001 and their comparison with sediment samples collected in 1989," *Marine Pollution Bulletin*, vol. 50, no. 6, pp. 638–651, 2005.

[2] K. Hylland, K.-E. Tollefsen, A. Ruus, et al., "Water column monitoring near oil installations in the North Sea 2001–2004," *Marine Pollution Bulletin*, vol. 56, no. 3, pp. 414–429, 2008.

[3] J. Zha, Z. Wang, and D. Schlenk, "Effects of pentachlorophenol on the reproduction of Japanese medaka (Oryzias latipes)," *Chemico-Biological Interactions*, vol. 161, no. 1, pp. 26–36, 2006.

[4] A. Brouwer, U. G. Ahlborg, M. Van den Berg, et al., "Functional aspects of developmental toxicity of polyhalogenated aromatic hydrocarbons in experimental animals and human infants," *European Journal of Pharmacology*, vol. 293, no. 1, pp. 1–40, 1995.

[5] C. L. Waldner, C. S. Ribble, E. D. Janzen, and J. R. Campbell, "Associations between oil- and gas-well sites, processing facilities, flaring, and beef cattle reproduction and calf mortality in western Canada," *Preventive Veterinary Medicine*, vol. 50, no. 1-2, pp. 1–17, 2001.

[6] OSPAR, "Discharges, Waste Handling and Air Emissions from Offshore Installations for 1998-1999," OSPAR Commission Report , 2001.

[7] OSPAR, "Environmental aspects of on and off-site injection of drill cuttings and produced water," OSPAR Commission Report, 2001.

[8] M. Laake, T. Bakke, and Schaanning, "Joint Study of Environmental Impact of Aquamul Cuttings and Test on Degradation and Environmental Effects of Thermal Treated Oily Cuttings under Natural Conditions," Report 2744, Norwegian Institute for Water Research, Oslo, Norway, 1992.

[9] U. Government, "Offshore Petroleum Activities (Oil Pollution Prevention and Control) Regulations," 2005.

[10] U. Government, "The Offshore Chemicals Regulations," Statutory Instrument (1355), 2002.

[11] "Technical Report—Offshore Drilling Waste Management Review," Canadian Association of Petroleum Producers 2001-0007, 2001.

[12] I. A. o. O. a. G. Producers, "E&P Forum Joint Study, Summary Report," Report 2.61/202, International Association of Oil and Gas Producers, London, UK, 1996.

[13] A. Rachel, B. Lavédrine, J.-P. Aguer, and P. Boule, "Photochemical study of 4, 4′-dinitrostilbene-2, 2′-disulfonate (DSD) degradation in water," *Journal of Photochemistry and Photobiology A*, vol. 151, no. 1–3, pp. 137–143, 2002.

[14] S. Malato, "New large solar photocatalytic plant: set-up and preliminary results," *Chemosphere*, vol. 47, no. 3, pp. 235–240, 2002.

[15] R. Dillert, A. E. Cassano, R. Goslich, and D. Bahnemann, "Large scale studies in solar catalytic wastewater treatment," *Catalysis Today*, vol. 54, no. 2-3, pp. 267–282, 1999.

[16] M. Abdullah, G. K. C. Low, and R. W. Matthews, "Effects of common inorganic anions on rates of photocatalytic oxidation of organic carbon over illuminated titanium dioxide," *Journal of Physical Chemistry*, vol. 94, no. 17, pp. 6820–6825, 1990.

[17] J. M. C. Robertson, P. K. J. Robertson, and L. A. Lawton, "A comparison of the effectiveness of TiO_2 photocatalysis and UVA photolysis for the destruction of three pathogenic micro-organisms," *Journal of Photochemistry and Photobiology A*, vol. 175, no. 1, pp. 51–56, 2005.

[18] O. M. Alfano, D. Bahnemann, A. E. Cassano, R. Dillert, and R. Goslich, "Photocatalysis in water environments using artificial and solar light," *Catalysis Today*, vol. 58, no. 2-3, pp. 199–230, 2000.

[19] https://www.og.berr.gov.uk/environment/opaoppcr.htm.

[20] S. Malato, J. Blanco, C. Richter, B. Braun, and M. I. Maldonado, "Enhancement of the rate of solar photocatalytic

mineralization of organic pollutants by inorganic oxidizing species," *Applied Catalysis B*, vol. 17, no. 4, pp. 347–356, 1998.

[21] T. Hirakawa, K. Yawata, and Y. Nosaka, "Photocatalytic reactivity for O_2^-. and OH. radical formation in anatase and rutile TiO_2 suspension as the effect of H_2O_2 addition," *Applied Catalysis A*, vol. 325, no. 1, pp. 105–111, 2007.

[22] P. K. J. Robertson, I. Campbell, and D. Russell, "Apparatus and method for treating a fluid by means of a transparent container," World Patent (WO2005033016), 2006.

[23] M. d. l. M. Ballari, R. Brandi, O. Alfano, and A. Cassano, "Mass transfer limitations in photocatalytic reactors employing titanium dioxide suspensions. I. Concentration profiles in the bulk," *Chemical Engineering Journal*, vol. 136, no. 1, pp. 50–65, 2008.

[24] M. d. l. M. Ballari, R. Brandi, O. Alfano, and A. Cassano, "Mass transfer limitations in photocatalytic reactors employing titanium dioxide suspensions. II. External and internal particle constrains for the reaction," *Chemical Engineering Journal*, vol. 136, no. 2-3, pp. 242–255, 2008.

[25] D. A. Hickman, M. Weidenbach, and D. P. Friedhoff, "A comparison of a batch recycle reactor and an integral reactor with fines for scale-up of an industrial trickle bed reactor from laboratory data," *Chemical Engineering Science*, vol. 59, no. 22-23, pp. 5425–5430, 2004.

[26] D. F. Ollis, E. Pelizzetti, and N. Serpone, "Destruction of water contaminants," *Environmental Science and Technology*, vol. 25, no. 9, pp. 1523–1529, 1991.

[27] R. W. Matthews, "Photooxidative degradation of coloured organics in water using supported catalysts. TiO_2 on sand," *Water Research*, vol. 25, no. 10, pp. 1169–1176, 1991.

[28] T. Hisanaga, K. Harada, and K. Tanaka, "Photocatalytic degradation of organochlorine compounds in suspended TiO_2," *Journal of Photochemistry and Photobiology A*, vol. 54, no. 1, pp. 113–118, 1990.

[29] V. Auguliaro, E. Davi, L. Palmisano, M. Schiavello, and A. Sclafani, "Influence of hydrogen peroxide on the kinetics of phenol photodegradation in aqueous titanium dioxide dispersion," *Applied Catalysis*, vol. 65, no. 1, pp. 101–116, 1990.

[30] B. J. P. A. Cornish, L. A. Lawton, and P. K. J. Robertson, "Hydrogen peroxide enhanced photocatalytic oxidation of microcystin-lR using titanium dioxide," *Applied Catalysis B*, vol. 25, no. 1, pp. 59–67, 2000.

[31] I. Liu, L. A. Lawton, B. Cornish, and P. K. J. Robertson, "Mechanistic and toxicity studies of the photocatalytic oxidation of microcystin-LR," *Journal of Photochemistry and Photobiology A*, vol. 148, no. 1–3, pp. 349–354, 2002.

Hindawi Publishing Corporation
International Journal of Photoenergy
Volume 2008, Article ID 197346, 7 pages
doi:10.1155/2008/197346

Research Article

Photocatalyzed Degradation of a Pesticide Derivative Glyphosate in Aqueous Suspensions of Titanium Dioxide

Mohammad Muneer[1,2] and Colin Boxall[1]

[1] *Centre for Material Science, University of Central Lancashire, Preston PR1 2HE, UK*
[2] *Department of Chemistry, Aligarh Muslim University, Aligarh-202002, India*

Correspondence should be addressed to Colin Boxall, cboxall@uclan.ac.uk

Received 24 July 2007; Revised 30 November 2007; Accepted 17 March 2008

Recommended by Russell Howe

The photocatalytic degradation of a herbicide derivative, glyphosate [(N-phosphonomethyl) glycine] has been investigated in aqueous suspensions of titanium dioxide at different pH values. This compound was found to degrade more efficiently under alkaline pH, where no adsorption takes place on the surface of the catalyst in the dark. The main degradation route involves the cleavage of the P–C bond giving rise to sarcosine and glycine as the intermediate products formed during the photooxidation process.

1. INTRODUCTION

A wide variety of organic pollutants especially pesticides are introduced into the water system from various sources such as industrial effluents, agricultural runoff, and chemical spills [1, 2]. Their toxicity, stability to natural decomposition, and persistence in the environment have been the cause of much concern to the societies and regulatory authorities around the world [3, 4].

The control of organic pollutants in water is an important measure in environmental protection. Among many processes proposed and/or being developed for the destruction of the organic contaminants, biodegradation has received the greatest attention. However, many organic chemicals, especially those that are toxic or refractory, are not amendable to microbial degradation [5]. Recently, considerable attention has been focused on the use of semiconductor photocatalysis as a means to oxidise toxic organic chemicals [6–18]. The mechanism constituting heterogeneous photocatalytic oxidation processes has been discussed extensively in the literature (see, inter alia, [19, 20]). In many of these studies, although the initial disappearance of the pollutant is rapid, a number of by products are formed which can also be potentially harmful to the environment.

The organophosphates exhibit considerable persistence in groundwaters and are highly hydrophilic. These compounds are the most prevalent pesticides and remain the choice of most farmers because of their effectiveness against large numbers of insect species. They are potent acetylcholinesterase inhibitors and are utilised to control chewing and sucking insects and spider mites on ornamental plants, citrus fruits, stone fruits, and other agriculture crops. For example, the pesticide derivative, glyphosate is a nonselective systemic herbicide that can control most annual and perennial plants [21]. It controls weeds by inhibiting the synthesis of aromatic amino acids necessary for protein formation in susceptible plants. Glyphosate is strongly adsorbed to soil particles, which prevents it from excessive leaching or from being taken up from the soil by nontarget plants [22–26]. It is degraded primarily by microbial metabolism, but strong adsorption to soil can inhibit microbial metabolism and slow degradation. The half-life of glyphosate ranges from several weeks to years, but averages are two months. In water, glyphosate is rapidly dissipated through adsorption to suspended and bottom sediments and has a half-life of 10–12 days [22–24, 27–29].

Although originally thought to be unaffected by sunlight [24], later studies found glyphosate to be susceptible to photodegradation. A half-life of 4 days in deionised water under UV light has been reported [30]. Recently, the photocatalytic degradation of glyphosate in the presence of TiO_2 has been reported by Shifu and Yunzhang [31]. However, no effort has

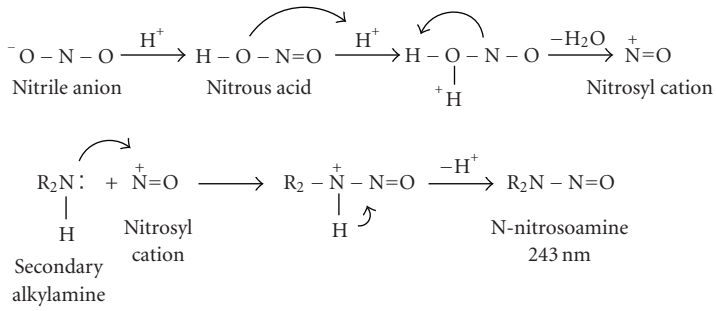

Scheme 1: Scheme showing the conversion of secondary amine to its N-nitroso derivative on treatment with nitrous acid in the presence of acid.

been made to look into the degradation products. Therefore, we have studied the degradation of glyphosate in aqueous suspension of TiO_2 with an aim to identify the products formed during the photooxidation process.

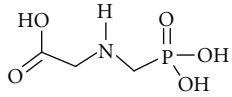

2. EXPERIMENTAL METHODS

2.1. Reagent and chemicals

Analytical grade glyphosate was obtained from Fluka and used without further purification. The water employed in this study was purified by a Millipore system. The photocatalyst titanium dioxide Degussa P25 was used in all the experiments reported here. Degussa P25 contains 75% anatase and 25% rutile with a specific BET surface area of $50\,m^2\,g^{-1}$ and a primary particle size of 20 nm [32].

2.2. Procedure

A solution of glyphosate at the desired concentration was prepared in water. For the irradiation experiments, $80\,cm^3$ of this desired solution was pipetted into a photochemical reactor. The pH of the reaction mixture was adjusted by adding a dilute aqueous solution of HNO_3 or NaOH. The photoreactor was comprised of a quartz glass reaction vessel equipped with a magnetic stirring bar, a water circulating jacket, and opening for gas supplies, placed within a bespoke circular photoirradiation system (photochemical reactors LTD Buckingham, UK) comprised of 12×15 watt Blacklight UVA lamps ($\lambda_{max} = 312$ nm), 42 cm long.

The required amount of the particulate photocatalyst was added to the glyphosate solution, and the solution was stirred in the dark for 10 minutes to allow equilibration of the system so that the loss of compound from the solution phase due to to-particle adsorption can be taken into account. The zero time reading was obtained from blank solution kept in the dark but otherwise treated similarly to the irradiated solution. Photodegradation experiments were conducted by irradiating the sample solutions with 312 nm light, the irradiated solutions being continuously purged with air throughout each experiment. Samples ($5\,cm^3$) were collected before and at regular intervals during the irradiation. These were centrifuged before being subjected to analysis.

2.3. Sample analysis

Elucidation of the mechanism and kinetics of photocatalytically driven glyphosate degradation requires a means to follow the concentration of glyphosate as a function of time. Secondary amines such as glyphosate and sarcosine are most easily determined by spectroscopic analysis of their nitro derivative. All secondary alkyl or aryl amines yield N-nitrosoamines with an absorbance at or about $\lambda = 243$ nm. Scheme 1 shows the route by which secondary amines are transformed to the N-nitroso compounds.

The procedure for both calibration measurements and the analysis of experimental samples, whether derived from dark adsorption experiments (*vide infra*) or photodegradation experiments, involves the shaking of centrifuged glyphosate adsorbed or irradiated solutions ($1\,cm^3$ of expt. sample or $1\,cm^3$ of $1 \times 10^{-3}\,mol\,dm^{-3}$calibration solution) in the presence of water ($5\,cm^3$), H_2SO_4(1 : 1, $0.5\,cm^3$), KBr (25 %, $0.1\,cm^3$), and $NaNO_2$ (0.2 N, $0.5\,cm^3$) in a $25\,cm^3$ red volumetric flask for 30 minutes followed by dilution with water to $25\,cm^3$. Absorbance was measured at 243 nm versus blank reagent containing all above reagents except glyphosate.

The product analysis was carried out using HPLC (Perkin Elmer 410 Bio) fitted with a nitrile column (cyanopropyl $5\,\mu m$). The eluent consisted of pure water; the compounds were detected employing a UV-detector at 254 nm.

3. RESULTS AND DISCUSSION

3.1. Dark adsorption of Glyphosate onto TiO_2

The possible dark adsorption of glyphosate on the surface of the photocatalyst was investigated by stirring aqueous solutions of glyphosate ($1 \times 10^{-3}\,mol\,dm^{-3}$, $35\,cm^3$) at a range of pH in the absence of illumination for 4 hours at different catalyst loadings ($2–10\,g\,dm^3$). Analysis of samples after centrifugation using the N-nitroso method (vide supra) showed that greatest adsorption occurs at lower pH values and that the extent of adsorption decreases as pH increases, as can be seen in Figure 1.

Table 1: Table showing different forms of glyphosate and the net charge on glyphosate and the surface of TiO_2 as a function of pH.

TiO_2 surface charge	Glyphosate species present	Net charge on glyphosate
	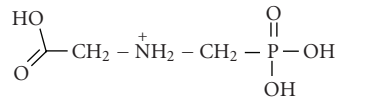	+1
	pKa = 2	
+	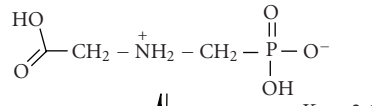	0
	pKa = 2.6	
~~	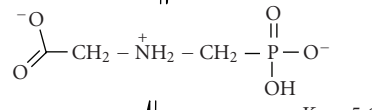	−1
	pKa = 5.6	
	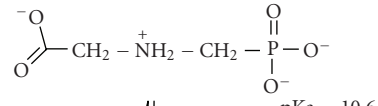	−2
−	pKa = 10.6	
	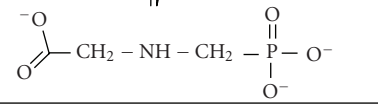	−3

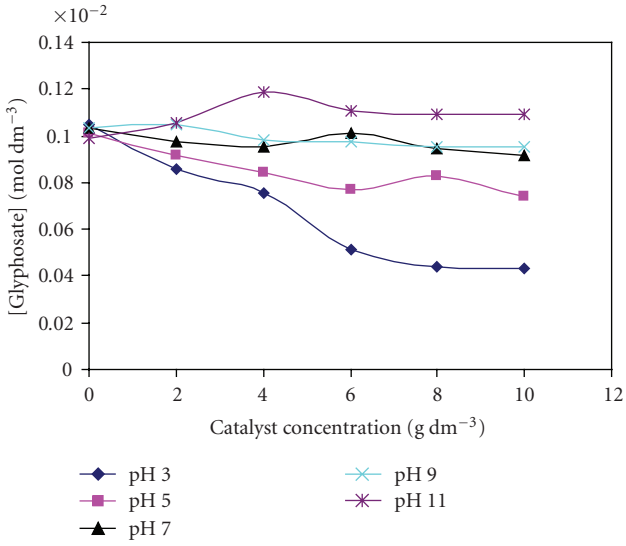

Figure 1: Glyphosate adsorption on the surface of Degussa P25 TiO_2 photocatalyst in the dark at different pH, assessed by measuring the concentration of free solution glyphosate as a function of solution loading of the catalyst.

This behaviour could be attributed to glyphosate containing three functional groups—phosphate, amino, and carboxylic—all of which can be protonated and deprotonated depending on individual functional group pKa values.

The point of zero charge (pzc) of TiO_2 (Degussa P25) is widely reported as pH ~6.25 [33]. With this in mind, Table 1 shows the ionic structure of glyphosate indicating the net charge on the molecule and TiO_2 surface as different pH values.

At low pH values (~pH 3), the TiO_2 surface will be positively charged, while the phosphate group of glyphosate will be negatively charged leading to the expectation that the compound will adsorb the surface of TiO_2. In contrast, at higher pH values, the catalyst surface as well as the compound will be negatively charged, and hence adsorption in dark would not be expected, as evident from the experimental results shown in Figure 1. The Langmuir constants at pH 3 (glyphosate uncharged, where phosphate is −1 and the TiO_2 surface has a net positive charge) and pH 5 (when glyphosate is −1 (phosphate and carboxlate are both −1) and TiO_2 is slightly positive/near neutral) have been calculated as being 88610 and 1087 $dm^3\ mol^{-1}$, respectively. At pH 7 (when glyphosate is −2 (phosphate −2, carboxylate −1) and the TiO_2 surface has a net negative charge), there is little evidence of any adsorption. Results at pH 9 and pH 11 are similar to those at pH 7. Therefore, the Langmuir adsorption pattern is congruent with that expected from columbic arguments. The magnitude of the adsorption coefficient at pH 3 compared with that at pH 5 suggests that the primary locus of adsorption is through phosphate group.

3.2. *Photocatalytic destruction of Glyphosate on TiO_2-loss of Glyphosate*

Irradiation of an aqueous suspension of glyphosate (80 cm^3, 1×10^{-3} mol dm^3) in the presence of TiO_2 (Degussa P25,

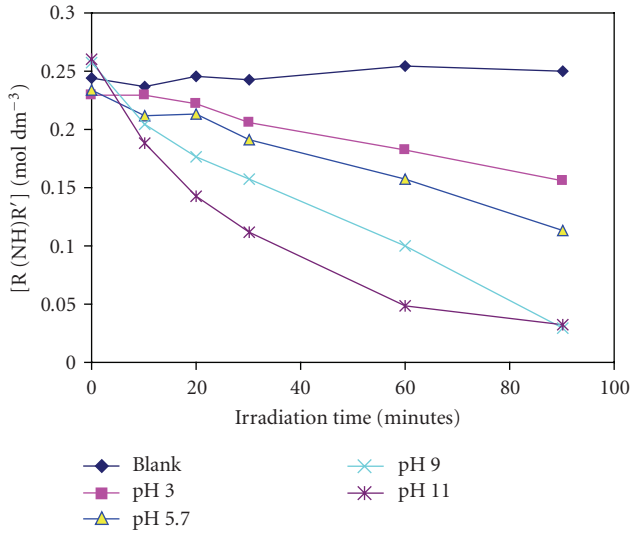

Figure 2: Photocatalytically induced loss of secondary amine functionality (measured using the N-nitroso method, see text) in glyphosate as a function of pH.

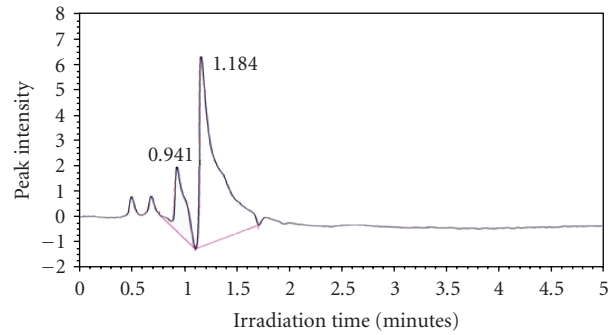

Figure 3: HPLC analysis of glyphosate in aqueous suspension of TiO_2 in the dark (zero irradiation time).

1 g dm^3) using 312 nm light in a tubular photochemical reactor with constant stirring and bubbling of air led to a decrease in glyphosate concentration as a function of time. The photodegradation was investigated at pH values 3, 5.7, 7, 9, and 11. The decrease in secondary amine concentration (as determined by the N-nitroso method, vide supra) as a function of irradiation time at different pH values is shown in Figure 2. The net loss and rate of loss of secondary amine was found to increase with the increase in pH, the highest rate being observed at pH 11. Further, for data recorded at pH 3 and pH 5.7, there appears to be an induction period during which no loss of secondary amine is observed for a time immediately after the onset of illumination. We will return to this point below.

3.3. Photocatalytic destruction of Glyphosate on TiO_2-product analysis

Figure 3 shows the HPLC trace of an aqueous suspension of glyphosate and TiO_2 at zero time irradiation indicating a strong peak at retention time R_t = 1.184 minutes and a medium peak at R_t = 0.941 minute. Irradiation of the

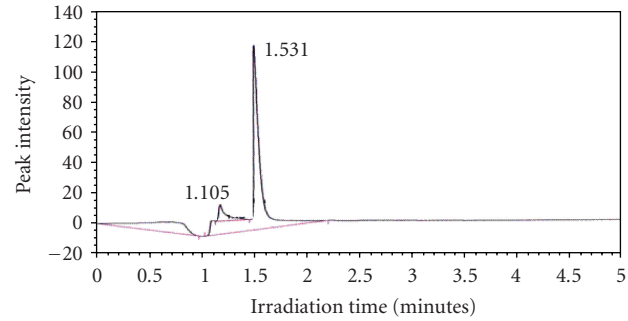

Figure 4: HPLC analysis of authentic sarcosine in aqueous solution.

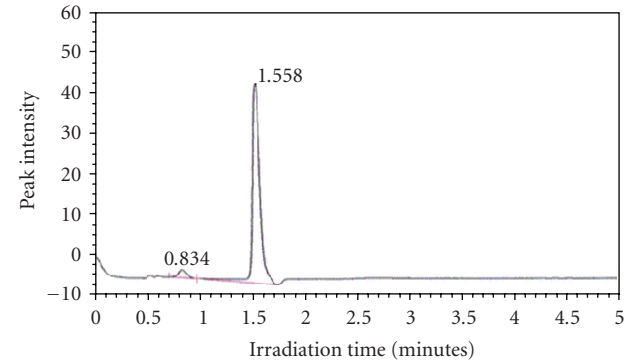

Figure 5: HPLC analysis of authentic glycine in aqueous solution.

solution for 90 minutes at pH 2 led to the formation of a product which is indicated by appearance of a strong peak at R_t = 1.651 minutes and a shoulder at R_t = 1.599 minutes in addition to the unchanged starting material (see Table 2). Said product exhibited an HPLC retention time and peak shape typical of a carboxylic acid (determined through comparison with HPLC analysis of methanoic and ethanoic acids on same instrument, not shown). However, during this period, no concomitant loss of secondary amine was observed leading us to conclude that the C–P bond had been broken in the formation of this product and that the product itself was most likely the amino acid sarcosine-N-methyl-2-aminoethanoic acid. The HPLC trace of authentic sarcosine is shown in Figure 4.

Primary product assignment was confirmed by adding authentic sarcosine to the photodegraded reaction mixture. Peaks in the HPLC trace recorded from this degraded sample/authentic sarcosine mix were found to be coincident with peaks in the HPLC trace recorded from the degraded reaction mixture alone (compare sample row 5 with sample row 4 in Table 2).

At longer times, both the concentration of secondary amine as determined by the N-nitroso method and the area of the peak at R_t = 1.523 minutes, associated with the secondary amine sarcosine, were seen to decrease with illumination time. The latter was accompanied by the concomitant formation of a second product peak at R_t = 1.56 minutes, in the vicinity of but not coincident with the sarcosine peak in the HPLC trace. Again, by addition of

Table 2: Table showing HPLC peaks retention times, R_t, for glyphosate, sarcosine, glycine (sample rows 1–3, resp.), irradiated mixtures of glyphosate at pH 3 and pH 11 (sample rows 4 and 6, resp.), and irradiated mixtures of glyphosate at pH 3 and pH 11 with authentic samples of sarcosine and glycine (sample rows 5 and 7, resp.). Peaks associated with glyphosate, sarcosine, and glycine are shown as **bold**, underlined, and double underlined text, respectively.

Sample	HPLC peak retention time (R_t)/minutes
1. Glyphosate (from Figure 3)	**0.941** (min), **1.184** (s)
2. Sarcosine (from Figure 4)	1.105 (w), 1.531 (s)
3. Glycine (from Figure 5)	0.834 (w),1.558 (s)
4. Glyphosate, 90 min Irradiation, pH3	**0.948** (min), 1.061 (min), **1.13** (s), 1.599 (min), 1.651 (s)
5. Glyphosate (90 min irradiation, pH3) + authentic Sarcocine	**0.948** (min), 1.039 (min), **1.117** (s), 1.523 (min), 1.651 (s),
6. Glyphosate (60 min irradiation, pH 11)	**1.161** (s), 1.548 (min), 1.662 (min)
7. Glyphosate (60 min irradiation, pH 11) + authentic Glycine	**1.108** (s), 1.543 (min), 1.665 (min)

s-strong, m-medium, w-weak.

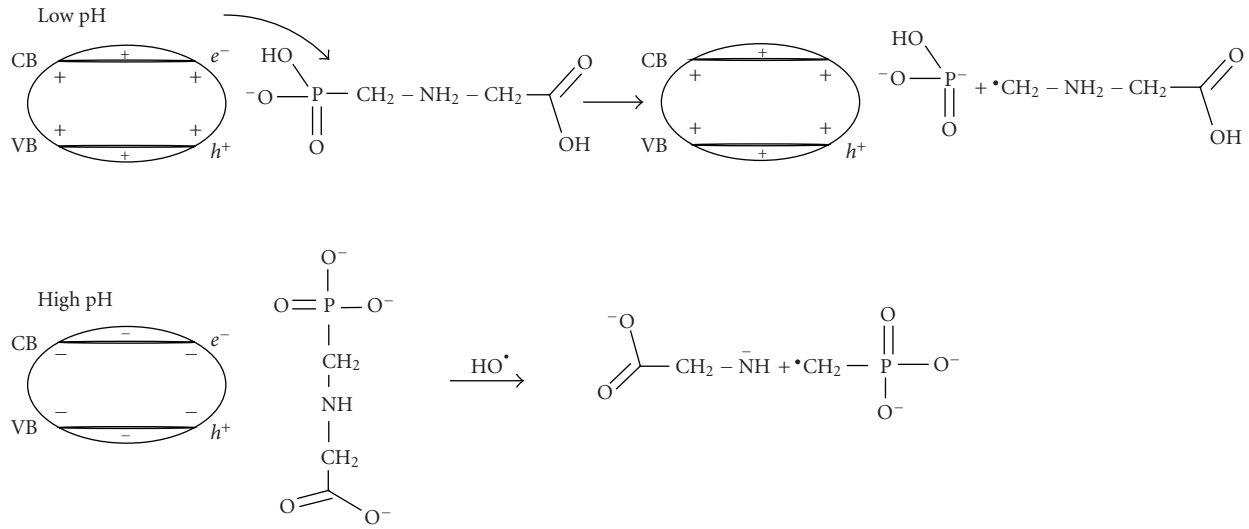

Figure 6: The interaction of glyphosate with the surface of TiO_2 in dark and the subsequent interaction of photogenerated electrons and hydroxyl radicals with glyphosate upon illumination of the TiO_2 with ultraband gap irradiation.

authentic material to photodegraded reaction mixtures, this second product was identified as glycine—2-aminoethanoic acid. The HPLC trace of authentic glycine is shown in Figure 5.

HPLC analysis of photodegraded reaction mixtures at pH 11 also indicates the formation of product (R_t = 1.548 and 1.662 minutes) in the vicinity of but not coincident with the sarcosine peak in the HPLC trace. No sarcosine peak was observed at any irradiation time at this pH. Following the methodology employed at pH 3, HPLC analyses of the photodegraded reaction mixture and samples of authentic materials shows that the primary reaction product is glycine (compare sample row 7 with sample row 6 in Table 2 and note coincidence of peaks at R_t = 1.548 minutes). This is most likely derived from C–N bond cleavage in nonadsorbed glyphosate (Figure 6).

The N-nitroso-based secondary amine analysis of Figure 2 indicates that at low pH, secondary amine is retained but glyphosate is lost due to loss of phosphate group and appearance of a peak in the carboxylic acid region of the HPLC trace. In conjunction with the product identification and the fact that adsorption occurs at low pH, the results suggest that at low pH the photocatalytic reaction is most likely initiated by from-particle electron transfer. In contrast, under alkaline pH where little adsorption is seen to occur (Figure 1) solution-phase hydroxyl radical attack plays an important role, said hydroxide radicals having been generated in the reaction medium by photogenerated holes.

Figure 6 provides a schematic summary of these processes, wherein it is assumed that, at low pH, the photogenerated electron on irradiated TiO_2 attacks through -phosphate-adsorbed-glyphosate leading to the formation of carbon centered radical which then reacts to form nonadsorbed sarcosine. Readsorption of sarcosine onto the positively charged TiO_2 surface is then inhibited by the anticipated net positive charge on the molecule, arising from the protonation of the secondary amino nitrogen at this pH. At high pH, photoelectrochemically generated hydroxyl radicals attack nonadsorbed glyphosate, causing C–N bond fracture and ultimately forming glycine. It is pertinent to

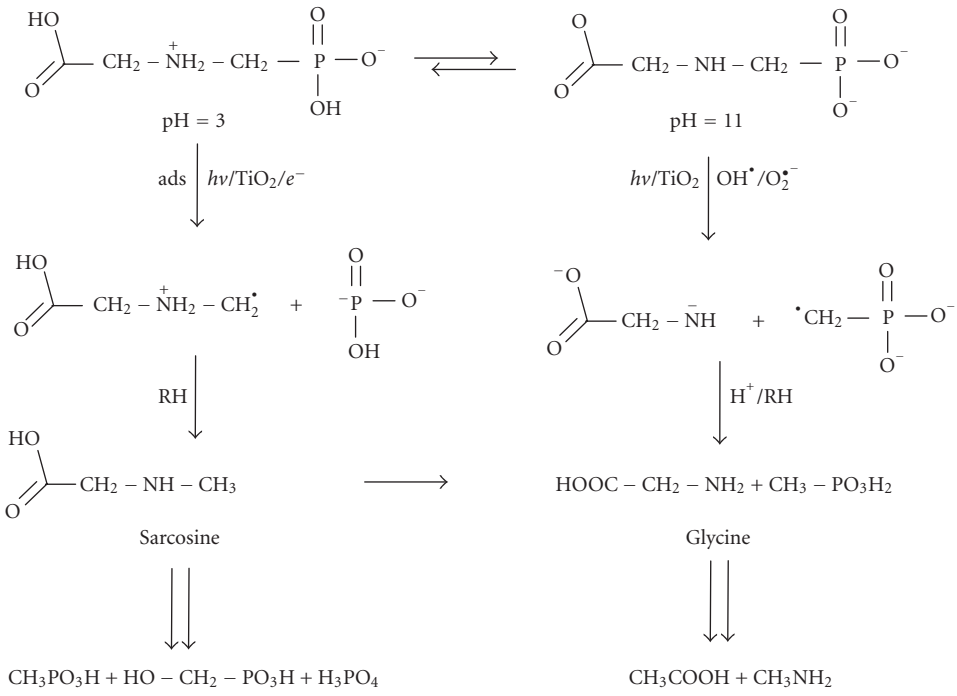

Scheme 2: Scheme showing the probable route for the degradation of glyphosate on irradiated TiO_2 at low and high pH.

mention here that photocatalysed degradation of glycine has a well-known mechanism and has been reported earlier [34]. Returning to pH 3, it can now be seen that sarcosine which is not adsorbed at the TiO_2 surface due to the loss of the phosphate group is then susceptible to similar solution-phase OH radical attack as nonadsorbed glyphosate at pH 11, so generating the same product, glycine. A mechanism consistent with these observations is shown in Scheme 2.

4. CONCLUSIONS

The pesticide derivative glyphosate has been found to degrade efficiently under alkaline conditions. Under acid conditions, it exhibits a strong, primarily coulombically driven dark adsorption onto the surface of the TiO_2 photocatalyst. Again, under acid conditions, the compound has been found to undergo efficiently photocatalytically promoted P–C bond cleavage leading to the formation of sarcosine and glycine like the main intermediate products. A probable degradation route involving a direct interfacial electron transfer reaction at low pH and hydroxyl radical /superoxide radical anion-mediated solution-phase oxidation at high pH on irradiated semiconductor particles has been proposed.

ACKNOWLEDGMENTS

Financial support from European Commission (Contract no. Mesocat 514289) and the award of a Marie Curie Incoming International Fellowship to Mohammad Muneer. are gratefully acknowledged.

REFERENCES

[1] Z. Z. Cohen, C. Eiden, and M. N. Lober, "Monitoring ground water for pesticides," in *Evaluation of Pesticides in Ground Water*, W. Y. Gernar, Ed., ACS Symposium Series 315, pp. 170–196, Washington, DC, USA, American Chemical Society, 1986.

[2] L. Muszkat, D. Raucher, M. Mogaritz, and D. Ronen, "Groundwater contamination by organic pollutants," in *Groundwater Contamination and Control*, pp. 257–272, Marcel Dekker, New York, NY, USA, 1994.

[3] J. A. Graham, "Monitoring groundwater and well water for crop protection chemicals," *Analytical Chemistry*, vol. 63, no. 11, pp. 631–622, 1991.

[4] R. M. Dowd, M. P. Anderson, and M. L. Johnson, "Ground water monitoring and geophysical method," in *Proceedings of the 2nd National Outdoor Action Conference on Aquifer Restoration, Ground Water Monitoring and Geophysical Methods*, pp. 1365–1379, National Water Well Association, Dublin, Ohio, USA, May 1988.

[5] J. Mönig, D. W. Bahnemann, and K.-D. Asmus, "One electron reduction of CCl_4 in oxygenated aqueous solutions: a $CCl_3O_2^{\bullet}$-free radical mediated formation of Cl^- and CO_2," *Chemico-Biological Interactions*, vol. 47, no. 1, pp. 15–27, 1983.

[6] D. M. Blake, "Bibliography of work on the photocatalytic removal of hazardous compounds from water and air," Tech. Rep. NREL/TP-510-31319, National Renewal Energy Laboratory, Cole Boulevard Golden, Colo, USA, 2001.

[7] M. Abu Tariq, M. Faisal, M. Muneer, and D. W. Bahnemann, "Photochemical reactions of a few selected pesticide derivatives and other priority organic pollutants in aqueous suspensions of titanium dioxide," *Journal of Molecular Catalysis A*, vol. 265, no. 1-2, pp. 231–236, 2007.

[8] D. W. Bahnemann, M. Muneer, and M. M. Haque, "Titanium dioxide-mediated photocatalysed degradation of few selected

organic pollutants in aqueous suspensions," *Catalysis Today*, vol. 124, no. 3-4, pp. 133–148, 2007.

[9] N. N. Rao and S. Dube, "Photocatalytic degradation of mixed surfactants and some commercial soap/detergent products using suspended TiO_2 catalysts," *Journal of Molecular Catalysis A*, vol. 104, no. 3, pp. L197–L199, 1996.

[10] I.-W. Huang, C.-S. Hong, and B. Bush, "Photocatalytic degradation of PCBs in TiO_2 aqueous suspensions," *Chemosphere*, vol. 32, no. 9, pp. 1869–1881, 1996.

[11] M. M. Haque, M. Muneer, and D. W. Bahnemann, "Semiconductor-mediated photocatalyzed degradation of a herbicide derivative, chlorotoluron, in aqueous suspensions," *Environmental Science & Technology*, vol. 40, no. 15, pp. 4766–4770, 2006.

[12] J. Blanco-Galvez, P. Fernández-Ibáñez, and S. Malato-Rodríguez, "Solar photocatalytic detoxification and disinfection of water: recent overview," *Journal of Solar Energy Engineering*, vol. 129, no. 1, pp. 4–15, 2007.

[13] K. Tanaka, S. M. Robledo, T. Hisanaga, R. Ali, Z. Ramli, and W. A. Bakar, "Photocatalytic degradation of 3,4-xylyl *N*-methylcarbamate (MPMC) and other carbamate pesticides in aqueous TiO_2 suspensions," *Journal of Molecular Catalysis A*, vol. 144, no. 3, pp. 425–430, 1999.

[14] J. Lobedank, E. Bellmann, and J. Bendig, "Sensitized photocatalytic oxidation of herbicides using natural sunlight," *Journal of Photochemistry and Photobiology A*, vol. 108, no. 1, pp. 89–93, 1997.

[15] K. Vinodgopal, D. E. Wynkoop, and P. V. Kamat, "Environmental photochemistry on semiconductor surfaces: photosensitized degradation of a textile azo dye, acid orange 7, on TiO_2 particles using visible light," *Environmental Science & Technology*, vol. 30, no. 5, pp. 1660–1666, 1996.

[16] I. Liu, L. A. Lawton, B. Cornish, and P. K. I. Robertson, "Mechanistic and toxicity studies of the photocatalytic oxidation of microcystin-LR," *Journal of Photochemistry and Photobiology A*, vol. 148, no. 1–3, pp. 349–354, 2002.

[17] R. Borello, C. Minero, E. Pramauro, E. Pelizzetti, N. Serpone, and H. Hidaka, "Photocatalytic degradation of DDT mediated in aqueous semiconductor slurries by simulated sunlight," *Environmental Toxicology and Chemistry*, vol. 8, no. 11, pp. 997–1002, 1989.

[18] J.-M. Herrmann, "Heterogeneous photocatalysis: fundamentals and applications to the removal of various types of aqueous pollutants," *Catalysis Today*, vol. 53, no. 1, pp. 115–129, 1999.

[19] C. S. Turchi and D. F. Ollis, "Photocatalytic degradation of organic water contaminants: mechanisms involving hydroxyl radical attack," *Journal of Catalysis*, vol. 122, no. 1, pp. 178–192, 1990.

[20] R. W. Matthews and S. R. McEvoy, "Photocatalytic degradation of phenol in the presence of near-UV illuminated titanium dioxide," *Journal of Photochemistry and Photobiology A*, vol. 64, no. 2, pp. 231–246, 1992.

[21] J. E. Franz, M. K. Mao, and J. A. Sikorski, *Glyphosate: A Unique Global Herbicide*, chapter 4, American Chemical Society, Washington, DC, USA, 1997.

[22] P. Sprankle, W. F. Meggitt, and D. Penner, "Rapid inactivation of glyphosate in the soil," *Weed Science*, vol. 23, no. 3, pp. 224–228, 1975.

[23] P. Sprankle, W. F. Meggitt, and D. Penner, "Adsorption, mobility and microbial degradation of glyphosate in the soil," *Weed Science*, vol. 23, no. 3, pp. 229–234, 1975.

[24] M. L. Rueppel, B. B. Brightwell, J. Schaefer, and J. T. Marvel, "Metabolism and degradation of glyphosate in soil and water," *Journal of Agricultural Food Chemisry*, vol. 25, no. 3, pp. 517–528, 1977.

[25] R. L. Glass, "Adsorption of glyphosate by soils and clay minerals," *Journal of Agricultural Food Chemistry*, vol. 35, no. 4, pp. 497–500, 1987.

[26] D. N. Roy, S. K. Konar, S. Banerjee, D. A. Charles, D. G. Thompson, and R. Prasad, "Persistence, movement, and degradation of glyphosate in selected Canadian boreal forest soils," *Journal of Agricultural Food Chemistry*, vol. 37, no. 2, pp. 437–440, 1989.

[27] N. S. Normura and H. W. Hilton, "The adsorption and degradation of glyphosate in five Hawaiian sugarcane soils," *Weed Research*, vol. 17, no. 2, pp. 113–121, 1977.

[28] J. Malik, G. Barry, and G. kishore, "The herbicide glyphosate," *BioFactors*, vol. 2, no. 1, pp. 17–25, 1989.

[29] S. M. Carlisle and J. T. Trevorrs, "Glyphosate in the environment," *Water, Air, & Soil Pollution*, vol. 39, no. 3-4, pp. 409–420, 1988.

[30] K. Lund-Høie and H. O. Friestad, "Photodegradation of the herbicide glyphosate in water," *Bulletin of Environmental Contamination and Toxicology*, vol. 36, no. 1, pp. 723–729, 1986.

[31] C. Shifu and L. Yunzhang, "Study on the photocatalytic degradation of glyphosate by TiO_2 photocatalyst," *Chemosphere*, vol. 67, no. 5, pp. 1010–1017, 2007.

[32] "Highly Dispersed Metallic Oxides Produced by the AEROSIL® Process," *Degussa Technical Bulletin*, no. 56, p. 8, 1984.

[33] R. I. Bickley, T. Gonzalez-Carreno, J. S. Lees, L. Palmisano, and R. J. D. Tilley, "A structural investigation of titanium dioxide photocatalysts," *Journal of Solid Sate Chemistry*, vol. 92, no. 1, pp. 178–190, 1997.

[34] S. Horikoshi, N. Serpone, J. Zhao, and H. Hidako, "Towards a better understanding of the initial steps in the photocatalyzed mineralization of amino acids at the titania/water interface. An experimental and theoretical examination of L-alanine, L-serine and L-phenylalanine," *Journal of Photochemistry and Photobiology A*, vol. 118, no. 2, pp. 123–129, 1998.

Hindawi Publishing Corporation
International Journal of Photoenergy
Volume 2008, Article ID 205358, 11 pages
doi:10.1155/2008/205358

Research Article

TiO_2 Nanoparticles-Photocatalytic Oxidation of Selected Cycloalkanols

Omima S. Mohamed, Saleh A. Ahmed, Mostafa F. Mostafa, and Aboel-Magd A. Abdel-Wahab

Chemistry Department, Faculty of Science, Assiut University, Assiut 71516, Egypt

Correspondence should be addressed to Aboel-Magd A. Abdel-Wahab, wahab_47@hotmail.com

Received 26 July 2007; Accepted 20 December 2007

Recommended by Russell Howe

Photocatalytic oxidation of cyclohexanol (**1**), cyclopentanol (**2**), and cycloheptanol (**3**) was investigated by using titanium dioxide (Degussa P25) as a semiconductor photocatalyst .The effect of different operational parameters such as the catalyst, the solvent, time, and oxidant was also studied. Results showed a high percentage of conversion for **1**–**3** (71.6%, 94.2%, and 100%, resp.) and that the primary photocatalytic oxidation products are the corresponding cycloalkanones (**4**–**6**). They were formed with high selectivity (>85%). Several other products were also identified using GC, GC/MS techniques and authentic samples. The photocatalytic activity is explained by a photoinduced electron transfer mechanism through the formation of electron-hole pair at the surface of the semiconductor particles. A first-order kinetic model was observed for the photocatalytic oxidation of the investigated cycloalkanols.

1. INTRODUCTION

Photocatalysis represents one of the promising technologies for photoenergy conversion started with the pioneer findings of Fujishima and Honda [1]. Its applications in water recycling, air-pollution treatment, as well as in organic synthesis have found a great interest [2–6].

There are many studies focused on the photocatalytic oxidation and degradation of several classes of organic compounds catalyzed by TiO_2 semiconductor particulates [7–13].

Photocatalytic oxidation and degradation of alcohols catalyzed by TiO_2 and other semiconductor particulates have found some interest. For example, Harvey et al. [14] studied photocatalytic oxidation of liquid propan-2-ol to propanone using suspensions of titanium dioxide irradiated with filtered UV radiation. The dependence of reaction rate on the square root of the intensity of the incident radiation, together with low quantum yields, reflects the dominance of photoelectron and photohole recombination within the TiO_2. Cameron and Bocarsly [15] studied the photocatalytic oxidation of ethanol, benzyl alcohol, cinnamyl alcohol, n-hexyl alcohol, isopropyl alcohol, cyclopentanol, and cyclohexanol which converted to the corresponding aldehyde or ketone by using oxygen gas and visible light 488 nm (85 mW) illumination from an Ar laser. The process was catalyzed by the presence of H_2PtCl_6 and $CuCl_2$.

Nishimoto et al. [16] studied the photocatalytic dehydrogenation of aliphatic alcohols by aqueous suspensions of platinized titanium dioxide, photoirradiation ($\lambda_{ex} > 300$ nm) of Ar-purged aqueous propan-2-ol solution gave hydrogen and acetone. The regioselectivity in the semiconductor-mediated photooxidation of 1,4-pentanediol was studied in 1989 by Fox et al. [17].

We also studied the photocatalytic oxidation of selected aryl alcohols [18, 19]. The main oxidation products were the corresponding aldehydes or ketones and acids. Kinetic studies revealed a second-order reaction rate for benzyl alcohol as a model alcohol. Also photocatalytic oxidation of fluoren-9-ol and 4,5-diazafluoren-9-ol in nonaqueous oxygen saturated TiO_2 suspension to the corresponding ketones was formed in a high yield, in addition to minor amount of the corresponding hydrocarbon and other decomposition products. Interestingly, photocatalytic oxidation of the parent fluorene afforded fluorenone under the same conditions. Similarly, Phenyl-4-pyridylmethanolas an acyclic

simulant gave the corresponding ketone and hydrocarbon. Furthermore, the effect of solvent polarity has been tested [18, 19].

Pillai and Salhe-Demessie [20] studied the selective oxidation of primary and secondaryaliphatic alcohols to their corresponding carbonyl compounds in gas phase. In 2006, Wu et al. [21] studied the long-term photocatalytic stability of Co^{2+}-modified P25-TiO_2 powders for the H_2 production from aqueous ethanol solution. In this paper, the long-term stability of photocatalytic activity of Co^{2+} doped P25-TiO_2 nanoparticles for hydrogen production from aqueous ethanol solution was discussed in detail using a photoelectrochemical method.

It is clear from the previous survey that the effect of ring size and conditions on the photocatalytic oxidations of secondary cycloalkanols has not been tackled. So, this study will be of great interest.

2. EXPERIMENTAL

2.1. Materials

Titanium dioxide P25 (Degussa-Hűs AG, powder) was dried at 120°C for 24 hrs before use, these particles are composed mostly of anatase with surface area of 37.7 m^2g^{-1}, average particle size 21 nm, and pore diameter 31.0. Oxygen was dried by passage through a drying calcium chloride tube. Acetonitrile and acetone (Sigma Aldrich, St. Louis, USA, HPLC grade) were distilled before use. Hydrogen peroxide was 30% (v/v). Cyclohexanol (**1**), cyclopentanol (**2**) and cycloheptanol (**3**) were purchased from Aldrich chemical company and were distilled before use. The authentic samples cyclohexanone (**4**), cyclopentanone (**5**), cycloheptanone (**6**), and 1,4-cyclohexadione (**7**) were obtained from Aldrich, whereas cyclohexyl formate (**8**) [22], 2-cyclohexenone (**9**) [23], 2-hydroxycyclohexanone (**10**) [24], n-hexanoic acid (**11**) [25], cyclohexyl hexanoate (**12**) [22], n-pentanoic acid (**13**) [22, 26], cyclopentyl pentanoate (**14**) [22], and n-heptanoic acid (**15**) [27] were synthesized as described in literatures. All the prepared authentic samples were analyzed by IR, ^{1}H-NMR, GC, and GC/MS analyses as synthetic mixture.

2.2. Apparatus

A 450 W medium pressure mercury lamp (ACE glass, immersion type) with a pyrex well was used as the light source, which has a maximum emission range 296.7–578 nm (4.18 − 2.15 eV). The system was covered with aluminum foil which served as light reflector to decrease light loss and the apparatus was set up in a metallic cabinet. The distance between sample and irradiation source was 5 cm.

IR spectra were recorded using IR-470, IR spectrophotometer-Shimadzu using thin film and NaCl disks. The electronic absorption spectra were recorded using UV-2101 PC, UV-VIS scanning spectrophotometer-Shimadzu. ^{1}H-NMR spectra were carried out using 90 MHz Varian 390 in $CDCl_3$ and TMS as an internal standard. GC analyses were performed employing Perkin Elmer, Autosystem XLGC using capillary column (5% diphenyl–95% dimethyl polysiloxane), length 30 m, internal diameter 0.32 mm, film thickness 0.25 μm. The initial temperature of column is 40°C and the final temperature is 280°C, the rate of heating is 20°C/min. The injector temperature is 300°C and the detector used is a flame ionization detector at 250°C. GC/MS analysis were carried out using GC model: GC 2000 thermo, capillary column DB-5 (5% phenyl–95% methyl polysiloxane, L. 30 m, I.D. 0.25 mm, F.T. 0.25 μm, temperature of column from 50°C to 300°C, 10°C/min. and injector temperature 250°C), attached with mass spectrometer: model SSQ 7000 produced by Finnigan. All melting points were determined on a Gallen-Kamp melting point apparatus.

2.3. General procedure

A 75 ml (0.1 M) solution of the investigated cycloalkanols (**1–3**) was prepared in the used solvent, 75 mg of titanium dioxide (P25 Degussa-Hűs AG) was added to the solution, the mixture was transferred to the reaction vessel and sonicated in an ultrasonic bath for 15 minutes. The stirred suspension was bubbled with a stream of oxygen gas at a flow rate (30 ml/min) and then illuminated for 20 hours using 450 W medium pressure mercury lamp.The reaction progress was monitored by GC. After irradiation, the titanium dioxide powder was removed by filtration using a medium porosity frit and the solvent was evaporated by using rotatory evaporator. The reaction mixture was analyzed by using GC and GC/MS techniques, and then the products were identified and estimated with convincing match qualities compared with the standard mass spectra in the mass spectral libraries and with their retention time matched with authentic samples.

3. RESULTS AND DISCUSSIONS

Application of photocatalysis in our daily life and chemical industries has found a great interest. As reported in the introduction, the superior TiO_2 photocatalyst was elegantly used for several photocatalytic oxidation processes. The present work is directed for synthesis, mechanistic, and selectivity studies as well as for decontamination purposes.

The target starting materials include three selected alicyclic alcohols; cyclohexanol (**1**), cyclopentanol (**2**), and cycloheptanol (**3**); of different ring sizes.

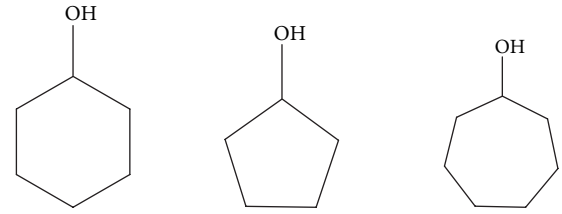

Cyclohexanol (**1**) Cyclopentanol (**2**) Cycloheptanol (**3**)

Results obtained in this work will be presented for each individual alcohol; and collective table and figures are also available in the following discussion.

3.1. PCO of cyclohexanol (1) and cyclohexanone (4)

3.1.1. PCO of 1 in acetonitrile

After irradiation of **1** in dry acetonitrile, the photolysis product, using GC/MS technique, were cyclohexanone (**4**, 45.6%), 1,4-cyclohexanedione (**7**, 3.2%), cyclohexyl formate (**8**, 2.5%), 2-cyclohexenone (**9**, 1.8%), 2-hydroxycyclohexanone (**10**, 1.1%), n-hexanoic acid (**11**, 4.0%), 5-hexenal(**16**, 2.9%), 4-hydroxycyclohexanone (**17**, 4.4%), and cyclohexyl hexanoate (**12**, 3.0%), and other product (**19**, 2.9%) (Table 1, Exp. 1).

Cyclohexanol (**1**) is a sensitive probe, for it has been established that two electron oxidation will give cyclohexanone (**4**) [17] as a primary product, whereas single electron oxidation selectively produces the open-chain unsaturated aldehyde 5-hexenal (**16**) [17], also 5-hexenal (**16**) formed by intramolecular hydrogen transfer reaction of cyclohexanone. Cyclohexanone was also oxidized to n-hexanoic acid (**11**) [28, 29].

Cyclohexanone (**4**) can be hydroxylated by $^{\bullet}$OH radical to 4-hydroxycyclohex-anone (**17**) and 2-hydroxycyclohexanone (**10**). 1,4-cyclohexanedione (**7**) is most probably formed by oxidation of 4-hydroxycyclohexanone (**17**) [30] and 2-cyclohexenone (**9**) was probably formed by dehydration of 2-hydroxycyclohexanone (**10**) [14, 17], respectively. 3-hydroxycyclohexanone may be formed also, but not detected, and dehydrated to 2-cyclohexenone (**9**). This is because the heat of formation [31] of the three hydroxylated cyclohexanones are close to each other (−101.61, −99.88, −103.64 Kcal/mol, resp.). This means that they are close in stability and probability of formation. 5-hexenal (**16**) oxidation by double bond cleavage to formaldehyde [32] which by further oxidation gives formic acid. Cyclohexanol (**1**) can react with formic acid to give cyclohexyl formate (**8**), and with n-hexanoic acid (**11**) to give cyclohexyl hexanoate (**12**), (Scheme 1).

3.1.2. PCO of 1 in acetone:

After irradiation of **1** in acetone, the photolysis products analyzed by GC/MS technique were cyclohexanone (**4**, 25.2%), 1,4-cyclohexanedione (**7**, 3.4%) cyclohexyl formate (**8**, 2.3%), 2-hydroxycyclohexanone (**10**, 0.5%), n-hexanoic acid (**11**, 5.4%), 5-hexenal (**16**, 1.9%), and 4-hydroxycyclohexanone (**17**, 3.5%),1,1′-bicyclohexyl-1,1′-diol (**18**, 2.5%) (Table 1, Exp. 4).

GC chromatogram and the suggested mechanism of these products showed that nearly all products formed in acetone are the same as the products formed in acetonitrile, but in lower conversion. From Table 1, the conversion of cyclohexanol (**1**) in dry acetonitrile was 71.6%, while in dry acetone equals to 45% (Figure 1). This is because the dielectric constant (DEC) of acetonitrile is much higher than that of acetone, 37.5 and 21.4, respectively [33]. A plausible explanation is that increase of solvent polarity increases the stabilization of the intermediate radical cations which in turn raise the percentage of the oxidation products [33].

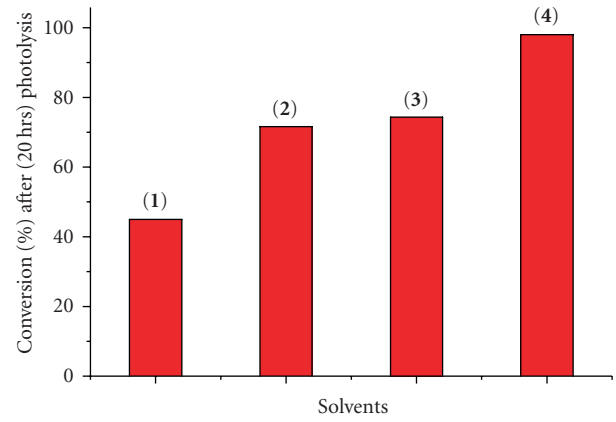

(**1**) $(CH_3)_2CO$
(**2**) CH_3CN
(**3**) CH_3CN-H_2O (4 : 1)
(**4**) CH_3CN-30% H_2O_2 (4 : 1)

Figure 1: Effect of solvents on photocatalytic oxidation of cyclohexanol (**1**).

This supports the electron/hole mechanism in photocatalytic oxidation of the investigated alcohols.

3.1.3. PCO of 1 in acetonitrile-water (4 : 1)

Irradiation products of **1** in acetonitrile-water mixture (4 : 1), as analyzed by GC/MS, were cyclohexanone (**4**, 39.7%), 1,4-cyclohexanedione (**7**, 3.7%), cyclohexyl formate (**8**, 1.43%), 2-cyclohexenone (**9**, 2.4%), 2-hydroxycyclohexanone (**10**, 7.8%), 5-hexenal (**16**, 1.8%), 4-hydroxycyclohexanone (**17**, 11.0%) and 1,4-cyclohexanediol (**20**, 6.5%), (Table 1, Exp. 2).

The products formed in aqueous acetonitrile are almost similar to those formed in acetonitrile, but the experimental conversion and yield distribution are different (Table 1). Conversion of **1** in aqueous acetonitrile (4 : 1) is 74.3% more than in dry acetonitrile (71.6%) this is because the dielectric constant (DEC) of water is 78.3 [34] (Figure 1). Also primary oxidant in this reaction is expected to be the strong oxidant $^{\bullet}$OH radical generated by trapping a photohole at an adsorbed water molecule [35]. The percentage of hydroxylated compounds increased from 5.5% to 25.3%, and a new product is formed 1,4-cyclohexanediol (**20**).

3.1.4. PCO of 1 in acetonitrile-30% H_2O_2 (4 : 1)

Irradiation of **1** in acetonitrile-30% hydrogen peroxide (4 : 1) without oxygen passage, using GC/MS analyses of the photolysat gave cyclohexanone (**4**, 13.6%), 1,4-cyclohexanedione (**7**, 8.7%), 2-cyclohexenone (**9**, 5.1%), 2-hydroxycyclohexanone (**10**, 10.2%), 4-hydroxycyclohexanone (**17**, 10.5%) and 1,4-cyclohexadiol (**20**, 8.2%), glutaric acid (**21**, 12.0%) and adipic acid (**22**, 29.8%) (Table 1, Exp. 3).

Table 1: Photocatalytic oxidation of the investigated cyclalkanols **1–3**.

Exp.	Substrate	Solvents	Time (hrs)	Conv. (%)	Products (No, yield%)
1	Cyclohexanol (**1**)	CH_3CN	20	71.6	Cyclohexanone (**4**, 45.6), 1,4-Cyclohexanedione (**7**, 3.2), Cyclohexyl formate (**8**, 2.5), 2-Cyclohexenone (**9**, 1.8), 2-Hydroxycyclohexanone (**10**, 1.1) n-Hexanoic acid (**11**, 4.0), Cyclohexyl hexanoate (**12**, 3.0), 5-Hexenal (**16**, 2.9), 4-Hydroxycyclohexanone (**17**, 4.4), Other product (**19**, 2.9).
2	Cyclohexanol (**1**)	CH_3CN+H_2O (4 : 1)	20	74.3	Cyclohexanone (**4**, 39.7), 1,4-Cyclohexadione (**7**, 3.7), Cyclohexyl formate (**8**, 1.4), 2-Cyclohexenone (**9**, 2.4), 2-Hydroxycyclohexanone (**10**, 7.8), 5-Hexenal (**16**, 1.8), 4-Hydroxycyclohexanone (**17**, 11.0), 1,4-Cyclohexanediol (**20**, 6.5).
3	Cyclohexanol (**1**)	CH_3CN+H_2O_2 (4 : 1)	20	98.0	Cyclohexanone (**4**, 13.6), 1,4-Cyclohexadione (**7**, 8.7), 2-Cyclohexenone (**9**, 5.1), 2-Hydroxycyclohexanone (**10**, 10.2), 4-Hydroxycyclohexanone (**17**, 10.5), 1,4-Cyclohexanediol (**20**, 8.2), Glutaric acid (**21**, 12.0), Adipic acid (**22**, 29.8).
4	Cyclohexanol (**1**)	H_3COH_3	20	45	Cyclohexanone (**4**, 25.2), 1,4-Cyclohexadione (**7**, 3.4), Cyclohexyl formate (**8**, 2.3), 2-Hydroxycyclohexanone (**10**, 0.5) n-Hexanoic acid (**11**, 5.4), 5-Hexenal (**16**, 1.9), 4-Hydroxycyclohexanone (**17**, 3.5), 1,1′-Bicyclohexyl-1,1′-diol (**18**, 2.5).
5	Cyclopentanol (**2**)	CH_3CN	20	94.2	Cyclopentanone (**5**, 72.7), n-Pentanoic acid (**13**, 4.3), Cyclopentyl pentanoate (**14**, 2.8), 4-Pentenal (**23**, 3.7), Other products (**24**, 3.1), (**25**, 5.8), (**26**, 1.8).
6	Cycloheptanol (**3**)	CH_3CN	20	100	Cycloheptanone (**6**, 79.9), n-heptanoic acid (**15**, 3.2), 6-Heptenal (**27**, 1.8), 4-Hydroxycycloheptanone (**28**, 4.1), 1,4-Cycloheptadione (**29**, 4.7), 2-Hydroxycycloheptanone (**30**, 1.5).

GC chromatogram and the suggested mechanismof these products showed that most of products formed in acetonitrile-30% H_2O_2 (4 : 1) mixture are the same as formed in dry acetonitrile with almost complete conversion of **1** (98%), that is, more than in dry acetonitrile or in aqueous acetonitrile (Figure 1). Electrons are donated from TiO_2 to hydrogen peroxide because it is a stronger oxidant than molecular oxygen [30]. When hydrogen peroxide accepts an electron, $^{\bullet}OH$ radical may be produced according to (**1**) [35], so the $^{\bullet}OH$ radicals are generated in large amounts, so the percentage of hydroxylated compounds increased, for example, the % of compound **10** increased from 1.1% to 7.8% to 10.2% in cases of acetonitrile, aqueous acetonitrile or acetonitrile-30% H_2O_2, respectively, and new products were formed such as glutaric acid (**21**) and adipic acid (**22**).

$$TiO_{2(e^-)} + H_2O_2 \longrightarrow TiO_2 + O\overline{H} + {}^{\cdot}OH. \quad (1)$$

The addition of H_2O_2 is a well-known technique for increasing the rate of photocatalytic degradation with higher quantum yield of formation of $^{\bullet}OH$ [30]. Consequently, the increased oxidation rate is expected by the addition of H_2O_2 as shown in Table 1 (Exps. 1–3).

It is worthy to mention that no oxidation products could be detected with cyclohexanol in the absence of catalyst and/or light [30]. This is a good proof for the role of each parameter (H_2O_2, TiO_2 and light) in the photocatalytic oxidation process.

Table 2: Photocatalytic Oxidation of the Investigated Ketones **4**–**6**:

Exp.	Substrate	Solvents	Time (hrs)	Conv. (%)	Products (No,%)
7	Cyclohexanone (**4**)	CH_3CN	20	19.8	1,4-Cyclohexadione (**7**, 4.1), 2-Cyclohexenone (**9**, 1.4), 2-Hydroxycyclohexanone (**10**, 0.3) n-Hexanoic acid (**11**, 6.2), 5-Hexenal (**16**, 3.5), 4-Hydroxycyclohexanone (**17**, 3.8).
8	Cyclopentanone (**5**)	CH_3CN	20	26.3	n-Pentanoic acid (**13**, 15.9), 4-Pentenal (**23**, 10.4).
9	Cycloheptanone (**6**)	CH_3CN	20	29.9	n-heptanoic acid (**15**, 6.8), 6-Heptenal (**27**, 4.1), 4-Hydroxycycloheptanone (**28**, 7.8), 1,4-Cycloheptanedione (**29**, 7.8), 2-Hydroxycycloheptanone (**30**, 3.4).

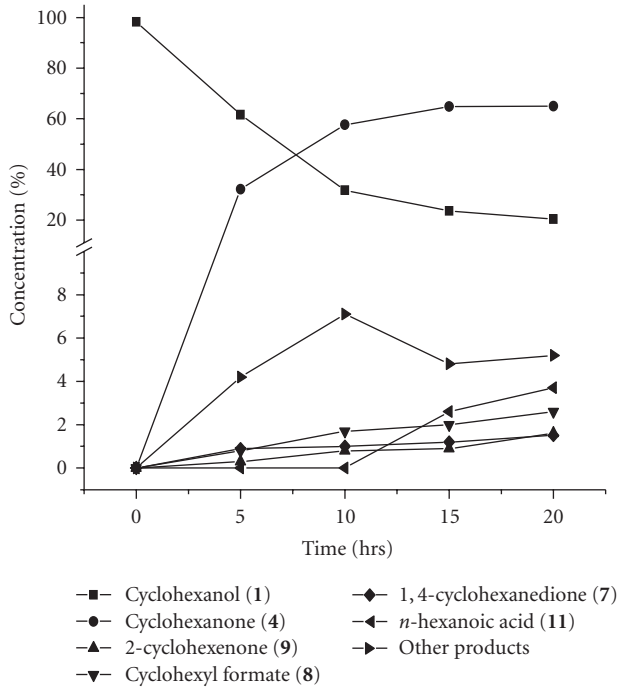

Figure 2: Photocatalytic Oxidation of cyclohexanol (**1**) in acetonitrile.

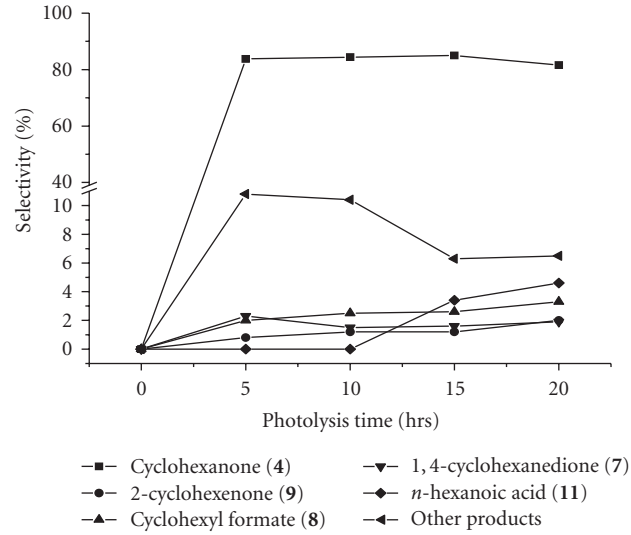

Figure 3: Selectivity of products of PCO of **1** in acetonitrile.

3.1.5. PCO of cyclohexanone (4) in acetonitrile

To shed more light on the formation and fate of the primary photooxidation products, cyclohexanone was irradiated at the same previous conditions. The conversion was only 19.8% after 20 hours irradiation. The GC/MS analyses of the photolysis products were 1,4-cyclohexanedione (**7**, 4.1%), 2-cyclohexenone (**9**, 1.4%), 2-hydroxycyclohexanone (**10**, 0.3%), n-hexanoic acid (**11**, 6.2%), 5-hexenal (**16**, 3.5%), and 4-hydroxycyclohexanone (**17**, 3.8%) (Table 2, Exp.7).

GC chromatogram and the suggested mechanism of these products matches those obtained from photocatalytic oxidation of cyclohexanol (**1**).

3.2. PCO of cyclopentanol (2) and cyclopentanone (5)

3.2.1. PCO of 2 in acetonitrile using TiO_2

After irradiation of **2** in acetonitrile, the residue was analyzed by GC/MS. The photolysis products were cyclopentanone (**5**, 72.7%), n-pentanoic acid (**13**, 4.3%), cyclopentyl pentanoate (**14**, 2.8%), 4-pentenal (**23**, 3.7%), and some other unidentified low concentration products (**24**, 3.1%, **25**, 5.8%, and **26**, 1.8%) (Table 1, Exp. 5).

GC chromatogram and the suggested mechanism of these products showed that cyclopentanol (**2**) via two electron oxidation gave cyclopentanone (**5**) [17] as a primary product, whereas single electron oxidation selectively produces open chain unsaturated aldehyde 4-pentenal (**23**) [17]. Also 4-pentenal (**23**) may be formed by intramolecular hydrogen atom transfer reaction of cyclopentanone [28]. Cyclopentanone was also oxidized to n-pentanoic acid (**13**), which reacted with cyclopentanol (**2**) to give cyclopentyl pentanoate (**14**) (Scheme 2).

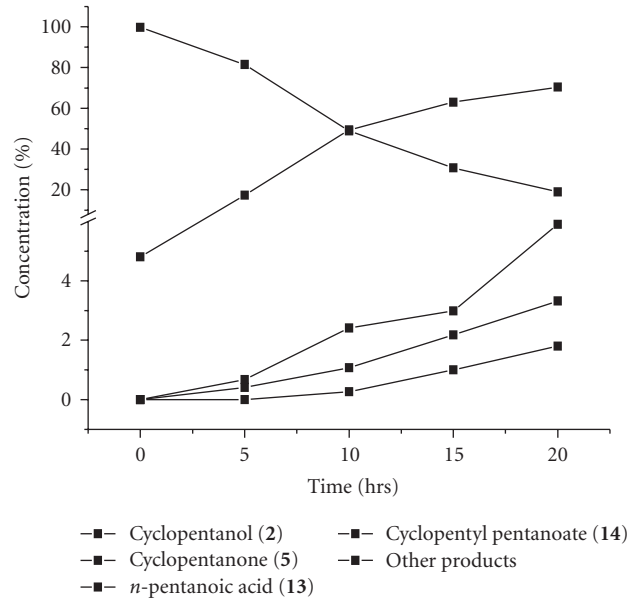

Figure 4: Photocatalytic oxidation of cyclopentanol **2** in acetonitrile.

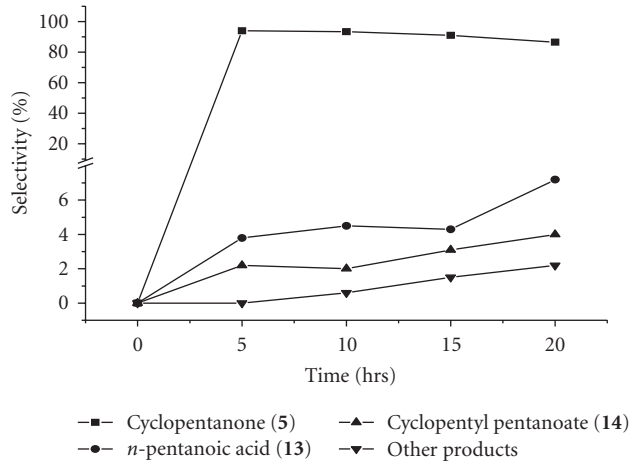

Figure 5: Selectivity of products of PCO of **2** in acetonitrile.

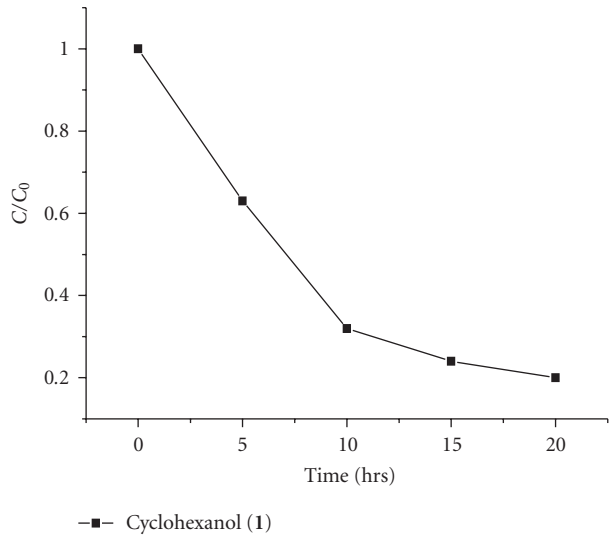

Figure 6: Photocatalytic disappearance of **1** in acetonitrile.

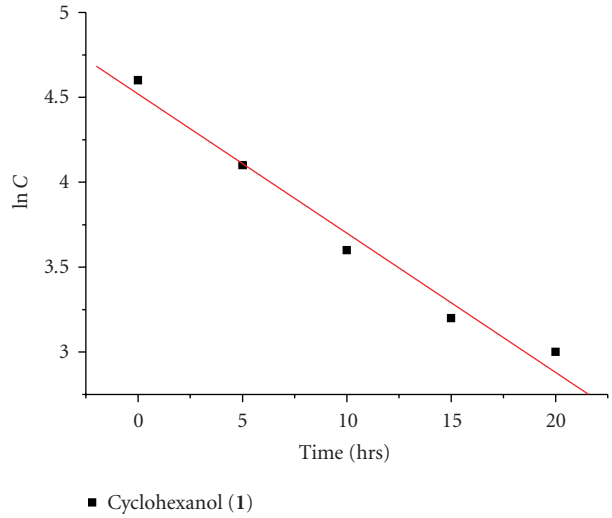

Figure 7: First-order PCO of **1** in acetonitrile ($r = 0.9886$, $k = -0.083\ \mathrm{hr}^{-1}$).

3.2.2. PCO of cyclopentanone (5) in acetonitrile

Great attention was focused on the oxidation of the primary oxidation product, cyclopentanone. Therefore, the photocatalytic oxidation of **5** under the same previous condition was investigated. Low conversion (26.3%) was observed and the photolysis products were n-pentanoic acid (**13**, 15.9%), and 4-pentenal (**23**, 10.4%) (Table 2, Exp. 8).

The suggested mechanism of these products is in agreement with the suggested mechanism of photocatalytic oxidation of cyclopentanol.

3.3. PCO of cycloheptanol (3) and cycloheptanone (6)

3.3.1. PCO of 3 in acetonitrile using TiO_2

After irradiation of **3** in acetonitrile, the photolysis products, analyzed by GC/MS, were cycloheptanone (**6**, 79.9%), n-heptanoic acid (**15**, 3.2%), 6-heptenal (**27**, 1.8%), 4-hydroxycycloheptanone (**28**, 4.1%), 1,4-cycloheptadione (**29**, 4.7%) and 2-hydroxycycloheptanone (**30**, 1.5%) (Table 1, Exp. 6).

The suggested mechanism of these products showed that cycloheptanol (**3**) is a sensitive probe, therefore it has been established that two electron oxidation will give cycloheptanone (**6**) [17], whereas a single electron oxidation selectively produces the open-chain unsaturated

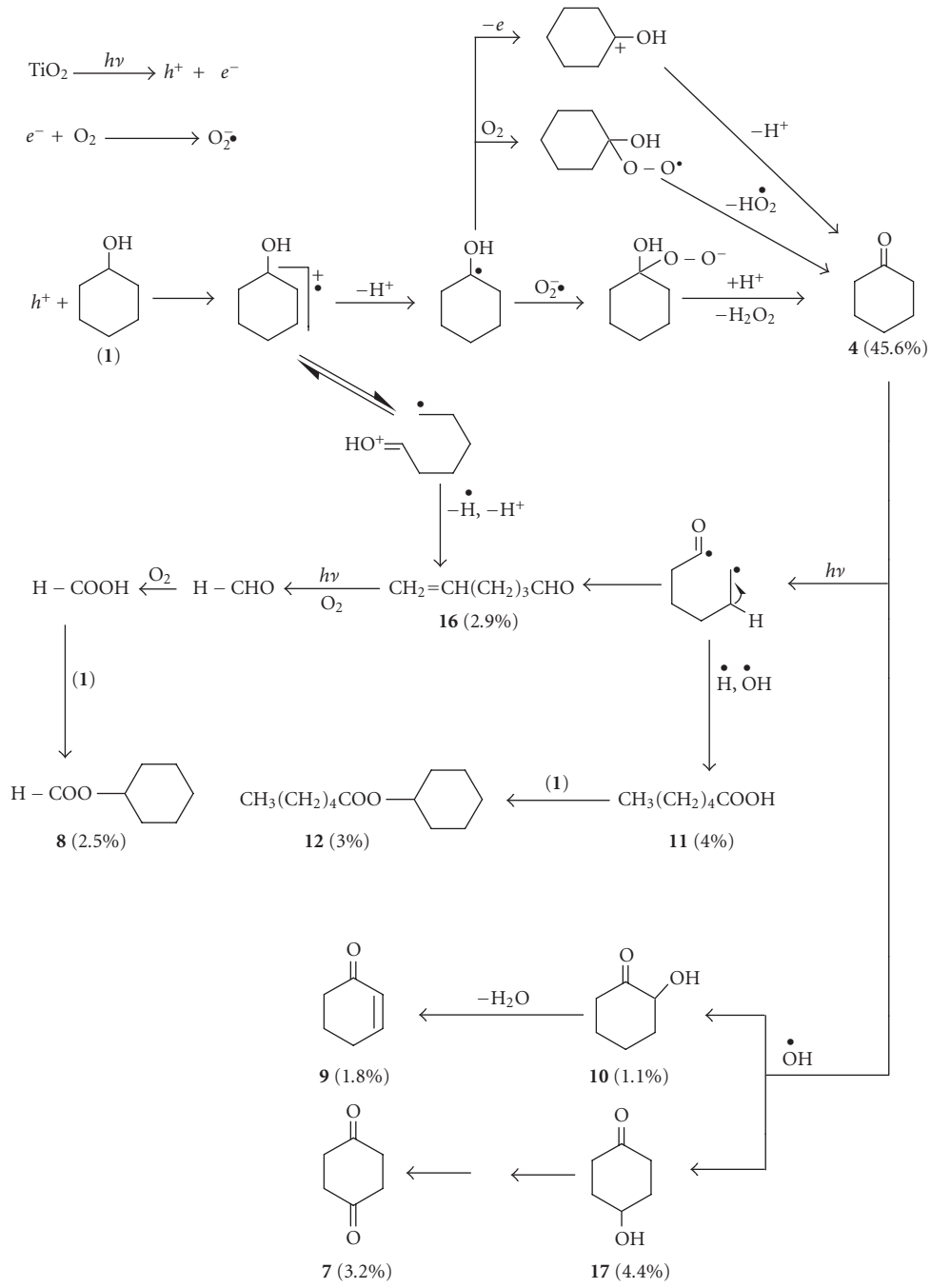

Scheme 1: Suggested mechanism of PCO of **1** in acetonitrile.

aldehyde 6-heptenal (**27**) [17]. Also 6-heptenal (**27**) was formed by intramolecular hydrogen transfer reaction for cycloheptanone [28]. Cycloheptanone oxidiation affored n-heptanoic acid (**15**). Also cycloheptanone (**6**) was hydroxylated by ·OH radical to give 4-hydroxycycloheptanone (**28**) and 2-hydroxycycloheptanone (**30**). 1,4-cycloheptandione (**29**) was most probably generated by oxidation of 4-hydroxycycloheptanone (**28**) [30] (Scheme 2).

3.3.2. PCO of Cycloheptanone (6) in Acetonitrile Using TiO_2

Photocatalytic irradiation of **6** in dry acetonitrile, resulted in 29.9% conversion. The photolysis products were 6-heptenal (**27**, 4.1%), n-heptanoic acid (**15**, 6.8%), 4-hydroxycycloheptanone (**28**, 7.8%), 1,4-cycloheptadione (**29**, 7.8%), and 2-hydroxycycloheptanone (**30**, 3.4%) (Table 2, Exp. 9).

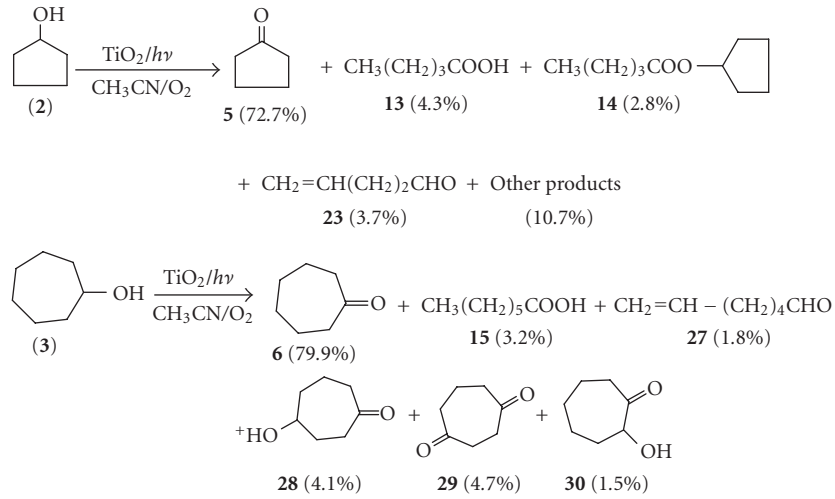

Scheme 2: Photocatalytic oxidation of **2** and **3**.

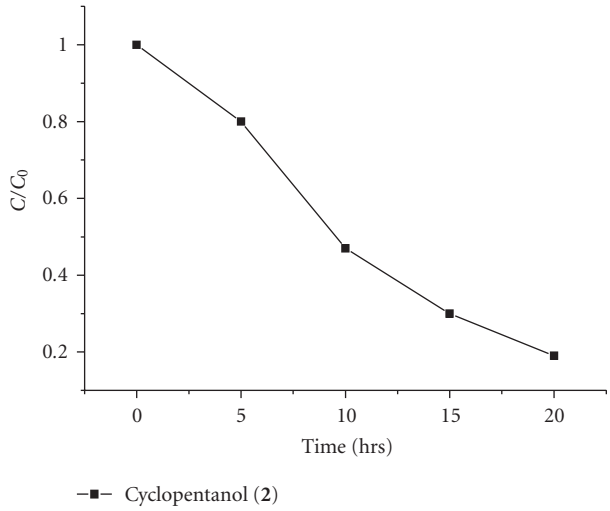

Figure 8: Photocatalytic disappearance of **2** in acetonitrile.

GC chromatogram and the suggested mechanism of these products are similar to the photocatalytic oxidation of cycloheptanol (**3**).

The obtained results indicated that the percentage conversion of **3** > **2** > **1**, the same as that of corresponding ketones where **7** > **6** > **5**. This is in agreement with their heat of formation (ΔH_f = **−60.83, −66.98, and −80.22) Kcal/mol, respectively**. Of course cyclohexanol (**1**), the most stable one [31] (ΔH_f = −80.22 Kcal/mol), has the lowest percentage of conversion compared with **2** and **3**.

4. DISCUSSION

The main objectives of the present work include photocatalytic oxidation (PCO) of the selected alicyclic alcohols (**1–3**) of different ring sizes in the presence of aerated titanium dioxide (Degussa P25) suspensions in anhydrous acetonitrile and other solvent mixtures. A polar, nonhydroxylic solvent (CH_3CN) represents the best opportunity for controlling oxidative reactivity at the interface between a liquid reaction mixture and a solid irradiated photocatalyst [18, 19, 36]. To evaluate the role of each parameter in the system using cyclohexanol (**1**) as a model alcohol, we studied the effect of catalyst, light, oxygen, solvent polarity, and the effect of hydrogen peroxide as oxidizing agent instead of oxygen gas.

No oxidation products were detected upon irradiation of cyclohexanol (**1**) in the absence of catalyst and/or of light. Furthermore, experiments carried out in the absence of oxygen showed also no significant evidence of products formed. All these results confirm the essential role of oxygen, TiO_2 and light in the photocatalytic oxidation process [18, 19, 33].

Furthermore, the UV absorption spectra of the target compounds have been inspected to shed some light on their behavior upon irradiation. The maximum absorption of the investigated alcohols (**1–3**) ranges between 277.1 nm for **2** and 287.1 nm for **3**, a range that will be cutoff by pyrex glass [18, 19]. As the maximum emission of the used 450 W medium pressure mercury lamp ranges between 296.7 nm–578.0 nm (4.18 − 2.15 eV), the obtained products are therefore originated through initial band gap excitation of TiO_2 (3.23 eV) [7, 37], but not through direct excitation of the alcohol.

In a photocatalytic process, the primary step following the radiation absorption by the photocatalyst is the generation of electron-hole pairs (**2**), which must be trapped in order to avoid recombination, that is, charge separation is essential for any photocatalytic electroprocess.

$$TiO_2 \xrightarrow{h\nu} [TiO_2{}^*] \longrightarrow e^-_{CB} + h^+_{VB}. \quad (2)$$

Despite the contributions from a number of research groups, detailed mechanisms of the photocatalytic oxidation processes at the TiO_2 surface remain elusive for many important organic materials particularly regarding the initial steps involved in the redox radical reactions, which may

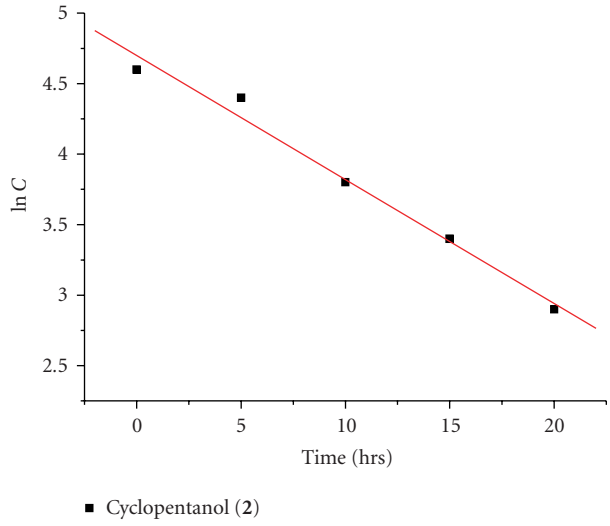

Figure 9: First-order PCO of **2** in acetonitrile ($r = 0.9918$, $k = -0.094\,\mathrm{hr}^{-1}$).

involve one or more of the following radicals $O_2^{\bullet-}$, $^{\bullet}OH$, $HOO^{\bullet}$, $Cl^{\bullet}$, and so on. The use of nonaqueous reaction medium rules out the participation of hydroxy radicals generated by water trapping of the hole, in the oxidation process [38].

From the product distribution and reaction products profiles, the reaction mechanism of TiO_2 sensitized photooxidation of the target alcohols (**1–3**) in aerated acetonitrile has been proposed.

The efficiency of the oxidation was governed by the oxidation potential of the alcohol, the avability of α-hydrogens and the tightness of the association with the photocatalyst.

Cyclic voltammetric measurement using glassy carbon electrode revealed anodic oxidation potential of the model alcohol, cyclohexanol equals to (+0.85 V) which is less positive than the hole potential (+2.35 V), meaning that photocatalytic oxidation of cyclohexanol is thermodynamically possible. Also as the reduction potential of oxygen (−0.39 V) is less negative than the conduction band electron (−0.88 V), formation of the superoxide $O_2^{\bullet-}$ is thermodynamically allowed in the reaction medium [18, 19, 33].

It is useful to stress on the point that in a photoreaction occurring on a semiconductor catalyst powder both the oxidation and reduction processes must occur on the same particle, although reaction sites for these processes may be different. Adsorbed oxygen species are the traps for electrons according to the following (3), (4), forming the radical anion $O_2^{\bullet-}$ (superoxide).

$$O_2(\text{solution}) \rightleftharpoons O_2(\text{ads}), \tag{3}$$

$$O_2(\text{ads}) + e^- \longrightarrow O_2^{\bullet-}(\text{ads}). \tag{4}$$

On the other hand, the adsorbed alcohol species in dry acetonitrile are the likely traps for holes forming the radical cation, by single electron transfer, which rapidly deprotonated producing α-hydroxy radical of reasonable stability [17] as follows (5).

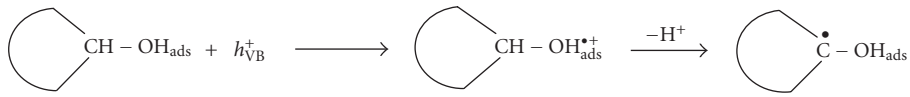

(5)

Two fates are available to such radical. (1) **A second electron oxidation:** the latter intermediate is extremely easily oxidized [17] by loss of a second electron generating a protonated carbonyl intermediate. This intermediate gives the proton to the environmental forming the corresponding carbonyl compound **(two-electrons mechanism).** (2) **Trapping of $O_2^{\bullet-}$ and/or $O_2^{\bullet-}$:** An alternative mechanism is the trapping of the α-hydroxy radical by oxygen forming the peroxy radical or by superoxide ($\mathbf{O_2^{\bullet-}}$) forming peroxy anion, decomposition of which would be expected to occur rapidly to produce the carbonyl products [17] (6), (7).

Formation of the open-chain carbonyl compounds (8) can be produced by **ring rupture** of the α-hydroxy radical cation [17] (**single-electron mechanism**).

These suggested mechanisms can be represented in general as follows:

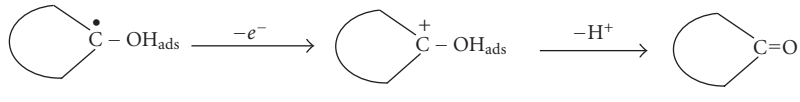

(6)

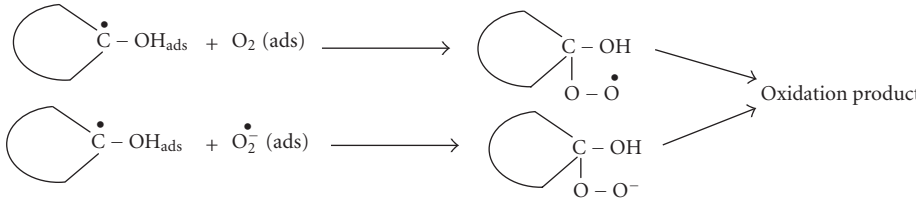

(7)

(8)

Accordingly, the proposed photocatalytic oxidation (PCO) of cyclohexanol (**1**), for example, could be present as in Scheme 1. Also the PCO of **2** and **3** are summarized in Scheme 2.

5. KINETIC STUDIES

The photocatalytic oxidation reactions of cyclohexanol (**1**) and cyclopentanol (**2**) in acetonitrile were followed up by GC, as shown in Figures 2 and 4, respectively.

Selectivity of photocatalytic oxidation of cyclohexanol (**1**), cyclopentanol (**2**) are shown in Figures 3 and 5, respectively.

From these results, we can conclude that the photocatalytic oxidation of secondary alcohols **1, 2** have high selectivity to form ketones by more than 85%.

The kinetic disappearance [39] of the investigated alcohols (**1, 2**) from an initial concentration in acetonitrile was shown in Figures 6 and 8, respectively.

The semilogarithmic plots [39] of concentration data gave a straight line for cyclohexanol (**1**) and cyclopentanol (**2**) in acetonitrile as shown in Figures 7 and 9, respectively. These findings indicate that the photocatalytic oxidation of the investigated alcohols in TiO_2 suspension can be described by the first-order kinetic model; $\mathrm{Ln}C = -kt + \mathrm{Ln}C_o$, where C_o is the initial concentration and C is the concentration of alcohols at time t. This is in agreement with the former work of Cinar on m-cresol [39].

REFERENCES

[1] A. Fujishima and K. Honda, "Electrochemical photolysis of water at a semiconductor electrode," *Nature*, vol. 238, no. 5358, pp. 37–38, 1972.

[2] A. Fujishima, K. Hashimoto, and T. Watanabe, *TiO_2 Photocatalysis Fundaments and Applications*, BKC, Tokyo, Japan, 1999.

[3] J. Peral, X. Domènech, and D. F. Ollis, "Heterogeneous photocatalysis for purification, decontamination and deodorization of air," *Journal of Chemical Technology & Biotechnology*, vol. 70, no. 2, pp. 117–140, 1997.

[4] K. Hofstadler, R. Bauer, S. Novalic, and G. Heisler, "New reactor design for photocatalytic wastewater treatment with TiO_2 immobilized on fused-silica glass fibers: photomineralization of 4-chlorophenol," *Environmental Science & Technology*, vol. 28, no. 4, pp. 670–674, 1994.

[5] S.-L. Kuo and C.-J. Liao, "Solar photocatalytic degradation of 4-chlorophenol in kaolinite catalysts," *Journal of the Chinese Chemical Society*, vol. 53, no. 5, pp. 1073–1083, 2006.

[6] H. Yu, K. Zhang, and C. Rossi, "Theoretical study on photocatalytic oxidation of VOCs using nano-TiO_2 photocatalyst," *Journal of Photochemistry and Photobiology A*, vol. 188, no. 1, pp. 65–73, 2007.

[7] A. A. Abdel-Wahab and A. M. Gaber, "TiO_2-photocatalytic oxidation of selected heterocyclic sulfur compounds," *Journal of Photochemistry and Photobiology A*, vol. 144, no. 3, pp. 213–218, 1998.

[8] A. Danion, J. Disdier, C. Guillard, and N. Jaffrezic-Renault, "Malic acid photocatalytic degradation using a TiO_2-coated optical fiber reactor," *Journal of Photochemistry and Photobiology A*, vol. 190, no. 1, pp. 135–140, 2007.

[9] O. Prieto, J. Fermoso, and R. Irusta, "Photocatalytic degradation of toluene in air using a fluidized bed photoreactor," *International Journal of Photoenergy*, vol. 2007, Article ID 32859, 8 pages, 2007.

[10] H. Vosooghian and M. H. Habibi, "Photooxidation of some organic sulfides under UV light irradiation using titanium dioxide photocatalyst," *International Journal of Photoenergy*, vol. 2007, Article ID 89759, 7 pages, 2007.

[11] S.-S. Kim, J. Jo, C. Chun, J.-C. Hong, and D.-Y. Kim, "Hybrid solar cells with ordered TiO_2 nanostructures and MEH-PPV," *Journal of Photochemistry and Photobiology A*, vol. 188, no. 2-3, pp. 364–370, 2007.

[12] H. Maeda, H. Nakagawa, and K. Mizuno, "TiO_2-catalyzed photooxygenation of cinnamic acid derivatives via their radical cations," *Journal of Photochemistry and Photobiology A*, vol. 189, no. 1, pp. 94–99, 2007.

[13] M. Bettoni, T. D. Giacco, C. Rol, and G. V. Sebastiani, "Titanium dioxide photosensitised oxidation of α,β-dihydroxybenzyl derivatives in CH_3CN," *Journal of Photochemistry and Photobiology A*, vol. 190, no. 1, pp. 34–40, 2007.

[14] P. R. Harvey, R. Rudham, and S. Ward, "Photocatalytic oxidation of liquid propan-2-ol by titanium dioxide," *Journal of the Chemical Society, Faraday Transactions 1*, vol. 79, no. 6, pp. 1381–1390, 1983.

[15] R. E. Cameron and A. B. Bocarsly, "Photoactivated oxidation of alcohols by oxygen," *Journal of the American Chemical Society*, vol. 107, no. 21, pp. 6116–6117, 1985.

[16] S.-I. Nishimoto, B. Ohtani, and T. Kagiya, "Photocatalytic dehydrogenation of aliphatic alcohols by aqueous suspensions of platinized titanium dioxide," *Journal of the Chemical Society, Faraday Transactions 1*, vol. 81, no. 10, pp. 2467–2474, 1985.

[17] M. A. Fox, H. Ogawa, and P. Pichat, "Regioselectivity in the semiconductor-mediated photooxidation of 1,4-pentanediol," *Journal of Organic Chemistry*, vol. 54, no. 16, pp. 3847–3852, 1989.

[18] O. S. Mohamed, "Photocatalytic oxidation of selected fluorenols on TiO_2 semiconductor," *Journal of Photochemistry and Photobiology A*, vol. 152, no. 1–3, pp. 229–232, 2002.

[19] M. A. Fox and A. A. Abdel-Wahab, "Photocatalytic oxidation of multifunctional organic molecules. The effect of an intramolecular aryl thioether group on the semiconductor-mediated oxidation/dehydrogenation of a primary aliphatic alcohol," *Journal of Catalysis*, vol. 126, no. 2, pp. 693–696, 1990.

[20] U. R. Pillai and E. Salhe-Demessie, "Selective oxidation of alcohols in gas phase using light-activated titanium dioxide," *Journal of Catalysis*, vol. 211, no. 2, pp. 434–444, 2002.

[21] Y. Wu, G. Lu, and S. Li, "The long-term photocatalytic stability of Co^{2+}-modified P25-TiO_2 powders for the H_2 production

from aqueous ethanol solution," *Journal of Photochemistry and Photobiology A*, vol. 181, no. 2-3, pp. 263–267, 2006.

[22] A. I. Vogel, *Textbook of Practical Organic Chemistry*, Longman, New York, NY, USA, 4th edition, 1978.

[23] F. C. Whitmore and G. W. Pedlow, "Δ^2-cyclohexenone and related substances," *Journal of the American Chemical Society*, vol. 63, no. 3, pp. 758–760, 1941.

[24] J. C. Sheehan, R. C. O'Neill, and M. A. White, "The formation of five and six-membered rings by the acyloin condensation. I. The cyclization of glutaric and adipic esters," *Journal of the American Chemical Society*, vol. 72, no. 8, pp. 3376–3378, 1950.

[25] H. B. Hass and J. R. Marshall, "Syntheses from natural-gas hydrocarbons I—caproic acid from pentane," *Industrial & Engineering Chemistry*, vol. 23, no. 4, pp. 352–253, 1931.

[26] R. Adams and C. S. Marvel, "Organic chemical reagents. VI. Reagents from *n*-butyl alcohol," *Journal of the American Chemical Society*, vol. 42, no. 2, pp. 310–320, 1920.

[27] J. R. Ruhoff, "*N*-heptanoic acid," in *Organic Syntheses Collective*, C. R. Noller and M. Patt, Eds., vol. 2, pp. 315–316, John Wiley & Sons, New York, NY, USA, 1943.

[28] A. A. Scala and D. G. Ballan, "Vacuum ultraviolet photolysis of cyclohexanone," *Journal of Physical Chemistry*, vol. 76, no. 5, pp. 615–620, 1972.

[29] R. Srinivasan, "Photoisomerization processes in cyclic ketones. II. Cyclohexanone and 2-methylcyclohexanone," *Journal of the American Chemical Society*, vol. 81, no. 11, pp. 2601–2604, 1959.

[30] T. Ohno, T. Mitsui, and M. Matsumura, "TiO_2-photocatalyzed oxidation of adamantane in solutions containing oxygen or hydrogen peroxide," *Journal of Photochemistry and Photobiology A*, vol. 160, no. 1-2, pp. 3–9, 2003.

[31] E. V. Anslyn and D. A. Dougherty, *Modern Physical Organic Chemistry*, C.Taylor, Edwards Brothers, Sausalito, Calif, USA, 2004.

[32] M. A. Fox, *Advances in Photochemistry*, John Wiley & Sons, Austin, Tex, USA, 1986.

[33] O. S. Mohamed, A. M. Gaber, and A. A. Abdel-Wahab, "Photocatalytic oxidation of selected aryl alcohols in acetonitrile," *Journal of Photochemistry and Photobiology A*, vol. 148, no. 1–3, pp. 205–210, 2002.

[34] S. Yamazaki, N. Yamabe, S. Nagano, and A. Fukuda, "Adsorption and photocatalytic degradation of 1,4-dioxane on TiO_2," *Journal of Photochemistry and Photobiology A*, vol. 185, no. 2-3, pp. 150–155, 2007.

[35] S. Senthilkumaar and K. Porkodi, "Heterogeneous photocatalytic decomposition of crystal violet in UV-illuminated sol-gel derived nanocrystalline TiO_2 suspensions," *Journal of Colloid and Interface Science*, vol. 288, no. 1, pp. 184–189, 2005.

[36] M. A. Fox and A. A. Abdel-Wahab, "Selectivity in the TiO_2-mediated photocatalytic oxidation of thioethers," *Tetrahedron Letters*, vol. 51, no. 32, pp. 4533–4536, 1990.

[37] M. A. Fox, "Mechanistic photocatalysis in organic synthesis," in *Photocatalysis: Fundamentals and Applications*, N. Serpone and E. Pelizzetti, Eds., pp. 421–455, Wiley-Interscience, New York, NY, USA, 1990.

[38] P. F. Schwarz, N. J. Turro, S. H. Bossman, A. M. Braun, A. A. Abdel-Wahab, and H. Dürr, "A new method to determine the generation of hydroxyl radicals in illuminated TiO_2 suspensions," *Journal of Physical Chemistry*, vol. 101, no. 36, pp. 7127–7134, 1997.

[39] A. Hatipoğlu, N. San, and Z. Çinar, "An experimental and theoretical investigation of the photocatalytic degradation of *meta*-cresol in TiO_2 suspensions: a model for the product distribution," *Journal of Photochemistry and Photobiology A*, vol. 165, no. 1–3, pp. 119–129, 2004.